OPTIMIZING ENERGY PERFORMANCE AND INDOOR ENVIRONMENTAL QUALITY OF BUILDINGS USING ENERGY SIMULATION, GENERIC OPTIMIZATION AND COMPUTATIONAL FLUID DYNAMICS

Rajaguru Mudiyanselage Priyantha Senarath Bandara

(128002 P)

Thesis submitted in partial fulfillment of the requirements for the degree
Doctor of Philosophy in Mechanical Engineering

Department of Mechanical Engineering

University of Moratuwa
Sri Lanka

May 2018

Declaration, copyright statement and the statement of the supervisor

I declare that this is my own work and this thesis does not incorporate without acknowledgement any material previously submitted for a Degree or Diploma in any other University or institute of higher learning and to the best of my knowledge and belief it does not contain any material previously published or written by another person except where the acknowledgement is made in the text.

Also, I hereby grant to University of Moratuwa the non-exclusive right to reproduce and distribute my thesis, in whole or in part in print, electronic or other medium. I retain the right to use this content in whole or part in future works (such as articles or books.)

Signature: Date:

The above candidate has carried out research for the PhD thesis under my supervision.

Name of supervisor:

Signature of the supervisor: Date:

DEDICATION

I dedicate this thesis to my beloved late father, Mr. R M Navaratne Bandara (1943-2016), who had been the live wire throughout my life. Without his never ending support and encouragement, I would not have come this far.

ACKNOWLEDGMENT

I wish to express my sincere gratitude to Professor R A Attalage, my supervisor, for his invaluable guidance and continuous support extended to me throughout my PhD study programme. His enormous encouragement and motivation had been the driving force in overcoming challenges and obstacles that enabled me to complete this endeavour successfully.

I would also like to extend by gratitude to Professor R A R C Gopura, Head of Department and Dr. D Chathuranga, postgraduate research coordinator of the Department of Mechanical Engineering, University of Moratuwa for their valuable administrative support.

I am highly grateful to Professor R G N De S Munasinghe (Professor, Department of Material Science and Engineering) and Dr. W K Wimalsiri (Former Head of Department of Mechanical Engineering), members of my progress review committee for their invaluable comments and advice that contributed immensely in enhancing the outcome of the research study.

I am also thankful to Eng. M. Vignarajah, Senior Lecturer, Department of Civil Engineering of University of Jaffna, Dr. (Mrs.) W C D K Fernando, Dean, Faculty of Engineering of General Sir John Kotelawala Defence University and Eng. G Herath, Deputy Director General of the Public Utilities Commission of Sri Lanka for their valuable technical inputs that assisted me to a great extent in creating the computational models of buildings and in setting up numerical schemes for optimization. The great support extended by Mr. V Nimarshana, Department of Mechanical Engineering and Professor C Jayasinghe and Mr. L Dissanayaka of the Department of Civil Engineering of the University of Moratuwa in conducting indoor environmental measurements is also highly appreciated.

Finally, I would like to extend my special gratitude to my parents, wife and children for their support, encouragement, understanding and love throughout this challenging endeavour.

Abstract

A building is a complex system with multiple interacting physical processes taking place simultaneously. Various aspects influence the performance of buildings and the building envelope is one of the major contributors in this regard. Building orientation, Aspect ratio, Window to wall ratio, Location and types of fenestration, Envelope materials and their characteristics etc. can have a major impact on the energy consumption and life cycle cost of buildings. However, the best combination of the said envelope elements for optimizing the performance of buildings is difficult to determine and is not known. Whole building simulation tools are often used in making building performance predictions. Building energy simulation is generally used on a scenario-by-scenario basis, with the designer generating a solution and subsequently having the computer evaluating it. This is however, a slow and a tedious process and only a few cases are evaluated in a large range of scenarios, possibly leading to sub-optimal envelope designs. By coupling a generic optimization tool with a whole building energy simulation tool, it is possible to optimize the performance of buildings by determining the best combination of envelope elements, subject to predefined constraints. First part of the thesis explains optimization of energy performance and life cycle cost of buildings through this methodology. Secondly, drawbacks of whole building simulation tools that lead to issues in energy performance predictions of buildings are discussed in detail. The issues have been addressed by coupling the whole building simulation tool with a computational fluid dynamics tool on a complementary data exchange platform. It is observed that with this approach more reliable building performance predictions can be made. Final section of the thesis discusses on optimizing indoor environmental quality using computational fluid dynamics with respect to identified mechanical ventilation configurations. Model predictions have been validated using a detailed experimental design where computational model predictions closely agree with the actual measurements.

Keywords: Performance, Envelope, Simulation, Optimization, Computational Fluid Dynamics

TABLE OF CONTENTS

LIST OF FIGURES

LIST OF TABLES

1. INTRODUCTION

1.1 Overview

The chapter provides with an overview on the background issues together with the rationale and the significance of the study. According to the International Energy Agency (2016), global building sector has consumed approximately 122 EJ (equivalent to 34 x 10^6 GWh) in 2014, which is over 30% of the total energy consumption in the world. Figure 1.1 shows the energy consumption and intensity by subsector in the global building sector from 1990 to 2014.

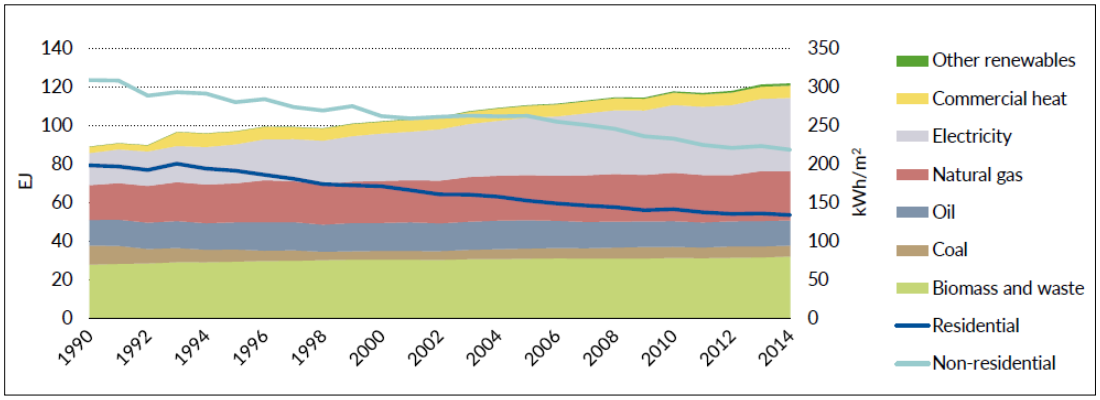

Figure 1.1: Global building sector energy consumption and intensity by sub-sector, 1990-2014

Source: IEA (2016)

According to the United States Energy Information Administration (2016), end-user energy consumption in buildings may increase by an average of 1.5% per annum from 2012 to 2040. In this context, energy utilization in the residential sector may account for nearly 13% of the global end-user energy consumption in 2040 (EIA, 2016). Furthermore, as reported by the Global Alliance for Buildings and Construction (2016), buildings have also accounted for 50% of the global electricity demand, with electrical energy consumption increasing by more than 500% in certain regions of the world since 1990. The report further states that, if no action is taken to improve the energy performance of buildings, energy demand in the global building sector could increase by another 50% by 2050. Moreover, it is seen that

approximately 80% of the said growth takes place in developing countries and emerging economies, where there are plenty of opportunities available for improving the performance of buildings.

On the other hand, greenhouse gas emissions from buildings have reached 9.18 GT of CO_2 equivalent in 2010, which has more than doubled compared to the amount emitted in 1970 (Lucon et al., 2014). It accounts for 19% of energy-related greenhouse gas emissions with nearly one third of black carbon emissions. Figure 1.2 shows emissions generated by the building subsectors from 1970 to 2010.

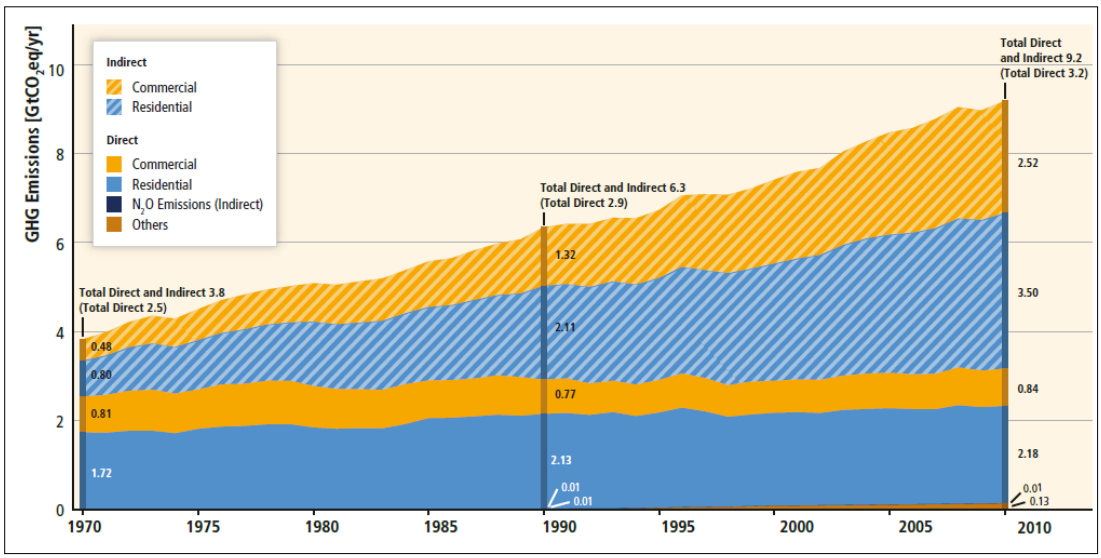

Figure 1.2: Direct and indirect emissions (from electricity and heat production) in the building sub-sectors, 1970 - 2010

Source: Lucon et al. (2014)

According to Figure 1.2, majority of the greenhouse gas emissions fall under indirect CO_2 emissions due to energy consumption in buildings that has undergone a substantial growth during the stipulated period. It is also observed that in contrast, direct emissions have stagnated during the same period.

Buildings could last for decades and hence the decisions made on them today have a long lasting impact on the future global energy consumption and emissions. The rapid increase of energy consumption and CO_2 emissions in buildings has made energy efficiency and energy saving strategies a priority in the formulation of energy

policies in most countries (Lombard, Ortiz, & Pout, 2008). High-impact measures especially taken during the early design stage can significantly reduce energy consumption and emissions in buildings. In this context, high emphasize can be given for the reduction of energy consumption and carbon footprint by optimizing the performance and resource utilization of buildings.

1.2 Research problem analyzed

A building is a complex system with multiple interacting physical processes taking place simultaneously. The building envelope is the interface through which interactions between indoor and outdoor environment take place. Different aspects influence the performance of buildings and building envelope is one of the major contributors in this regard. According to the United States Department of Energy (2003), building envelope is responsible for approximately 25% of energy usage in buildings. It further states that, it can increase up to 42% in the residential sector and 57% in the commercial sector. Building envelope also accounts for 15-40% of the total construction cost and can contribute to an additional 40% cost when impacted by building services (Wigginton & Harris, 2002). Hence, it is evident that the decisions made on the building envelope during the conceptual design stage have substantial impacts on building performance during operation. The choice on building orientation, Aspect ratio, Window to Wall Ratio (WWR), Location and types of fenestration, Envelope materials and their characteristics, Glazing and shading aspects etc. can have a major impact on the annual energy consumption and life cycle cost of buildings. As per Cofaigh et al. (1999), simply making buildings the right shape and correct orientation, it is possible to reduce the energy consumption by 30-40% at no extra cost. Fenestrations on the building envelope have the potential to utilize the freely available daylight and reduce the demand for artificial lighting substantially. Furthermore, building envelope can highly influence the indoor environmental quality, especially thermal comfort of the occupants.

However, the best combination of the aforementioned envelope elements for optimizing the performance of buildings is difficult to determine and is not known mainly due to the existence of nonlinear relationships among different envelope

elements. Finding a solution to this problem can be carried out by analyzing building performance in terms of its envelope elements, which is one of the main objectives of the present study.

1.3 Performance of buildings and optimization criteria

In general, performance of buildings can be analyzed based on the following criteria:

- Energy performance
- Indoor environmental quality for human comfort and health
- Environmental degradation
- Economic aspects

Building performance analysis is mostly conducted through energy modelling. This is an approach that analyses thermal aspects, day-lighting, moisture, acoustics, airflow and indoor air quality of buildings (Mumovic & Santamouris, 2009). The main objective of building design is to optimize the performance of buildings through a whole-building approach. A whole building energy simulation tool can serve this purpose to a certain extent, by providing valuable inputs through building energy modelling during the design process. However, building energy modelling is generally carried out on a scenario-by-scenario basis, where the designer generates a solution and subsequently utilizes the computer to evaluate it. The process is generally implemented by changing one design variable at a time while keeping all other variables constant and then making a comparison between the new design and the base design related to the performance of the building. Hence, it is a slow and a tedious process and generally, only a few cases are evaluated in a large range of possible scenarios. When the number of design variables increases, the process becomes even more difficult and cumbersome and it often becomes difficult to understand the impact of the design modifications on the building performance due to the existence of nonlinear relationships among different design variables. Furthermore, there is every possibility that the designer ends up with only a sub-optimal design. Although many building simulation tools have been developed, all of them adopt the inherent trial and error procedure for the enhancement of building performance. It is a time consuming and ineffective task because of the difficulty in

handling a large solution space. Hence, instead of evaluating the building performance with respect to individual design variables, changing one at a time, it is necessary to consider a strategy for optimizing the building performance through an integrated approach.

On the other hand, optimizing building performance may be carried out firstly, by establishing an objective function as per desired building performance criterion, and subsequently by applying an appropriate generic optimization tool through an iterative process to determine the minimal of the said objective function. This involves computing the objective function value and comparing it with that of the same at the previous iterative step, until a minimal of the objective function is achieved. Generally, objective functions found in the building optimization problems are highly nonlinear and complex in nature and hence cannot be readily solved (Wetter & Wright, 2004). However, whole building simulation tools are capable of evaluating such complex nonlinear functions with their advanced solvers and hence they can be readily used to evaluate the aforementioned objective functions. Furthermore, generic optimization tools have the capability of varying the design variables simultaneously during the optimization process, which is not a feasible task during energy modelling alone. Hence, it is clear that both energy modelling and generic optimization, when applied in isolation are not very effective tools since they have their own limitations and drawbacks. However, if they are integrated on a common platform, the respective tools can operate hand-in-hand by combining their strengths for establishing an efficient building performance optimization process. On this basis, by combining a generic building performance optimization tool with a whole building simulation tool, it is possible to optimize the performance of buildings successfully by determining the best combination of building envelope elements, subject to predefined constraints. This methodology that adopts a procedure of iterative nature is often known as numerical optimization or simulation-based optimization (Nguyen, Reiter, & Rigo, 2014).

Present work involves optimizing performance of buildings under the following two criteria:

- Annual Primary Energy Consumption
- Life Cycle Cost

Both tasks are carried out through combined performance modelling and generic optimization or simulation-based optimization approach. This enables the designers to determine the best solution, in a field of feasible solutions for optimizing the desired performance of buildings through building envelope elements under the influence of a set of predefined constraints.

However, the most essential requirement of this whole task is to give realistic predictions for annual energy consumption and life cycle cost of the building concerned. It is revealed that there are certain inherent drawbacks of the current whole building energy simulation tools that may lead to unrealistic building performance predictions (Loutzenhiser, Manz, Moosberger, & Maxwell, 2009; Zhai, Chen, Klems, & Haves, 2001). This is because whole building energy simulation tools do not have the capacity to model air flow within buildings comprehensively and also due to their dependence on empirical correlations. As a solution to this issue, the whole building simulation tool may be coupled with a Computational Fluid Dynamics (CFD) tool on an interoperable platform, enabling data exchange between the said tools. This coupled simulation, although computationally very expensive, provides a mechanism of giving realistic predictions for building performance. This approach is elaborated in detail in the chapters to follow.

1.4 Indoor environmental quality

Optimizing building energy performance is meaningless if health and comfort of building occupants is sacrificed by the optimal envelope design. Hence, during the second stage of this work, emphasis is given for enhancing Indoor Environmental Quality (IEQ) with the optimized building envelope. During this task, focus will be on the microscopic level analysis of the indoor environment using Computational Fluid Dynamics.

Following factors determine the IEQ that directly influences the physical and mental state (health and comfort) of occupants (Bluyssen, 2009):

- Thermal comfort: Determined by moisture level, air velocity, air temperature etc.
- Indoor air quality: A complex phenomenon comprised of indoor pollutant levels, odour, fresh air supply etc.
- Acoustical quality: Influenced by outside and indoor noise levels etc.
- Visual or lighting quality: Determined by view, illuminance, luminance ratios, reflection etc.

It is worth considering as to why IEQ should be given high priority during the design stage. According to the United States Department of Health and Human Services (2006), during the past several years it is observed that air within buildings can be more polluted than outdoor air even in the largest and most industrialized cities. It further states that, people spend almost 90% of their time indoors and as a result indoor pollutant levels could reach 2 to 5 times higher than outdoor levels (United States Department of Health and Human Services [USDHHS], 2006). Hence, if not addressed accordingly, this scenario may lead to serious health issues for many occupants. According to the United States Environmental Protection Agency (1995), occupants exposed to indoor air pollutants for the longest periods are those who are most vulnerable to such effects. Such occupants include young children, elderly people and patients suffering from respiratory or cardiovascular diseases. The depth of the problem is further justified by the World Health Organization (2018) by reporting that 4.3 million deaths have taken place in 2012 due to household air pollution.

On the other hand, undesirable thermal comfort levels can affect productivity of occupants in a drastic manner, especially for office employees. Also, high temperature and humidity levels increase the concentration of certain pollutants and growth of microorganisms in the indoor environment as revealed by the USDHHS (2006).

Wu, Jacobs, Mitchell, Miller, and Karol (2007) explained the complexity of the relationship between the indoor environment and the hazards generated as a consequence and the ultimate health effects. According to this explanation,

characteristics of the building, attributes of the occupants and activities within the building contribute to the quality of the indoor environment. Eventually, it can lead to a variety of adverse health effects including respiratory, neurological and dermatologic etc. as illustrated in Figure 1.3.

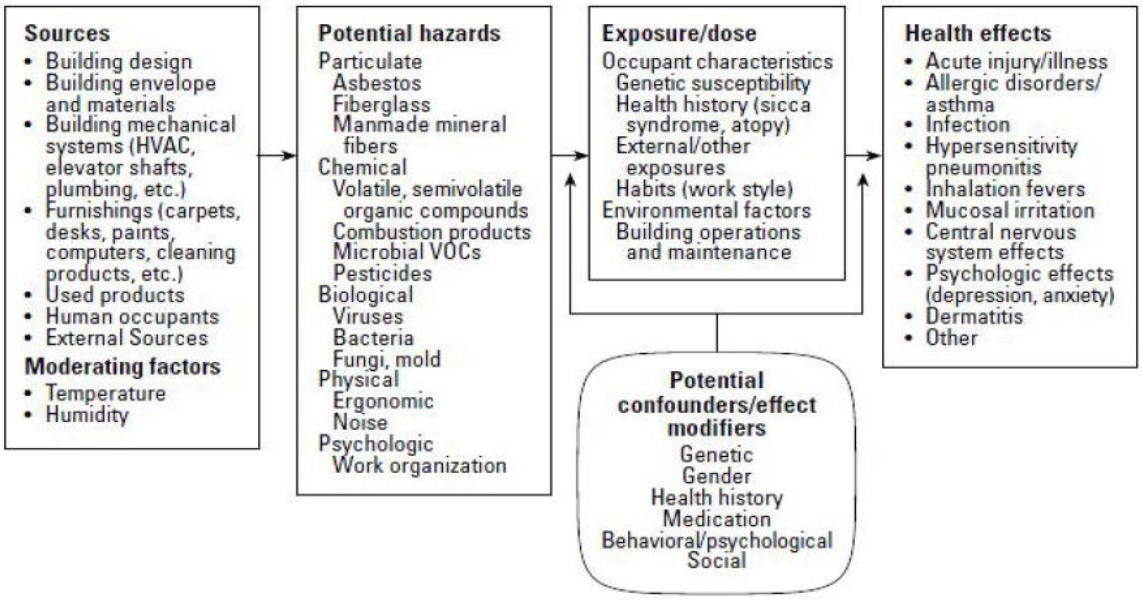

Figure 1.3: Relationship between IEQ and health effects

Source: Wu et al. (2007)

Mechanical ventilation is one of the main mechanisms responsible for maintaining acceptable IEQ in modern buildings. However, these systems themselves can also account for the issues associated with IEQ, such as undesirable thermal comfort levels and high levels of air contaminants, due to insufficient rate of air flow and lack of circulation of ventilation air. One solution for this issue is to simply increase the rate of ventilation supplied to the occupied space. However, this approach often conflicts with building energy efficiency requirements as it leads to higher consumption of energy. An alternative solution is to enhance the efficiency of the mechanical ventilation system so that requirement for increasing rate of ventilation is minimal in meeting the acceptable pollutant levels. In this case, efficiency of the mechanical ventilation system refers to the effective delivery of conditioned ventilation air to the occupants, or more specifically, ventilation performance of the

building, rather than solely referring to the mechanical performance of the particular ventilation system. Hence, it is clear that IEQ can be optimized by enhancing ventilation performance of buildings.

To enhance the ventilation performance, it is important to analyze the relationship between the configuration of the mechanical ventilation system and the respective air flow field generated. However, the challenge is how this analysis can be conducted at the early design stage of a building. Analytical methods have limited applicability to handle this type of complex real flows in buildings. Experimental approach is fairly costly and a considerable time has to be spent on planning, constructing prototypes and taking measurements. Hence, it can be applied only for a limited number of selected cases. In this context, the only feasible and cost effective option available is the numerical approach. Selection of numerical techniques to handle such complex real flow problems may also be quite tricky and uncertain since they generate only approximate solutions and hence need to undergo validation prior to accepting model predictions for design purposes. In addition, the said numerical tools should be capable of handling time bound dynamic flow problems that are typical in indoor air flow scenarios of buildings at microscopic level. In this context, Computational Fluid Dynamics (CFD) is considered as a powerful tool that is capable of assessing the ventilation performance of buildings at microscopic level that eventually enables the designers to optimize the IEQ. Latter part of the thesis focuses on this aspect. However, the scope of present work will be limited to predicting IEQ of buildings in terms of thermal comfort and indoor CO_2 level through CFD modelling.

1.5 Research objectives

Objectives of the research study are as follows:

- Develop a methodology to generate optimal solutions on the performance of buildings with respect to energy consumption and life cycle cost using the simulation-based generic optimization approach in terms of building envelope elements
- Establish an algorithm coupling Energy Simulation (ES) and Computational Fluid Dynamics (CFD) to predict a detailed level of performance of buildings

- Predict thermal comfort and indoor air quality of buildings in terms of CO_2 with respect to identified mechanical ventilation configurations using CFD
- Validate CFD predictions through experimental measurements in terms of indoor air velocity, air temperature and CO_2 concentration

1.6 Organization of thesis

The thesis is organized as follows:

- Chapter 2 reviews the literature on Energy Modelling, Building energy simulation tools, Building performance optimization methods and algorithms, Optimization programs, previous studies carried out with regard to building performance modelling and optimization and future trends on the same.
- Concepts for establishing the optimization process on building performance are explained in Chapter 3.
- Chapter 4 elaborates the methodology adopted for optimizing the performance of buildings during the study.
- Chapter 5 presents and interprets the results obtained with respect to the building performance optimization.
- Strategies to improve building performance predictions are discussed in Chapter 6.
- Chapter 7 reviews the literature related to Indoor Environmental Quality in buildings and application of different approaches on modelling the same.
- Modelling of indoor environmental quality using Computational Fluid Dynamics is explained in Chapter 8.
- Chapter 9 presents the experimental procedure for assessing the Indoor Environmental Quality together with the validation of model predictions using the same.
- Chapter 10 concludes the thesis by giving a summary of the research findings and discussing relevant issues and recommendations for future work.

1.7 Limitations of study

The study has the following limitations:

- The study confines itself for optimizing building performance using a single-criterion optimization (Annual primary energy consumption or Building life cycle cost) with predefined constraints. It focuses on methods applicable for early stages of the building design process. The design decisions considered are only with respect to the building envelope elements.
- The whole building simulation tool assumes a well-mixed model for each thermal zone and hence variation of air flow characteristics at microscopic level within the thermal zone has not been taken into account.
- A novel optimization algorithm has not been developed during the study, while the standard algorithms available in the library of the optimization tool are modified and adopted accordingly to meet user requirements.
- Although present approach incorporates a computer-aided design and modelling environment, development of a novel Graphical User Interface (GUI) in order to transfer data to the computational model of the building has not been conducted. (Data transfer is performed through a standard in-built text based GUI in EnergyPlus.)
- Indoor Environmental Quality was assessed in terms of only thermal comfort and indoor CO_2 concentration at steady state. Acoustical quality and visual quality have not been considered as building performance criteria in the analysis. Emissions from envelope materials were not taken into account.
- CFD modelling is performed only through Reynolds Averaged Navier-Stokes (RANS) approach due to limitations in computational power.

1.8 Summary

The chapter provides with an overview on the background issues with respect to energy consumption and emissions of buildings in particular. Furthermore, it explains the rationale, significance, objectives and limitations of the study undertaken. It also provides with an overview on the organization of the thesis at the end.

2. MODELLING PERFORMANCE OF BUILDINGS

2.1 Overview

Modelling is a powerful methodology capable of predicting and analyzing the dynamic behaviour of buildings with respect to various building performance criteria. It enables the designers to simulate the behaviour of complex building systems thereby providing access to detailed information on the performance of the same. Analysis of the energy performance of buildings is carried out through a process known as Energy Modelling. There are two basic levels of building energy modelling; namely; simplified method and the detailed method (Knipe & Day, 1986). The simplified method uses degree-day method, suitable for predicting energy consumption of small buildings and the modified-bin method which has better accuracy for predicting energy consumption in larger buildings (Knebel, 1983). Detailed method performs a whole building energy simulation for every hour of the year. It takes into consideration exact sun angles, extent of cloud cover, wind velocity, outdoor temperature and relative humidity etc. on an hourly basis in order to predict the energy consumption of the building (Knebel, 1983). During energy modelling input data is taken from different sources as shown in Figure 2.1.

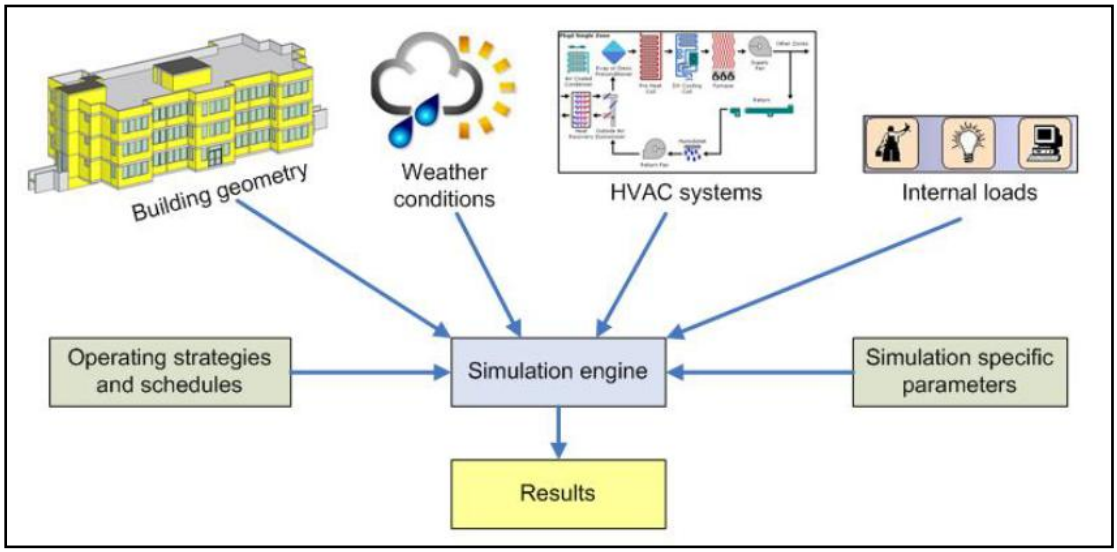

Figure 2.1: Inputs for Energy Modelling

Source: Maile, Fischer, and Bazjanac (2007)

The inputs mainly consists of the building geometry, weather data, HVAC systems and components, internal loads of the building, operating strategies and schedules and simulation specific parameters. Energy modelling is based on the principles of energy and mass conservation. Since the governing equations involved are complex and nonlinear, appropriate simplifying assumptions are made. Building geometry is represented in terms of a solid model or a Computer Aided Drafting (CAD) format. The building model is divided into multiple thermal zones to facilitate modelling of different components and processes. Properties and characteristics of building materials, glazing and shading aspects also have to be provided as inputs. Internal and external loads provide vital information for the energy balance in a thermal zone. External loads are strongly influenced by weather conditions of the building location and hence, statistically assembled weather data are used in energy modelling (Maile et al., 2007). Weather data files are available for a large number of cities and regions in the world to be used particularly for building performance modelling purposes.

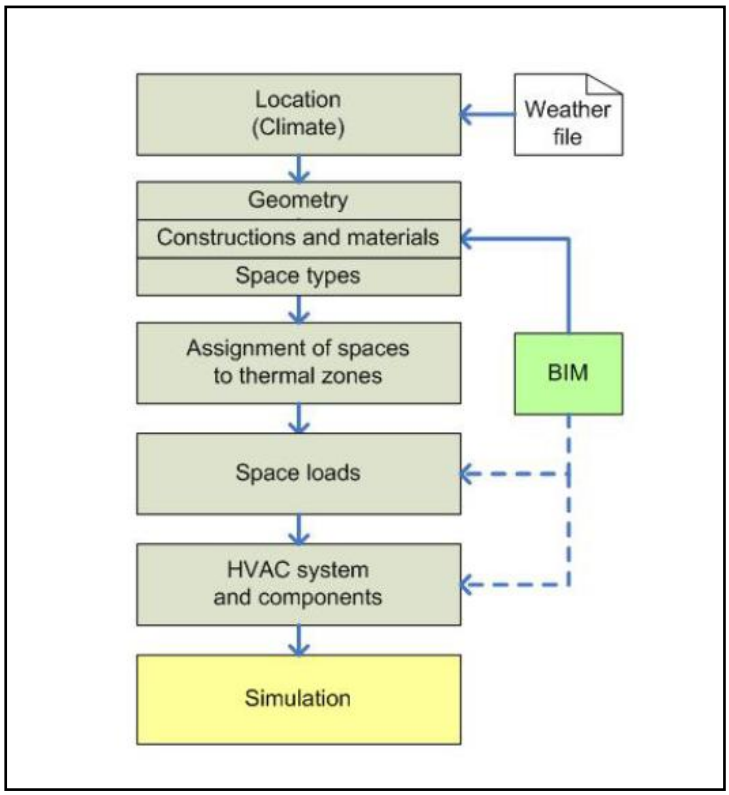

Figure 2.2: Workflow related to Energy Modelling

Source: Maile et al. (2007)

Weather files do not represent a specific year, but provide with a statistical reference for the typical weather parameters of a specific location (Maile et al., 2007). Internal loads represent thermal and electrical loads due to lighting, occupancy and equipment. The workflow related to the process of energy modelling is illustrated in Figure 2.2. The location of the building has to be defined in order to establish a link to weather data. Information related to building geometry, construction and materials and types of occupied spaces etc. has to be preferably imported from a Building Information Model (BIM). Based on geometry definitions, building model is subdivided into thermal zones. Subsequently internal space loads are assigned to the relevant thermal zones. HVAC system and components are then defined through the manual user interface or are imported from the BIM. Finally, simulation can be performed after specifying additional simulation-specific parameters (such as numerical tolerances, simulation period etc.).

2.2 Building energy simulation tools

Evolution of the building energy simulation tools from traditional manual methods to contemporary simulators is summarized in Table 2.1.

Table 2.1: Evolution of building energy simulation tools

Generation	Characteristics	Consequences
1	• Handbook oriented • Simplified and piecemeal • Familiar to practitioners	Easy to use, Difficult to translate to real world, Non-integrative, Application limited, Deficiencies hidden ↓ Increasing integrity *vis-à-vis* the real world ↓ Deficiencies overt, Easy to use and interpret, Predictive and multi-variate, Ubiquitous and accessible
2	• Building dynamics stressed • Less simplified, still piecemeal • Based on standard theories	
3	• Field problem approach • Shifted to numerical methods • Integrated modelling stressed • Graphical User Interface • Partial interoperability enabled	
4 and beyond	• Good match with reality • Intelligent knowledge-based • Fully integrated • Network compatible / interoperable	

Source: Extracted from Clarke (2001)

Traditionally designers used a range of different calculation techniques to quantify and assess building performance at the design stage (Clarke, 2001). These calculations were based on analytical formulations, incorporating many simplifying assumptions. In the mid 70s second generation programmes began to emerge (Clarke, 2001). They used frequency domain response factors to model the dynamic response of construction elements and HVAC system modelling was limited to the steady state scenario. With the advent of more powerful personal computers, third generation programs began to emerge in the mid 80s (Clarke, 2001). This was the beginning of integrated modelling where thermal, visual and acoustic aspects of performance are considered together. In the mid 90s new developments concerned with program interoperability, knowledge-based user-interfaces, application quality control and user training took place (Clarke, 2001).

During the last sixty years, numerous energy simulation tools were developed and used by the building energy simulation community throughout the world. Due to the increasing demand on building energy simulation, several organizations developed popular as well as powerful building energy simulation software. Some of them are DOE-2, ESP-r, CLIM 2000 and DeST developed by Lawrence Berkeley National Laboratory in the United States, British Energy System Research Unit, Electricity Applications in Building Branch of the French Utility Company and Chinese Tsinghua University respectively (Han, Liu, & Chang, 2014). Some of the popular modern building energy simulation tools used at present includes EnergyPlus, eQUEST, ESP-r, TRNSYS, DesignBuilder, IES-VE, ECOTECT, DeST etc. Many of these tools have established a community that continues to develop new components or modules on a regular basis.

Aforementioned software have their own unique capabilities and features. Table 2.2 makes a comparison among some of the popular building energy simulation software with respect to their main features. Sections to follow will elaborate on the main features of the aforementioned software.

Table 2.2: Comparison of features of the building energy simulation software

Feature	Building Energy Simulation Software				
	TRNSYS	**eQUEST**	**EnergyPlus**	**ESP-r**	**DeST**
Ability to import CAD drawings	√	√	√	√	-
Ability to export CAD drawings	-	-	√	√	-
Variable time step	-	√	√	√	-
Ability to generate standard output reports	√	√	√	√	√
Heat balance calculations	√	√	√	√	√
Humidity calculations	√	√	√	-	√
Thermal comfort calculations	√	-	√	√	-
Natural ventilation calculations	√	√	√	√	√
Day-lighting illumination and controls	-	√	√	√	-
Renewable energy calculations	√	√	√	√	-
Greenhouse gas calculations	-	√	√	√	-
Coupling with other software	√	-	√	√	√
Standard life cycle costing	√	√	-	√	-

Source: Extracted from Crawley, Hand, Kummert, and Griffith (2005)

2.2.1 EnergyPlus

EnergyPlus (Crawley et al., 2001) is a state-of-the-art building energy modelling tool, initially released in 2001. It has earned an enormous reputation for the high accuracy of results it produces. It is a new generation building energy modelling tool based on DOE–2 and BLAST (Building Loads Analysis and System Thermodynamics), with numerous added capabilities. EnergyPlus was developed collectively by Lawrence Berkeley National Laboratory, University of Illinois, U.S. Army Construction Engineering Research Laboratory, GARD Analytics Inc., and Oklahoma State University, with the support from the United States Department of Energy, Office of Building Technology and State & Community Programs (Crawley et al., 2001). EnergyPlus can model heating, cooling, lighting, ventilation, other energy flows and water usage in buildings. The software includes many innovative simulation capabilities such as lower time-steps (less than an hour), modular systems integrated with the heat balance-based zone simulation, multi-zone air flow network, thermal comfort and water usage calculations, modelling of natural ventilation and

photovoltaic systems in buildings etc. (Crawley et al., 2001). Workflow chart and modules of EnergyPlus are shown in Figures 2.3 and 2.4 respectively.

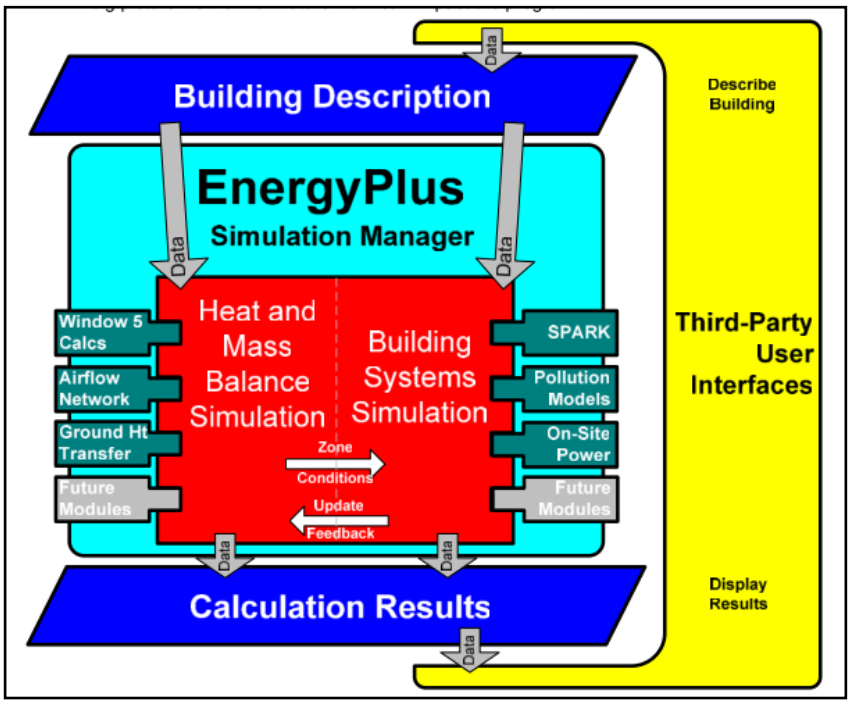

Figure 2.3: EnergyPlus workflow chart

Source: Crawley et al. (2001)

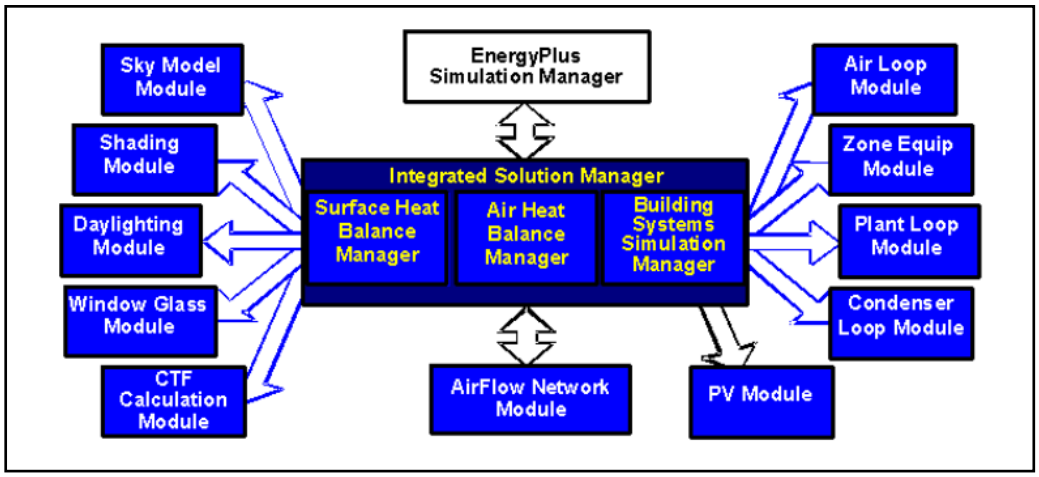

Figure 2.4: EnergyPlus modules

Source: Crawley et al. (2001)

Another advantage of EnergyPlus is that the source code of the programme is open for public inspection, revision etc. Hence, the programme is not intended to be a

black box to the users and developers. The main limitation of the software is that the graphical user interface is not very user-friendly.

2.2.2 eQUEST

eQUEST is a building energy modelling software in the public domain developed by James Hirsch and Associates for Southern California Edison and is based on DOE-2.2 (Maile et al., 2007). It performs building energy modelling by combining two building creation wizards, an energy efficiency measure wizard and a graphical results display module with a simulation engine. Building creation wizards include schematic design wizard and the design-development wizard. The wizards will guide the user through a series of steps designed for fully describing the principal energy related features of the building design. The schematic design wizard is designed to support the early design phase when information is limited (Maile et al., 2007). It allows the user to describe the architectural features of the building and its HVAC system. The design-development wizard is designed for more detailed design. It is also better suited for larger, more complicated structures or with more detailed internal loads, schedules and HVAC system requirements (Maile et al., 2007). The energy efficiency measures wizard assists the user to explore energy performance of the preferred design alternatives easily and reliably. Interactions of the wizards in eQUEST are illustrated in Figure 2.5.

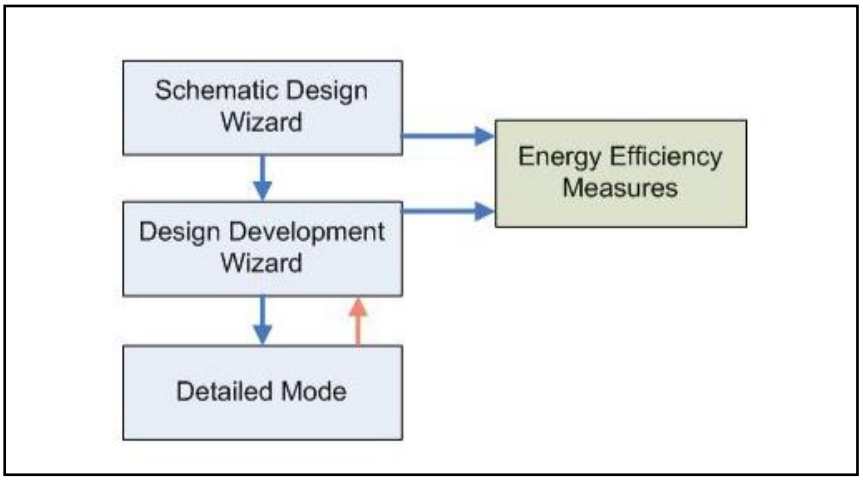

Figure 2.5: Wizards in eQUEST

Source: Maile et al. (2007)

2.2.3 ESP-r

ESP-r (Energy Simulation Program for research) was developed in 1970s by the Energy System Research Unit of the University of Strathclyde in the United Kingdom (Han et al., 2014). It is a general purpose simulation environment which allows an in-depth analysis on the energy and environmental performance of buildings ("The European Portal for Energy Efficiency in Buildings", 2010). ESP-r is comprised of a central project manager, around which databases, a simulator, various performance assessment tools and a variety of third party applications are arranged for computer aided drafting, visualization and report generation ("The European Portal for Energy Efficiency in Buildings", 2010). The software allows the designer to explore the complex relationships among building's form, fabric, air flow, plant and control through a finite volume based approach in which the building performance modelling problem is transformed into a set of conservation equations ("The European Portal for Energy Efficiency in Buildings", 2010). They are then integrated at successive time steps in response to climate, occupant and control system influences. ESP-r also has the capability to simulate many innovative technologies including daylight utilization, natural ventilation, contaminant distribution, combined heat and electrical power generation and photovoltaic facades, transient CFD, multi-gridding (2D and 3D conduction) and control systems ("ESP-r Overview", 2011).

2.2.4 DeST

Designer's Simulation Toolkit (DeST) was developed by Tsinghua University of China during the early 1980s. DeST can be used to simulate and analyze both building energy consumption and HVAC systems (Han et al., 2014). It has been designed for improving reliability of system design, to ensure the quality of the system performance and to reduce energy consumption in buildings. Furthermore, DeST can focus on different stages of the building design process and possesses five main simulation stages: Building thermal process, System scheme analysis, Air handling unit system analysis, Duct/pipe networks and Plant analysis (Yan & Jiang, 2005). The aforementioned simulation stages provide accurate results to fulfill the needs of different stages of the building systems design. DeST applies advanced

multi-zone heat and mass balance methodology based on the state space method in the thermal environment simulations, while maintaining high accuracy (Yan & Jiang, 2005). The Graphical User Interface of DeST is coupled with AutoCAD. The software is also capable of coupling building energy simulations with Computational Fluid Dynamics tools. DeST has been widely used in China for various large building projects, in addition to some applications in Europe and Japan (Han et al., 2014).

2.2.5 TRNSYS

TRNSYS (Transient System Simulation Program) is an energy simulation programme with a modular system approach. It is one of the most flexible tools available for modelling a variety of energy systems that are at different levels of complexity ("TRNSYS", 2016). It facilitates addition of mathematical models, add-on components, etc. and has the capability to carry out multi-zone building energy modelling while interfacing with other simulation programmes. The software has been commercially available since 1975, and continues to develop through international collaboration of the United States, France and Germany ("TRNSYS 17", 2012). TRNSYS includes a graphical user interface, a simulation engine, and a library of components that is comprised of various building models, standard HVAC equipment and emerging technologies. This simulation package has been used for HVAC analysis and sizing, multi-zone air flow analyses, electrical power simulation, solar energy design, building thermal performance, analysis of control schemes, etc ("TRNSYS", 2016).

2.2.6 Trend of usage

Figure 2.6 shows an approximate share of utilization of the major building simulation programmes based on a study conducted by Nguyen et al. (2014). According to Figure 2.6, it is evident that EnergyPlus, TRNSYS, DOE-2 and ESP-r share the major portion of the distribution. Possible cause for this scenario is likely to be the existence of a large global user community who makes use of the strong features possessed by the said software tools.

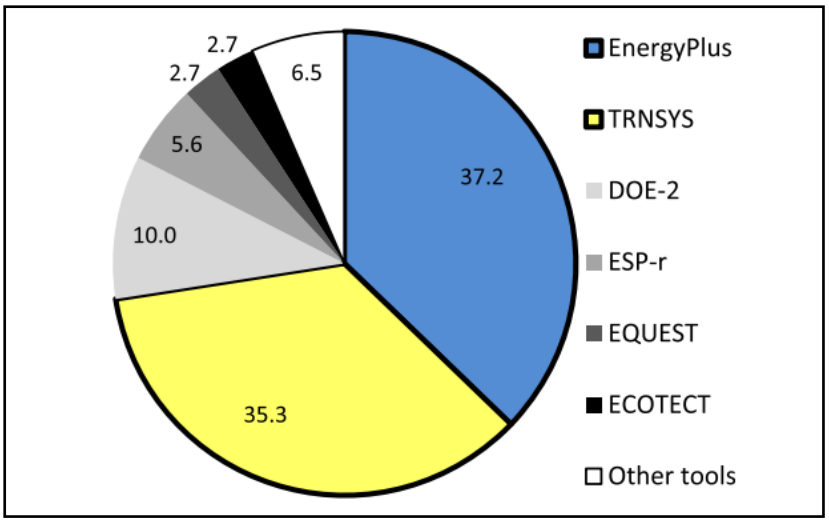

Figure 2.6: Utilization proportions of major building energy simulation tools

Source: Nguyen et al. (2014)

2.3 Building performance optimization

Even though the use of mathematical models in building design is relatively new, application of optimization methods to various building design problems has been in use since the 1950s (Al-Homoud & Degelman, 1994). Such applications range from spatial allocation to the design of structural and mechanical systems in buildings, with different degrees of success.

Most optimization problems related to building performance can be formulated as non-linear constrained problems (Wetter & Wright, 2004). Furthermore, they are inherently multivariate and multi-criteria in nature having their own unique characteristics. The governing parameters are consisted of a mixture of both continuous and discrete variables (Al-Homoud & Degelman, 1994). Continuous variables are real numbers that may vary continuously between the lower and upper bounds. Building design process also involves the selection of various components that are included in the design. Choosing a particular one from different building components is a discrete process. Therefore, variables specifying the selection of building components may be represented by discrete values.

During optimization, the best solution that satisfies preset objectives, among a field of feasible solutions, is sought under the restriction of a set of preset constraints. Optimization utilizes mathematical techniques systematically to model and analyze certain quantitative measures to establish the best course of action possible for a decision problem (Al-Homoud, 1997). An optimization problem generally consists of:

- A set of independent variables or design parameters
- A set of constraints that bound the respective domains of the independent and dependent variables
- An objective function to be optimized

Classification of an optimization problem is generally based on the following factors (Roy, Hinduja, & Teti, 2008; Sahab, Toropov, & Gandomi, 2013):

- Number of design variables
- Nature and type of design variables
- Number of objective functions being optimized
- Nature of objective functions
- Presence of constraints and their nature
- Problem domain etc.

Although a wide range of optimization methods are in existence, not all of them are applicable to building performance optimization (Wetter & Wright, 2004). Many building performance optimization problems are comprised of both multi-modal and discontinuous (hence non-differentiable) objective functions (Kampf & Robinson, 2009). As per Wetter and Wright (2004), some optimization algorithms fail due to the existence of substantial discontinuities in the aforementioned objective functions. Hence, selection and application of optimization methods for building optimization problems has to be done with utmost care. Selection of an optimization method for a given building optimization problem is usually based on a number of considerations as given below (Nielsen, 2002; Wetter, 2009):

- Nature of design variables: continuous, discrete or both
- Presence of constraints on the objective function

- Nature of objective function (linear or nonlinear, convex or non-convex, continuous or discontinuous, number of local minima etc.)
- Availability of first and second order derivatives of the objective function
- Characteristics of the problem (static or dynamic etc.)
- Performance of respective algorithms

Providing a generic rule for selecting an optimization method is generally infeasible due to the complexity and the diversity of real world building optimization problems (Nguyen et al., 2014). The different methods applicable for building performance optimization are elaborated in the sections to follow.

2.4 Optimization methods

In order to deal with different types of optimization problems, a large number of optimization methods have been developed. Optimization methods may be broadly classified as follows (Belegundu & Chandrupatla, 2011; Nguyen et al., 2014):

- Local or Global methods
- Heuristic or Meta-heuristic methods
- Deterministic or Stochastic methods
- Derivative-based or Derivative-free methods
- Trajectory or Population-based methods
- Bio-inspired or Non bio-inspired methods
- Single or Multi-objective optimization methods

2.5 Optimization algorithms

This section elaborates on optimization algorithms widely applied for building performance optimization.

2.5.1 Adaptive optimization algorithms

Direct search algorithms, gradient-based techniques and evolutionary search methods are categorized as adaptive optimization algorithms (Belegundu & Chandrupatla, 2011). They take the results of the previous evaluation into consideration in determining a new search point. Direct search algorithms handle objective functions

only through ranking of a countable set of values. They do not make use of the partial derivatives of the objective function and hence are also called non-gradient or zeroth order algorithms (Belegundu & Chandrupatla, 2011). Exhaustive search, Coordinate search algorithm, Hooke-Jeeves algorithm (Hooke & Jeeves, 1961), Rosenbrock algorithm (Rosenbrock, 1960), Simplex algorithm of Nelder and Mead (Nelder & Mead, 1965), Powell's conjugate directions algorithm (Powell, 1964), Mesh adaptive search algorithm, Generating set search algorithm are some of the popular direct search optimization algorithms.

In the Hooke-Jeeves algorithm, an initial step size is chosen and the search is initiated from a given starting point. The method involves steps of exploration and pattern search as shown in Figure 2.7.

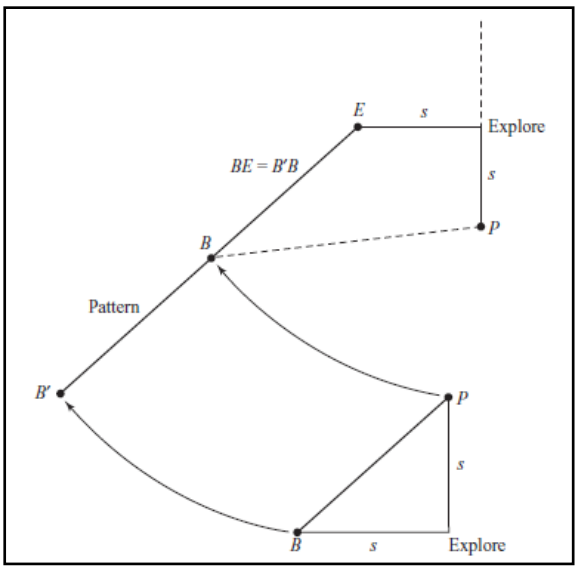

Figure 2.7: Exploration and pattern search in the Hooke-Jeeves algorithm
Source: Belegundu and Chandrupatla (2011)

Exploration is used to explore the local behaviour of the objective function and the pattern search is applied to take advantage of the pattern direction. In this algorithm, the pattern direction is established with a search in the coordinate directions. Once a pattern direction is established, new information related to the function is available. Hence, a new set of orthogonal directions can be developed using this information.

In Rosenbrock's method, the search is carried out in *n* orthogonal directions at any stage. New orthogonal directions are established at the subsequent stages. The orthogonal setting makes this method robust and efficient (Rosenbrock, 1960).

The Simplex algorithm of Nelder and Mead makes use of geometrical properties of the *n*-dimensional space (Nelder & Mead, 1965). In an *n*-dimensional space, *n*+1 points form a simplex. An initial simplex in *n*-dimensions is easily created by choosing the origin as one corner and *n* points, each marked at a set distance, c from the origin along the coordinate axes as shown in Figure 2.8.

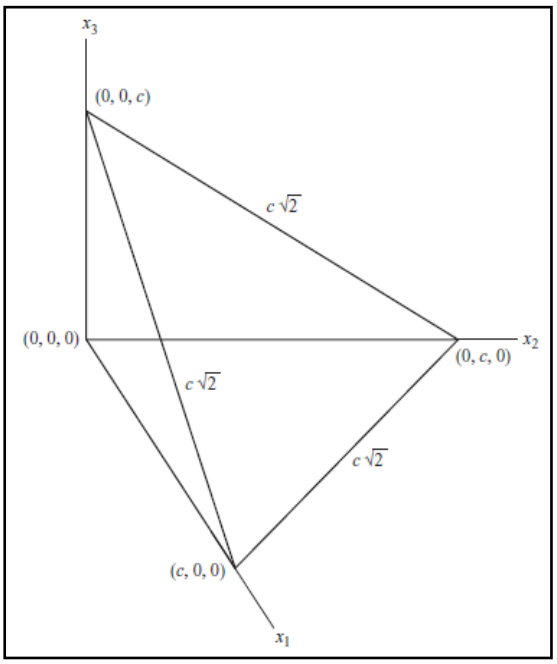

Figure 2.8: Simplex in 3-D in the Nelder and Mead algorithm

Source: Belegundu and Chandrupatla (2011)

Powell (1964) developed an approach using the idea of conjugate directions defined with respect to the quadratic form. If minimization is carried out along successive directions, which are conjugate with respect to all the previous directions, status of convergence can be achieved. Powell developed the idea of constructing the conjugate directions without using derivatives.

The concepts of simulated annealing, genetic and differential evolution algorithms also come under the same category. Simulated annealing is a stochastic search

method that has analogy to the physical annealing process where steel is cooled gradually so that a state of minimal energy is achieved. It avoids getting stuck in local optima and keeps track of the overall best objective function value (Carson & Maria, 1997).

Genetic algorithm is a technique used to automate the process of searching for an optimal solution. It is observed that the probability of the search getting trapped in local minima is limited (Caldas & Norford, 2002). Genetic algorithms start searching by randomly sampling within a solution space, and then stochastic operators are applied to direct the process based on objective function values (Goldberg, 1989). Genetic operators control the evolution of successive generations. The three basic steps of the process are selection, crossover and mutation (Goldberg, 1989). A genetic algorithm starts by generating a number of possible solutions to a problem, subsequently evaluates them and applies the basic genetic operators to the initial population as per fitness of each individual. This process generates a new population with higher average fitness than in the previous step, which in turn will be evaluated. The cycle is repeated for the number of generations specified by the user, which is dependent on the complexity of the problem (Caldas & Norford, 2002).

Gradient-based methods are based on the derivatives or gradients of the objective function. Some of the algorithms of this category include Steepest descent (Cauchy) method, Conjugate gradient (Fletcher-Reeves) method, Newton's method, Levenberg-Marquardt algorithm, Discrete Armijo gradient algorithm and Quasi-Newton method (Belegundu & Chandrupatla, 2011). In the steepest descent method as shown in Figure 2.9, search starts from an initial trial point and iteratively moves along the steepest descent directions until the optimal point is reached. The convergence technique of the steepest descent method can be greatly improved with the concept of conjugate gradient (Belegundu & Chandrupatla, 2011).

Newton's method is based on the Taylor's series expansion. Marquardt algorithm is a combination of both the steepest descent algorithm and Newton's method, which has the advantages of both the methods in terms of the movement of the function value towards the optimal point at a fast convergence rate.

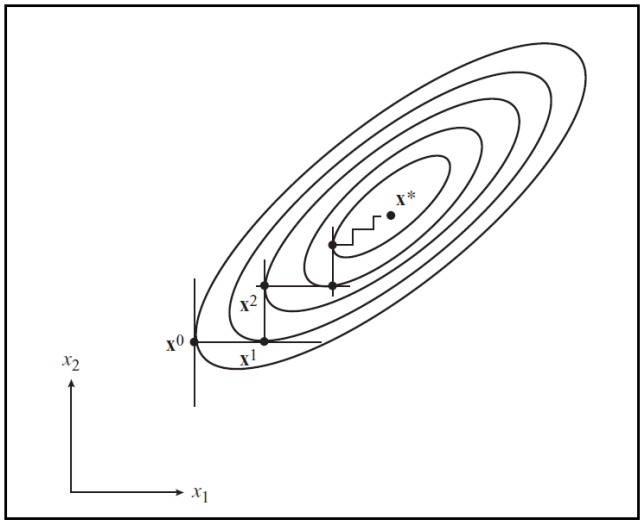

Figure 2.9: Steepest descent method

Source: Belegundu and Chandrupatla (2011)

Quasi-Newton methods are well known algorithms for finding the optimal of nonlinear functions. However, it should be noted that the aforementioned gradient-based algorithms can only be used for solving unconstrained optimization problems (Belegundu & Chandrupatla, 2011).

Similar to genetic algorithms (GA), evolutionary search methods adopt optimization algorithms that apply the principles of natural evolution as a method to solve optimization problems. The strategy is to apply mutation and selection, alternating on a population or a single solution in order to gradually improve its function value. They are considered to be robust search algorithms that can be used for optimizing non-differentiable functions (Belegundu & Chandrupatla, 2011). Some of them are Particle swarm optimization (PSO), Ant colony algorithm, Bee colony algorithm and Intelligent water drop (Nguyen et al., 2014). PSO algorithms are population based probabilistic optimization algorithms firstly proposed by Kennedy & Eberhart (1995). In this case, at each iteration step, objective function value of a finite set of points known as particles are compared. The change of each particle from one iteration to the next is modelled based on the social behaviour of flocks of birds or schools of fish (Wetter & Wright, 2004).

2.5.2 Non-adaptive optimization algorithms

Non-adaptive algorithms initially determine all search points at which the objective function is to be evaluated. Subsequently they evaluate the objective function at all aforementioned locations and determine the optimal solution approximately. Design of experiments and random sampling come under this category.

2.5.3 Pareto optimization algorithms

Pareto optimization algorithms are used for handling multi-objective optimization problems (Ellis, 2006). Pareto optimality applies the concept of dominated and non-dominated solutions. A solution is Pareto optimal if it is not dominated by any other solution. In this case the optimization search is formulated as a multi-criteria, or multi-objective search for a set, or Pareto-optimal front, of optimal solutions. Figure 2.10 uses one such possible optimization for cost and performance (solutions that are down and to the left are better) to illustrate a Pareto front. A designer, who is presented with such results, then has a range of possible solutions (which are all optimal) that can be utilized for decision making (Ellis, 2006).

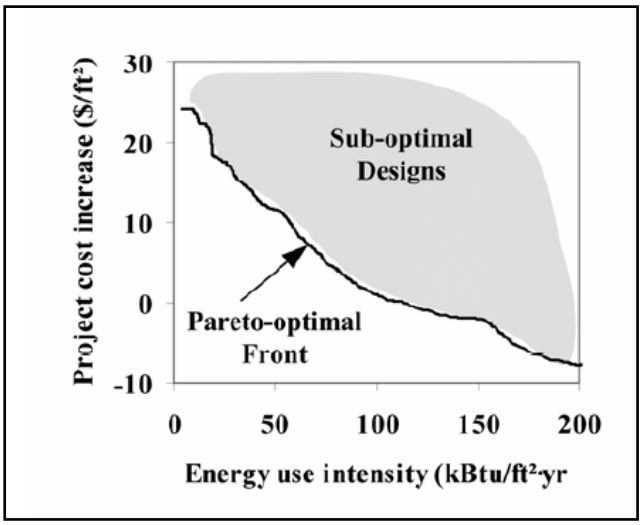

Figure 2.10: Pareto front of optimal solutions

Source: Ellis (2006)

2.5.4 Hybrid optimization algorithms

Hybrid optimization algorithms include two or more optimization algorithms operating sequentially. They show a remarkable performance in dealing with discontinuous, highly constrained mixed integer and/or multi-modal problems as typically found in building simulation outputs (Nguyen et al., 2014). Popular hybrid algorithms include Particle Swarm Hooke-Jeeves (PSO-HJ) algorithm (Wetter, 2011), Covariance Matrix Adaptation Evolution Strategy and Hybrid Differential Evolution (CMA-ES/HDE) algorithm (Kämpf & Robinson, 2009), Genetic and Generalized Pattern Search (GA-GPS) algorithm (Palonen, Hasan, & Siren, 2009), Harmony Search Broyden-Fletcher-Goldfarb-Shanno (HS-BFGS) algorithm etc. Hybrid algorithms combine strengths and limit weaknesses of the individual algorithms that it is made of (Nguyen, et al., 2014). PSO-HJ algorithm conducts a particle swarm optimization on a mesh for the initial iterations. This is carried out through a user-specified number of generations. Subsequently, Hooke-Jeeves algorithm is initiated at the mesh point that generated the lowest objective function value by the PSO algorithm and continues searching for the optimal point.

Wetter and Wright (2004) compared the performance of eight algorithms in optimizing simple and complex building models and found that PSO-HJ algorithm achieved the overall best reduction of value of the objective function. The performance of two hybrid algorithms: PSO-HJ and CMA-ES/HDE were compared on optimizing five standard benchmark functions using EnergyPlus by Kampf, Wetter and Robinson (2010). The study revealed that both of these algorithms performed well in solving building optimization problems on EnergyPlus models.

2.5.5 Trend of usage

The trend of using algorithms in building performance optimization studies is given in Figure 2.11. These results have been derived from more than 200 building optimization studies published by SciVerse Scopus of Elsevier (Nguyen, et al., 2014). According to Figure 2.11, it is evident that Genetic algorithms, Particle Swarm Optimization and Hybrid algorithms are the most preferred algorithms in studies related to building performance optimization.

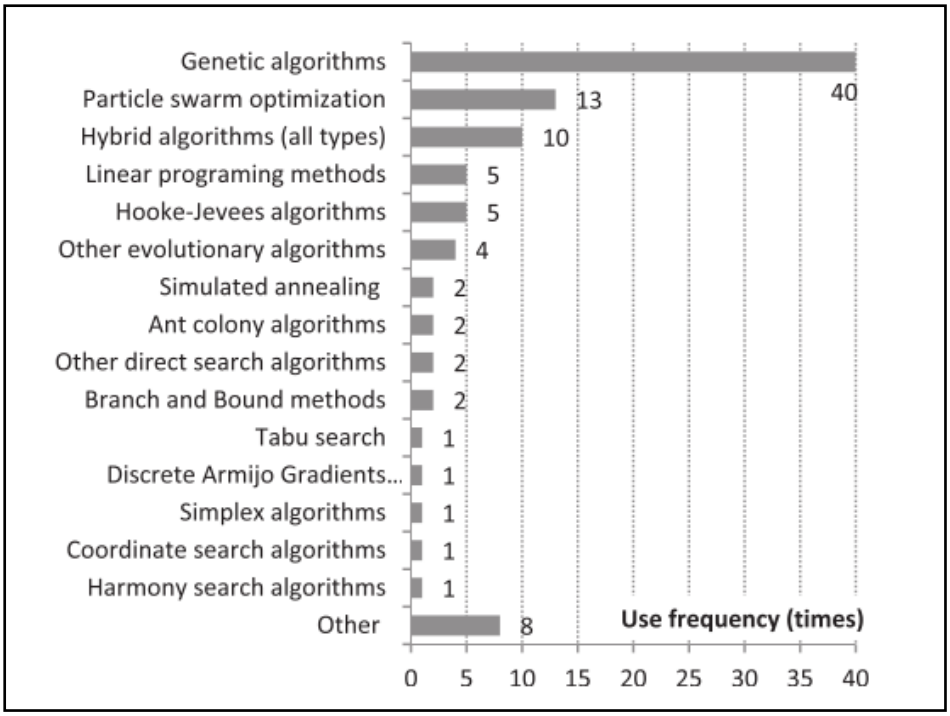

Figure 2.11: Usage frequency of algorithms in building performance studies
Source: Nguyen et al. (2014)

According to literature (Wetter & Wright, 2004), gradient-based algorithms often fail in handling building performance optimization problems since they are sensitive to discontinuities in the objective function. Furthermore, Wetter and Wright (2004) stated that when detailed simulation models have been used some of the direct search algorithms also tend to fail, mainly due to the large steps that are taken in the global exploration. Hence, simple GA and Hybrid algorithms have been recommended as the best options available in this regard (Nguyen et al., 2014; Wetter & Wright, 2004). On this basis, the hybrid algorithm, Generalized Pattern Search Particle Swarm Optimization with Constriction Coefficient Hooke-Jeeves (GPSPSOCCHJ) is applied in the present work. It consists of the Particle Swarm Optimization with Constriction Coefficient (PSOCC) algorithm, which is a stochastic population-based algorithm and the Hooke-Jeeves (HJ) algorithm, which is a direct search algorithm. This hybrid algorithm initially performs a particle swarm optimization and then switches to the HJ algorithm to further refine the results. The main advantage of this algorithm is that the global search of the PSOCC algorithm increases the chances of

getting close to the global minimum, rather than getting trapped in a local minimum. Subsequently the HJ algorithm further refines the search locally.

2.6 Optimization tools

A number of optimization tools applicable for building performance optimization can be found in the literature and only the most popular ones are elaborated here. Following section gives a brief explanation of some of the popular optimization tools used in building performance optimization.

2.6.1 GenOpt

GenOpt (Wetter, 2011) is a generic optimization tool whose main field of application is building energy usage or operational cost optimization. It can be combined with any whole building simulation tool that reads its input from text files and writes its output to text files (Wetter, 2011). GenOpt automatically finds the values of user defined independent variables that optimize any given objective function. The independent variables can be continuous variables (possibly with lower and upper bounds), discrete variables or both. Constraints on dependent variables can be implemented using penalty or barrier functions. GenOpt initiates the optimization task, checks for possible simulation errors, reads the value of the objective function to be optimized from the simulation output file and then determines the new set of input parameters for the next run (Wetter, 2011). The whole process is repeated iteratively until an optimal of the objective function is achieved. The interface between GenOpt and the simulation program is shown in Figure 2.12. GenOpt uses the following input files during the optimization process:

- Initialization file: Specification of file locations (input files, output files, log files etc.)
- Command file: Specification of parameter names, initial values, upper and lower bounds, optimization algorithm etc.
- Configuration file: Configuration of simulation programme (error indicators, start command, etc.)
- Simulation input template: Templates of simulation input files

GenOpt has a library of local and global one-dimensional and multi-dimensional optimization algorithms and algorithms for performing parametric runs.

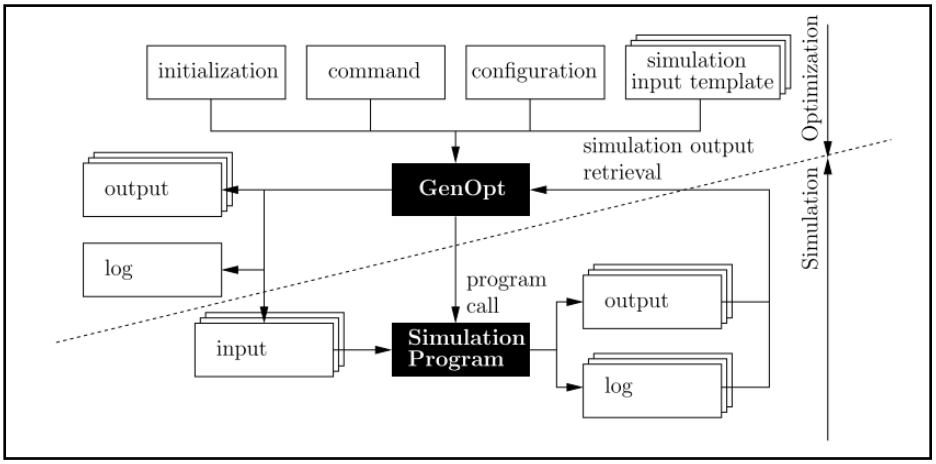

Figure 2.12: Interface between GenOpt and simulation programme

Source: Wetter (2011)

The platform independence and the general interface make GenOpt applicable to a wide range of optimization problems (Wetter, 2011). The main limitation of GenOpt is that it does not have any multi-objective optimization algorithms at its disposal.

2.6.2 MATLAB

MATLAB is a high-level language and an interactive environment capable of performing numerical computations, visualization, and programming (Dar, 2017). It consists of a family of add-on application-specific solutions called toolboxes. Toolboxes are comprehensive collections of MATLAB functions (M-files) that extend the MATLAB environment to solve different classes of problems. Some of the areas in which toolboxes are available include signal processing, control systems, neural networks, fuzzy logic, simulation etc. (Dar, 2017). MATLAB optimization toolboxes are not specially designed for building performance optimization applications and hence in order to use them more complex skills are required. However, the neural network toolbox allows users to replace a computationally expensive model by a surrogated model (Nguyen et al., 2014). Furthermore, MLE+ is a MATLAB toolbox designed for performing co-simulation with EnergyPlus. It is designed for engineers and researchers who are already familiar with MATLAB and for those who wants to apply the software for solving building energy optimization

problems. MLE+ is particularly useful for (Bernal, Behl, Ngheim, & Mangharam, 2012):

- Controller design where the energy simulation is carried out by EnergyPlus while the controller is designed and implemented in MATLAB
- Data acquisition for a large number of simulations, with different scenarios, can be carried out and their execution data is read, stored and processed in MATLAB. The data can then be used for understanding the building system and for establishing a regression model or a neural network model
- Simulation-based optimization where a non-linear optimizer, such as MATLAB global optimization toolbox, can be used to find the optimal (or sub-optimal) parameters or control sequences of the building system, by considering the building as a black-box whose execution is performed through simulations by EnergyPlus.

2.6.3 DAKOTA

DAKOTA (Design Analysis Kit for Optimization and Tera-scale Applications) (Adams et al., 2010) provides a flexible, extensible interface between the simulation code and a variety of iterative methods and strategies. It provides engineers and scientists with a systematic and rapid means of obtaining improved or optimal designs or understand sensitivity or uncertainty using simulation-based models. Recent versions of the software have been expanded to interface with other types of iterative analysis methods such as quantification of uncertainty with nondeterministic propagation methods, sensitivity/variance analysis with general purpose design of experiments and parameter study capabilities (Adams et al., 2010). One of the primary advantages of DAKOTA is its access to a broad range of iterative capabilities obtained through a single, relatively simple interface between DAKOTA and the simulator. It is executed using the commands that the user provides in an input file which specify the type of analysis to be performed such as parametric study, optimization, uncertainty analysis etc., along with the file names associated with the user's simulation code. DAKOTA is not specifically designed for building performance optimization. However, DAKOTA allows users to replace a computationally expensive model by a surrogated model (Nguyen et al., 2014).

2.6.4 MOBO

MOBO (Multi-Objective Building Optimization) (Palonen et al., 2013) is a generic freeware capable of handling single and multi-objective optimization problems with continuous and discrete variables and constraint functions. It can be coupled with many external simulation programmes that calculate the values of objective functions. MOBO has a library of different types of algorithms and hence capable of handling multi-modal functions (Palonen et al., 2013). It possesses a GUI for defining the optimization problem and the progress of the optimization process can also be monitored. Since the software is developed with the Java programming language, it is platform independent. As per Nguyen et al. (2014), MOBO shows promising capabilities and may become the major optimization engine in the future.

Table 2.3: Comparison of main features of optimization tools

Feature	**Optimization Tools**			
	GenOpt	MATLAB	DAKOTA	MOBO
Whether an open source software?	√	X	√	√
Ability to perform multi-objective optimization	X	√	√	√
Ability to perform parallel computing	√	√	√	√
Ability to handle both discrete and continuous variables	√	√	√	√
Ability to perform parametric studies	√	√	√	X
Ability to perform sensitivity analysis	X	√	√	X
Availability of multiple algorithms	√	√	√	√
Availability of a user interface	X	√/X	√	√
Possess objective function flexibility	√	√	√	√
Possess parameter flexibility	√	√	√	√
Possess algorithmic extensibility	√	√	Unknown	√
Ability to apply of surrogated models	X	√	√	X
Operating system	Independent	Windows/ Mac/Linux	Windows/ Linux	Independent

Source: Extracted from Nguyen et al. (2014)

Table 2.3 makes a comparison among some of the optimization tools with respect to their main features.

From a study carried out by Attia (2012), it was revealed that GenOpt and MATLAB are the most frequently used building performance optimization tools. GenOpt has become very popular since it is a platform-independent free optimization tool specifically designed for optimizing building performance applications. Hence, it is suitable and applicable for multiple purposes in the field of building performance with acceptable complexity (Nguyen et al., 2014). MATLAB optimization toolboxes and DAKOTA have not been specifically designed for building performance optimization and hence can be considered only as generic tools. MOBO is a tool in the public domain that has high potential to become the major optimization engine in the future (Nguyen et al., 2014).

2.7 Major studies on building performance optimization

Many previous studies carried out on optimizing the performance of buildings can be found in the literature. This section summarizes some of the major studies published over the years in chronological order, covering various aspects of building performance optimization.

A model based on thermal discomfort as the criterion of optimality was established by Gupta (1970) and Gupta and Spencer (1970) through application of a sequential simplex type of search procedure. The study optimized the thermal performance of buildings under periodic indoor and outdoor design conditions on a typical outdoor weather cycle during the summer in Australian cities over several design variables.

An optimization model was established by Wilson and Templeman (1976) for determining the thermal design of an office building with minimal initial and operating costs. The total discounted cost of the entire heating and insulation process was used as the criterion of optimality.

Design of parallelepiped open plan office buildings was carried out by D'Cruze and Radford (1987) that was based on multi-criteria optimization, considering thermal load, daylight availability, net usable area and capital cost. Dynamic programming

approach was used for optimization with respect to design variables of window geometry, wall and roof construction, building orientation, massing, floor area and shape of the building.

An optimization technique to set the level of insulation of the building envelope to maximize net energy savings in passive as well as in air-conditioned buildings was suggested by Kumar, Ashutosh, and Sodha (1989).

A direct search optimization coupled with an hourly thermal simulation tool was performed by Al-Homoud (1997) for minimizing the energy consumption for heating and cooling in residential buildings.

The optimal technology mix was determined for selected building projects by Peippo, Lund, and Vartiainen (1999). This method considered design parameters such as the shape of the building, orientation, amount of insulation and window areas etc. In order to find the optimal parameter values, this method established a multivariate problem formulation, taking into consideration the total annual cost for the building, as well as the total annual energy consumption. The optimization procedure was comprised of cyclic coordinate search as well as the Hooke-Jeeves direct search method.

In another approach, Bouchlaghem (2000), not only simulated the thermal performance of the building, but also applied numerical optimization techniques to determine the design variables, that optimized the thermal comfort of the building. This method took into account design variables related to the building envelope and fabric, such as the aspect ratio, building orientation and the glazing ratio etc. This method investigated different objective functions, which represented six different ways of quantifying the thermal comfort involving decision variables that were subjected to linear constraints. The resulting constrained optimization problem was solved using a combination of the Nelder and Mead simplex method, and the complex method described by Mitchell and Kaplan (1968).

Nielsen and Svendsen (2002) determined the optimal values with respect to the amount of insulation, type of glazing, window to wall ratio in a constrained

optimization problem, where the life cycle cost of the building was taken as the objective function. Furthermore, energy required by the building, the number of hours where overheating occurred and the daylight factors were taken as constraints. The resulting optimization problem consisted of discrete as well as continuous variables. They used the simulated annealing method for optimizing the discrete parameters and the method suggested by Hooke and Jeeves (1961) for optimizing the continuous variables.

Dimensions of windows were optimized with the objective of minimizing the energy required for heating and artificial lighting in a building by Caldas and Norford (2002). The optimization was based on the results generated by the building simulation software. The software automatically adjusted the amount of artificial lighting, so that the required illumination level was achieved. This resulted in an unconstrained optimization problem that was solved using the genetic algorithm described by Goldberg (1989).

Jedrzejuk and Marks (2002) disintegrated the design optimization problem into sub-problems related to optimization of internal partitions and shape of the building considering the ease of coordinating the solution. Shape of the building was represented by design parameters such as wall lengths, number of storeys, window-to-wall ratio etc. This method was based on a constrained multi-criteria formulation that took building construction costs, seasonal demand for energy for heating, and pollutant levels emitted by heat sources, as objective functions. The optimization problem was solved using a combination of analytical and numerical methods.

Multi-criteria optimization has been applied to optimize the shape of energy-saving buildings by Jedrzejuk and Marks (2002). The criteria focused on minimizing the thermal load and capital cost and to maximize the net usable area.

Wang, Zmeureanu, and Rivard (2005) considered aspects of green building design during their study. They determined optimal values related to building orientation, aspect ratio and window to wall ratio. This method was based on a multi-criteria formulation, with building life cycle cost and life cycle environmental impact of the building taken as objective functions. The optimization problem was solved using the

multi-objective genetic algorithm of Fonseca and Flemming (1998). The method provided the Pareto set for the two objective functions, which was used for assessing the level of compromise between optimizing economic aspects of the building and optimizing environmental impact of the same.

In a study related to a large office building, Kampf et al. (2010) found means of reducing the total energy consumption by 7.1% in Florida, United States.

Suh, Park, and Kim (2011) found 24% and 33% reduction of heating and cooling energy in a post office building in Korea respectively, using a knowledge-based design method and a simulation-based optimization method, respectively.

Castro-Lacouture, Sefair, Florez, and Medaglia (2009), Bambrook, Sproul, and Jacob (2011) and Fesanghary, Asadi, and Geem (2012) studied the design of high performance buildings using optimization techniques.

Nguyen (2013) improved thermal comfort and energy consumption in three typical existing dwellings in two running modes under three hot and humid climates by performing optimization using calibrated EnergyPlus models.

A multi-objective optimization model for life-cycle cost analysis and retrofitting planning of buildings was developed by Wang, Xia, and Zhang (2014). The model was optimized in terms of both energy savings and economic benefits during a selected time frame using a differential evolution algorithm.

Negendahl and Nielsen (2015) applied multi-objective genetic algorithms for holistic building design, assigning building energy usage, capital cost, daylight distribution and thermal indoor environment as optimization criteria. It presents a fast evaluation method suitable for the early design stage of buildings.

Li, Pan, Xue, Jiang, and Mao (2017) presented an efficient optimization framework to facilitate design of buildings by utilizing several simulation software. Performance of three optimization strategies: GenOpt method, artificial neural network method and their proposed methodology have been investigated in this study.

It is observed that the aforementioned studies have considered following criteria as objective functions in order to optimize the performance of buildings:

- Cost of heating
- Thermal load
- Thermal comfort and level of thermal discomfort
- Total annual cost
- Annual energy consumption
- Energy consumption for heating and cooling
- Energy required for heating and artificial lighting
- Building construction cost
- Seasonal demand for energy for heating
- Pollutant levels emitted by heat sources
- Building life cycle cost
- Net energy savings
- Building life cycle environmental impact
- Daylight distribution

Furthermore, following design variables have been considered in optimizing the relevant objective functions:

- Building orientation
- Wall/Window/Floor area and Window to wall ratio
- Shape of the building expressed in terms of aspect ratio
- Number of storeys
- Amount of insulation in the building envelope
- Thermal Mass
- Construction characteristics of building elements
- Window type and dimensions
- Glazing and shading aspects

The aforementioned studies have applied both single and multi-criteria schemes for optimizing the performance of buildings. According to Nguyen et al. (2014), approximately 60% of the building optimization studies found in the literature have

used single objective approach. In addition, problems with both unconstrained and constrained conditions have been considered for optimization. The respective objective functions consist of continuous, discrete or both types of variables.

In the field of building performance simulation, optimization does not necessarily mean determining the global optimal solution(s) to a problem, since it may be infeasible to find the same at all times due to the nature of the problem being considered (Baños et al., 2011; Wetter & Wright, 2004). Furthermore, some authors have interpreted the term "optimization" simply to indicate an improvement of performance using computer simulations in order to achieve merely suboptimal solutions. Some researchers adopted a sensitivity analysis as an approach to optimize performance of buildings without carrying out a rigorous mathematical optimization. However, it is generally accepted among the simulation-based optimization communities that "optimization" refers to an automated process which is entirely based on numerical simulations and mathematical optimization (Attia, 2012).

2.8 Future trends on building performance optimization

With the increasing demand for high performance buildings, there is an upward trend of the number of building performance optimization studies carried out by the global building research community as shown in Figure 2.13.

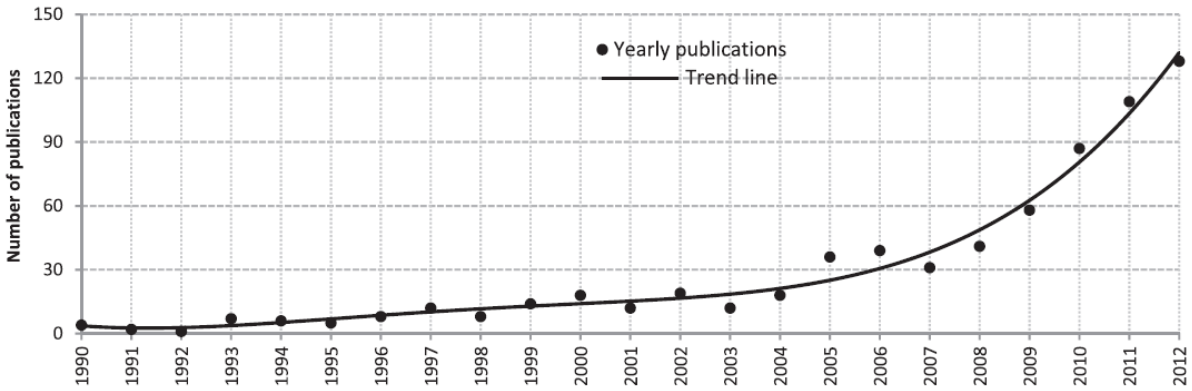

Figure 2.13: Trend of the number of optimization studies on building performance

Source: Nguyen et al. (2014)

Availability of high computing power, whole building simulation and optimization tools and also due to the stringent regulations on the performance of buildings at present, may have contributed substantially to this scenario.

Simulation-based optimization is an approach undoubtedly having a great potential at present. This is a complex multi-disciplinary approach that involves several scientific fields such as mathematics, engineering, environmental science, economics, computer science etc. (Nguyen et al., 2014). The major obstacles in implementing this approach include complex nature of the building simulation outputs, high computational cost, scale of the problem being handled, multi-objective design problems and uncertainty of variables and constraints etc. (Nguyen et al., 2014). Moreover, application of building performance optimization for real-world problems is still in the early stage of development. Hence, research efforts are underway towards improving the efficiency of search techniques and algorithms in order to reduce computational time and to mitigate uncertainties involved. In spite of all the said challenges, there is high possibility that, simulation-based optimization approach will become a standard practice in the global building design sector in the near future.

2.9 Summary

This chapter provided with an in-depth analysis on building energy modelling, optimization methodologies and related concepts, relevant tools and their features and the major building performance optimization studies found in the literature.

3. GOVERNING ASPECTS OF BUILDING PERFORMANCE

3.1 Overview

In order to optimize the performance of buildings, heat and mass transfer processes that take place in a building need to be thoroughly understood, quantified and incorporated. Heat and mass transfer processes in buildings can be incorporated and modelled successfully using whole building energy simulation tools. An overview of heat and mass transfer processes in a typical building is illustrated in Figure 3.1.

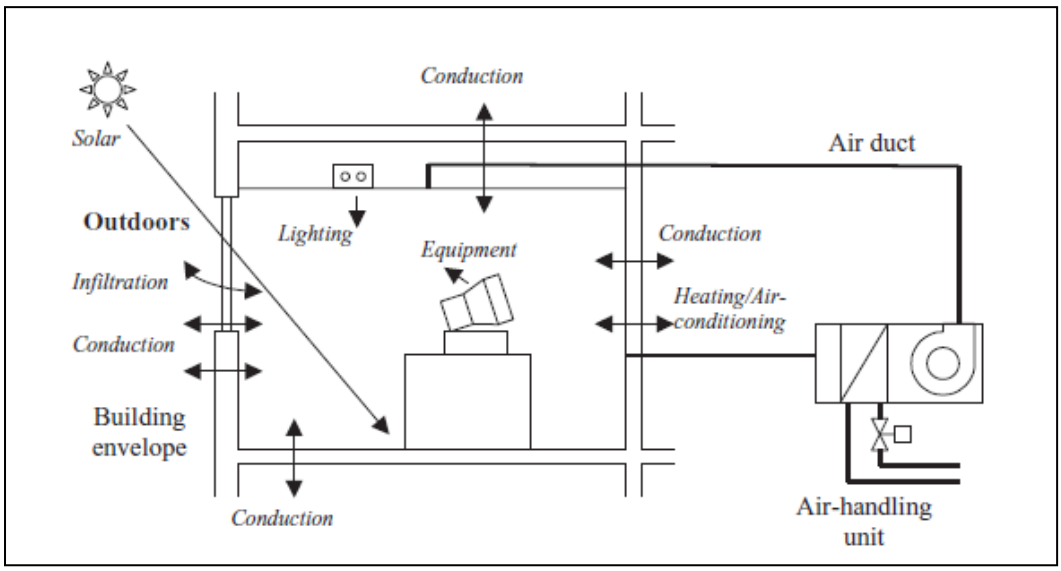

Figure 3.1: Heat and mass transfer processes in a typical building

Source: Underwood and Yik (2004)

According to Figure 3.1, it is evident that majority of heat and mass transfer takes place across the building envelope. Interior air of buildings and envelope elements are the main contributors in this regard. Furthermore, lighting, equipment and occupants influence the heat and mass transfer in the indoor environment. The sections to follow focus on the governing aspects related to the aforementioned processes.

3.2 Heat balance in buildings

The basis for building performance analysis is the formulation of heat balance encompassing different elements of the building. This task is of two-fold. Both air in

buildings and building envelope elements need to be considered in establishing the heat balance equations. Consequent to a number of lumped mass based assumptions, this results in a set of linear ordinary differential equations (resulting from non-linear partial differential equations) that need to be solved in order to calculate the corresponding heat transfer quantities. Most whole building simulation tools apply the predictor-corrector approach for solving the aforementioned differential equations ("EnergyPlus Engineering Reference", 2013). Eventually, heat transfer quantities are made use of in predicting the building energy performance.

3.2.1 Heat balance for zonal air

Heat balance for air in a particular thermal zone of a building can be expressed as in equation 3.1 ("EnergyPlus Engineering Reference", 2013):

$$C_z \frac{dT_z}{dt} = \sum_{i=1}^{N} \dot{Q}_i + \sum_{i=1}^{N_{surfaces}} h_i A_i (T_{si} - T_z) + \sum_{i=1}^{N_{zones}} \dot{m}_i C_p (T_{zi} - T_z) + \dot{Q}_{sys} + \dot{m}_{\text{inf}} C_p (T_\infty - T_z) \quad (3.1)$$

where

$\sum_{i=1}^{N} \dot{Q}_i$ - Sum of the convective internal loads

$\sum_{i=1}^{N_{surfaces}} h_i A_i (T_{si} - T_z)$ - Convective heat transfer from the zone surfaces

$\dot{m}_{inf} C_p (T_\infty - T_z)$ - Heat transfer due to infiltration of outside air

$\sum_{i=1}^{N_{zones}} \dot{m}_i C_p (T_{zi} - T_z)$ - Heat transfer due to inter-zone air mixing

$\dot{Q}_{sys}$ - Output of air system

$C_z \frac{dT_z}{dt}$ - Rate of energy storage in zonal air

$$C_z = \rho_{air} C_p C_T \quad (3.2)$$

where

ρ_{air} - Density of zonal air

C_p - Specific heat capacity of zonal air

C_T - Sensible heat capacity multiplier

In simple terms the heat balance equation for building air takes the form as given in equation 3.3 (Zhai et al., 2001):

$$\sum_{i=1}^{N} q_{ic}A_i + Q_{light} + Q_{occup} + Q_{equip} + Q_{inf} - Q_{heat\_extrct} = \rho_{air}V_{building}C_p\frac{dT}{dt} \quad (3.3)$$

where

q_{ic} - Convective heat flux from building surface i

A_i - Area of building surface i

$V_{building}$ - Volume of building

$\frac{dT}{dt}$ - Rate of change of temperature of building air

Q_{light}, Q_{occup}, Q_{equip}, Q_{inf}, Q_{heat_extrct} denote heat transfer due to lighting, occupants, equipment, infiltration and heat extraction from the building respectively.

Buildings gain or lose heat by infiltration and exfiltration, depending on the surrounding conditions. Heat transfer in this case consists of both sensible and latent components. The sensible heat transfer rate due to infiltration, Q_{si} is given in equation 3.4 ("EnergyPlus Engineering Reference", 2013):

$$Q_{si} = \dot{m}_o C_{pm}(T_o - T_i) = \dot{V}_o \rho_o C_{pm}(T_o - T_i) \quad (3.4)$$

The latent heat transfer rate due to infiltration Q_{li} is given in equation 3.5 ("EnergyPlus Engineering Reference", 2013):

$$Q_{li} = \dot{m}_o h_{fg}(\omega_o - \omega_i) = \dot{V}_o \rho_o h_{fg}(\omega_o - \omega_i) \quad (3.5)$$

where

$\dot{m}_o$ - Mass flow rate of outdoor air due to infiltration

$\dot{V}_o$ - Volumetric flow rate of outdoor air due to infiltration

C_{pm} - Average specific heat capacity of moist air

h_{fg} - Latent heat of vapourization of water

T_o - Outdoor dry bulb temperature

T_i - Indoor dry bulb temperature

ω_o - Outdoor moisture content

ω_i - Indoor moisture content

ρ_o - Density of outdoor air

3.2.2 Heat balance for building envelope elements

Heat balance for a particular building envelope element is illustrated in Figure 3.2.

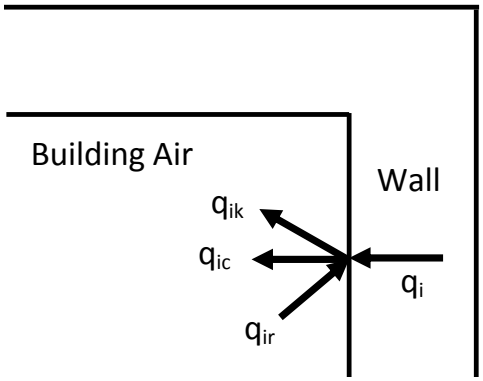

Figure 3.2: Heat balance for a particular building envelope element

Source: Zhai et al. (2001)

Heat balance for a certain building envelope element can be expressed as in equation 3.6 (Zhai et al., 2001):

$$q_i + q_{ir} = \sum_{k=1}^{N} q_{ik} + q_{ic} \tag{3.6}$$

where q_i and q_{ic} denote conductive heat flux through element i and convective heat exchange between element surface i and building air respectively. q_{ir} and q_{ik} represent radiative heat exchange from internal heat sources and solar radiation and the net radiative heat exchange between element surface i and other surfaces respectively. N is the number of envelope elements in the building.

Surface conductive heat fluxes (q_i) are computed using the Conduction Transfer Functions (CTF) method (Ceylan & Meyers, 1980; Seem, 1987) by most whole building simulation solvers. The basic time series solution represents the response factor equation as given in equation 3.7 ("EnergyPlus Engineering Reference", 2013):

$$q(t) = \sum_{j=0}^{\infty} X_j T_{o,t-j\delta} - \sum_{j=0}^{\infty} Y_j T_{i,t-j\delta} \quad (3.7)$$

where q and T are heat flux and temperature respectively. Subscripts i and o signify inside and outside of the building element respectively whereas t represents the current time step. X and Y are the response factors.

Convective heat flux may be determined by equation 3.8 (Zhai et al., 2001):

$$q_{ic} = h_c(T_i - T_{building}) \quad (3.8)$$

where h_c and $T_{building}$ denote convective heat transfer coefficient and building air temperature respectively.

Radiative heat flux from surface i to surface k in a building can be given as expressed in equation 3.9 (Zhai et al., 2001):

$$q_{ik} = h_{ik,r}(T_i - T_k) \quad (3.9)$$

where

$h_{ik,r}$ - Linearized radiative heat transfer coefficient between surfaces i and k

T_i - Temperature of interior surface i

T_k - Temperature of interior surface k

Solar gain through fenestrations can be expressed as in equation 3.10:

$$q_{ir} = A(SHGF).(SC) \quad (3.10)$$

where

A - Area of fenestration exposed to solar radiation

SHGF - Solar heat gain factor

SC - Shading coefficient

Solar heat gain factor is expressed in equation 3.11:

$$SHGF = \left[I_t\left(\tau + \frac{\alpha U}{h_o}\right)\right] \quad (3.11)$$

where

I_t - Solar radiation incident on the fenestration

τ - Solar transmissivity of fenestration medium

α - Solar absorptivity of fenestration medium

U - Overall heat transfer coefficient

h_o - External convective heat transfer coefficient

The shading coefficient generally depends upon the type of fenestration medium and the nature of the shading device.

Using equations 3.6 to 3.11 expressing conductive, convective and radiative heat fluxes on each envelope element of the building, relevant surface temperatures can be determined, if the temperature of the building air ($T_{building}$) is assumed to be known. This task is generally performed by the whole building simulation tool.

3.3 Mass balance in buildings

A building is an open thermodynamic system with its envelope acting as the interface with the external environment. Various mass transfer processes take place across the building envelope throughout its life cycle. Mass balance in a building is governed by the principle of conservation of mass or continuity. The transient mass balance of air in a thermal zone takes the general form as given in equation 3.12 ("EnergyPlus Engineering Reference", 2013):

$$\rho V_z C_\omega \frac{d\omega_z}{dt} = \sum_{i=1}^{N} \dot{m}_{shedload} + \sum_{i=1}^{N} A_i h_{mi} \rho_z (\omega_i - \omega_z) + \sum_{i=1}^{N} \dot{m}_i (\omega_{zi} - \omega_z) + \dot{m}_{inf}(\omega_\infty - \omega_z) + \dot{m}_{sys}(\omega_{sup} - \omega_z) \quad (3.12)$$

where

$\rho V_z C_\omega \frac{d\omega_z}{dt}$ - Change in zone air humidity ratio

$\sum_{i=1}^{N} \dot{m}_{shedload}$ - Scheduled latent loads

$\sum_{i=1}^{N} A_i h_{mi} \rho_z (\omega_i - \omega_z)$ - Latent loads from the zone surfaces

$\sum_{i=1}^{N} \dot{m}_i (\omega_{zi} - \omega_z)$ - Multi-zone air flow loads

$\dot{m}_{inf}(\omega_\infty - \omega_z)$ - Outdoor air infiltration load

$\dot{m}_{sys}(\omega_{sup} - \omega_z)$ - Ventilation/Supplied air flow load

C_ω - Humidity capacity multiplier

N - Number of thermal zones/building surfaces

3.4 Problem of building performance optimization

Notation

$a \triangleq b$ - a is equal to b by definition

f (x) - Objective function

$\mathbb{R}^n$ - Euclidean space of n-tuplets of real numbers

$\mathbb{Z}$ - Set of integers

$\mathbb{Q}$ - Set of rational numbers

$\mathbb{N} \triangleq \{0,1, \dots\}$ - Set of natural numbers

$\mathbb{Q}_+ \triangleq \{q \in \mathbb{Q} \mid q > 0\}$

$f(\cdot)$ - Function of undesignated variables

$f: A \to B$ - Domain of $f(\cdot)$ is in the space A and its range in the space B.

Building performance optimization problems considered during present work take the form as in equation 3.13 (Wetter & Wright, 2004):

$$\min_{x \in X} f(x) \tag{3.13}$$

where $x \in X$ is the vector of independent variables, $f: X \to \mathbb{R}$ is the objective function, and $X \subset \mathbb{R}^n$ is the set of constraints, defined as:

$$X \triangleq \left\{ x \in \mathbb{R}^n \mid l^i \leq x^i \leq u^i, i \in \{1, \dots, n\} \right\} \tag{3.14}$$

with $-\infty \ll l^i < u^i \ll \infty$, for all $i \in \{1, \dots, n\}$, where $x \in X \subset \mathbb{R}^n$ is the set of design parameters, X is the feasible set for x. $l \in \mathbb{R}^n$and $u \in \mathbb{R}^n$denote lower and upper bounds of the design parameter respectively.

The optimization tool makes use of the relevant algorithm to optimize the objective function as per constraints imposed. The value of the objective function is computed by the whole building simulation tool and transferred back, at each iteration of the optimization process.

3.5 Building performance optimization algorithm

Present work utilizes the hybrid Particle Swarm Optimization and Hooke-Jeeves (PSO-HJ) algorithm for optimizing the performance of buildings. It initially performs a particle swarm optimization on a mesh for a user-specified number of generations $n_G \in \mathbb{N}$. Subsequently, the process switches over to the Hooke-Jeeves

generalized pattern search algorithm. The algorithm can accommodate both continuous and discrete variables. Dimensions of the continuous and discrete independent variables are denoted by $n_c \in \mathbb{N}$ and $n_d \in \mathbb{N}$ respectively.

Let $k \in \mathbb{N}$ denote the generation number and let $n_p \in \mathbb{N}$ denote the number of particles in each generation. Also let $x_i(k) \in \mathbb{R}^n, i \in \{1, \dots, n_p\}$ denote i[th] particle of the k[th] generation.

The objective function $f: \mathbb{R}^n \times \mathbb{R}^n \times \mathbb{Q}_+ \times \mathbb{R}^n \to \mathbb{R}$ is defined by equation 3.15 (Wetter & Wright, 2004):

$$f(x; x_0, \Delta, s) \triangleq f(\gamma(x)) \tag{3.15}$$

where $\gamma(x) \in \mathbb{M}(x_0, \Delta, s) \cap X$ is the closest feasible mesh point and the mesh is of the form:

$$\mathbb{M}(x_0, \Delta_k, s) \triangleq \left\{ x_0 + \Delta_k \sum_{i=1}^{n} m^i s^i e_i \mid m \in \mathbb{Z}^n \right\} \tag{3.16}$$

The PSO algorithm is run with user specified initial iterate $x_o \in X \triangleq X_c \times X_d \subset \mathbb{R}^{n_c} \times \mathbb{Z}^{n_d}$ for a user specified number of generations $n_G \in \mathbb{N}$, where the continuous independent variables are restricted on the mesh defined in equation (3.16). The set of constraints $X_c \subset \mathbb{R}^{n_c}$ defined in equation (3.14) have finite lower and upper bounds $l^i, u^i \in \mathbb{R}$, for all $i \in \{1, \dots, n_c\}$.

3.6 State of Convergence

The objective function to be optimized is a series comprised of a finite number of terms. As per D'Angelo and West (2000), a series is said to be convergent if it approaches some limit L. The infinite series $\sum_{n=1}^{\infty} a_n$ is convergent, if the sequence of partial sums $S_n = \sum_{k=1}^{n} a_k$ is convergent. If $\sum u_k$ and $\sum v_k$ are convergent series then $\sum(u_k + v_k)$ and $\sum(u_k - v_k)$ are convergent. If c≠0, then both $\sum u_k$ and $c\sum u_k$ converge. For any sequence$\{a_1, a_2, a_3, \dots\}$, $a_n \leq |a_n|$ for all n. Hence,

$$\sum_{n=1}^{\infty} a_n \leq \sum_{n=1}^{\infty} |a_n| \tag{3.17}$$

If $\sum_{n=1}^{\infty}|a_n|$ converges then, $\sum_{n=1}^{\infty} a_n$ also converges. If the series $\sum_{n=1}^{\infty}|a_n|$ converges, then the series $\sum_{n=1}^{\infty} a_n$ is absolutely convergent.

3.7 Summary

This chapter explained governing principles related to performance of buildings. Energy and mass balance equations form the basis for such analysis. Furthermore, the chapter elaborates on the theoretical aspects of generic optimization and on the PSO-HJ algorithm applied during optimization of building performance.

4. METHODOLOGY FOR PERFORMANCE OPTIMIZATION

4.1 Introduction

The methodology adopted for optimizing the performance of buildings is discussed in this chapter. The overall exercise can be broadly categorized into several main tasks as explained in the sections to follow. The main tasks include:

- Development of the objective functions
- Generation of the whole building simulation model
- Linking simulation model with the optimization tool through user defined files and coding
- Setting up of optimization algorithm
- Performing the simulation
- Interpretation of results

Three types of building envelope designs have been optimized in terms of annual primary energy consumption and life cycle cost with respect to different building envelope variables coming under continuous and discrete categories. Furthermore, saving potential of the optimal envelope design with respect to the aforesaid criteria have also been predicted.

4.2 Objective functions

The objective function represents the criterion to be optimized subjected to predefined constraints. During present work objective functions were developed for annual energy consumption and life cycle cost of the building. Equation 4.1 shows the general form of the objective function f(x) to be optimized:

$$f(x) \cong a(x) + p(x) \tag{4.1}$$

where

$a(x)$ - Function representing the performance of the building

$p(x)$ - Penalty function

The purpose of including a penalty function, p(x) in the objective function is to make sure that the optimal envelope design does not aggravate the thermal comfort in the

occupied space. As per ASHRAE standards (ANSI/ASHRAE/IESNA 55, 2010), recommended range for thermal comfort in a building in terms of Predicted Mean Vote (PMV) is $-0.5 \leq PMV \leq +0.5$. However, if this criterion is maintained for all optimization scenarios, only sub-optimal building envelope designs will be generated with respect to energy consumption and life cycle cost. This is because in order to meet the aforesaid optimal thermal comfort criteria, the building envelope elements related to optimal energy consumption for cooling has to be sacrificed for a higher energy consuming envelope. Hence, in order to trade off these contradictory criteria, the penalty function was included in the objective function, only when it was really necessary. The penalty function takes the following general form as given in Equation 4.2:

$$p(x) \cong A.(PMV)^n \tag{4.2}$$

where A and n are constants. To ensure that the penalty imposed is high enough, A is set to energy consumed by equipment (E_{equip}) in the thermal zone. With some analysis it is evident that when n = 4 necessary high penalty can be achieved in the objective function. Hence the penalty function takes the form:

$$p(x) \cong E_{equip}.(PMV)^4 \tag{4.3}$$

4.2.1 Annual energy consumption

Objective function for annual energy consumption of the building was developed, incorporating different forms of energy flows taking place within as well as through the building envelope. There are two forms of energy flows taking place in a typical building; thermal and electrical energy. Energy required for building heating and cooling are generally expressed in terms of thermal energy, whereas energy required for artificial lighting and electrical equipment (process and non-process) is expressed in terms of electrical energy. In order to obtain the total annual energy consumption of the building, thermal and electrical energy quantities have to be added together. This can be done only after bringing them down to a common form of primary energy. This is achieved by assigning corresponding primary energy factors to the different energy forms (Jagemar, 1996). Hence, the annual primary energy consumption (E_{tot}) of the building may be expressed by equation 4.4:

$$f(x) \cong E_{tot} = \alpha_{th}\left(\frac{Q_{heat}}{\eta_{heat}} + \frac{Q_{cool}}{\eta_{cool}}\right) + \alpha_{el}\left(E_{light} + E_{equip.}\right) \quad (4.4)$$

where

- Q_{heat} - Energy consumption for heating
- Q_{cool} - Energy consumption for cooling
- E_{light} - Energy consumption for lighting
- E_{equip} - Energy consumption by equipment
- η_{heat} - Mean plant efficiency for heating
- η_{cool} - Mean plant efficiency for cooling
- α_{th} - Primary energy factor for thermal energy
- α_{el} - Primary energy factor for electrical energy

Thermal and electrical energy quantities are assigned with primary energy factors 1.0 and 3.0 respectively. By assigning the aforementioned primary energy factors, electrical energy is weighted thrice more than thermal energy enabling both forms to be converted to the same form of primary energy. Hence the objective function takes the form:

$$f(x) \cong E_{tot} = \frac{Q_{heat}}{\eta_{heat}} + \frac{Q_{cool}}{\eta_{cool}} + 3\left(E_{light} + E_{equip.}\right) \quad (4.5)$$

4.2.2 Life cycle cost (LCC)

The objective function for life cycle cost was developed incorporating the different cash flows taking place related to the building envelope during the lifetime of the building. To be more precise, difference in building life cycle cost ($dLCC_j$) between the life cycle cost of any envelope design (LCC_j) and that of the existing base design (LCC_0) is taken as the objective function to be optimized. The objective function is given by equation 4.6:

$$f(x) \cong dLCC_j = LCC_j - LCC_0 \quad (4.6)$$

Furthermore objective function can be expressed as:

$$f(x) \cong dLCC_j = \sum dIC_j + \sum dOC_j \quad (4.7)$$

where

dIC_j - Difference in investment cost of any specific building element/component in a particular envelope design and that of the existing base envelope design (Rs.)

dOC_j - Difference in present value (PV) of the operating cost of a certain item of a particular envelope design and that of the existing base envelope design, occurring at a particular point in time during lifetime of the building (Rs.)

Hence,

$$\sum dIC_j = dIC_{walls} + dIC_{windows} + dIC_{HVAC} \tag{4.8}$$

where

dIC_{walls} - Difference in investment cost with respect to walls

$dIC_{windows}$ - Difference in investment cost with respect to windows

dIC_{HVAC} - Difference in investment cost with respect to the Heating, Ventilation and Air Conditioning (HVAC) system

Real discount rate is calculated as shown in equation 4.9.

$$d = \frac{D - I}{1 + I} \tag{4.9}$$

where

d - Real discount rate

D - Nominal discount rate

I - Rate of inflation

Hence,

$$\sum dOC_j = \sum_{1}^{n} \frac{(1+e)^j E_p(dE_j) + (1+g)^j G_p(dG_j)}{(1+d)^j} \tag{4.10}$$

where

E_p - Current price of electrical energy (in the base year) (Rs./kWh)

dE_j - Difference in annual electrical energy consumption between a particular envelope design and that of the existing base envelope design occurring at a particular point in time (kWh)

G_p - Current price of fuel (in the base year) (Rs./MJ)

dG_j - Difference in annual fuel consumption between a particular envelope design and that of the existing envelope design occurring at a particular point in time (MJ)

e - Annual rate of escalation in electrical energy price

g - Annual rate of escalation in fuel price

n - Lifetime of the building (yrs.)

Hence, the objective function takes the form:

$$f(x) \cong dIC_{walls} + dIC_{windows} + dIC_{HVAC} + \sum_{1}^{n} \frac{(1+e)^j E_p(dE_j) + (1+g)^j G_p(dG_j)}{(1+d)^j} \quad (4.11)$$

4.3 Tools for analysis of performance of buildings

This section explains the tools used during the analysis.

4.3.1 Whole building simulation tool

EnergyPlus v. 8.0 is used as the whole building simulation tool during present work. It is a new generation building energy modelling tool with numerous capabilities.

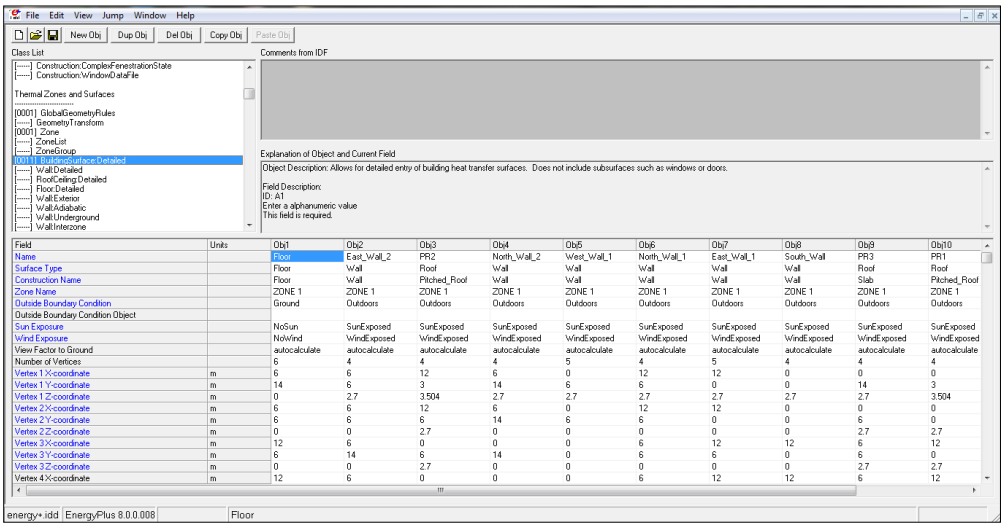

Figure 4.1: Graphical user interface of EnergyPlus

EnergyPlus can model heating, cooling, lighting, ventilation, other energy flows (process and non-process), water usage etc. in buildings and includes many innovative simulation capabilities. Furthermore, it can be coupled directly with the optimization tool. GUI of EnergyPlus is shown in Figure 4.1.

4.3.2 Geometry modelling tool

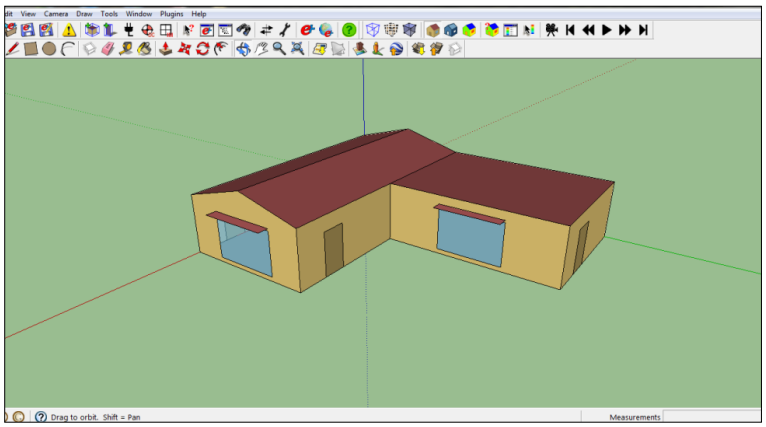

Figure 4.2: Graphical user interface of Legacy OpenStudio Plug-in for SketchUp

The Legacy OpenStudio Plug-in for Google SketchUp facilitates using standard SketchUp tools to create and edit building geometries and thermal zones. It is possible to manipulate EnergyPlus input files by using all of the standard SketchUp 3D capabilities. Hence, both Legacy OpenStudio Plug-in for SketchUp and EnergyPlus can work hand in hand in developing the simulation model of a building. GUI of Legacy OpenStudio Plug-in for SketchUp is shown in Figure 4.2.

4.3.3 Optimization tool

GenOpt v. 3.1.0 is used as the optimization tool during the present analysis. It is a generic optimization programme whose main field of application is building energy usage or operating cost optimization. It can be combined with any whole building simulation tool that reads its input from text files and writes its output to text files. GenOpt is capable of handling both continuous and discrete variables. GUI of GenOpt is shown in Figure 4.3.

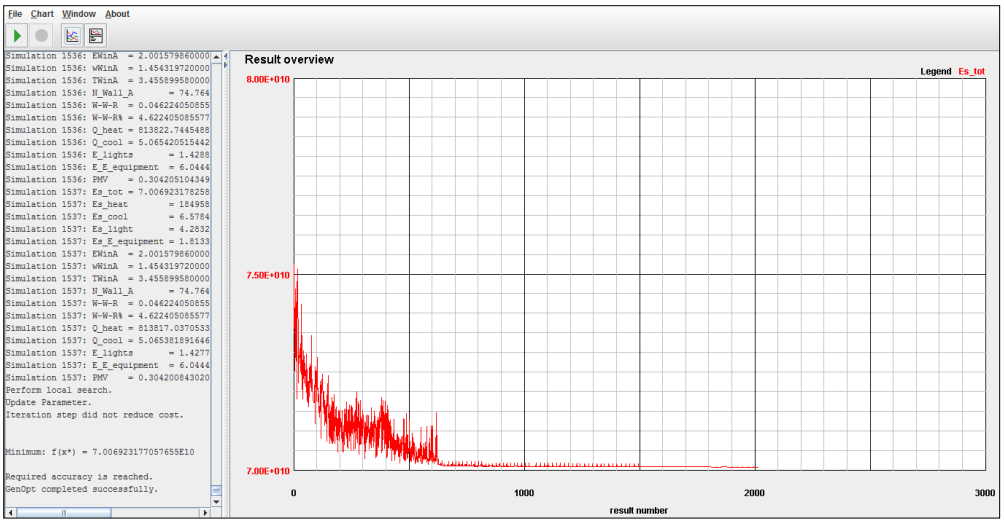

Figure 4.3: Graphical user interface of GenOpt

4.3.4 Optimization algorithm

Selection of the optimization algorithm was one of the crucial decisions to be made with utmost care. A detailed literature survey was conducted in order to decide on the best optimization algorithm for building performance optimization. According to the literature (Nguyen et al., 2014; Wetter & Wright, 2004), Genetic and Hybrid algorithms are the most suited in handling nonlinear non-differentiable objective functions typically found in building performance optimization problems. Furthermore, extensive numerical tests were conducted on the aforesaid algorithms with respect to their stability during simulations before arriving at a decision. On this basis, hybrid algorithm-Generalized pattern search particle swarm optimization with constriction coefficient Hooke-Jeeves (GPSPSOCCHJ) was selected as the best option for the present analysis based on its performance with respect to stability and accuracy. It is comprised of the particle swarm optimization with constriction coefficient (PSOCC) algorithm, which is a stochastic population-based algorithm and the Hooke-Jeeves (HJ) algorithm, which is a direct search algorithm. This hybrid algorithm initially performs a particle swarm optimization and then switches over to the HJ algorithm to further refine the results. The main advantage of this algorithm is that the global search of the PSOCC algorithm increases the chances of getting close to the global minimum, rather than getting trapped in a local minimum. Subsequently, HJ algorithm further refines the search locally.

4.3.5 Output visualization tool

xEsoView was used for visualizing EnergyPlus simulation results. It is capable of displaying variations of different parameters in the building thermal zones related to the time period covered by the simulation. GUI of xEsoView is shown in Figure 4.4.

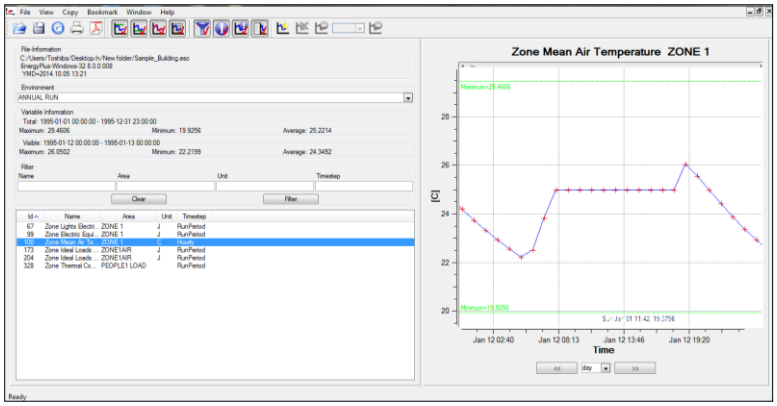

Figure 4.4: Graphical user interface of xEsoView

4.4 Optimization framework

Figure 4.5 illustrates the framework for optimizing the performance of buildings during present analysis. EnergyPlus simulation file is created by the Legacy OpenStudio Plug-in for Google SketchUp and IDF Editor utilizing information related to building geometry, thermal and electrical loads, characteristics of construction materials, occupancy schedules etc. EnergyPlus is coupled to GenOpt through user-defined files that carry information relevant to the objective function, independent variables, constraints, optimization algorithm, simulation settings, reporting of errors etc. GenOpt initiates the optimization process and calls EnergyPlus iteratively to perform simulations for a certain set of variable values and subsequently to calculate the value of the objective function. Optimization algorithm then compares the value of the objective function with that of the same at the previous iterative step and directs the optimization process accordingly until an optimal value for the objective function is achieved. This phenomenon is known as the state of convergence of the numerical solution. The optimal value of the objective function (for annual energy consumption or life cycle cost) and the corresponding values of the building envelope variables related to the optimal solution are recorded and made available for visualization and for post processing.

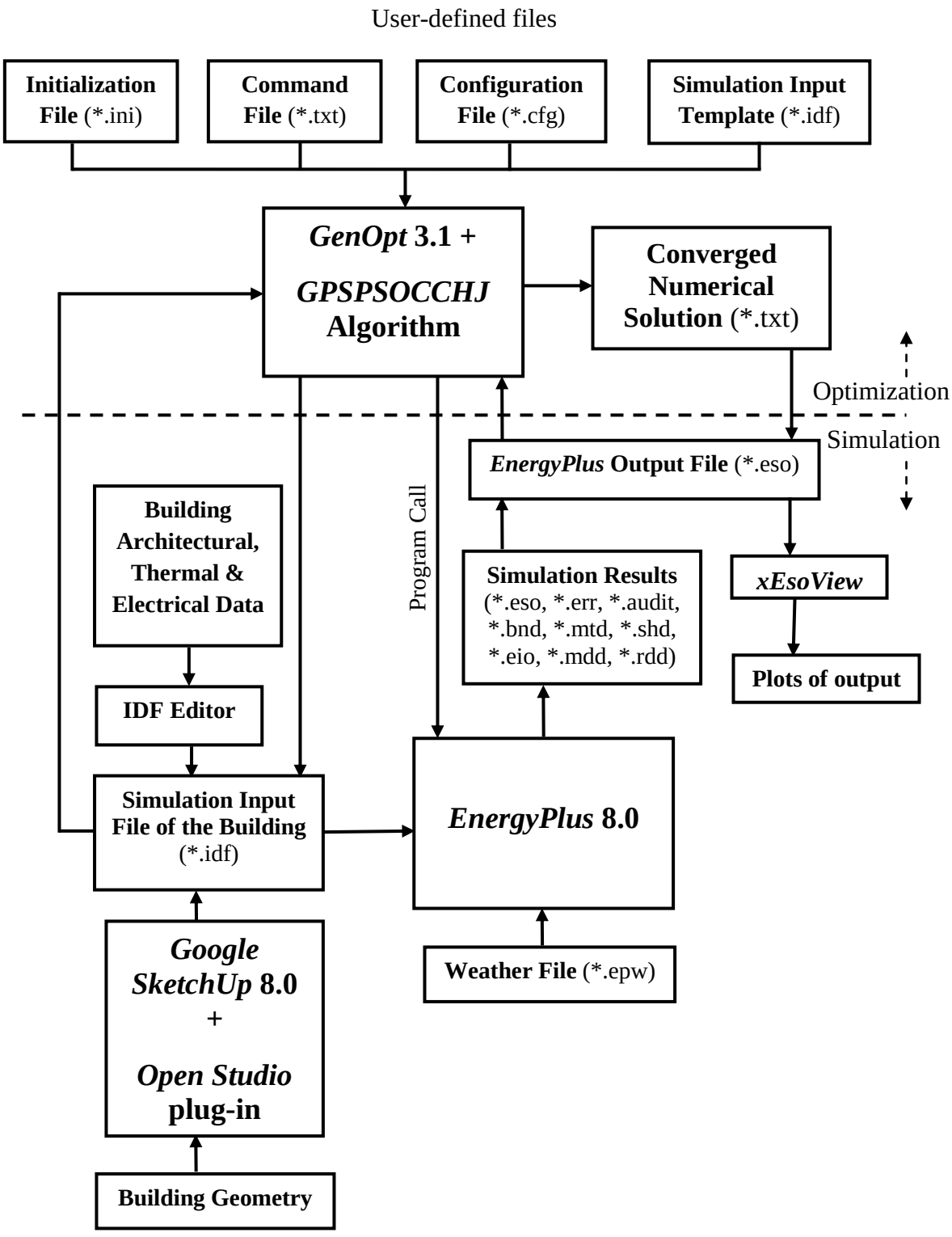

Figure 4.5: Building performance optimization framework

4.5 User-defined and associated files

Several user-defined and associated files have to be created and/or linked to the system before the optimization process is implemented. Sections below elaborate on each of them.

4.5.1 Initialization file

The initialization file having the .ini file format initializes the optimization process by specifying the following information:

- Location of relevant files of the current optimization problem
- Simulation files to be saved for later inspection
- Additional strings that have to be passed to the command that initiates the simulation (such as the name of the simulation input file)
- Number assigned for the objective function value in the simulation output file
- Whether and if so, how the objective function value(s) have to be post-processed
- Which simulation programme is being used

4.5.2 Command file

The command file specifies optimization-related settings such as the independent variables, stopping criteria and the optimization algorithm being used. Independent variables, both continuous and discrete type can be specified in the command file. Continuous variables can take on any values, possibly constrained by lower and upper bound settings. Discrete variables can take on only user-specified discrete values, to be specified in this file. If any variable or input function is specified in the command file, it should appear in the simulation input template file. Command file has .txt file format.

4.5.3 Configuration file

The configuration file contains information related only to the simulation programme used and not to the optimization problem. Hence, it has to be written only once for each simulation programme and relevant operating system. It is recommended to place this file in the directory “cfg” so that it can be used for different optimization

projects. Some configuration files are provided with the GenOpt installation. Configuration file has .cfg file format.

4.5.4 Simulation input file

The simulation input file forms the simulation model of the building under consideration. It consists of the following information related to the building whose performance needs to be optimized:

- Building geometry
- Architectural data
- Materials and construction data
- Building surface, fenestration and shading data
- Electrical loads and schedules
- HVAC system, other building services related data and schedules
- Lighting system and lighting control mechanisms
- Occupancy related data and schedules etc.

Both EnergyPlus IDF Editor and Legacy OpenStudio Plug-in for SketchUp may be used hand in hand to create the simulation input file. It has .idf file format.

4.5.5 Simulation input template file

The simulation input template file is same as the simulation input file but incorporates independent variables governing the optimization process. The variables appearing in this file should be the same as those included in the command file. Simulation input template file has .idf file format.

4.5.6 Weather file

Weather data for more than 2100 locations are now available in EnergyPlus weather format. Weather files for nine locations in Sri Lanka are also available in this database. Weather file contains information on general weather data at a particular location such as dry bulb temperature, dew point temperature, wind speed/direction, atmospheric pressure, solar radiation, cloud conditions, precipitation etc. Weather data do not represent a particular year as such, but represent the typical long-term

weather patterns established through comprehensive analysis of trends. Weather file has .epw file format.

4.5.7 EnergyPlus output file

EnergyPlus output file records all results for a particular EnergyPlus simulation. Type of results appearing in this file depends on the output variables specified in the simulation input file for the building. During the optimization process GenOpt reads and writes data to the EnergyPlus output file by calling EnergyPlus in an iterative manner until an optimal value for the objective function is found. EnergyPlus output file has .eso file format.

4.6 Building case studies

Actual buildings with three different types of envelope designs are optimized in terms of their envelope elements. Selection of envelope designs is based on common architectural practices in Sri Lanka. The sections to follow explain them in detail.

4.6.1 Single-storey building

The single storey building has overall dimensions of 8.0 m x 6.0 m x 3.5 m. Existing base envelope design of the building is shown in Figure 4.6.

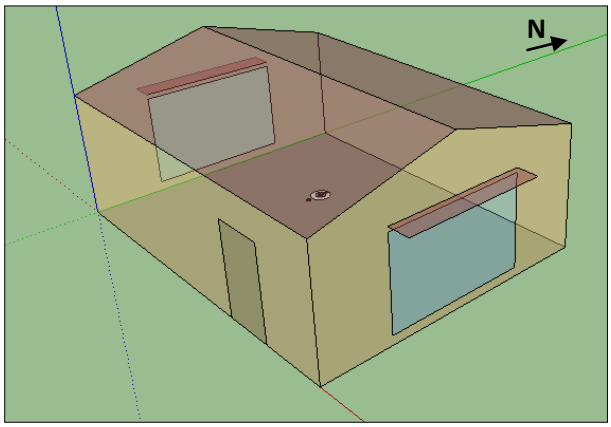

Figure 4.6: Simulation model of the single-storey building

Simulation model of the building consists of a single thermal zone. Table 4.1 gives the details of thermal and electrical loads of the building. Tables 4.2 and 4.3 show construction details of the envelope and details of the envelope variables used in the optimization process respectively.

Table 4.1: Thermal and electrical loads: Single-storey building

Load / System	Description
Occupancy	10 nos. of occupants involved in general office work with a specified occupancy schedule
Heating	Liquefied petroleum gas-fired boiler system with a seasonal efficiency of 85%
Cooling	Chilled water system with a mean plant efficiency of *70%
Temperature control	Temperature control through dual set point, where 20 ^{0}C for heating and 25 ^{0}C for cooling.
Rated artificial lighting	200 W (4.17 W/m^2)
Rated electrical equipment	500 W (10.42 W/m^2)
Building lighting control mechanism	Continuously dims artificial lights to match an illumination set point of 500 lx at the centre of the building at a working plane of 0.8 m above the floor level, with the variation of day light.

*This is an equivalent effective efficiency generally used for chilled water cooling systems

Table 4.2: Construction details: Single-storey building envelope

Element	Construction Details	
Walls	9 inch thick standard brickwork	8 inch thick masonry block work
Roof	Pitched roof of 15^0 with 25 mm thick Calicut tiles	Pitched roof of 15^0 with 6 mm thick Asbestos sheets
Floor	10 mm thick ceramic tiles on a 150 mm thick reinforced concrete slab.	
Door	Each of 1.1 m x 2.0 m made of plywood.	
Windows	3.0 m x 2.0 m double pane windows with 4 mm thick glass and 2 mm thick air space. There exists 0.2 m of wall below the window and 0.5 m of wall above the window. The edge of each window is located 1.5 m from the respective wall edge.	
Shading overhangs	Depth 0.5 m with 0.1 m height above the window. Tilt angle is 90^0.	

Table 4.3: Details of building envelope variables: Single-storey building

Envelope Variable	Type of Variable	Minimum Value	Maximum Value	Base Case Value
Building Azimuth Angle (^{0})	Continuous	0	360	0
Window-to-Wall Ratio (WWR) (%)	Continuous	3.7	34.3	18.1
Horizontal position of east window (m)	Continuous	0.50	2.50	1.50
Vertical position of east window (m)	Continuous	0.20	0.80	0.20
Horizontal position of west window (m)	Continuous	0.50	2.50	1.50
Vertical position of west window (m)	Continuous	0.20	0.80	0.20
Depth of shading overhangs (m)	Continuous	0.30	1.00	0.50
Wall material	Discrete	Brickwork		Masonry Blocks
Roof material	Discrete	Calicut Tiles		Asbestos Sheets

4.6.2 Three - storey building

The three-storey building has overall dimensions of 8.0 m x 12.0 m x 8.9 m. Existing base envelope design of the building is shown in Figure 4.7. It is comprised of six occupancy blocks and each is represented by a separate thermal zone in the simulation model. Table 4.4 gives details of building envelope variables used in the optimization process. Tables 4.5 and 4.6 show details of thermal and electrical loads of the building and construction details of the envelope respectively.

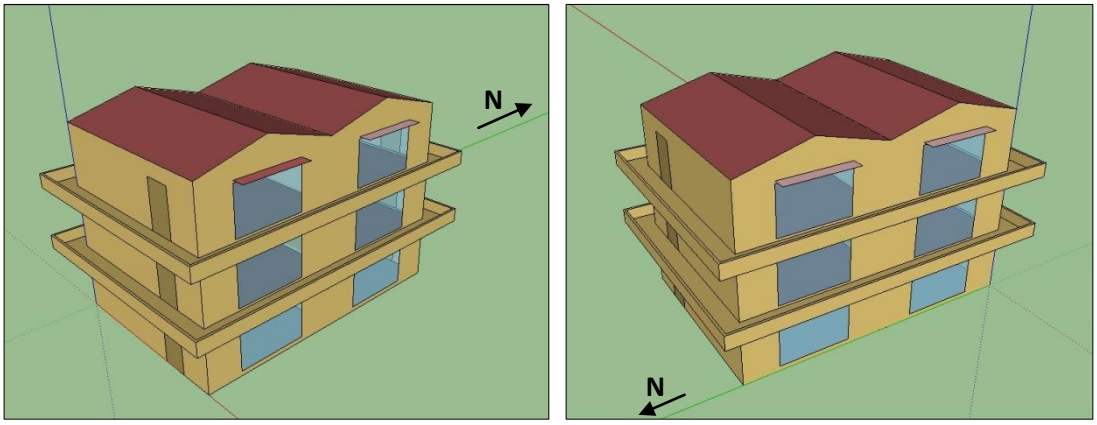

Figure 4.7: Simulation model of the three-storey building

Table 4.4: Details of building envelope variables: Three-storey building

Envelope Element	Type of Variable	Minimum Value	Maximum Value	Base Case Value
Building Azimuth Angle (^{0})	Continuous	0	360	0
Window-to-Wall Ratio (WWR) (%)	Continuous	4.0	62.4	29.9
Horizontal position of east windows (m)	Continuous	0.50	2.50	1.50
Vertical position of east windows (m)	Continuous	0.20	0.80	0.20
Horizontal position of west windows (m)	Continuous	0.50	2.50	1.50
Vertical position of west windows (m)	Continuous	0.20	0.80	0.20
Depth of east shading overhangs (m)	Continuous	0.30	1.00	0.50
Depth of west shading overhangs (m)	Continuous	0.30	1.00	0.50
Wall material	Discrete	Brickwork		Masonry Blocks
Roof material	Discrete	Calicut Tiles		Asbestos Sheets

Table 4.5: Thermal and electrical loads: Three-storey building

Load / System	Description
Occupancy	60 nos. of occupants involved in general office work with a specified occupancy schedule
Heating	Liquefied petroleum gas-fired boiler system with a seasonal efficiency of 85%
Cooling	Chilled water system with a mean plant efficiency of 70%
Temperature control	Temperature control through dual set point, where 20 ^{0}C for heating and 25 ^{0}C for cooling
Rated artificial lighting	1.2 kW (12.50 W/m^2)
Rated electrical equipment	3.0 kW (31.25 W/m^2)
Building lighting control mechanism	Continuously dims artificial lights to match an illumination set point of 500 lx at the centre of each occupancy block at a working plane of 0.8 m above the floor level, with the variation of day light

Table 4.6: Construction details: Three-storey building envelope

Element	Construction Details	
Walls	9 inch thick standard brickwork	8 inch thick masonry block work
Roof	Pitched roof of 15^0 with 25 mm thick Calicut tiles	Pitched roof of 15^0 with 6 mm thick Asbestos sheets
Floor	10 mm thick ceramic tiles on a 150 mm thick reinforced concrete slab	
Doors	Each of 1.1 m x 2.0 m, made of plywood	
Windows	3.0 m x 2.0 m double pane windows with 4 mm thick glass and 2 mm thick air space. There exists 0.2 m of wall below the window and 0.5 m of wall above the window. The edge of each window is located 1.5 m from the respective wall edge.	
Shading overhangs on 3rd floor windows	Depth 0.5 m with 0.1 m height above the window. Tilt angle is 90^0.	

For the two case studies, objective function for the annual primary energy consumption takes the form:

$$f(x) \cong E_{tot} = \frac{Q_{heat}}{0.85} + \frac{Q_{cool}}{0.70} + 3\left(E_{light} + E_{equip.}\right) \tag{4.12}$$

4.6.3 L - shape building

The L-shape building has overall dimensions of 12.0 m x 14.0 m x 3.5 m. Base envelope design of the building is shown in Figure 4.8. This building is comprised of two thermal zones. Table 4.7 gives details of building envelope variables used in the optimization process. Tables 4.8 and 4.9 show details of thermal and electrical loads of the building and the construction details of the envelope respectively.

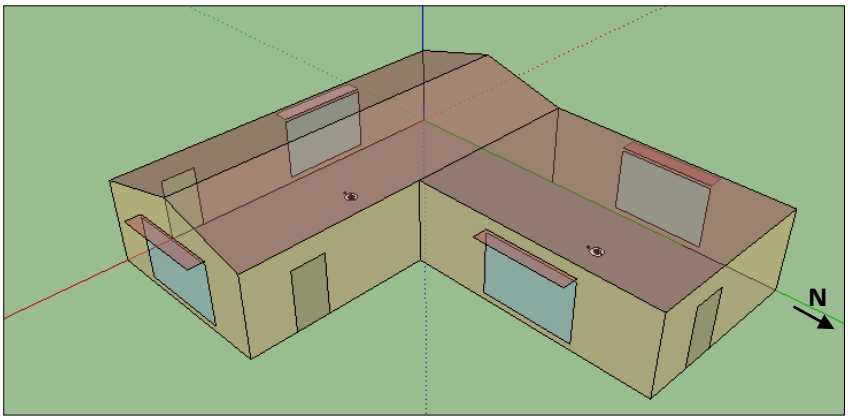

Figure 4.8: Simulation model of the L-shape building

Table 4.7: Details of building envelope variables: L-shape building

Envelope Variable	Type of Variable	Minimum Value	Maximum Value	Base Case Value
Building Azimuth Angle (^{0})	Continuous	0	360	0
Window-to-Wall Ratio (WWR) (%)	Continuous	3.0	53.0	20.9
Horizontal position of east window 1 (m)	Continuous	0.50	2.50	1.50
Vertical position of east window 1 (m)	Continuous	0.20	0.80	0.20
Horizontal position of east window 2 (m)	Continuous	7.50	9.50	8.50
Vertical position of east window 2 (m)	Continuous	0.20	0.80	0.20
Horizontal position of west window (m)	Continuous	7.50	9.50	8.50
Vertical position of west window (m)	Continuous	0.20	0.80	0.20
Horizontal position of south window (m)	Continuous	2.00	4.00	3.00
Vertical position of south window (m)	Continuous	0.20	0.80	0.20
Depth of east window 1 overhang (m)	Continuous	0.30	1.00	0.50
Depth of east window 2 overhang (m)	Continuous	0.30	1.00	0.50
Depth of west window overhang (m)	Continuous	0.30	1.00	0.50
Depth of south window overhang (m)	Continuous	0.30	1.00	0.50
Wall material	Discrete	Brickwork		Masonry Blocks
Roof material	Discrete	Calicut Tiles		Asbestos Sheets

Table 4.8: Thermal and electrical loads: L-shape building

Load / System	Rating and Description
Occupancy	20 nos. of occupants involved in general office work with a specified occupancy schedule
Heating	Liquefied petroleum gas-fired boiler system with a seasonal efficiency of 85%
Cooling	Direct application of electrical energy using DX units
Temperature control	Temperature control through dual set point, where 20 ^{0}C for heating and 25 ^{0}C for cooling
Rated artificial lighting	400 W (3.33 W/m^2)
Rated electrical equipment	1 kW (8.33 W/m^2)
Building lighting control mechanism	Continuously dims artificial lights to match an illumination set point of 400 lx at two reference points at a working plane of 0.8 m above the floor level, with the variation of day light

Table 4.9: Construction details: L-shape building envelope

Element	Construction Details	
Walls	9 inch thick brickwork	8 inch thick masonry block work
Pitched Roof	Pitch angle of 15^0 with 25 mm thick Calicut tiles	Pitched roof of 15^0 with 6 mm thick Asbestos sheets
Slab	150 mm thick reinforced concrete slab	
Floor	10 mm thick ceramic tiles on a 150 mm thick reinforced concrete slab	
Doors	Each of 1.1 m x 2.0 m, made of plywood	
East Windows	02 nos. of 3.0 m x 2.0 m double pane windows with 4 mm thick glass and 2 mm thick air space. There exists 0.2 m of wall below the windows and 0.5 m of wall above the windows. The edge of the two windows is located 1.5 m and 2.5 m from the corresponding wall edge respectively.	
West Window	3.0 m x 2.0 m double pane window with 4 mm thick glass and 2 mm thick air space. There exists 0.2 m of wall below the window and 0.5 m of wall above the window. The edge of the window is located 2.5 m from the wall edge.	
South Window	3.0 m x 2.0 m double pane window with 4 mm thick glass and 2 mm thick air space. There exists 0.2 m of wall below the window and 0.5 m of wall above the window. The edge of the window is located 3.0 m from the wall edge.	
Shading overhangs on all windows	Depth 0.5 m with 0.1 m height above the window. Tilt angle is 90^0.	

Hence objective function for the annual primary energy consumption takes the form:

$$f(x) \cong E_{tot} = \frac{Q_{heat}}{0.85} + 3\left(E_{cool} + E_{light} + E_{equip.}\right) \quad (4.13)$$

Tables 4.10 and 4.11 show the economic data used for the building life cycle cost analysis and settings of the GPSPSOCCHJ algorithm for the optimization process respectively. Settings of the optimization algorithm were established based on recommendations found in the literature and as per numerical experiments conducted during the study, mainly focusing on the stability and level of convergence of the simulations. Data in Tables 4.10 and 4.11 are common for all building case studies considered. Furthermore, all buildings are assumed to be located in the Ratmalana area.

Table 4.10: Economic data for building life cycle cost analysis

Parameter	Value
Lifetime of the building under study (n)	25 yrs.
Nominal discount rate (D)	10.00 %
Rate of inflation (I)	4.70 %
Real discount rate (d)	5.06 %
Annual rate of escalation in electrical energy price (e)	10.00 %
Annual rate of escalation in LPG price (g)	3.00 %
Current price of electrical energy (E_p)	Rs. 12.50 / kWh
Current price of LPG (G_p)	Rs. 2.58 / MJ
Investment cost on envelope walls	Rs. 4500.00 /m^2
Investment cost on envelope windows	Rs. 1100.00 /m^2
Investment cost on HVAC system	Rs. 80,000.00 per Ton

Table 4.11: Settings of the GPSPSOCCHJ algorithm

Parameter	Setting
Neighbourhood Topology	Von-Neumann
Neighbourhood Size	1
Number of Particles	16
Number of Generations	20
Seed	0
Cognitive Acceleration	2.8
Social Acceleration	1.3
Maximum Velocity Gain - Continuous	0.5
Maximum Velocity - Discrete	1.0
Constriction Gain	1.0
Mesh Size Divider	2
Initial Mesh Size Exponent	0
Mesh Size Exponent Increment	1
Number of Step Reductions	20

For all building case studies, objective function for life cycle cost takes the form:

$$f(x) \cong dIC_{walls} + dIC_{windows} + dIC_{HVAC} + \sum_{1}^{25} \frac{(1.1)^j (12.5)\left(dE_j\right) + (1.03)^j (2.58)\left(dG_j\right)}{(1.0506)^j} \quad (4.14)$$

4.7 Summary

This chapter describes the methodology adopted in the study. Development of objective functions representing annual primary energy consumption and life cycle cost has been explained. Furthermore, it elaborates on the optimization framework, numerical scheme and the tools and resources necessary for the analysis. Three buildings with different envelope designs are considered for optimization of performance.

5. OPTIMIZATION RESULTS

5.1 Simulation environment

Extensive numerical tests were conducted prior to modelling and optimizing building case studies. Tests were performed in order to establish the best possible settings for the GPSPSOCCHJ algorithm in terms of stability of the optimization process. Tools were installed and run on an Intel Core i5 2.6 GHz dedicated workstation of 4.0 GB RAM. The sections to follow elaborate on the optimization results for the case studies with respect to annual energy consumption and life cycle cost.

5.2 Single-storey building

5.2.1 Annual energy consumption

Results for the optimal annual energy consumption of the single-storey building are explained here. For the bricks and calicut tiles combination**,** simulations took 2010 iterations, consuming 1 hour and 21 minutes for the solution to converge as shown in Figures 5.1 to 5.3. For other material combinations also similar type of plots were generated. Table 5.1 conducts a comparison among base case and optimal values of the building envelope elements for all material combinations. Table 5.2 gives a summary of comparison between the base case and optimal envelope designs with respect to annual energy consumption for all material combinations.

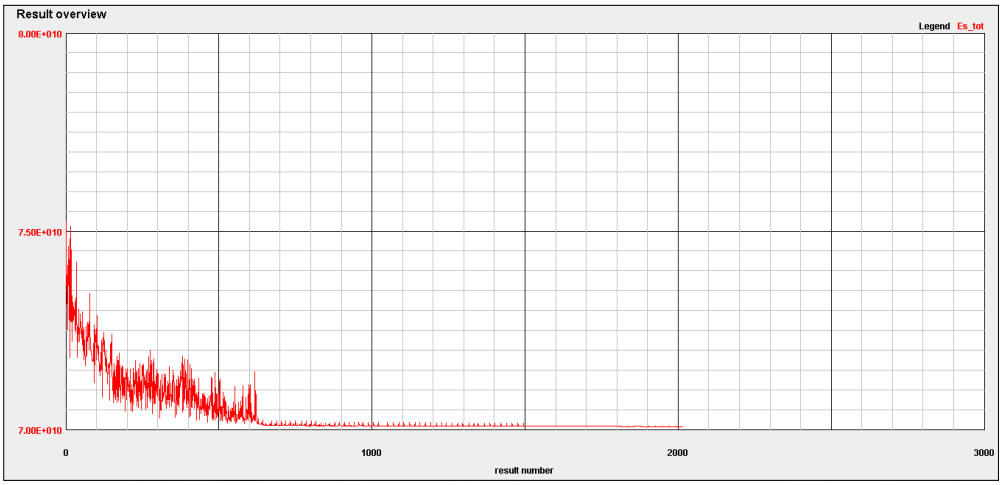

Figure 5.1: Solution for optimal annual energy consumption reaching convergence: Single-storey building

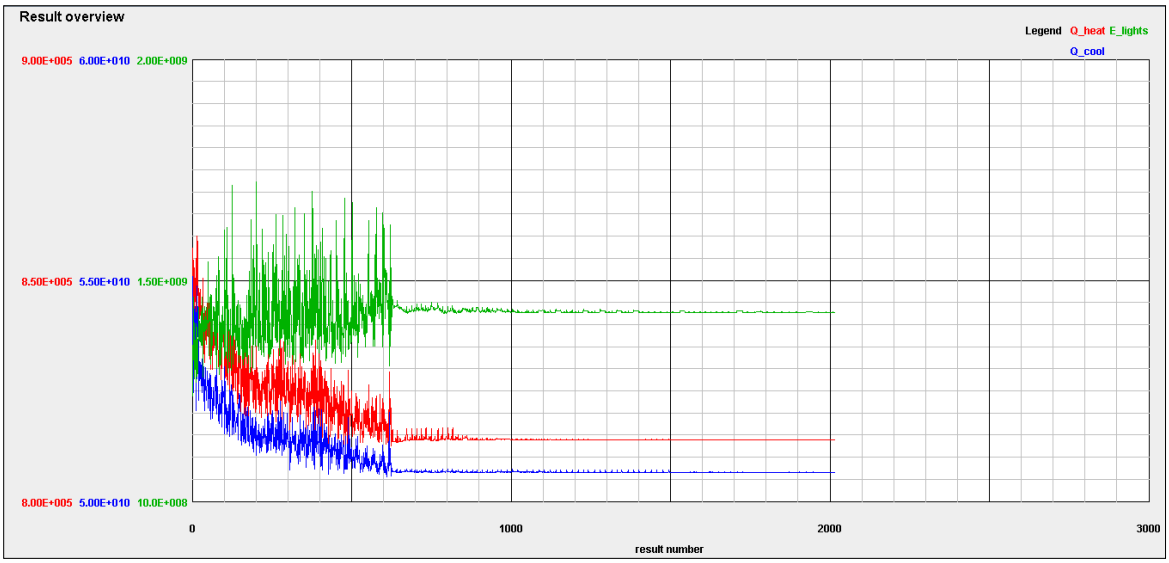

Figure 5.2: Solution for optimal energy consumption for heating, cooling and lighting reaching convergence: Single-storey building

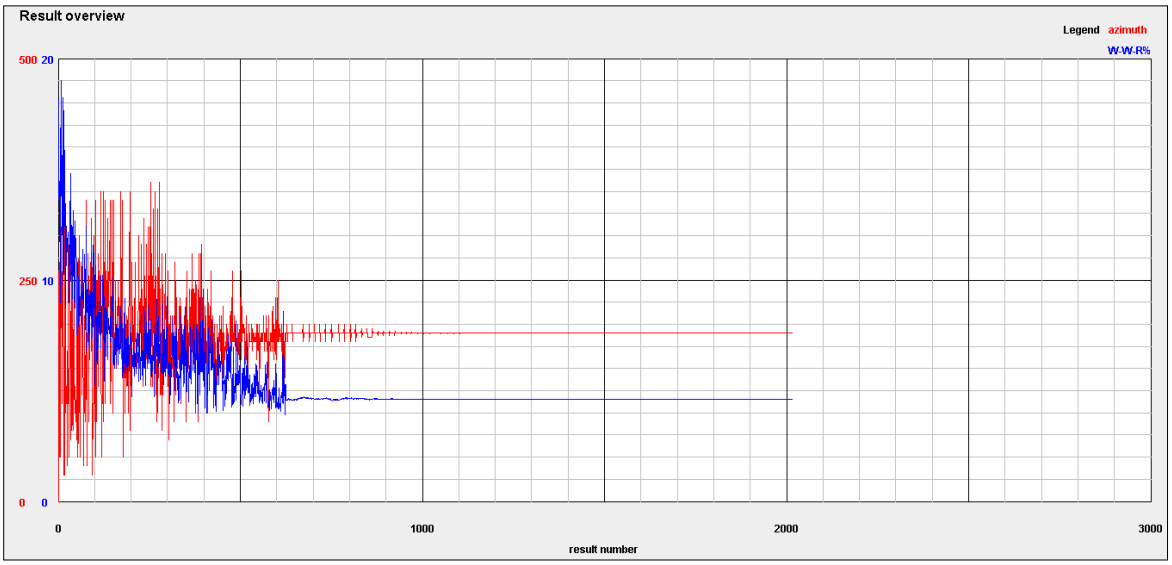

Figure 5.3: Solution for optimal azimuth angle and WWR reaching convergence: Single-storey building

Table 5.2 shows saving potential of the optimal envelope design related to annual primary energy consumption with respect to different wall and roof material combinations. It is observed that the highest saving potential is achieved by the brickwork/calicut tiles combination.

Table 5.1: Comparison among base case and optimal envelope elements: Single-storey building

Envelope Element	Base Case Value	Optimal Value			
		Bricks and Calicut tiles	Bricks and Asbestos sheets	Masonry blocks and Calicut tiles	Masonry blocks and Asbestos sheets
Building Azimuth Angle (^{0})	0	190	190	190	190
Window-to-Wall Ratio (WWR) (%)	18.1	4.6	5.2	4.9	6.0
Horizontal position of east windows (m)	1.50	2.46	2.38	2.10	2.20
Horizontal position of west windows (m)	1.50	2.46	2.34	2.44	2.03
Vertical position of east windows (m)	0.20	0.80	0.80	0.80	0.80
Vertical position of west windows (m)	0.20	0.80	0.80	0.80	0.80
Depth of east shading overhang (m)	0.50	1.00	1.00	1.00	1.00
Depth of west shading overhang (m)	0.50	1.00	1.00	1.00	1.00

Table 5.2: Comparison of annual primary energy consumption: Single-storey building

Wall material	Roof material	Envelope Design	Annual Energy Consumption (GJ)				PMV**
			Q_{heat} x 10^{-3}	Q_{cool}	E_{light}	E_{tot}*	
Bricks	Calicut tiles	Base Case	0.86	55.08	1.24	75.25	0.35
		Optimal	0.81	50.65	1.43	70.07	0.30
		Saving (%)	5.1	8.0	-15.3	6.9	-
Bricks	Asbestos sheets	Base Case	1.17	80.66	1.26	108.53	0.61
		Optimal	0.93	76.36	1.46	103.54	0.59
		Saving (%)	21.1	5.3	-16.1	4.6	-
Masonry blocks	Calicut tiles	Base Case	0.87	56.19	1.24	76.69	0.44
		Optimal	0.84	52.46	1.40	72.33	0.41
		Saving (%)	3.5	6.6	-12.9	5.7	-
Masonry blocks	Asbestos sheets	Base Case	0.90	80.14	1.26	107.84	0.70
		Optimal	0.89	76.39	1.39	103.39	0.68
		Saving (%)	0.9	4.7	-10.9	4.1	-

*Annual primary energy consumption for heating, cooling and lighting
**Predicted Mean Vote of the occupied space

5.2.2 Building life cycle cost

Results for the optimal life cycle cost of the single-storey building are discussed in this section. For bricks and calicut tiles combination**,** simulations took 1700 iterations, consuming 1 hour and 27 minutes for the solution to reach state of convergence as shown in Figures 5.4 to 5.6. For other material combinations also similar type of plots were generated. Table 5.3 makes a comparison among base case and optimal values of the building envelope elements for all material combinations. Table 5.4 provides with a comparison of life cycle cost between the base case and optimal envelope designs for all material combinations.

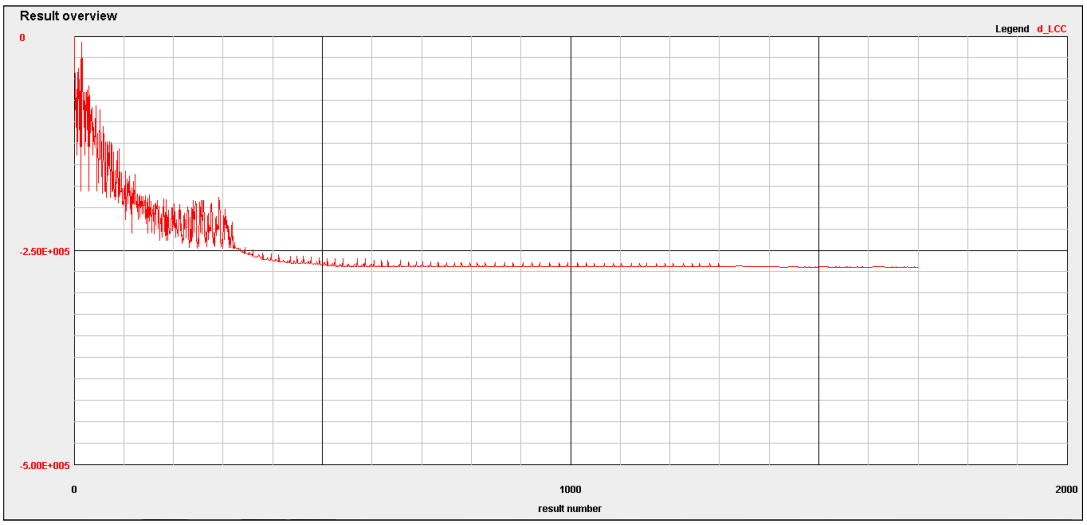

Figure 5.4: Solution for optimal life cycle cost reaching convergence

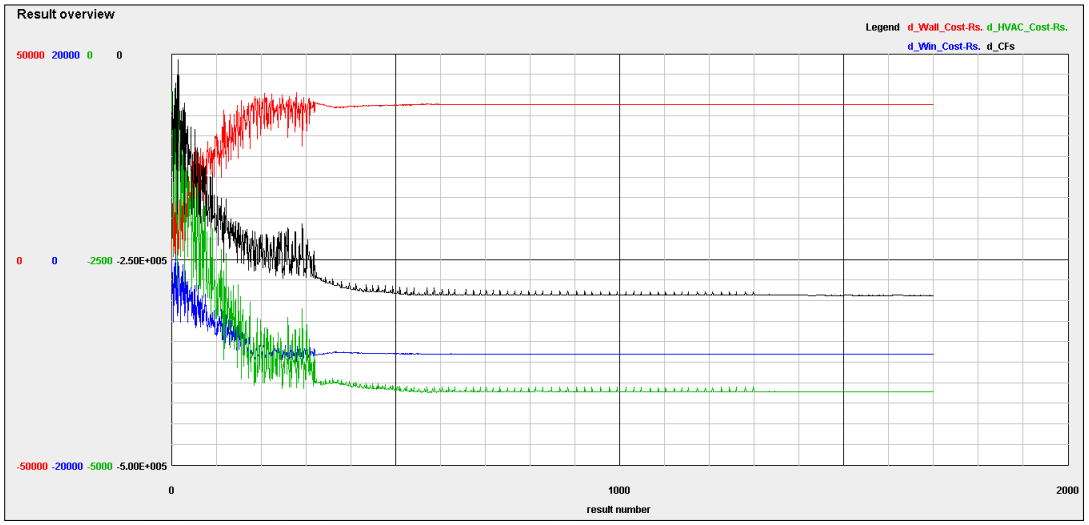

Figure 5.5: Optimal investment and operating costs reaching convergence

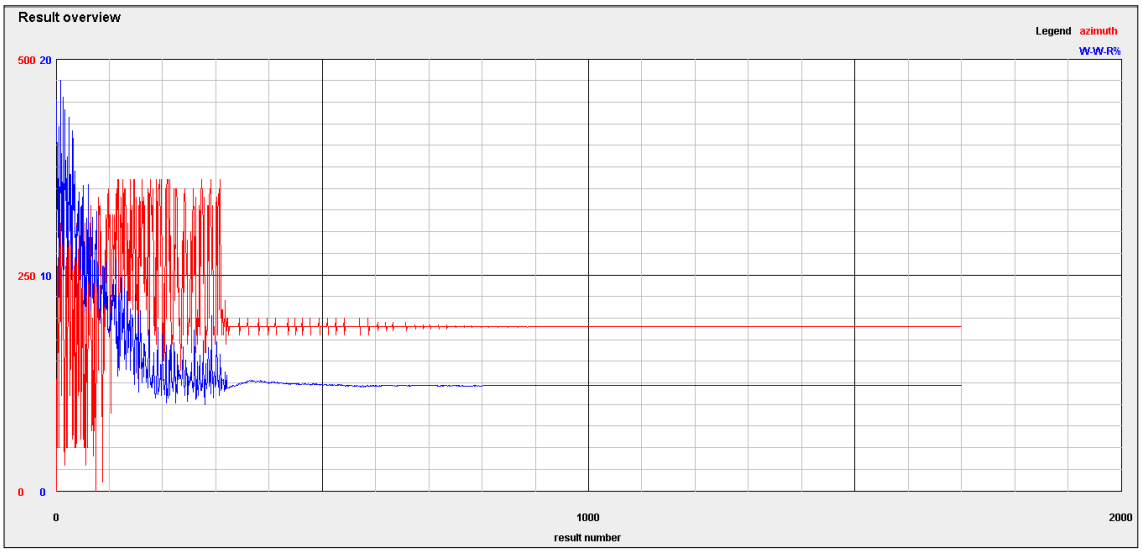

Figure 5.6: Solution for optimal azimuth angle and WWR reaching convergence

Table 5.3: Comparison among base case and optimal values of envelope elements: Single-storey building

Envelope Element	Base Case Value	Optimal Value			
		Bricks and Calicut tiles	Bricks and Asbestos sheets	Masonry blocks and Calicut tiles	Masonry blocks and Asbestos sheets
Building Azimuth Angle (^{0})	0	190	190	190	190
Window-to-Wall Ratio (WWR) (%)	18.1	4.9	5.5	5.2	5.6
Horizontal position of east windows (m)	1.50	2.11	2.46	2.12	2.48
Horizontal position of west windows (m)	1.50	2.45	2.32	2.47	2.33
Vertical position of east windows (m)	0.20	0.80	0.80	0.80	0.80
Vertical position of west windows (m)	0.20	0.80	0.80	0.80	0.80
Depth of east shading overhang (m)	0.50	1.00	1.00	1.00	1.00
Depth of west shading overhang (m)	0.50	1.00	1.00	1.00	1.00

Table 5.4: Building life cycle cost for optimal case: Single-storey building

Material	Change in Life Cycle Cost (dLCC) (Rs.)				Cost Saving (%)	Thermal Comfort	
	Investment Cost (dIC)		Operational Cost (dOC)	dLCC		Envelope Design	PMV*
Bricks and Calicut tiles	dIC_{walls}	37683.00	ΣdOC= -293975.47	-269616.96	5.8	Existing	0.35
	$dIC_{windows}$	-9211.40				Optimal	0.30
	dIC_{HVAC}	-4113.09					
	ΣdIC	24358.51					
Bricks and Asbestos sheets	dIC_{walls}	35604.00	ΣdOC= -283584.34	-260682.54	4.0	Existing	0.61
	$dIC_{windows}$	-8703.20				Optimal	0.59
	dIC_{HVAC}	-3999.00					
	ΣdIC	22901.80					
Masonry blocks and Calicut tiles	dIC_{walls}	36486.00	ΣdOC= -246807.31	-222690.69	4.7	Existing	0.44
	$dIC_{windows}$	-8918.80				Optimal	0.41
	dIC_{HVAC}	-3450.58					
	ΣdIC	24116.62					
Masonry blocks and Asbestos sheets	dIC_{walls}	35226.00	ΣdOC= -252324.75	-229287.80	3.5	Existing	0.70
	$dIC_{windows}$	-8610.80				Optimal	0.68
	dIC_{HVAC}	-3578.25					
	ΣdIC	23036.95					

*Predicted Mean Vote of the occupied space

Table 5.4 shows saving potential of the optimal envelope designs related to life cycle cost with respect to different wall and roof material combinations. Accordingly, as in the case of annual primary energy consumption, highest saving potential of LCC is achieved by the brickwork/calicut tiles combination.

5.3 Three-storey building

5.3.1 Annual energy consumption

Results for the optimal annual energy consumption of the three-storey building are shown below. For the bricks and Calicut tiles combination**,** simulations took 1015 iterations, consuming 2 hours and 54 minutes for the solution to converge as shown in Figures 5.7 to 5.9. For other material combinations also similar type of optimization simulations were conducted. Table 5.5 provides with a comparison among base case and optimal values of the building envelope elements for all material combinations. Table 5.6 gives a comparison of annual energy consumption between base case and optimal envelope designs.

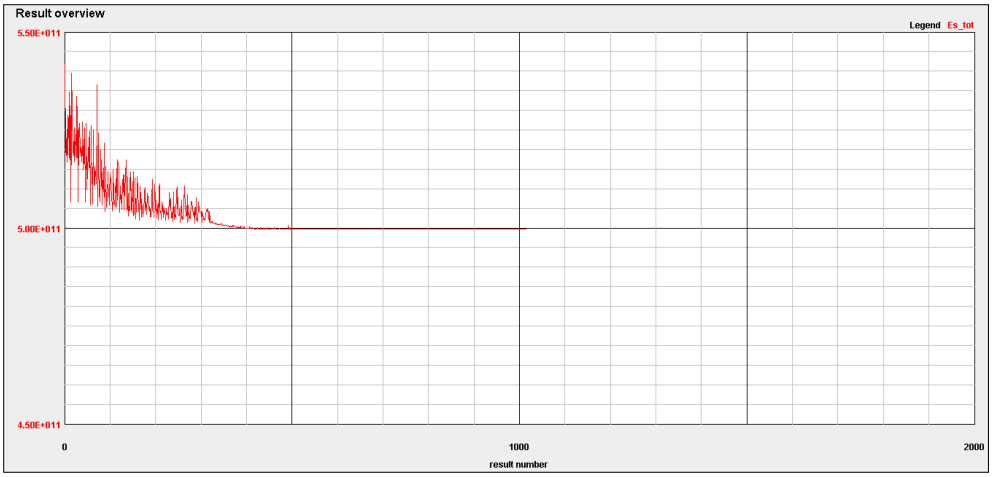

Figure 5.7: Solution for optimal annual energy consumption reaching convergence

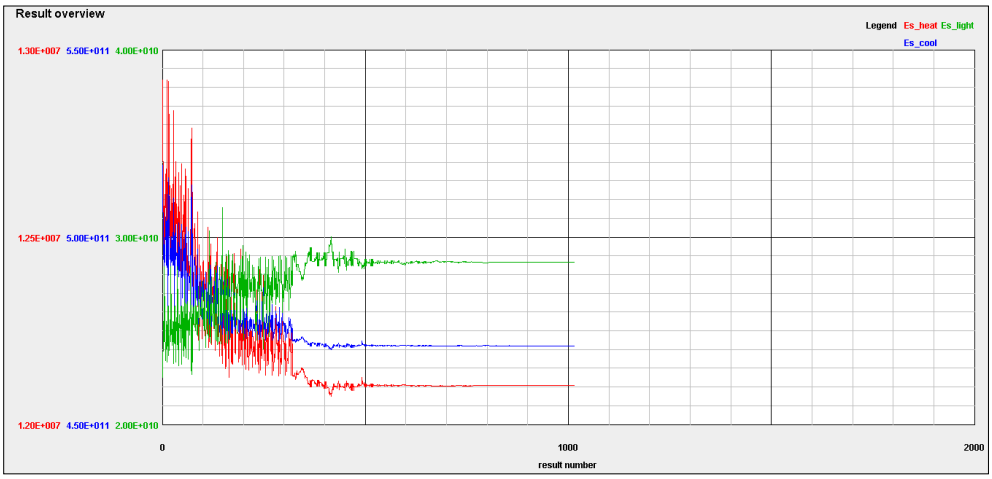

Figure 5.8: Solution for optimal energy consumption for heating, cooling and lighting reaching convergence

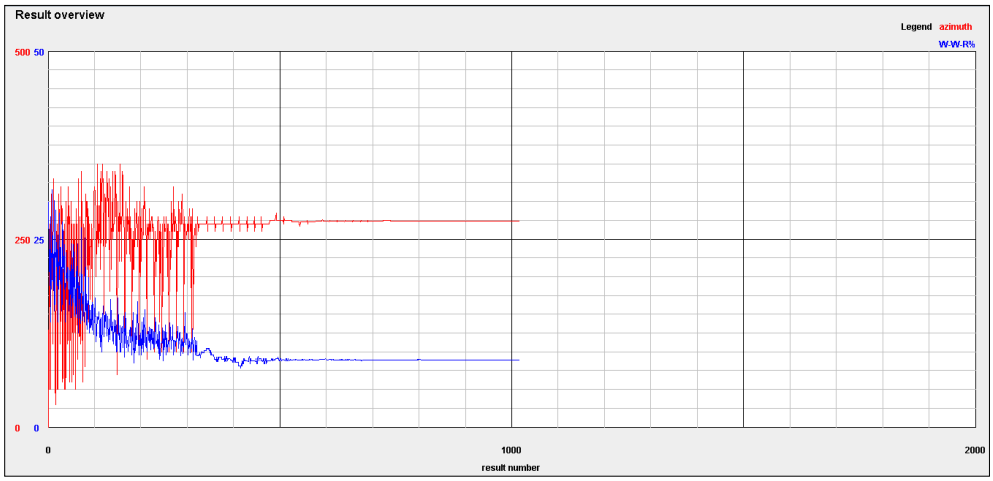

Figure 5.9: Solution for optimal azimuth angle and WWR reaching convergence

Table 5.5: Comparison of values of envelope elements: Three-storey building

Envelope Element	Base Case Value	Optimal Value			
		Bricks and Calicut tiles	Bricks and Asbestos sheets	Masonry blocks and Calicut tiles	Masonry blocks and Asbestos sheets
Building Azimuth Angle (^{0})	0	274	274	274	274
Window-to-Wall Ratio (WWR) (%)	29.9	8.9	9.1	9.3	9.4
Horizontal position of east windows (m)	1.50	2.24	2.24	2.19	2.20
Horizontal position of west windows (m)	1.50	2.39	2.38	2.35	2.30
Vertical position of east windows (m)	0.20	0.80	0.80	0.80	0.80
Vertical position of west windows (m)	0.20	0.80	0.80	0.80	0.80
Depth of east shading overhangs (m)	0.50	1.00	1.00	1.00	1.00
Depth of west shading overhangs (m)	0.50	1.00	1.00	1.00	1.00

Table 5.6: Comparison of annual energy consumption: Three-storey building

Material	Envelope Design	Annual Energy Consumption (GJ)				$PMV_{weighted}$ **
		$Q_{heat} \times 10^{-3}$	Q_{cool}	E_{light}	E_{tot} *	
Bricks and Calicut tiles	Base Case	5.68	399.81	7.51	541.78	0.75
	Optimal	5.32	362.65	9.55	499.65	0.70
	Saving (%)	6.3	9.3	-27.2	7.8	-
Bricks and Asbestos sheets	Base Case	5.73	452.20	7.52	609.86	0.83
	Optimal	5.39	415.73	9.56	568.61	0.79
	Saving (%)	5.9	8.1	-27.1	6.8	-
Masonry blocks and Calicut tiles	Base Case	5.73	404.90	7.51	548.38	0.77
	Optimal	5.43	370.02	9.42	508.83	0.72
	Saving (%)	5.2	8.6	-25.5	7.2	-
Masonry blocks and Asbestos sheets	Base Case	5.77	456.13	7.52	614.96	0.85
	Optimal	5.49	421.70	9.44	576.00	0.82
	Saving (%)	4.8	7.5	-25.5	6.3	-

*Annual primary energy consumption for heating, cooling and lighting
**Weighted Predicted Mean Vote based on the cooling load of each thermal zone

Table 5.6 shows the saving potential of the optimal building envelope design related to annual primary energy consumption with respect to wall and roof material combinations. Accordingly, the highest saving potential is recorded by the brickwork/calicut tiles combination.

5.3.2 Building life cycle cost

Optimization results for the optimal life cycle cost of the three-storey building are shown below. For bricks and Calicut tiles combination**,** simulations took 1183 iterations, consuming 3 hours and 18 minutes for the solution to converge as shown in Figures 5.10 to 5.12. For other material combinations also optimization results were generated.

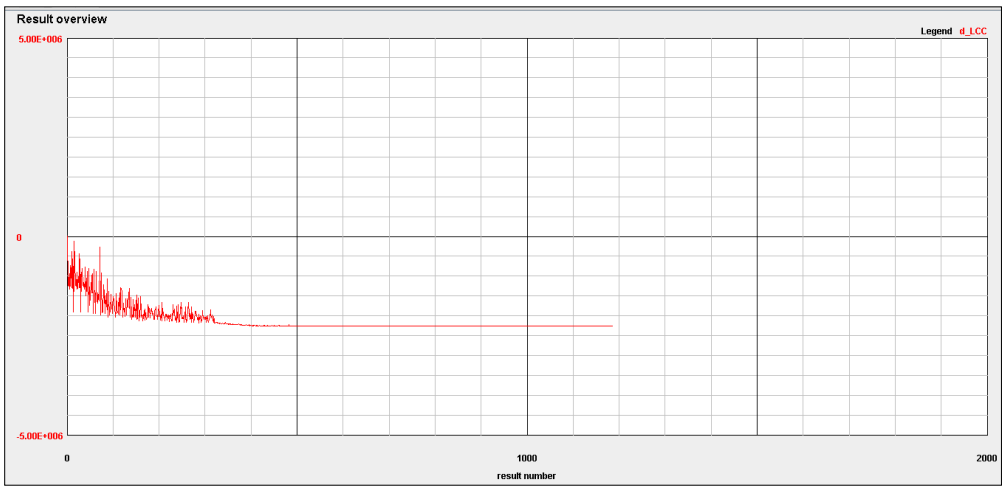

Figure 5.10: Solution for optimal life cycle cost reaching convergence

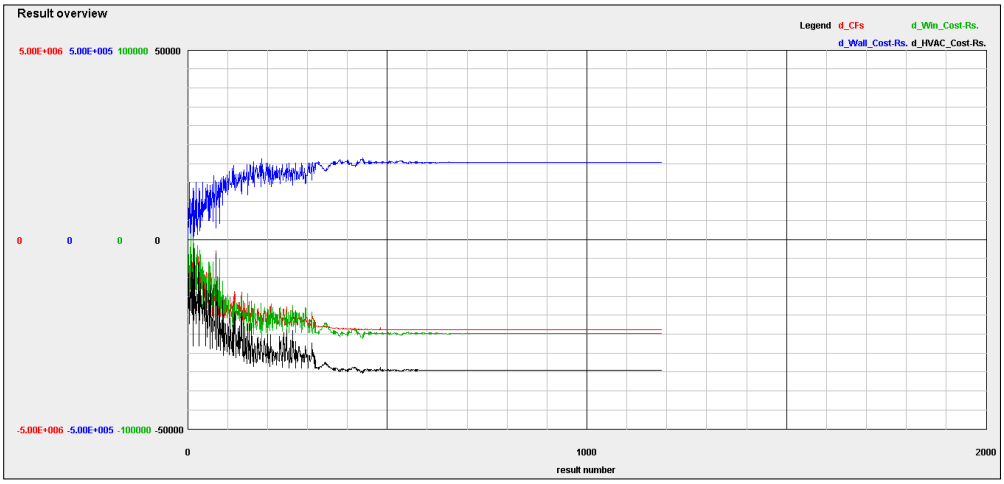

Figure 5.11: Optimal investment and operating costs reaching convergence

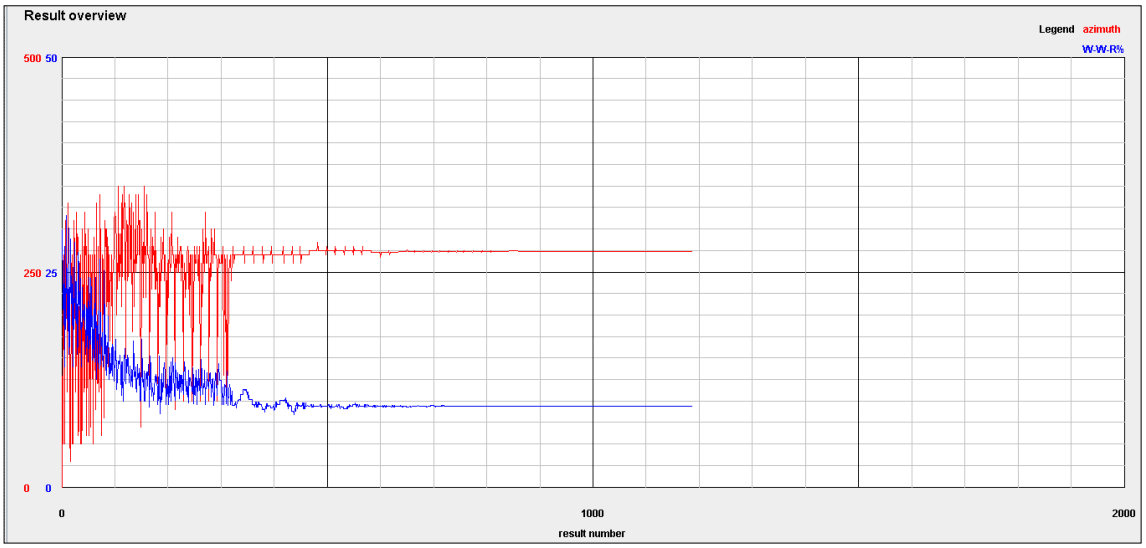

Figure 5.12: Solution for optimal azimuth angle and WWR reaching convergence

Table 5.7 shows a comparison among existing and optimal values of building envelope elements for all material combinations. Table 5.8 gives a comparison of life cycle cost between the base case and optimal envelope designs for all material combinations.

Table 5.7: Comparison of values of envelope elements: Three-storey building

Envelope Element	**Base Case Value**	**Optimal Value**			
		Bricks and Calicut tiles	**Bricks and Asbestos sheets**	**Masonry blocks and Calicut tiles**	**Masonry blocks and Asbestos sheets**
Building Azimuth Angle (^{0})	0	274	274	274	274
Window-to-Wall Ratio (WWR) (%)	29.9	9.4	9.6	9.8	9.9
Horizontal position of east windows (m)	1.50	2.21	2.17	2.10	2.15
Horizontal position of west windows (m)	1.50	2.36	2.31	2.31	2.27
Vertical position of east windows (m)	0.20	0.80	0.80	0.80	0.80
Vertical position of west windows (m)	0.20	0.80	0.80	0.80	0.80
Depth of east shading overhangs (m)	0.50	1.00	1.00	1.00	1.00
Depth of west shading overhangs (m)	0.50	1.00	1.00	1.00	1.00

Table 5.8: Building life cycle cost for optimal case: Three-storey building

Material	Change in Life Cycle Cost (dLCC) (Rs.)				Cost Saving (%)	Thermal Comfort	
	Investment Cost (dIC)		Operational Cost (dOC)	dLCC		Envelope Design	PMV*
Bricks and Calicut tiles	dIC_{walls}	203508.81	ΣdOC = -2385423.25	-2266230.54	7.0	Existing	0.75
	$dIC_{windows}$	-49746.60				Optimal	0.70
	dIC_{HVAC}	-34569.50					
	ΣdIC	119192.71					
Bricks and Asbestos sheets	dIC_{walls}	200983.90	ΣdOC = -2335082.09	-2217127.34	6.1	Existing	0.83
	$dIC_{windows}$	-49129.40				Optimal	0.79
	dIC_{HVAC}	-33899.75					
	ΣdIC	117954.75					
Masonry blocks and Calicut tiles	dIC_{walls}	198621.38	ΣdOC = -2238206.90	-2120549.86	6.5	Existing	0.77
	$dIC_{windows}$	-48551.89				Optimal	0.72
	dIC_{HVAC}	-32412.45					
	ΣdIC	117657.04					
Masonry blocks and Asbestos sheets	dIC_{walls}	196890.11	ΣdOC = -2205274.15	-2088516.29	5.7	Existing	0.85
	$dIC_{windows}$	-48128.69				Optimal	0.82
	dIC_{HVAC}	-32003.56					
	ΣdIC	116757.86					

*Weighted Predicted Mean Vote based on the cooling load of each thermal zone

Table 5.8 shows saving potential of the optimal building envelope design related to life cycle cost with respect to different wall and roof material combinations. Accordingly, as in the case of annual energy consumption, the highest saving potential for LCC is predicted for the brickwork/calicut tiles combination.

5.4 L - shape building

5.4.1 Annual energy consumption

Optimization results for the optimal annual energy consumption of the L- shape building are shown below. For the bricks and calicut tiles combination**,** the simulation took 3170 iterations, consuming 3 hours and 48 minutes for the solution to converge as shown in Figures 5.13 to 5.15. For other material combinations also similar type of plots were generated. Table 5.9 performs a comparison among existing and optimal values of the building envelope elements for all material combinations. Table 5.10 gives a comparison of annual energy consumption between the base case and optimal envelope designs for all material combinations.

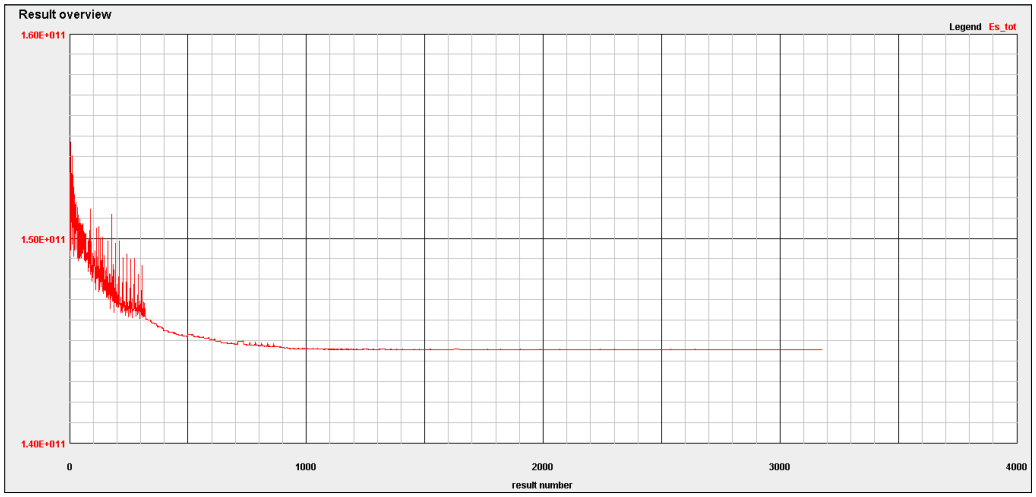

Figure 5.13: Optimal annual primary energy consumption reaching convergence

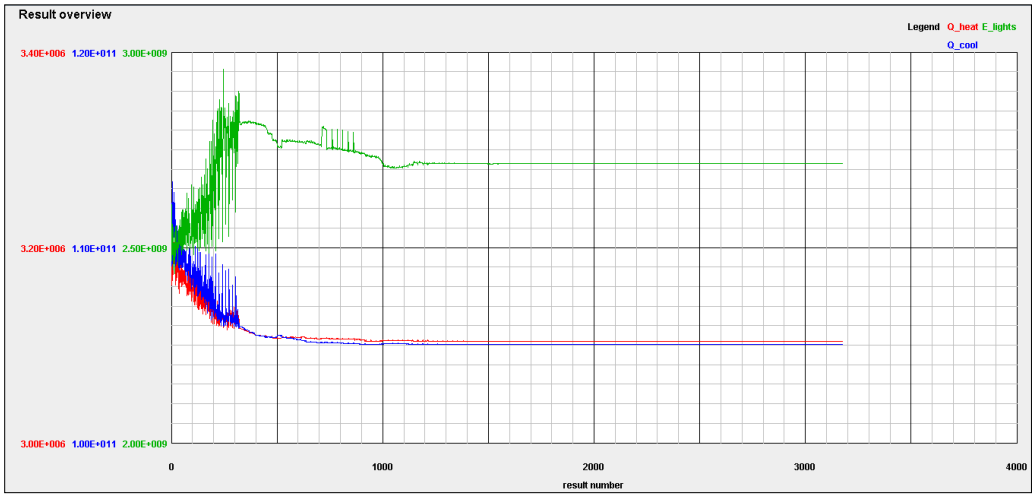

Figure 5.14: Solution for optimal energy consumption for heating, cooling and lighting reaching convergence

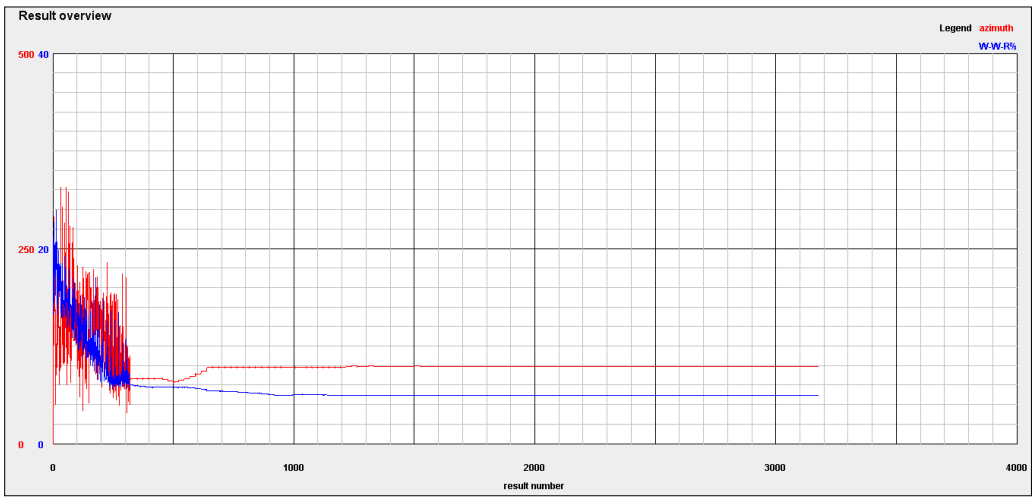

Figure 5.15: Solution for optimal azimuth angle and WWR reaching convergence

Table 5.9: Comparison among base case and optimal values of envelope elements: L-shape building

Envelope Element	Base Case Value	Optimal Value			
		Bricks and Calicut tiles	**Bricks and Asbestos sheets**	**Masonry blocks and Calicut tiles**	**Masonry blocks and Asbestos sheets**
Building Azimuth Angle (^{0})	0	99	82	100	170
Window-to-Wall Ratio (WWR) (%)	20.9	5.0	5.4	5.0	5.4
Horizontal position of east window 1 (m)	1.50	2.50	2.50	2.50	2.50
Horizontal position of east window 2 (m)	8.50	9.50	9.50	9.50	9.50
Horizontal position of west window (m)	8.50	9.50	9.50	9.50	9.50
Horizontal position of south window (m)	3.00	4.00	4.00	4.00	4.00
Vertical position of east window 1 (m)	0.20	0.80	0.80	0.80	0.80
Vertical position of east window 2 (m)	0.20	0.80	0.80	0.80	0.80
Vertical position of west window (m)	0.20	0.80	0.55	0.80	0.80
Vertical position of south window (m)	0.20	0.80	0.80	0.80	0.80
Depth of east window 1 overhang (m)	0.50	1.00	1.00	1.00	1.00
Depth of east window 2 overhang (m)	0.50	1.00	1.00	1.00	1.00
Depth of west window overhang (m)	0.50	1.00	1.00	1.00	1.00
Depth of south window overhang (m)	0.50	1.00	1.00	1.00	1.00

Table 5.10: Comparison of annual energy consumption: L-shape building

Material	Envelope Design	Annual Energy Consumption (GJ)				PMV**
		Q_{heat} x 10^{-3}	E_{cool}	E_{light}	E_{tot}*	
Bricks and Calicut tiles	Base Case	3.19	150.77	2.46	153.23	0.43
	Optimal	3.10	141.85	2.71	144.56	0.39
	Saving (%)	2.7	5.9	-10.1	5.7	-
Bricks and Asbestos sheets	Base Case	3.30	197.06	2.49	199.55	0.61
	Optimal	3.26	188.37	2.72	191.09	0.58
	Saving (%)	1.1	4.4	-9.2	4.2	-
Masonry blocks and Calicut tiles	Base Case	3.23	153.71	2.46	156.17	0.50
	Optimal	3.16	145.77	2.70	148.47	0.47
	Saving (%)	2.1	5.2	-9.8	4.9	-
Masonry blocks and Asbestos sheets	Base Case	3.32	197.80	2.49	200.29	0.67
	Optimal	3.29	189.73	2.65	192.38	0.65
	Saving (%)	1.1	4.1	-6.4	3.9	-

*Annual primary energy consumption for heating, cooling and lighting
**Predicted Mean Vote of the occupied space

Table 5.10 shows the saving potential of the optimal building envelope design related to annual primary energy consumption with respect to various wall and roof material combinations. Accordingly, the highest saving potential of annual energy consumption is predicted for the brickwork/calicut tiles combination.

5.4.2 Building life cycle cost

Optimization results for the optimal life cycle cost of the L-shape building are shown below. For the bricks and calicut tiles combination**,** simulations took 2533 iterations, consuming 2 hours and 36 minutes for the solution to reach the state of convergence as shown in Figures 5.16 to 5.18. For other material combinations also similar type of results were generated. Table 5.11 gives a comparison among existing and optimal values of the building envelope elements for all material combinations. Table 5.12 shows a comparison of life cycle cost between the base case and optimal envelope designs for all material combinations.

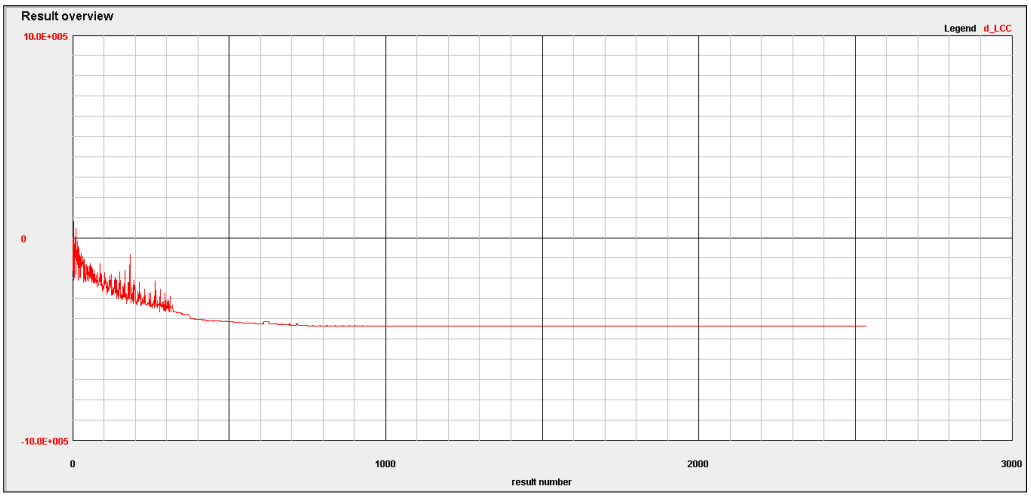

Figure 5.16: Solution for the optimal life cycle cost reaching convergence

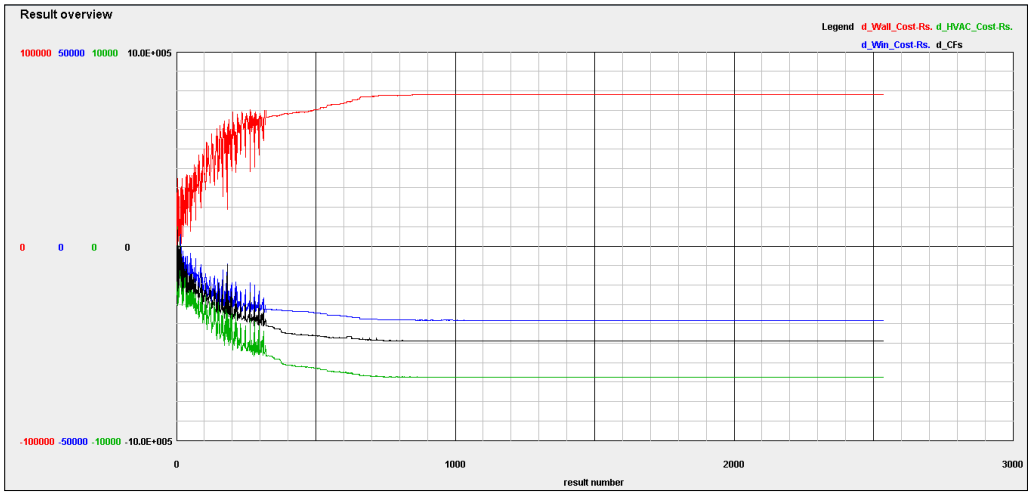

Figure 5.17: Optimal investment cost and operating cost reaching convergence

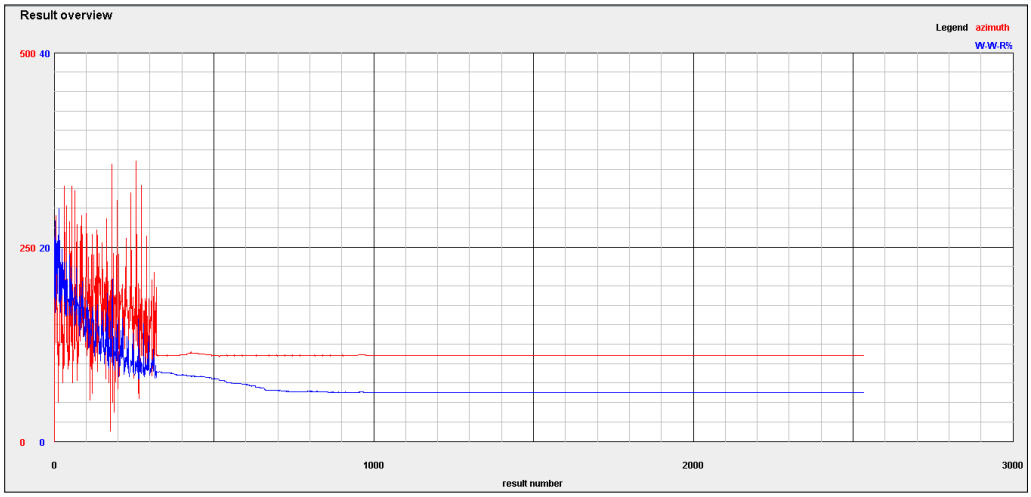

Figure 5.18: Solution for optimal azimuth angle and WWR reaching convergence

Table 5.11: Comparison among base case and optimal values of envelope elements: L-shape building

Envelope Element	Base Case Value	Optimal Value			
		Bricks and Calicut tiles	Bricks and Asbestos sheets	Masonry blocks and Calicut tiles	Masonry blocks and Asbestos sheets
Building Azimuth Angle (^{0})	0	111	170	112	95
Window-to-Wall Ratio (WWR) (%)	20.9	5.0	5.6	5.8	5.2
Horizontal position of east window 1 (m)	1.50	2.50	2.50	2.50	2.50
Horizontal position of east window 2 (m)	8.50	9.50	9.50	9.50	9.50
Horizontal position of west window (m)	8.50	9.50	9.50	9.08	9.45
Horizontal position of south window (m)	3.00	4.00	4.00	4.00	4.00
Vertical position of east window 1 (m)	0.20	0.80	0.80	0.80	0.80
Vertical position of east window 2 (m)	0.20	0.80	0.80	0.80	0.80
Vertical position of west window (m)	0.20	0.80	0.80	0.80	0.80
Vertical position of south window (m)	0.20	0.80	0.80	0.80	0.80
Depth of east window 1 overhang (m)	0.50	1.00	1.00	1.00	1.00
Depth of east window 2 overhang (m)	0.50	1.00	1.00	1.00	1.00
Depth of west window overhang (m)	0.50	1.00	1.00	1.00	1.00
Depth of south window overhang (m)	0.50	1.00	1.00	1.00	1.00

Table 5.12: Building life cycle cost for optimal case: L-shape building

Material	Change in Life Cycle Cost (dLCC) (Rs.)				Cost Saving (%)	Thermal Comfort	
	Investment Cost (dIC)		Operational Cost (dOC)	dLCC		Envelope Design	PMV*
Bricks and Calicut tiles	dIC_{walls}	78048.00	ΣdOC = -490030.68	-437827.39	4.7	Existing	0.43
	$dIC_{windows}$	-19078.40					
	dIC_{HVAC}	-6766.31				Optimal	0.39
	ΣdIC	52203.29					
Bricks and Asbestos sheets	dIC_{walls}	75114.00	ΣdOC = -497919.69	-447847.60	3.7	Existing	0.61
	$dIC_{windows}$	-18361.20					
	dIC_{HVAC}	-6680.71				Optimal	0.58
	ΣdIC	50072.09					
Masonry blocks and Calicut tiles	dIC_{walls}	73890.00	ΣdOC = -431148.05	-381173.18	4.0	Existing	0.50
	$dIC_{windows}$	-18062.00					
	dIC_{HVAC}	-5853.13				Optimal	0.47
	ΣdIC	49974.87					
Masonry blocks and Asbestos sheets	dIC_{walls}	77229.00	ΣdOC = -452694.84	-400590.33	3.3	Existing	0.67
	$dIC_{windows}$	-18878.20					
	dIC_{HVAC}	-6246.29				Optimal	0.64
	ΣdIC	52104.51					

*Predicted Mean Vote of the occupied space

Table 5.12 shows the saving potential of the optimal building envelope design related to life cycle cost with respect to different wall and roof material combinations. Accordingly, as in the case of annual energy consumption, the highest saving potential of life cycle cost is achieved by the brickwork/calicut tile combination.

5.5 Weighted Predicted Mean Vote (PMV)

The weighted PMV is predicted by EnergyPlus with respect to each building case study, for both the base case design and optimal envelope design. It was observed that the optimal envelope design always led to a better weighted PMV for the occupants in all case studies. For all three buildings modelled and optimized, worst weighted PMV was recorded with respect to Masonry blocks and Asbestos sheets combination. The penalty function included in the two objective functions has been successful in restricting the worst weighted PMV only to 0.82 in all cases.

5.6 Summary

This chapter interprets optimization results of building performance related to the three case studies with respect to annual energy consumption and life cycle cost. Predictions show that in all case studies, highest saving both in terms of annual energy consumption and life cycle cost is achieved for the combination of brickwork/Calicut tiles.

6. STRATEGIES FOR MAKING RELIABLE PREDICTIONS

6.1 Issues and challenges

It is observed that Energy Simulation (ES) tools such as EnergyPlus show certain inherent deficiencies in predicting the performance of buildings (Lomas, 1996; Loutzenhiser et al., 2009; Zhai et al., 2001). Several reasons have contributed to this situation. The said tools use a simplification of a uniform air temperature within the thermal zone due to application of the *well-mixed* model. This simplification may be acceptable for small buildings. However, for moderate and large buildings, i.e. those typically produce non-uniform air temperature distributions within the occupied space, such as displacement ventilation systems with stratified flow conditions and also for spaces with surfaces having substantially different temperatures, ES tools are not in a position to give acceptable and reliable energy consumption predictions (Zhai et al., 2001). Moreover, surface convective heat transfer coefficients applied by the ES tools are generally determined through predefined empirical correlations and hence have limited applicability due to simplifications made. The tools are unable to provide with information on the airflow field introduced by building spatial configurations, especially in natural ventilation (Zhai et al., 2001). EnergyPlus uses several empirical correlations to calculate convective heat transfer coefficients during building performance analysis as indicated below ("EnergyPlus Engineering Reference", 2013). The simple natural convection model in EnergyPlus uses constant convective heat transfer coefficients for different envelope surface configurations as given in Table 6.1.

Table 6.1: Simple natural convection model

Configuration	**h (W/m^2K)**
Horizontal surface with reduced convection	0.948
Horizontal surface with enhanced convection	4.040
Vertical surface	3.076
Tilted surface with reduced convection	2.281
Tilted surface with enhanced convection	3.870

Source: EnergyPlus Engineering Reference (2013)

The detailed natural convection model correlates mean surface convective heat transfer coefficient (h) to the surface orientation and the difference between the mean surface temperature and mean zone air temperature (ΔT) as expressed by equations 6.1 to 6.3.

- If ΔT = 0 or a vertical surface, then

$$h = 1.31|\Delta T|^{1/3} \tag{6.1}$$

- If ΔT < 0 with an upward facing surface or ΔT > 0 with an downward facing surface, then

$$h = \frac{9.482|\Delta T|^{\frac{1}{3}}}{7.283 - |cos\,\Sigma|} \tag{6.2}$$

  where Σ is the surface tilt angle.

- If ΔT > 0 with an upward facing surface or ΔT < 0 with an downward facing surface, then

$$h = \frac{1.810|\Delta T|^{\frac{1}{3}}}{1.382 + |cos\,\Sigma|} \tag{6.3}$$

The ceiling diffuser model correlates mean surface convective heat transfer coefficient to the air changes per hour (ACH) as shown in Table 6.2.

Table 6.2: Ceiling diffuser model

Building Element	**h (W/m^{2}K)**
Floors	$3.873 + 0.082(ACH)^{0.980}$
Ceilings	$2.234 + 4.099(ACH)^{0.503}$
Walls	$1.208 + 1.012(ACH)^{0.604}$

Source: EnergyPlus Engineering Reference (2013)

Furthermore, ES tools do not have the intention to model air circulation through the building space explicitly. However, knowledge on the airflow field is vital in predicting the temperature field of building air and also the heating and/or cooling load and eventually energy consumption of the building. Also spatially-averaged thermal comfort predictions by ES tools are not sufficient to satisfy advanced design requirements at present (Zhai et al., 2001). Hence on this basis, ES tools often find it

difficult to make reliable predictions on energy performance of buildings. It is observed that many energy simulation tools under-predict energy consumption in buildings, especially under sunny conditions (Loutzenhiser et al., 2009), typically experienced in a tropical country such as Sri Lanka. Spitler, Pedersen, Fisher, Menne, and Cantillo (1991) and Lomas (1996) found that this discrepancy of energy consumption may even reach up to 37%.

On the other hand, Computational Fluid Dynamics (CFD) tools can predict airflow paths, velocities, relative humidities and contaminant concentrations within an occupied space extensively (Zhai et al., 2001). Also, they are capable of determining the air temperature distribution within the building space and convective heat transfer coefficients at the building envelope. The predictions can be further extended to determine thermal comfort indices such as Predicted Mean Vote (PMV), Percentage of People Dissatisfied due to discomfort (PPD), Percentage Dissatisfied due to draft and ventilation effectiveness (Zhai et al., 2001). For CFD simulations, boundary of the solution domain is the internal surface of the building envelope. Hence, it is a challenging task to assign corresponding boundary conditions for CFD simulations since they depend on several parameters such as construction details of the building envelope, outside weather conditions etc. However, this information is readily available with energy simulation tools that can be transferred directly to CFD. On the other hand, envelope surface convective heat transfer coefficients predicted by CFD can be directly transferred to the ES tool in place of its in-built empirical correlations, in order to predict energy consumption of the building more accurately. On this basis, it is clear that if Energy Simulation and Computational Fluid Dynamics are coupled, more accurate and reliable predictions for building energy consumption can be made. This can be done through complementary data exchange in between the said tools on a common platform. This concept is elaborated in detail in the sections to follow.

6.2 ES and CFD coupling strategy

Many attempts have been made for coupling Energy Simulation and Computational Fluid Dynamics tools. Negrao (1995) performed a complete iterative coupling between ES and CFD. A full iterative strategy was implemented, where coupled

variables were exchanged at each iterative step until a convergence criterion was reached at each time step. Beausoleil-Morrison and Clarke (1998) and Beausoleil-Morrison (2000, 2001) continued the work of Negrao (1995, 1998) through investigation of coupling between ES and CFD.

Bartak et al. (2002) conducted an empirical validation of the coupled model of Beausoleil-Morrison (2000). Djunaedy, Hensen, and Loomans (2003, 2004) and Zhai et al. (2001) analyzed the pros and cons of internal coupling of ES and CFD. Zhai et al. (2002, 2003, 2004) investigated different coupling strategies extensively. Their results revealed that for spaces of moderate size, without having significant temperature stratification, coupling of ES and CFD gives marginal improvement in energy performance predictions. However, those with large temperature stratification, discrepancy between the coupled approach and ES alone can be as high as 42%. Wang and Chen (2005) and Wang (2007) proved that combined ES and CFD approach has a unique solution. Wang and Wong (2008) developed a text-based interface for establishing automated coupling in order to exchange information between ES and CFD tools. According to Djunaedy (2005), coupling strategies between ES and CFD can be categorized as:

- Internal coupling (Hard coupling): Two or more sets of equations are combined and solved at the same time (Conjugate heat transfer method)
- Internal coupling (Loose coupling): Two or more sets of equations are solved separately, and data exchanged during calculations
- External coupling (Loose coupling): Two or more sets of equations solved separately, in ES and CFD programmes, and data exchange takes place during calculations

The application of the conjugate heat transfer approach has several disadvantages. The difference in stiffness of the fluid and the solid side of the model leads to difficulties in obtaining a converged solution (Chen, Peng, & Van Passen, 1995). It is computationally expensive since the computing time increases drastically due to the difference in the time scales related to dynamics in fluids (few seconds) and dynamics in solids (few hours) encountered in buildings (Zhai et al., 2001). Although internal coupling (Loose coupling) solves some of the issues in the first method,

internal coupling approach as a whole is also a computationally expensive approach (Djunaedy, 2005). Benefits of external coupling include (Zhang, Lam, Yao, & Zhang, 2012):

- Computationally less expensive
- ES and CFD models can be maintained and updated individually

However, certain building simulation research (Djunaedy et al., 2004) revealed that the difference in results between internal and external coupling is not significant. Djunaedy (2005) stated that validation results clearly show that ES-CFD external coupling approach offered certain advantages over internal coupling method. Furthermore, he found out that external coupling has the capability to simulate dynamic changes in the building airflow pattern over the simulation period at the same accuracy as that of internal coupling.

Zhai et al. (2001) described an approach known as the staged coupling as shown in Figure 6.1. Definitions of "static" and "dynamic" coupling have been established based on the operating behaviour of coupling between ES and CFD tools (Zhai et al., 2001). Hence, dynamic coupling approach performs continuous exchange of data whereas static coupling involves occasional exchange of data between the two tools during the entire simulation period.

As per Zhai et al. (2001), static coupling performs one-step or two-step exchange of data between ES and CFD tools. They further argued that one-step static coupling is a good choice in an air conditioned room with low velocity mixing ventilation where inlet conditions and wall temperatures are needed for the CFD tool as inputs.

Dynamic coupling involves coupling between the two tools at every time step. This is applied when both ES and CFD solutions depend on boundary conditions that vary significantly with time (Zhai et al., 2001). It is evident that full dynamic coupling is the most accurate approach among those considered. However, it is also the most computationally expensive approach.

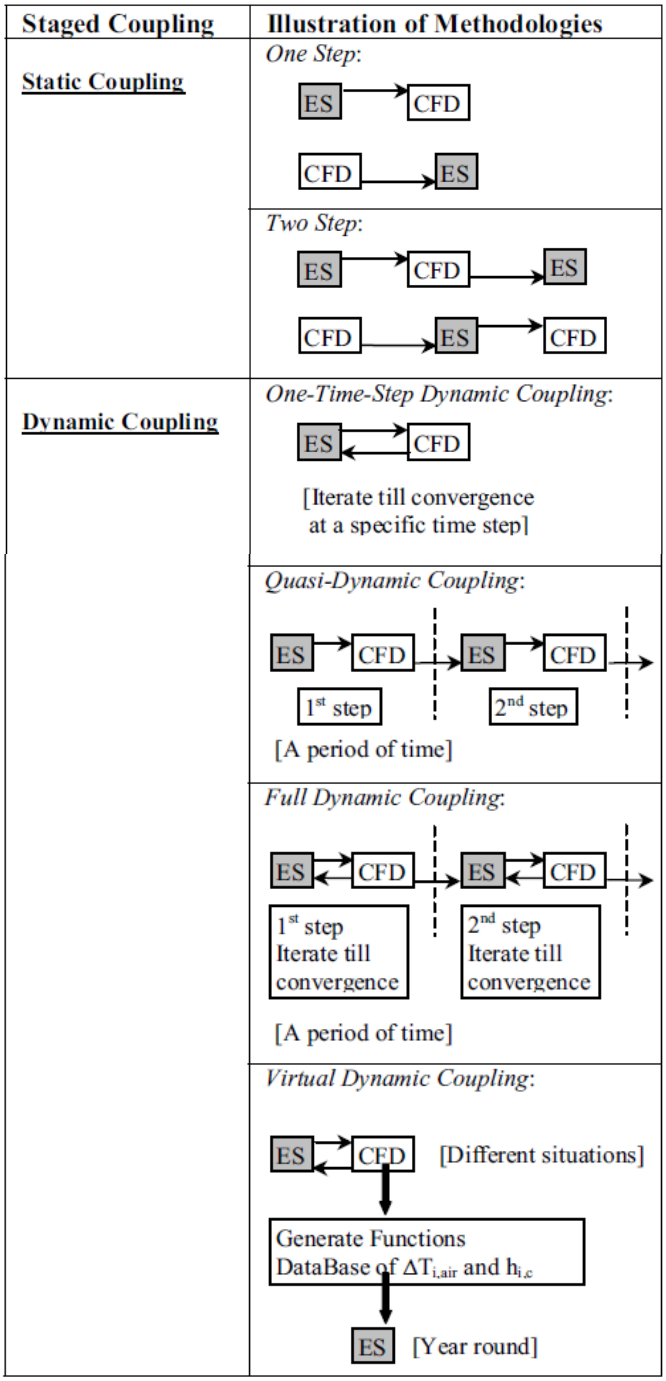

Figure 6.1: Staged coupling strategy (Zhai et al., 2001)

The main focus of ES-CFD coupling is on the convective heat transfer at internal surfaces of the building envelope elements, expressed as (Djunaedy, 2005):

$$q_{i,c} = h_{i,c}\left(\mathrm{T_i} - \mathrm{T_{i,air}}\right) \tag{6.4}$$

where

$q_{i,c}$ - Convective heat transfer

$h_{i,c}$ - Mean convective heat transfer coefficient

T_i - Internal surface temperature of the building envelope element

$T_{i,air}$ - Reference air temperature

Equation 6.4 can be rewritten as (Djunaedy, 2005):

$$q_{i,c} = h_{i,c}(T_i - T_{building}) - h_{i,c}\Delta T_{i,air} \quad (6.5)$$

where

$T_{building}$ - Mean building air temperature

and

$$\Delta T_{i,air} = T_{i,air} - T_{building} \quad (6.6)$$

As mentioned earlier, ES tools calculate surface convective heat transfer coefficients using empirical correlations. However, this methodology has drawbacks because of the "well-mixed" simplification taking $T_{building}$ as the reference temperature and hence local variation of air temperature within the thermal zone cannot be determined. On the other hand, CFD has the capability to calculate local convective heat transfer coefficients taking $T_{i,air}$ as the reference air temperature. In the indoor environment this reference air temperature can be the supply air temperature, free stream air temperature with respect to a particular envelope element or any other acceptable flow temperature depending on the problem being handled. Hence in CFD tools, this reference temperature will highly influence the calculated values of the convective heat transfer coefficient adjacent to the building envelope. Hence, it is observed that local convective heat transfer coefficients directly calculated by CFD tools are not very reliable. This issue has been addressed using a different approach as explained in section 6.3.

6.3 Methodology

The ideal approach would have been to allow exchange of variable data between ES and CFD tools at each iterative step of the corresponding simulations. However, this strategy is computational wise extremely expensive. Hence, external one-step static

data exchange approach was adopted for coupling EnergyPlus and Fluent on MATLAB platform in the present study in order to afford computational effort while acquiring an acceptable level of accuracy as recommended in the literature. In this context, tools achieve state of convergence separately before exchanging variable data between them. Internal mean surface temperature of building envelope elements (T_w) predicted by EnergyPlus and mean internal envelope surface convective heat transfer coefficients (h_c) predicted by Fluent and MATLAB are the exchange variables for the coupled simulation. Workflow of the coupled simulation is shown in Figure 6.2. Time step for complimentary data exchange was taken as 1 hour in order to establish compromise between computational time and accuracy of the solution.

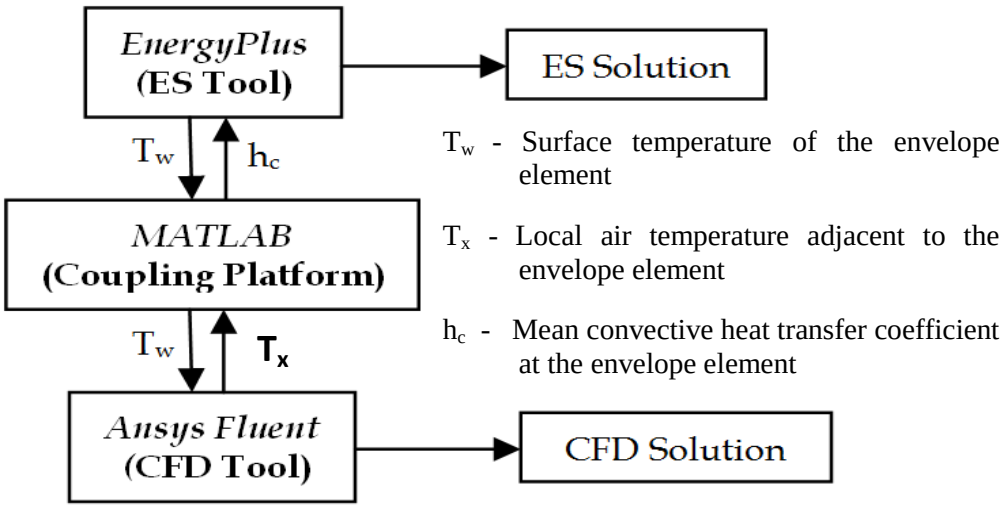

Figure 6.2: Workflow of the coupled ES-CFD simulation

The local convective heat transfer coefficient at each envelope element was calculated based on the air temperature at a point located just outside the boundary layer, placed directly in front of the centre of the corresponding envelope element. Temperature at this point (T_x) is predicted by ANSYS Fluent and MATLAB programme computes the local convective heat transfer coefficient (h_x) for that envelope element using equation 6.7:

$$q_x = h_x(T_w - T_x) \tag{6.7}$$

where q_x and T_w are surface convective heat flux and envelope surface temperature respectively. The mean convective heat transfer coefficient for the envelope element wall ($\bar{h}_x$) can be obtained by:

$$\bar{h}_x = \frac{1}{x}\int_0^x h_x = 2h_x = h_c \qquad (6.8)$$

Accordingly mean convective heat transfer coefficients (h_c) can be calculated for all envelope elements and eventually, energy consumption of the building is determined through the ES-CFD coupled simulation.

Since execution of the coupled simulation to predict energy consumption of the building for the entire year is highly computationally expensive, simulations were conducted only for the following cases during the present analysis:

- Scenario 1: Day recording the maximum outdoor dry bulb temperature
- Scenario 2: Day recording the minimum outdoor dry bulb temperature

Final ES solution provides the building energy consumption data for the particular scenario. Two case studies have been considered to demonstrate the aforementioned concept and they are discussed below in detail.

6.4 Case studies of coupled simulation

6.4.1 Case study 1: Single-storey building

The single storey building in 4.6.1 is reconsidered for the analysis. Wall and roof construction include standard brickwork and Calicut tiles respectively.

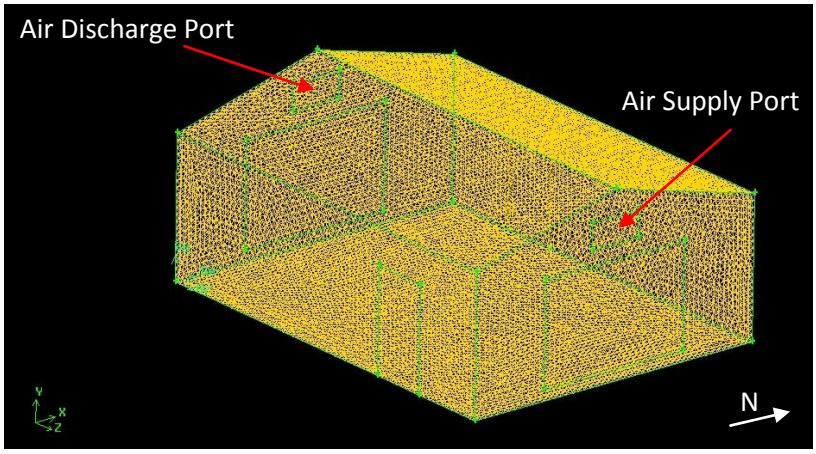

Figure 6.3: CFD model of the single-storey building

The CFD model of the building was created using the modelling software GAMBIT v. 2.2 and is shown in Figure 6.3. It consists of 1,686,789 hybrid mesh volumes in the computational domain. The resolution of the computational mesh has been checked for "grid independence". Separate boundary meshes were created for each envelope surface of the building. Average y-plus (y^+) for the mesh was 5.4.

As per literature (Chen, 1995; Gatski, Hussaini, & Lumley, 1996; Posner et al., 2003; Stamou & Katsiris, 2006) it is found that k-ε RNG turbulence model performs best in modelling indoor air flow with respect to experimental validation compared to other widely used turbulence models. Hence, the same turbulence model was incorporated in all case studies that demonstrated the ES-CFD coupled approach in this chapter. Table 6.3 gives modelling parameters for the CFD simulation.

Table 6.3: CFD modelling parameters: Single-storey building

Parameter	**Model/Value**
Air Supply	Cavity flow ventilation at 0.3 ms^{-1}
Supply air temperature	16 ^{0}C
Turbulence model	k-ε RNG
Discretization scheme	QUICK
Near-wall Treatment	Fine surface mesh

All envelope elements of the building can be approximated as flat plates. The supply air velocity (U_∞) is 0.3 ms^{-1} and the maximum characteristic length of an envelope element (L) of the building is found to be 8 m. Maximum Reynolds number of the airflow on any envelope surface is calculated as:

$$Re_{max} = \frac{U_\infty L}{\upsilon} = \frac{(0.3)(8)}{1.527 \times 10^{-5}} = 157{,}171 \qquad (6.9)$$

where kinematic viscosity of air (υ) at 20 ^{0}C obtained from property tables is 1.527 × 10^{-5} m^2s^{-1}. Since the calculated maximum Reynolds number on the envelope surface is less than the relevant critical Reynolds number (R_{cr}) of 500,000, flow on the envelope surface can be observed as laminar. The predicted Reynolds number (Re_x) and boundary layer thickness at the centre of the envelope wall (δ_x) is calculated as:

$$Re_x = \frac{U_\infty x}{\upsilon} = \frac{(0.3)(4)}{1.527 \times 10^{-5}} = 78585$$

$$\delta_x = \frac{4.91x}{\sqrt{Re_x}} = \frac{(4.91)(4)}{\sqrt{78585}} = 0.070 \text{ m} \tag{6.10}$$

The coupled ES and CFD setup was run on an Intel Core i5 3.2 GHz workstation of 4.0 GB RAM. It took 13 hours and 40 minutes for the coupled simulation to reach the state of convergence. Figures 6.4 and 6.5 illustrate the daily variation of internal envelope temperatures of the building predicted by EnergyPlus for scenarios 1 and 2.

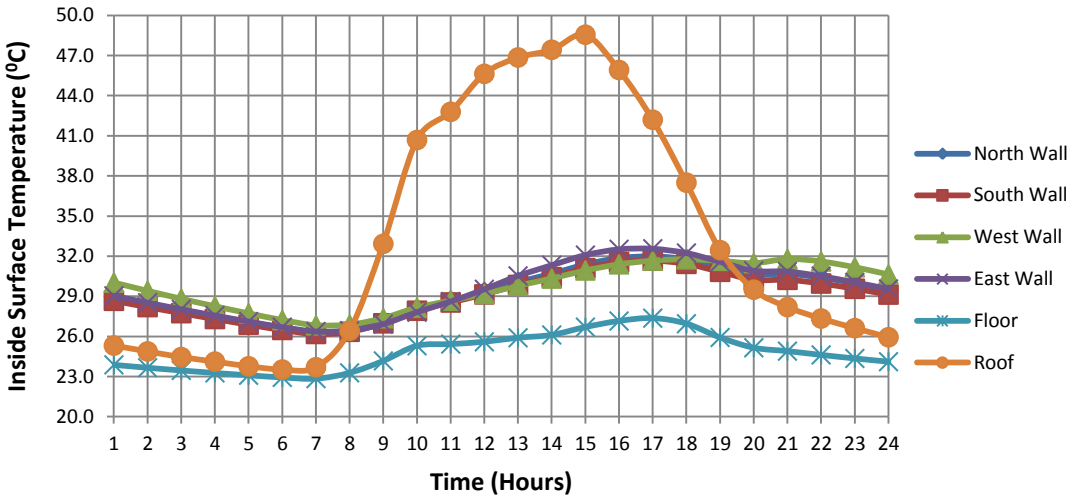

Figure 6.4: Daily variation of internal envelope temperature – Scenario 1

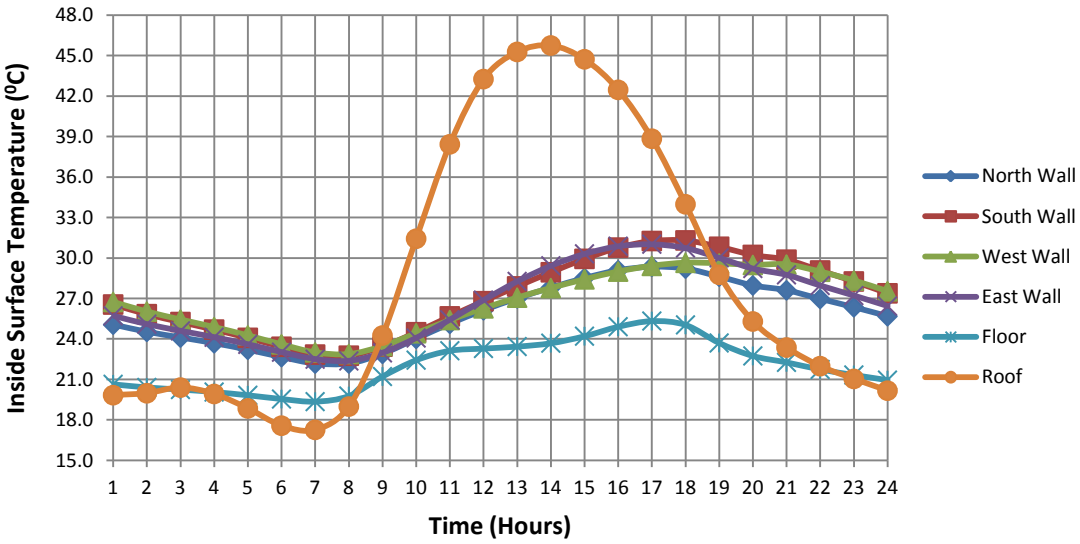

Figure 6.5: Daily variation of internal envelope temperature – Scenario 2

Figures 6.6 to 6.9 show daily variation of the mean internal envelope convective heat transfer coefficients related to ES only and ES-CFD coupled approach for both scenarios.

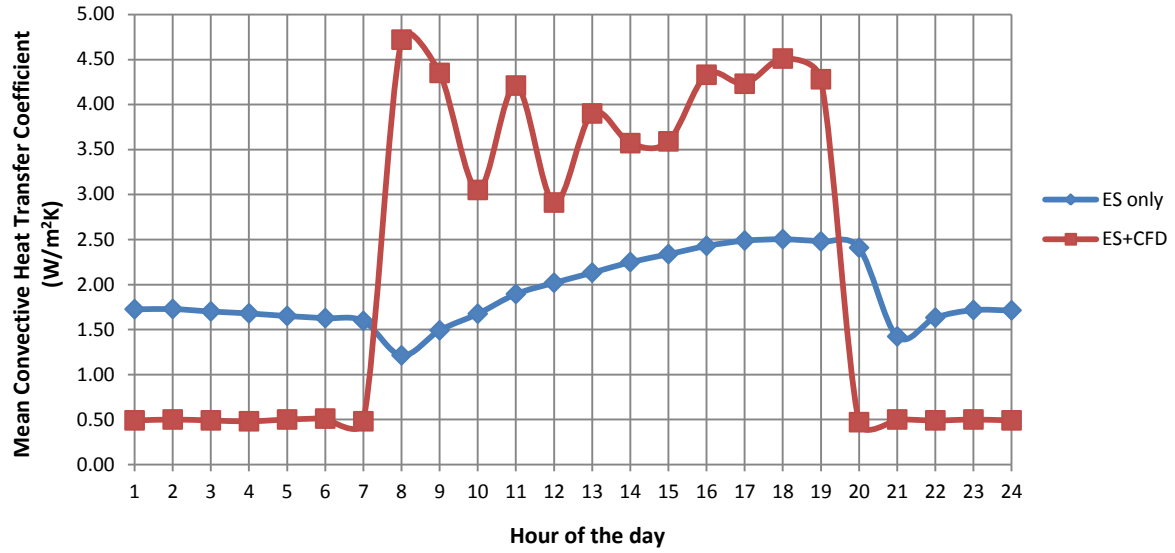

Figure 6.6: Variation of north wall mean convective heat transfer coefficient - Scenario 1

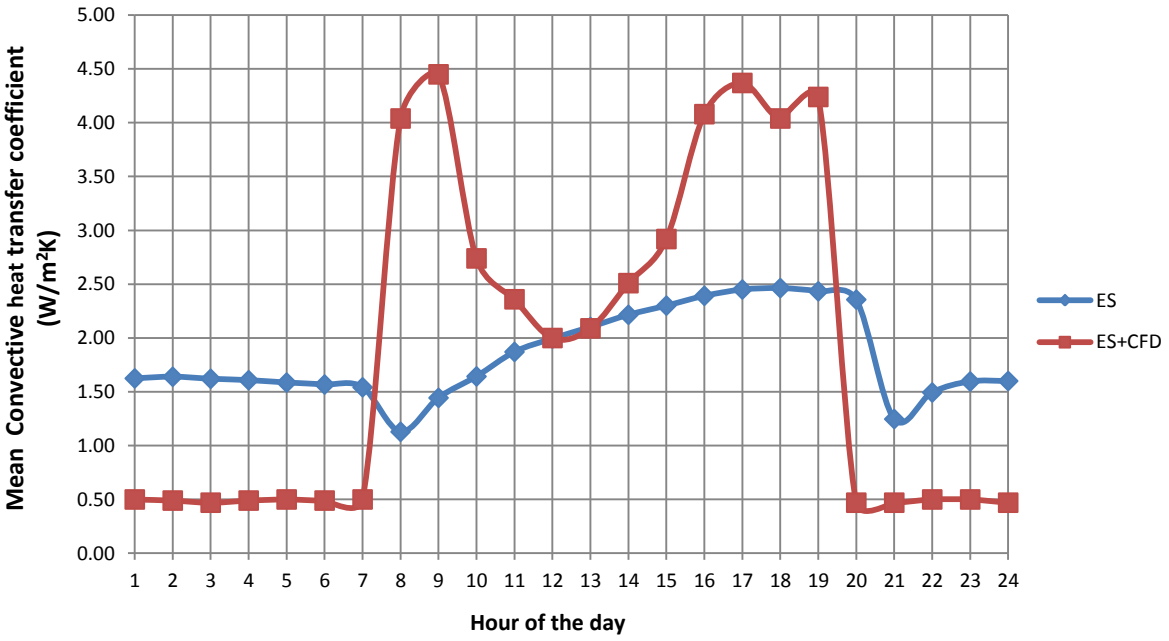

Figure 6.7: Variation of south wall mean convective heat transfer coefficient - Scenario 1

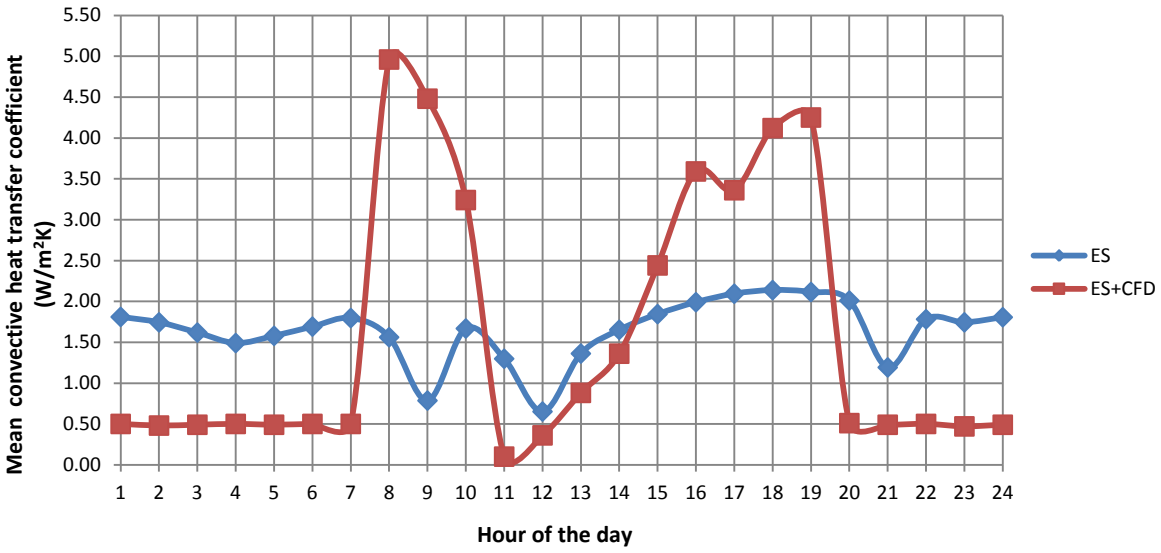

Figure 6.8: Variation of north wall mean convective heat transfer coefficient – Scenario 2

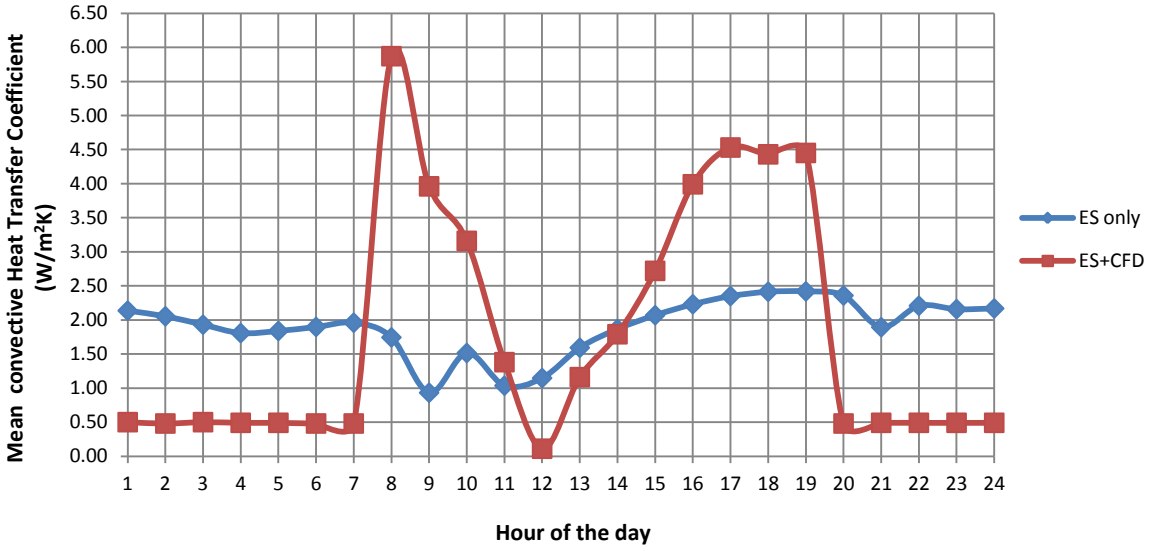

Figure 6.9: Variation of south wall mean convective heat transfer coefficient – Scenario 2

Figures 6.6 to 6.9 show that there is a considerable discrepancy between the respective mean wall convective heat transfer coefficients predicted by the two approaches. It is observed that there is a sudden decrease in mean convective heat transfer coefficients predicted by the ES-CFD coupled approach on both walls for the two scenarios (in scenario 2 in particular) around noon. This may be possibly due to stagnation of air because of very low indoor air velocities prevailing at that time

close to the envelope walls. However, this phenomenon could be accepted only after performing a comprehensive experimental validation. Table 6.4 gives a comparison of the building energy consumption related to the two approaches for both scenarios.

Table 6.4: Comparison of building energy consumption

Scenario	Energy Consumption (MJ)		Discrepancy (%)
	ES only	Coupled ES and CFD	
1	259	311	20.0
2	182	213	17.0

6.4.2 Case study 2: L- shape building

The L-shape building in 4.6.3 is reconsidered for the analysis. Wall and roof construction is comprised of standard brickwork and Calicut tiles respectively.

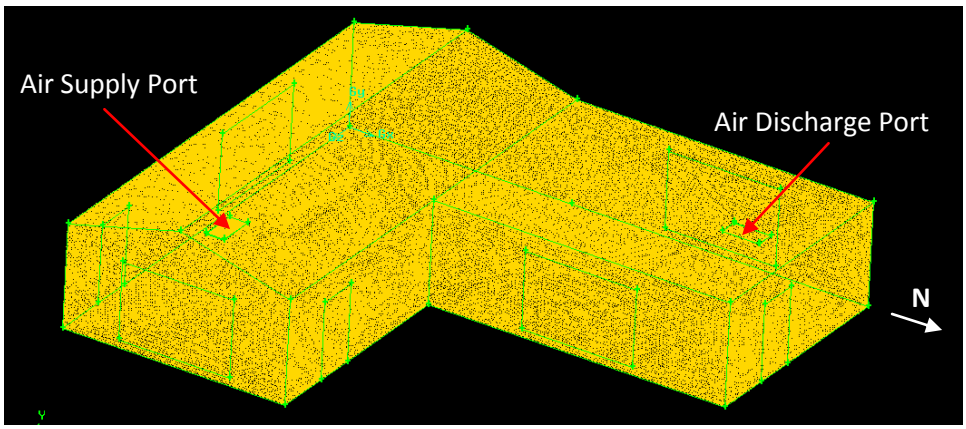

Figure 6.10: CFD model of L-shape building

CFD model of the building shown in Figure 6.10 consists of 1,736,647 hybrid mesh volumes in the computational domain. Separate boundary meshes were created for each envelope element surface. The resolution of the computational mesh has been checked for "grid independence". Average y-plus (y^+) for the mesh was 5.2. Table 6.5 gives the modelling parameters for the CFD simulation.

Table 6.5: CFD modelling parameters for L-shape building

Parameter	Model/Value
Air Supply	Mixing flow ventilation at 0.3 ms^{-1}
Supply air temperature	16 ^0C
Turbulence model	k-ε RNG
Discretization scheme	QUICK
Near-wall Treatment	Fine surface mesh

The maximum Reynolds number of flow (Re_{max}) on any envelope surface is found to be 275,049. Hence the boundary layer flow is laminar. The boundary layer thickness at the centre of this envelope surface (δ_x) is determined as 0.065 m. Calculation of average convective heat transfer coefficients and the energy consumption of the building is carried out as per methodology elaborated in Case 1.

The coupled simulation took 16 hours and 4 minutes for achieving the state of convergence. Figures 6.11 and 6.12 illustrate the daily variation of internal envelope temperatures of the building, predicted by EnergyPlus for scenarios 1 and 2.

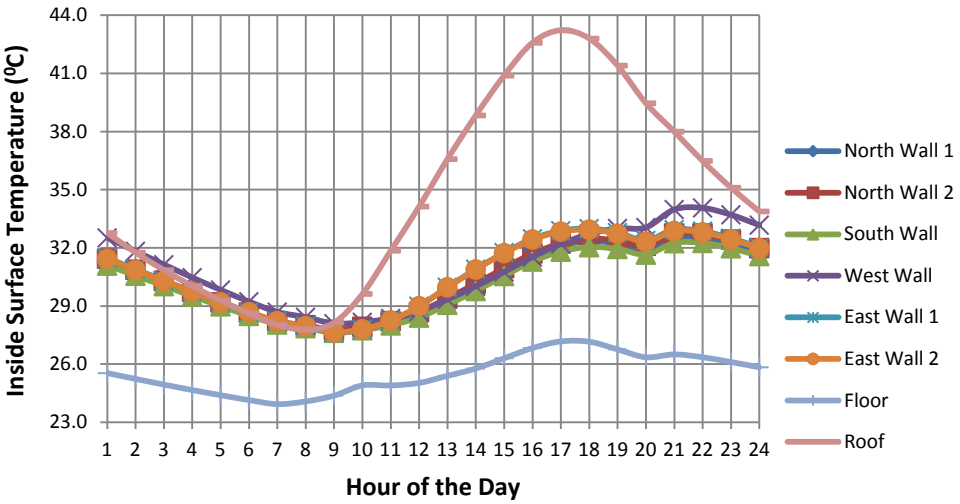

Figure 6.11: Daily variation of internal envelope temperature – Scenario 1

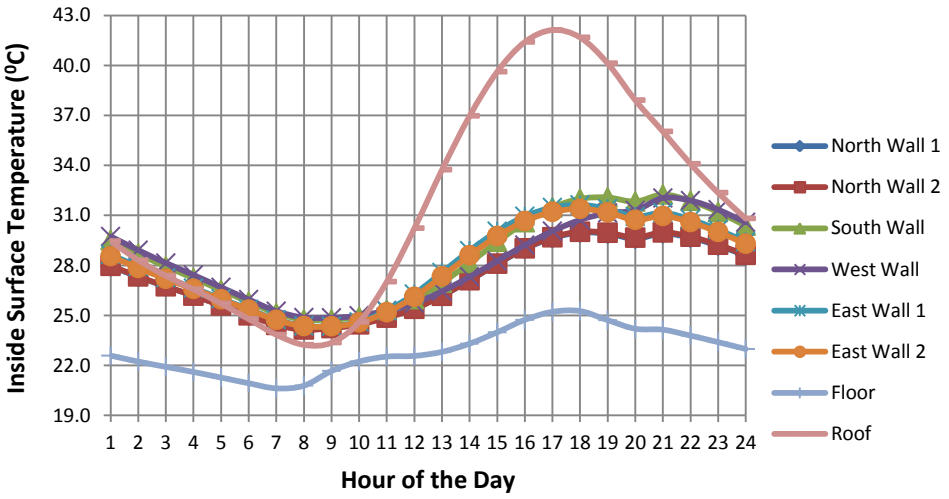

Figure 6.12: Daily variation of internal envelope temperature – Scenario 2

Figures 6.13 and 6.14 show the daily variation of internal envelope mean convective heat transfer coefficients related to ES only and ES-CFD coupled approach for both scenarios.

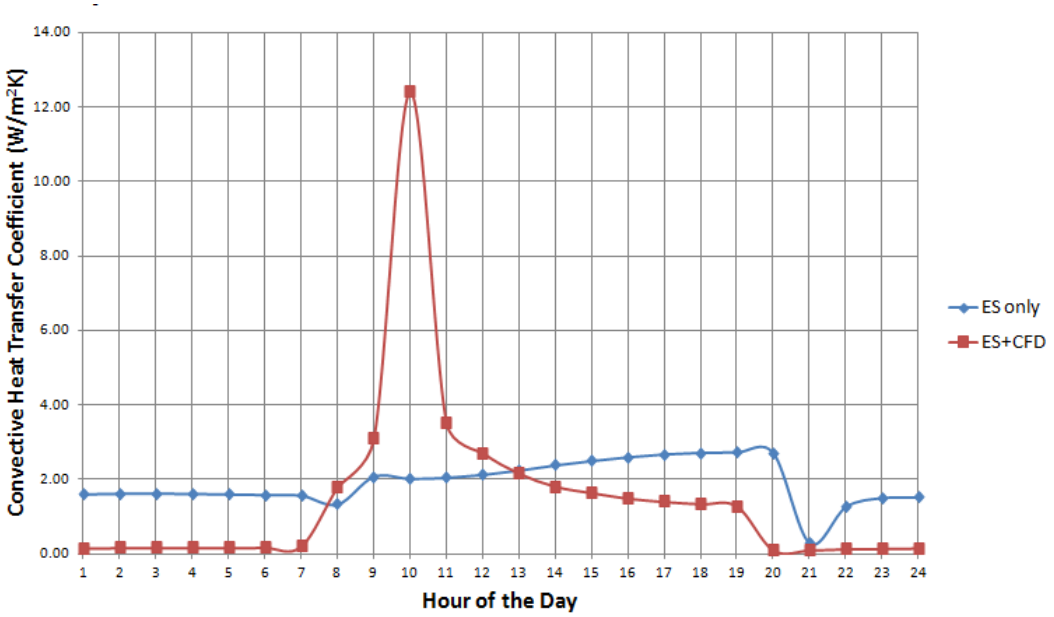

Figure 6.13: Variation of north wall convective heat transfer coefficient–Scenario 1

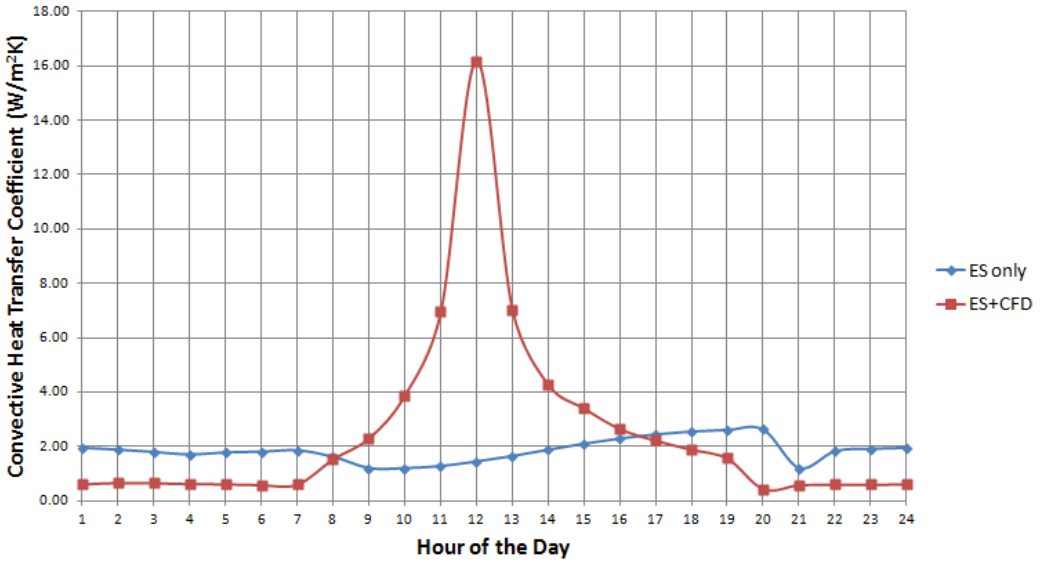

Figure 6.14: Variation of south wall convective heat transfer coefficient–Scenario 2

As per Figures 6.13 and 6.14, a peak related to the wall mean convective heat transfer coefficient is observed on both walls for the two scenarios. This may be due to increase in indoor flow velocity caused by turbulence close to the envelope walls at that time of the day. However, this prediction needs a detailed experimental

validation before being accepted. A distinct shift in the peak amplitude of the ES-CFD coupled convective heat transfer coefficient is observed for the south wall of scenario 2. This may be due to a time lag effect generated by the thermal mass phenomenon of the wall. Table 6.6 gives a comparison of building energy consumption related to the two approaches for both scenarios.

Table 6.6: Comparison of building energy consumption

Scenario	Energy Consumption (MJ)		Discrepancy (%)
	ES only	Coupled ES and CFD	
1	392	480	22.4
2	256	328	28.1

As per Table 6.6, discrepancy in scenario 2 has reached 28.1%. Present analysis considered only two scenarios in the aforementioned case studies, since it is not feasible to perform coupled simulation for the entire 365 days of the year due to high computational power demands involved. It is observed that for both scenarios considered, discrepancy related to predicted energy consumption between ES and the ES-CFD coupled approach is significant in both case studies. This is in good agreement with the previous studies found in the literature that were published by different researchers. However, this needs to be confirmed further through an in-depth experimental investigation. It is essential to analyze whether similar results are obtained for different air supply configurations of the building.

Coupled simulation has been demonstrated in this chapter for typical indoor flow conditions taking place in two different building envelope designs where a laminar boundary layer is formed on envelope surfaces. For higher supply velocities, air flow may become fully turbulent adjacent to envelope walls. In such situations, a turbulent boundary layer may be formed adjacent to the wall. The thickness of the turbulent boundary layer can be determined from equation 6.11 with usual notations.

$$\delta_x = \frac{0.38x}{(Re_x)^{0.2}} \tag{6.11}$$

However, there will always be a thin laminar sub layer immediately adjacent to the envelope wall that influences substantially on heat transfer between the solid surface and free stream. However, it may not be uniform at all times over the entire surface area due to inevitable interface effects.

6.5 Application of ES-CFD coupling in generic optimization

6.5.1 General framework

Figure 6.15 illustrates the general nature of building performance studies conducted in a qualitative manner as per literature survey conducted under the present study. It is observed that several previous studies on building energy simulation coupled with Computational Fluid Dynamics have been conducted. This includes mainly the work published by Negrao (1995), Beausoleil-Morrison (2000), Zhai and Chen (2003), Djunaedy (2005), Wang (2007) and Zhang et al. (2012). However, studies on building energy simulation coupled with CFD applied for generic performance optimization of buildings were rarely found in the literature. Hence, addressing this gap is considered to be worthwhile. Three approaches are proposed to carry out this task and relevant frameworks are illustrated in Figures 6.16 to 6.18.

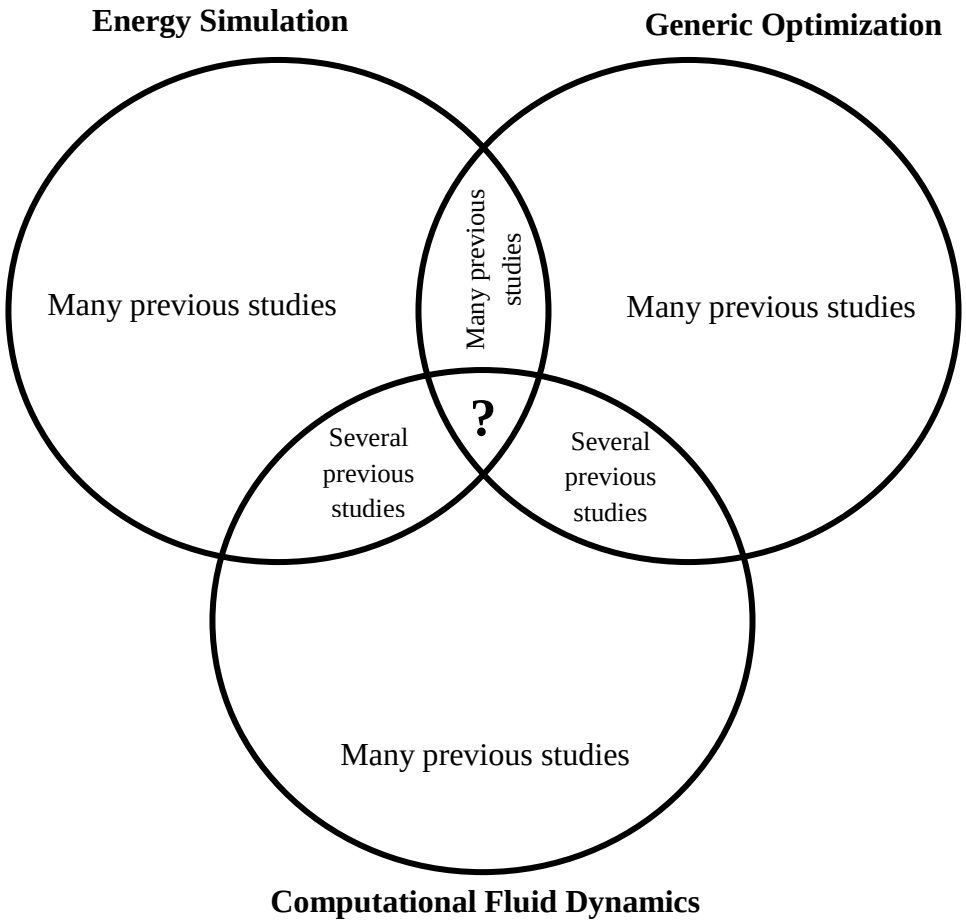

Figure 6.15: General nature of building performance studies in literature

6.5.2 Approach 1

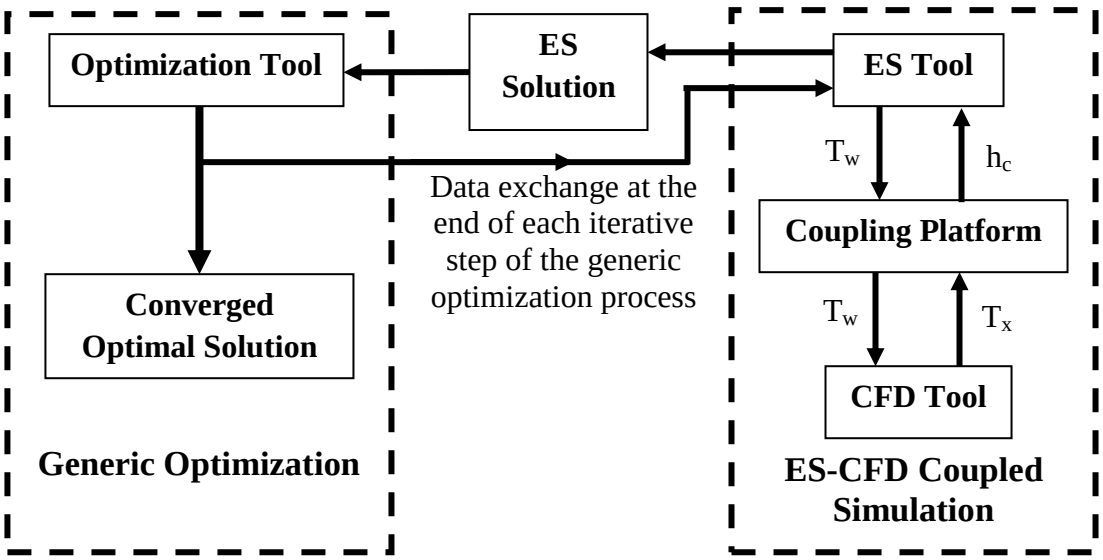

Figure 6.16: Proposed framework for optimizing building performance - Approach 1

Figure 6.16 illustrates the framework for the first approach. Two independent processes will run in parallel namely: ES-CFD coupled simulation and the Generic Optimization (GO) process exchanging data at each iterative step of the GO process. Firstly, ES-CFD coupled simulation will receive inputs from GO process. On convergence, ES-CFD simulation will produce the ES solution as explained in section 6.3 and then it is transferred to the GO process. At this stage the ES-CFD simulation will be withheld until it receives data from the GO process at the end of its second iterative step. Once the data is received, ES-CFD coupled simulation will commence and the process will continue until the GO process generates the optimal solution for the performance of the building. Although this approach has the highest accuracy among the approaches considered here, it is extremely computationally expensive, since data transfer takes place at each iterative step of the optimization process. Hence, this approach is not feasible to be implemented with its extreme computational demands.

6.5.3 Approach 2

In the second approach, as shown in Figure 6.17, exchange of data is performed only at certain specified iterative steps of the generic optimization process. Although this

strategy is not as computationally expensive as the first approach, still the computational demands are quite high.

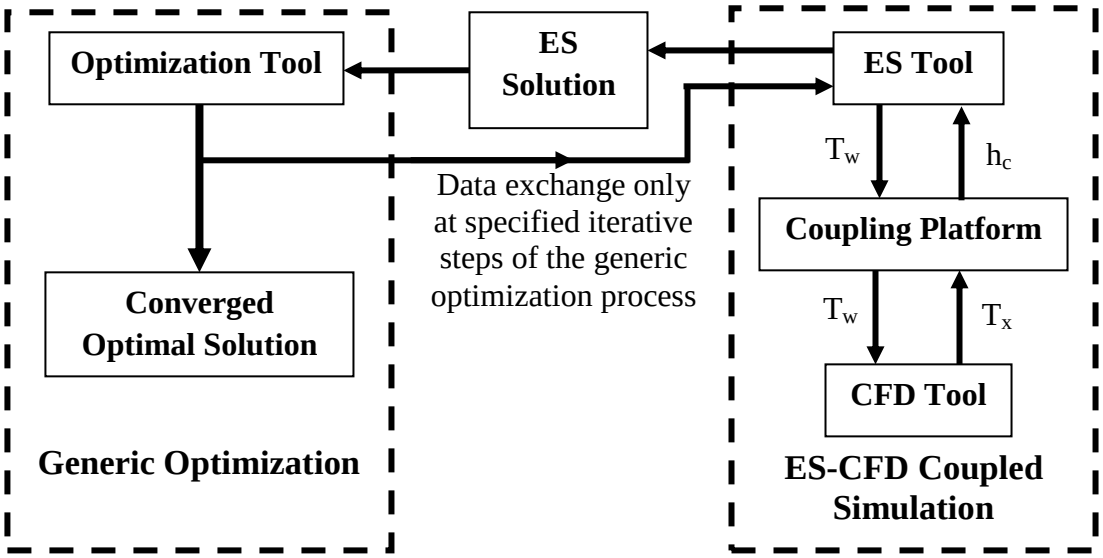

Figure 6.17: Proposed framework for optimizing building performance - Approach 2

Furthermore, intermittent data transfer between the two systems leads to stability and convergence problems during the optimization process.

6.5.4 Approach 3

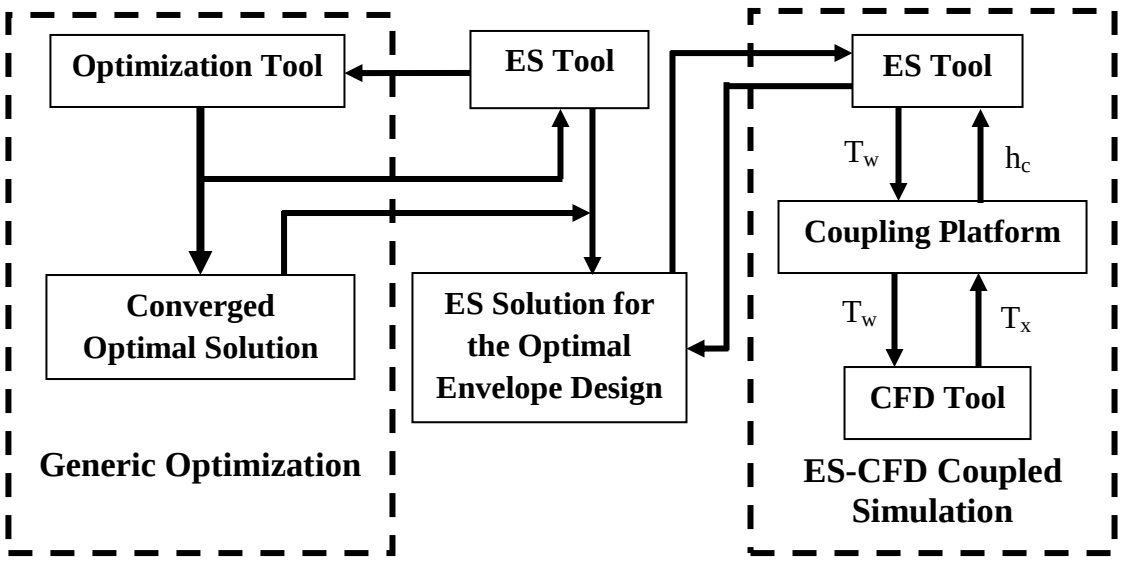

Figure 6.18: Proposed framework for optimizing building performance - Approach 3

In the third approach as shown in Figure 6.18, generic optimization process is first completed and the ES solution for the optimal envelope design is generated. Subsequently, ES-CFD coupled simulation is commenced, taking the aforementioned optimal ES solution as its initial input. The coupled simulation is run until state of convergence is achieved. The refined optimal ES solution gives a more realistic prediction for performance of the building. Among the three approaches considered, this approach has the least accuracy since generic optimization and ES-CFD coupled simulations are conducted separately and sequentially. However, it demands the least computational effort and hence can be recommended as the most feasible option among those considered here. The preference for the three options depends mainly on the computational resources at hand and the level of accuracy expected.

Present study elaborates only the third approach mainly due to the limitations in the computational power available. This approach is explained with two case studies below. EnergyPlus v. 8.0, Ansys Fluent v. 15.0, MATLAB v. R2012a and GenOpt v. 3.1 have been applied as ES tool, CFD tool, coupling platform and optimization tool respectively. The method was applied for the two scenarios namely:

- Scenario 1: Day recording the maximum outdoor dry bulb temperature
- Scenario 2: Day recording the minimum outdoor dry bulb temperature

6.5.5 Case study 1: Single-storey building

The single-storey building in 4.6.1 is reconsidered here with its optimal envelope design with respect to annual primary energy consumption as shown in Figure 6.19. Wall and roof are constructed with standard brickwork and Calicut tiles respectively.

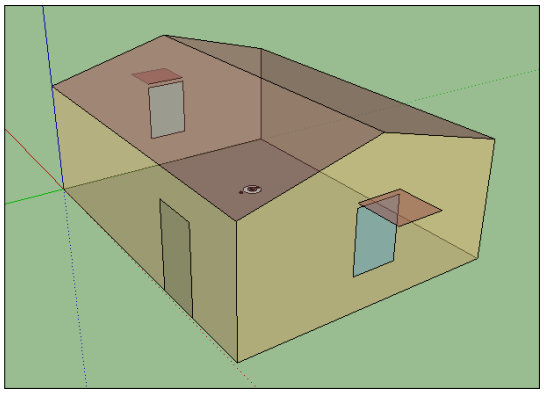

Figure 6.19: ES model of single-storey building with its optimal envelope design

Figure 6.20 shows the CFD model of the building.

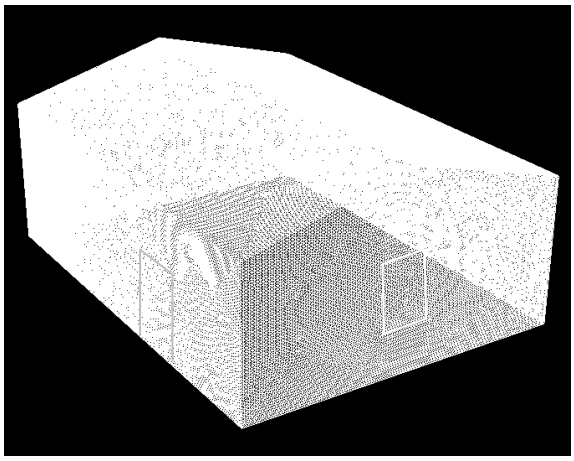

Figure 6.20: CFD model of single-storey building with its optimal envelope design

Table 6.7 compares the predicted primary energy consumption for heating, cooling and lighting for the two approaches for both scenarios.

Table 6.7: Comparison of predicted building energy consumption: Single-storey building

Scenario	**Primary Energy Consumption (MJ)**		**Discrepancy (%)**
	Generic Optimization only	**Generic Optimization + Coupled ES-CFD Approach**	
1	248	296	19.3
2	178	208	16.8

According to Table 6.7 it is observed that generic optimization with ES-CFD coupled approach predicts higher energy consumption than that predicted by generic optimization alone for both scenarios.

6.5.6 Case study 2: Three-storey building

Three-storey building in 4.6.2 is reconsidered here with its optimal envelope design with respect to annual primary energy consumption as shown in Figure 6.21. Wall and roof are constructed with standard brickwork and Calicut tiles respectively. Figure 6.22 shows the CFD model of the building.

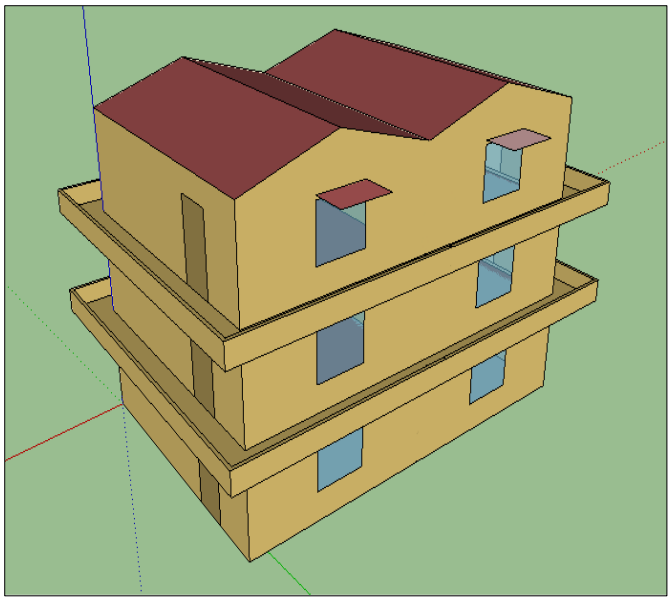

Figure 6.21: ES model of three-storey building with its optimal envelope design

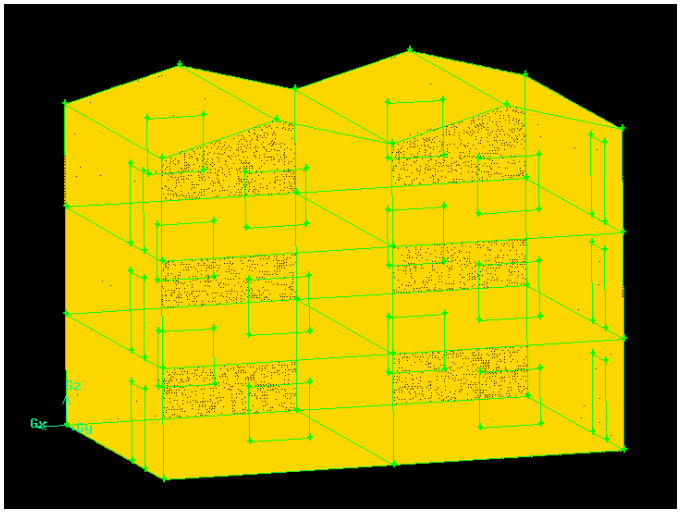

Figure 6.22: CFD model of three-storey building with its optimal envelope design

Table 6.8 compares the predicted primary energy consumption for heating, cooling and lighting for the two approaches for both scenarios.

Table 6.8: Comparison of predicted building energy consumption: Three-storey building

Scenario	**Primary Energy Consumption (MJ)**		**Discrepancy (%)**
	Generic Optimization only	**Generic Optimization + Coupled ES-CFD Approach**	
1	1907	2311	21.2
2	1174	1394	18.7

According to Table 6.8 the discrepancy between the two approaches is 21.2% for the scenario related to maximum outdoor dry bulb temperature.

6.6 Summary

This chapter explains drawbacks of the whole building energy simulation tools in predicting performance of buildings and subsequently emphasizes on the value addition to the study by coupling ES and CFD that enables more reliable predictions. This approach is elaborated by two case studies. Furthermore, three strategies are proposed in applying ES-CFD coupled approach in the generic optimization process of buildings performance and the most feasible strategy has been elaborated with relevant case studies.

7. CONCEPTS ON INDOOR ENVIRONMENTAL QUALITY

7.1 Overview

The objective of this chapter is to discuss the concepts related to indoor environmental quality of buildings. The main challenge faced by building designers at present, is to establish a sustainable and low-energy consuming built environment, while giving priority simultaneously to a healthy, comfortable and a safe indoor environment. During the past few decades, construction practices especially related to the building envelope, occupancy levels, use of heating, ventilation and air conditioning (HVAC) systems and user expectations have undergone drastic changes, leading to a growing interest on the indoor environmental quality. It is considered as one of the main factors influencing health, comfort and performance of occupants, since people spend most of their time inside buildings (Wargocki, 2009). Furthermore, indoor environmental factors have a substantial impact on the energy consumption of a building and hence, their assessment during the design process has been extensively discussed (Alfano et al., 2010; Santamouris et al., 2008). Indoor environmental quality is a broad concept and depends on many factors that fall into four major categories as shown in figure 7.1.

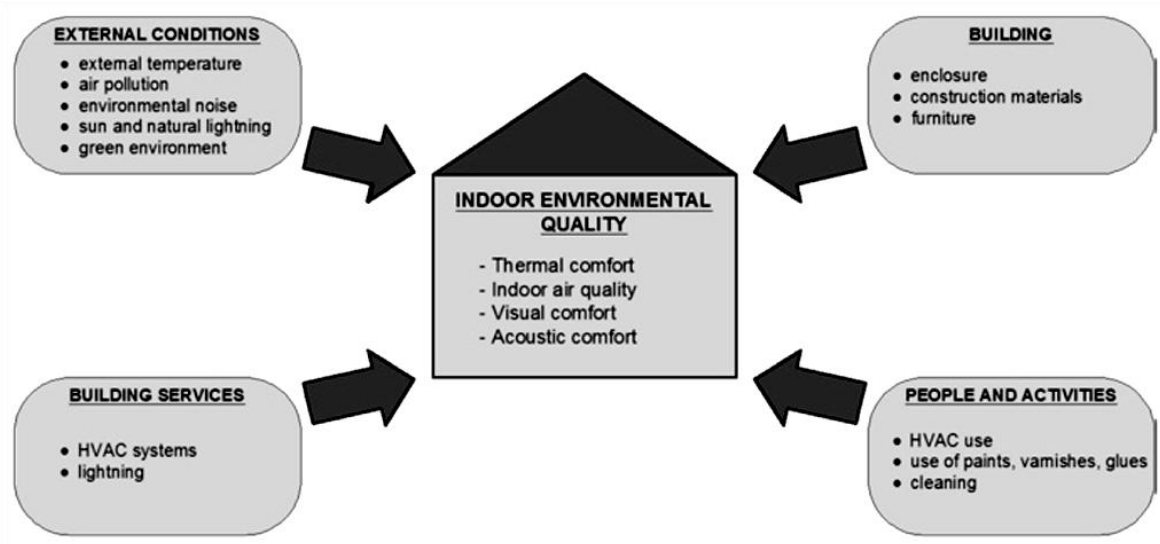

Figure 7.1: Factors affecting IEQ

Source: Adapted from REHVA (2010)

During present work, focus will be mainly on thermal comfort, indoor air quality and building ventilation in order to assess and optimize the IEQ in buildings. Hence, the aforementioned concepts are discussed further in the sections to follow.

7.2 Thermal comfort

Thermal comfort is a state of the mind of occupants that expresses satisfaction with the thermal environment (ASHRAE 55, 2017). Due to the existence of large variations, both physiologically and psychologically, from one individual to another, it is difficult to satisfy everyone in an occupied space. Relevant data have been collected through extensive laboratory and field tests to establish the statistical base in order to define conditions that a specified percentage of occupants will find thermally comfortable (ASHRAE 55, 2017). The following primary factors are considered when defining criteria for thermal comfort (ASHRAE 55, 2017):

- Metabolic rate
- Clothing insulation
- Air temperature
- Radiant temperature
- Air speed
- Humidity

The ASHRAE thermal sensation scale that was developed in order to quantify the thermal comfort of occupants is given in Table 7.1.

Table 7.1: ASHRAE thermal sensation scale

Thermal Sensation	Scale
Hot	+3
Warm	+2
Slightly Warm	+1
Neutral	0
Slightly Cool	-1
Cool	-2
Cold	-3

Source: ASHRAE 55 (2017)

The Predicted Mean Vote (PMV) index predicts the mean response of a large group of occupants as per ASHRAE thermal sensation scale by using heat balance principles relating aforementioned six main indoor environmental and personal variables (ASHRAE 55, 2017). The expression for calculating PMV is given by equation (7.1):

$$PMV = [0.303 \exp(-0.036M) + 0.028]L \tag{7.1}$$

where M is the metabolic activity and L is the thermal load on the body.

If W is external work then,

$$\begin{aligned} M - W = {} & 3.96 \times 10^{-8} f_{cl}[(t_{cl} + 273)^4 - (\bar{t}_r + 273)^4] + f_{cl}\mathrm{h}_c(t_{cl} - t_a) + \\ & 3.05[5.73 - 0.007(M - W) - p_a] + 0.42[(M - W) - 58.15] + \\ & 0.0173M(5.87 - p_a) + 0.0014M(34 - t_a) \end{aligned} \tag{7.2}$$

where

$$\begin{aligned} t_{cl} = {} & 35.7 - 0.0275(M - W) \\ & - R_{cl}\{(M - W) - 3.05[5.73 - 0.007(M - W) - p_a] \\ & - 0.42[(M - W) - 58.15] - 0.0173M(5.87 - p_a) \\ & - 0.0014M(34 - t_a)\} \end{aligned} \tag{7.3}$$

If PMV value generated by the model falls within the recommended range, thermal conditions of the occupied space are considered to be within the comfort zone. Acceptable thermal environment for general comfort is given by -0.5 < PMV < +0.5 (ASHRAE 55, 2017). Furthermore, the Predicted Percent Dissatisfied (PPD) index is related to the PMV as shown in the Figure 7.2.

The relationship between PPD and PMV is expressed as:

$$PPD = 100 - 95 \exp[-(0.03353PMV^4 + 0.2179PMV^2)] \tag{7.4}$$

The PMV-PPD model is widely used and accepted for design and field assessment of comfort conditions (ASHRAE 55, 2017).

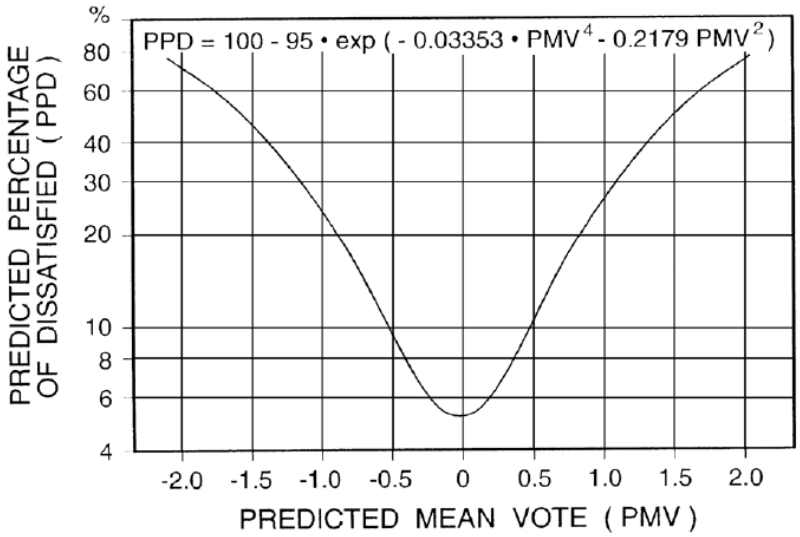

Figure 7.2: PPD as a function of PMV

Source: ASHRAE 55 (2017)

7.3 Indoor air quality

Indoor air quality (IAQ) is determined by the level of exposure of an occupant to the pollutants present in a building space (Bluyssen, 2009). This exposure is defined in terms of the concentration of the pollutants over time. According to Bluyssen (2009) concentration of the pollutants depends upon:

- Production of pollutants in the space expressed in terms of the rate of emission of the respective pollutants
- Rate of ventilation of occupied space in which the pollutants are produced
- Concentration of pollutants in the air supply

Exposure to indoor air pollutants in an occupied space is influenced by the rate of ventilation, air velocity, air temperature, relative humidity of air, occupant activities and time and duration of the exposure (Bluyssen, 2009). Sources of indoor air contaminants can be divided into the following categories (Bluyssen, 2009):

- Outdoor sources (traffic and industry sources)

- Occupant related activities and products (smoking, office equipment, consumer products etc.)
- Building materials and furnishings (paint, furniture, floor/wall covering etc.)
- HVAC system components (filters, ducts, humidifiers etc.)

The pollutants found in indoor air are mainly categorized as chemical and biological pollutants as shown in Table 7.2.

Table 7.2: Main categories of indoor air pollutants

Group	Subgroups	Description
Chemical	Gasses and vapours	Inorganic: CO, CO_2, NO_x, SO_x, O_3
		Organic: Volatile organic compounds (VOCs), formaldehyde
	Particulate matter	Fibres: asbestos, mineral wool, ceramic
		Respirable suspended particles, PM10
		Particulate organic matter, aromatic hydrocarbons
	Radioactive particles/gases	Radon
Biological	Micro-organisms, mould, fungi, mycotoxins, bio-aerosols pollens, mites, spores, allergens, bacteria, airborne infections, dust etc.	

Source: Adapted from Bluyssen (1996)

Poor IAQ may lead to a variety of health issues that have significant impact on the occupants who are affected directly, as well as on their families, employers and the society at large. Health issues associated with poor IAQ can be categorized mainly as building related illnesses and the "Sick building syndrome" (Childs, Argeles, Henderson, Horst, & Malin, 2006). "Sick building syndrome" refers to a general set of symptoms that affect occupants during their stay in the building and that diminish when they leave the building. This condition is further aggravated due to lack of ventilation in the occupied space. Nearly 75% of the building related health issues are categorized under the "Sick building syndrome" (Childs, et al., 2006). Common symptoms of this include headaches, nose, eye and throat irritation, dry cough, dry skin irritation, dizziness or nausea, difficulty in concentration and fatigue. Building related illnesses include specific diseases attributed to a particular material, product or system in a building. Some of them are Legionnaire's disease, Hypersensitivity

pneumonitis, Humidifier fever etc. (Childs, et al., 2006). Building related illnesses are generally characterized by a longer recovery time than the "Sick building syndrome" symptoms.

The key elements that contribute to the optimal IAQ include (Childs, et al., 2006):

- Supply and distribution of adequate air for ventilating buildings
- Close control of airborne contaminants
- Maintenance of acceptable temperature and relative humidity of air

On this basis, several international standards have been established in order to specify the maximum allowable limit of the said indoor pollutants and to closely control the same. Table 7.3 compares some of the said standards.

Table 7.3: Comparison of Indoor Air Quality Standards

Indoor pollutant	**[1]Canadian**	**[2]WHO/Europe**	**[3]NIOSH REL**	**[4]OSHA**	**[5]ACGIH**
CO_2	3500 ppm	-	5000 ppm	5000 ppm	5000 ppm
CO	25 ppm	25 ppm	35 ppm	50 ppm	25 ppm
NO_2	0.25 ppm	0.1 ppm	1 ppm	5 ppm	3 ppm
O_3	0.02 ppm	0.06 ppm	0.1 ppm	0.1 ppm	0.05 ppm
SO_2	0.019 ppm	0.047 ppm	2 ppm	5 ppm	2 ppm
PM2.5	0.1 mg/m^3	-	-	5 mg/m^3 (respirable fraction)	3 mg/m^3
PM10	-	-	-	-	10 mg/m^3
Total particles	-	-	-	15 mg/m^3	-

[1]Health Canada Exposure Guidelines for Residential Indoor Air Quality
[2]World Health Organization Air Quality Guidelines for Europe
[3]The National Institute for Occupational Safety and Health
[4]The U.S. Occupational Safety and Health Administration
[5]American Conference of Governmental Industrial Hygienists

Sources: Adapted from ASHRAE (2013) and ASHRAE 62.1 (2007)

7.4 Ventilation in buildings

Ventilation is the process of providing conditioned outdoor air of acceptable quality in specified quantities to buildings in order to maintain health, comfort and productivity of their occupants. It is also responsible for removing heat and contaminants generated indoors for maintaining indoor environmental quality

parameters at their respective desired levels. According to Bluyssen (2009), ventilation air flow patterns should be established so that fresh air reaches the occupants' heads as closely as possible, enabling the contaminated air to be removed as quickly as possible, before being mixed with fresh air.

Building ventilation can be provided through natural ventilation, mechanical ventilation or by both means (Hybrid ventilation). Natural ventilation is the passive means of exchanging air with outdoors and to evacuate indoor contaminants (Bluyssen, 2009). Air flow in this case takes place due to density gradients and subsequently by pressure differences resulting from temperature differences. Mechanical ventilation is applied when natural ventilation doesn't have the capacity to fulfill the demands, either due to extreme outdoor conditions or in locations that cannot be naturally ventilated (Bluyssen, 2009). Hybrid ventilation is a combination of both natural and mechanical ventilation. This offers opportunities for improving indoor environmental quality as well as to reduce energy demand in buildings.

Different types of mechanically driven ventilation configurations are utilized in buildings. Configuration of the ventilation system influences the ventilation performance in buildings. Selection of the appropriate configuration for ventilating a building depends on many factors including the function of the building itself. Some of the basic mechanical ventilation configurations include:

- Mixing ventilation
- Displacement ventilation
- Cavity flow ventilation
- Piston flow ventilation

They are explained in brief in the subsequent sections.

7.4.1 Mixing ventilation

Mixing ventilation has been the most popular mode of building ventilation since the inception of mechanical ventilation. In mixing ventilation, air is supplied to the building at a relatively high velocity to induce mixing as shown in figure 7.3.

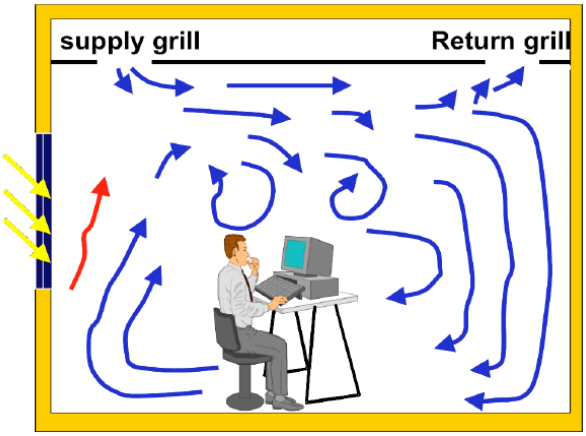

Figure 7.3: Mixing ventilation

Source: Adapted from Butler (2002)

Entrainment of building air in the supply jet leads to a high degree of mixing and as a result, temperature and contaminant concentrations tend to remain at a uniform level (Loomans, 1998). However, as a consequence, it may also lead to distribution of contaminants generated within the building (Arens, 2000). Generally, mixing ventilation is suited for both heating and cooling in buildings, for those do not possess a secondary heating system.

7.4.2 Displacement ventilation

In displacement ventilation, air is supplied at the floor level at a relatively low velocity. Supply air that flows across the building is warmed by the internal heat sources, producing buoyant plumes forcing the air to move vertically up towards the top of the building, where it will be exhausted as shown in figure 7.4.

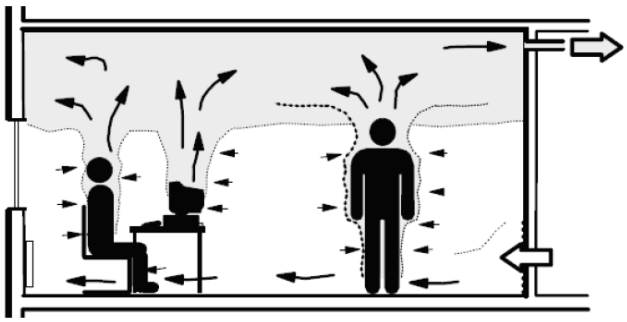

Figure 7.4: Displacement ventilation

Source: Extracted from Skistad et al. (2004)

A notable characteristic of displacement ventilation is the presence of vertical temperature and contaminant concentration gradients. Furthermore, it produces a sharp horizontal interface between the lower air layer, which is relatively cool and fresh and the upper air layer, which is relatively warm and contaminated (Loomans, 1998). Although the vertical temperature gradient may have a negative impact on the thermal comfort of occupants, displacement ventilation increases the ventilation effectiveness and hence the ventilation performance due to the vertical contaminant concentration gradient (Loomans, 1998).

7.4.3 Cavity flow ventilation

In cavity flow ventilation, air is supplied from one side of the building at a higher level and it is pushed towards the discharge port at the opposite facing wall also at a higher level. Hence, this allows air to circulate in the formed cavity as shown in figure 7.5.

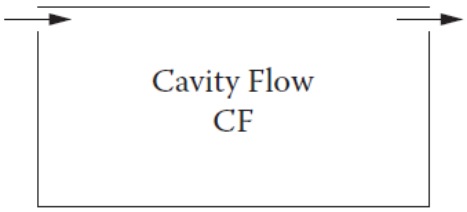

Figure 7.5: Cavity flow ventilation

Source: Khalil (2014)

7.4.4 Piston flow ventilation

Air is supplied from the roof at one or more supply ports and is discharged from the extraction ports on opposite walls near the floor as shown in figure 7.6. In this configuration, air is pushed from the roof towards the floor level.

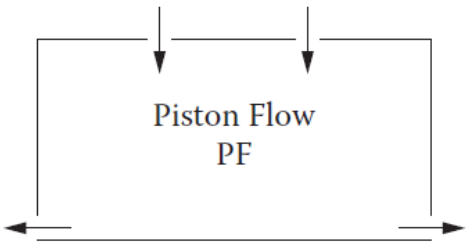

Figure 7.6: Piston flow ventilation

Source: Khalil (2014)

7.5 Modelling indoor environmental quality

The two widely accepted approaches for modelling indoor air flow and contaminant concentration are macro models and Computational Fluid Dynamics (CFD). Substantial progress has been achieved on modelling indoor environment with the application of full scale computer simulations since the beginning of 1960s (Kusuda, 2001).

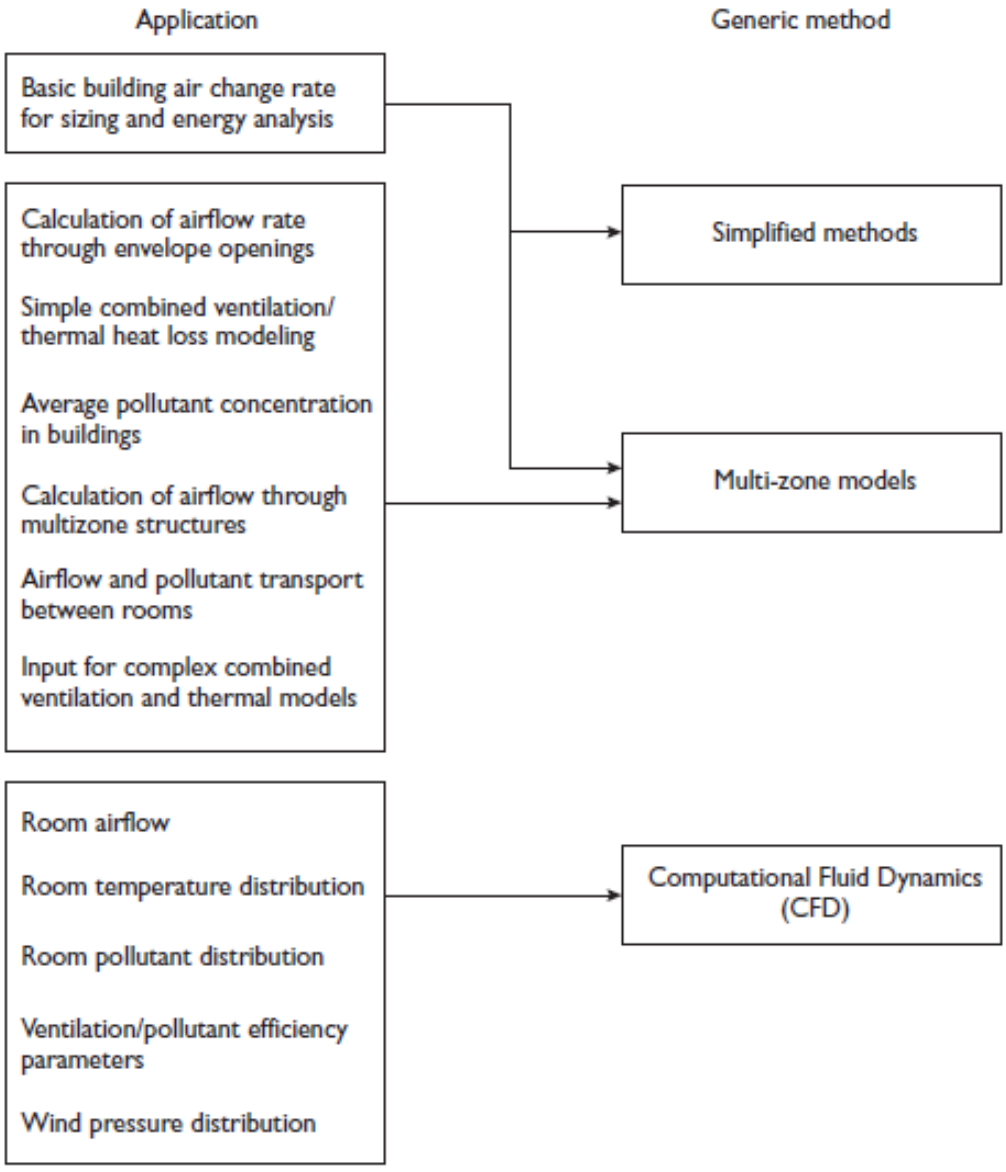

Figure 7.7: Overview of the typical building air flow modelling approaches

Source: Extracted from Malkawi and Augenbroe (2003)

This section describes the related concepts and applicability of the main indoor environmental quality modelling approaches: Semi-empirical or simplified approach, Zonal approach and CFD approach (Malkawi & Augenbroe, 2003). Figure 7.7 provides with an overview of the said air flow modelling approaches.

7.5.1 Simplified/Semi-empirical approach

This approach is mostly used to estimate air change rate and is frequently based on the estimates of building air-tightness (Malkawi & Augenbroe, 2003). In this approach air flow is modelled conceptually. Based on rules of thumb, engineering values and/or empirical relationships, it is up to the user to define direction and magnitude of air flow. The model is easy to set up and is readily understood since it originates from the conventional engineering practice. The models can easily be integrated with thermal network solvers in building performance simulation software (Malkawi & Augenbroe, 2003). In a semi-empirical model, air flow rate due to infiltration can be expressed as:

$$Q = L(A\Delta t + Bv^2)^{0.5} \tag{7.5}$$

where Q, L, A, Δt, B and v represent air flow rate, effective leakage area, stack coefficient, average outside/inside temperature difference, wind coefficient and average wind speed respectively.

7.5.2 Zonal approach

This approach is known under different terms such as zonal approach, mass balance network, nodal network etc. In the zonal approach, building and its systems are treated as a collection of nodes representing rooms, parts of rooms and system components, with inter-nodal connections representing the distributed flow paths associated with cracks, doors, ducts, etc. (Malkawi & Augenbroe, 2003). It is assumed that there is a simple, nonlinear relationship between the flow, through a connection and the pressure difference across it. Conservation of mass for the different flows taking place among each node leads to a set of simultaneous,

nonlinear equations that can be integrated over time to characterize the flow domain (Malkawi & Augenbroe, 2003).

The behaviour of air flow in the indoor environment is governed by pressure differences which may arise from any combination of wind, thermal buoyancy effects and mechanical ventilation. Air flow modelling is a prerequisite for predicting indoor environmental quality. Figure 7.8 illustrates how different governing factors influence individually or as a combination on indoor pressure distribution and eventually on the indoor air flow field. Feustel and Dieris (1992) defined two main zonal model categories: single-zone and multi-zone models.

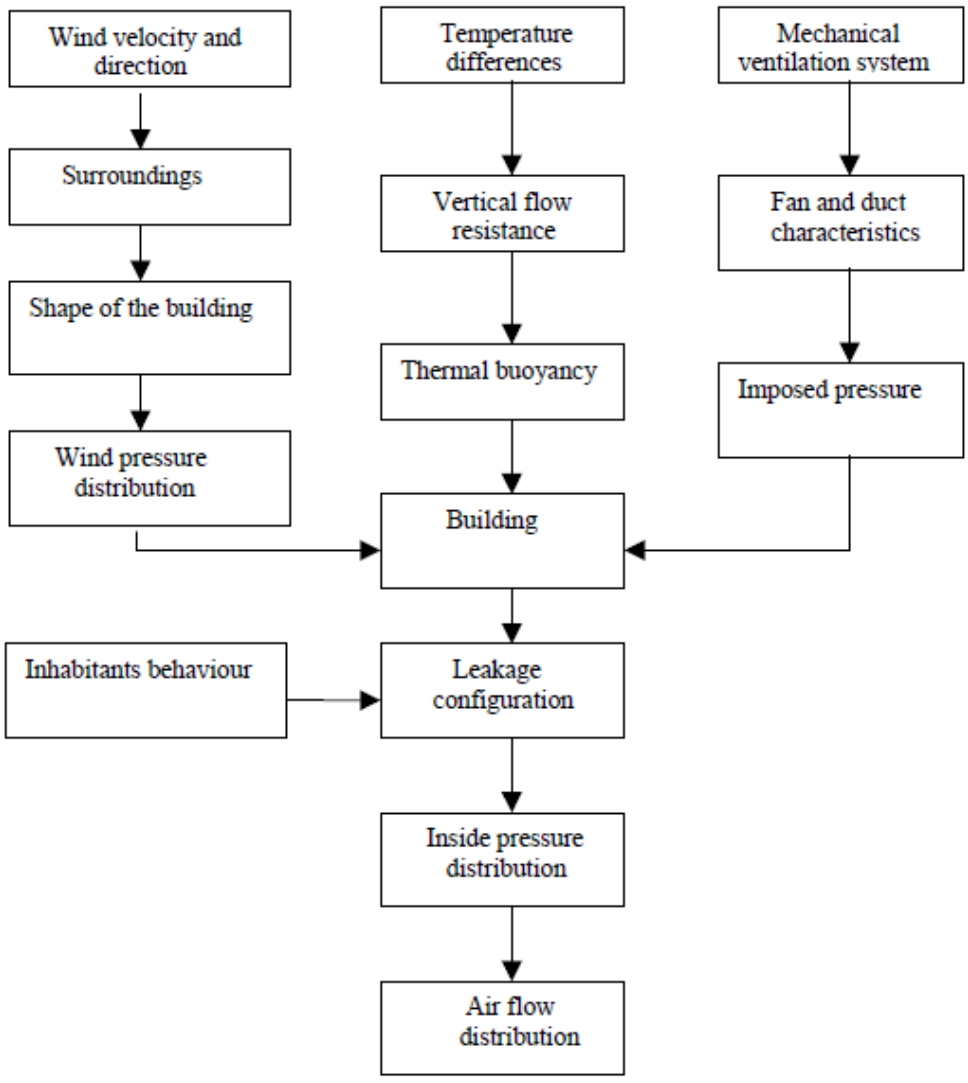

Figure 7.8: Influences on air flow distribution in buildings

Source: Feustel (1998)

Single-zone models assume that a building can be represented by a single well-mixed zone. These models are most often applied for single-storey buildings with simple construction and having no internal partitions. However their applicability will be very limited in real life problems. Single-zone models can be broadly categorized as empirical and physical models (Feustel & Sherman, 1989). Empirical models are based purely on knowledge from infiltration measurements. Infiltration rate can be assumed to be constant or obtained through tracer gas measurements. Physical models can be divided into two main groups; namely; crack models and single-zone network models (Feustel & Sherman, 1989). Crack model was the first major attempt for estimating leakage through the building envelope. In this approach, infiltration rate is assumed to be proportional to the product of crack coefficient and crack length and hence can be expressed by an empirical power law function as shown in equation 7.6 (Feustel & Sherman, 1989).

$$Q = al\Delta p^n = C\Delta p^n \tag{7.6}$$

where Q, a, l, C, Δp and n represent infiltration rate, crack flow coefficient, crack length, flow coefficient, design pressure and flow exponent respectively.

Single-zone network models are based on the mass balance of the building which takes into account all relevant flow paths. For a building with *k* flow paths the mass balance takes the form:

$$\sum_{j=0}^{k}\left[\rho C_j|p_{oj}-p_i|^n\left(\frac{p_{oj}-p_i}{|p_{oj}-p_i|}\right)\right]=0 \tag{7.7}$$

where p_{oj} and p_i are external pressure for flow path j and internal pressure respectively. The main drawback of this method is that it requires data such as, flow path distribution and characteristics, weather data, shielding and terrain roughness conditions and characteristics of the mechanical ventilation system. In order to overcome this issue, certain simplified single-zone models have been developed. In single-zone models, a particular zone is assumed as a fully mixed volume with a constant flow concentration. Hence, single-zone buildings are rarely found in reality. However, a smaller building without internal partitions or with open internal doors

can be modelled using single-zone approach with reasonable accuracy (Feustel & Sherman, 1989).

Multi-zone models are most suitable for buildings that can be represented by more than one well-mixed zone. Most buildings can be characterized as multi-zone structures even with the absence of internal partitions. The main characteristic of multi-zone models is that respective internal pressure in each zone must be known or needs to be determined. Moreover, flows taking place among zones are determined by a combination of pressure differences and a description of the flow paths among respective zones. Hence, network models are comprised of nodes that represent corresponding zones and inter-node flow paths. Multi-zone models are based on mass conservation as shown in equation 7.8:

$$\sum_{i=0}^{m}\left\{\sum_{j=0}^{k}\left[\rho C_{j,i}\left|p_{oj,i}-p_i\right|^{n_{j,i}}\left(\frac{p_{oj,i}-p_i}{\left|p_{oj,i}-p_i\right|}\right)\right]\right\}=0 \qquad (7.8)$$

where m and k represent number of zones and number of links of zone i respectively. Multi-zone model used in EnergyPlus is illustrated in Figure 7.9.

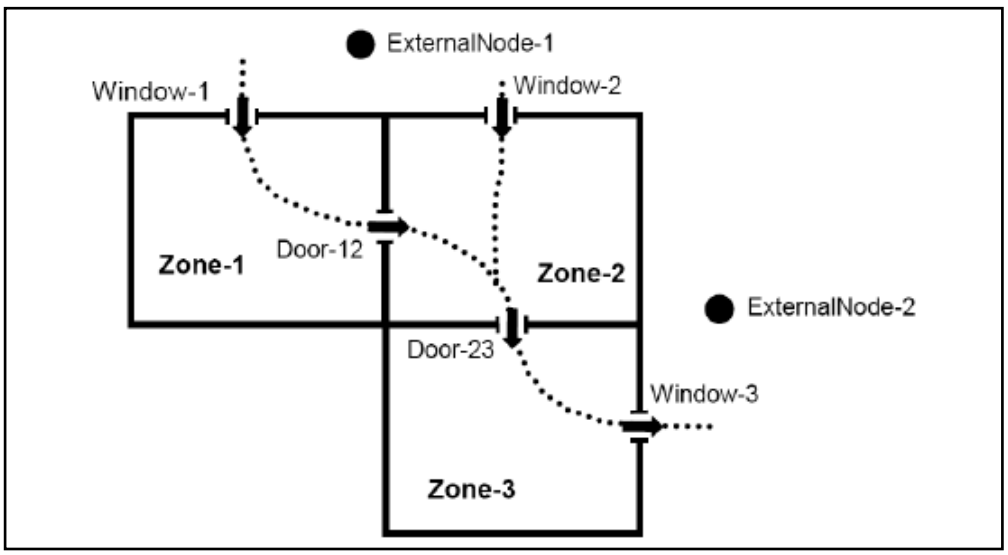

Figure 7.9: Air flow network model in EnergyPlus

Source: EnergyPlus Engineering Reference (2013)

Pressure difference between two nodes is calculated by the equation 7.9.

$$\Delta p = \left(p_n + \frac{\rho {V_n}^2}{2}\right) - \left(p_m + \frac{\rho {V_m}^2}{2}\right) + \rho g(Z_n - Z_m) + p_w \quad (7.9)$$

where

p_n, p_m - Entry and exit static pressures

V_n, V_m - Entry and exit air velocity

Z_n, Z_m - Entry and exit elevation

p_w - Pressure difference due to wind

Equation 7.10 relates the mass flow rate and pressure difference in the air flow network.

$$\dot{m}_\iota = C_i \rho \left(\frac{\Delta p_i}{\mu}\right) \quad (7.10)$$

where

$\dot{m}_\iota$ - Air mass flow rate at i^{th} linkage

C_i - Air mass flow coefficient

Δp_i - Pressure difference across i^{th} linkage

Unlike single-zone models, where there is only single internal pressure to be determined, in multi-zone models corresponding pressure for all zones has to be determined. This leads to substantial complexity of the numerical algorithm. However, the said models have wide applicability in predicting infiltration and ventilation air flow distribution in buildings.

7.5.3 Computational Fluid Dynamics approach

During the past few years, Computational Fluid Dynamics has gained a high popularity as a useful tool in design and analysis of the indoor environment. CFD was not developed specifically for modelling indoor air flows. It is a general purpose simulation tool whose main applications include Aeronautics, Astronautics, Hydrodynamics, Meteorology, Biomedical Engineering, Automotive Engineering, Combustion modelling, Performance of gas turbines etc. With the advent of CFD, Nielsen (1974) presented an attractive alternative approach for conducting empirical research on indoor air flows. Since then CFD has evolved to become a powerful tool

capable of predicting the indoor environment at a comprehensive and a detailed level with high flexibility. Extensive analysis on thermal comfort, indoor air quality and effectiveness of the building ventilation system can be performed through CFD in relation to the indoor air flow field, indoor air parameters and contaminant profiles. Latest developments in turbulence modelling and solver techniques have improved the accuracy of CFD predictions considerably. The ever increasing processing speeds and memory capacities of today's computers have facilitated immensely on the application of CFD to solve engineering real flow problems such as indoor air flows.

In the CFD approach, numerical techniques are applied for solving the governing Navier-Stokes equations for fluid flow and energy transfer, which take the non-linear partial differential form. The Navier-Stokes equations are derived through the application of conservation laws of mass (continuity), momentum, and energy to a fluid control volume. Furthermore, relevant governing equations for predicting turbulence, species transport, thermal comfort etc. may be incorporated with respect to modelling indoor air flows. Equations 7.11 to 7.16 show the conservation governing equations in partial differential form related to indoor air flow with respect to the three dimensional Cartesian coordinate system:

Conservation of mass (Principle of continuity)

$$\frac{\partial}{\partial x}(\rho u) + \frac{\partial}{\partial y}(\rho v) + \frac{\partial}{\partial z}(\rho w) = 0 \tag{7.11}$$

Conservation of momentum in x direction

$$\frac{\partial}{\partial t}(\rho u) + \frac{\partial}{\partial x}(\rho u u) + \frac{\partial}{\partial y}(\rho v u) + \frac{\partial}{\partial z}(\rho w u) = -\frac{\partial p}{\partial x} + \frac{\partial}{\partial x_j}\left[\mu\left(\frac{\partial u}{\partial x_j} + \frac{\partial u_j}{\partial x}\right)\right] \tag{7.12}$$

Conservation of momentum in y direction

$$\frac{\partial}{\partial t}(\rho v) + \frac{\partial}{\partial x}(\rho u v) + \frac{\partial}{\partial y}(\rho v v) + \frac{\partial}{\partial z}(\rho w v) = -\frac{\partial p}{\partial y} + \frac{\partial}{\partial x_j}\left[\mu\left(\frac{\partial v}{\partial x_j} + \frac{\partial u_j}{\partial y}\right)\right] \tag{7.13}$$

Conservation of momentum in z direction

$$\frac{\partial}{\partial t}(\rho w) + \frac{\partial}{\partial x}(\rho u w) + \frac{\partial}{\partial y}(\rho v w) + \frac{\partial}{\partial z}(\rho w w) = -\frac{\partial p}{\partial z} + \frac{\partial}{\partial x_j}\left[\mu\left(\frac{\partial w}{\partial x_j} + \frac{\partial u_j}{\partial z}\right)\right] = -\rho g \beta (T_\infty - T) \quad (7.14)$$

Conservation of energy

$$\frac{\partial}{\partial t}(\rho c_p T) + \frac{\partial}{\partial x}(\rho c_p u T) + \frac{\partial}{\partial y}(\rho c_p v T) + \frac{\partial}{\partial z}(\rho c_p w T) = \frac{\partial}{\partial x_j}\left(k \frac{\partial T}{\partial x_j}\right) + q \quad (7.15)$$

Conservation of species

$$\frac{\partial C}{\partial t} + \frac{\partial}{\partial x}(uC) + \frac{\partial}{\partial y}(vC) + \frac{\partial}{\partial z}(wC) = \frac{\partial}{\partial x_j}\left(D \frac{\partial C}{\partial x_j}\right) + S \quad (7.16)$$

Generation of flow field in the computational domain requires discretisation of the aforementioned partial differential Navier-Stokes equations into a set of linear equations using either finite difference (Patankar, 1980) or finite element (Baker, et al., 1994) method. The computational domain of interest such as an occupied space in a building is divided into a large number of control volumes, which is known as the computational mesh or grid. Generation of the computational mesh can be considered as the most crucial task in modelling with CFD since the size, shape and resolution of control volumes can influence the level of convergence, computational effort required and accuracy of the solution to a great extent. The numerical solution for the indoor flow field is generated by solving all governing equations on the computational mesh through an iterative process at each time step, until the state of convergence is reached. CFD is capable of generating numerical solutions at microscopic or nodal level for any indoor air flow scenario through which extensive data is at the disposal of the building designers in order to take vital decisions, especially during the early design stage.

Turbulent flows are often found in many engineering systems including indoor environment. Methodologies having different levels of complexity and computational intensity for modelling turbulence have been developed. The main approaches include: Direct Numerical Simulation (DNS), Large Eddy Simulation (LES) and Reynolds-Averaged Navier Stokes (RANS) approach (Tu, Yeoh, & Liu, 2008).

The most accurate approach for modelling turbulence is to directly solve the governing transport equations without averaging or approximating other than performing numerical discretization on them (Tu et al., 2008). This approach is known as the Direct Numerical Simulation where all turbulent elements and structures are captured during the calculations. Hence, DNS takes the behaviour of all small and large turbulent eddies in the computational domain into account as shown in figure 7.10.

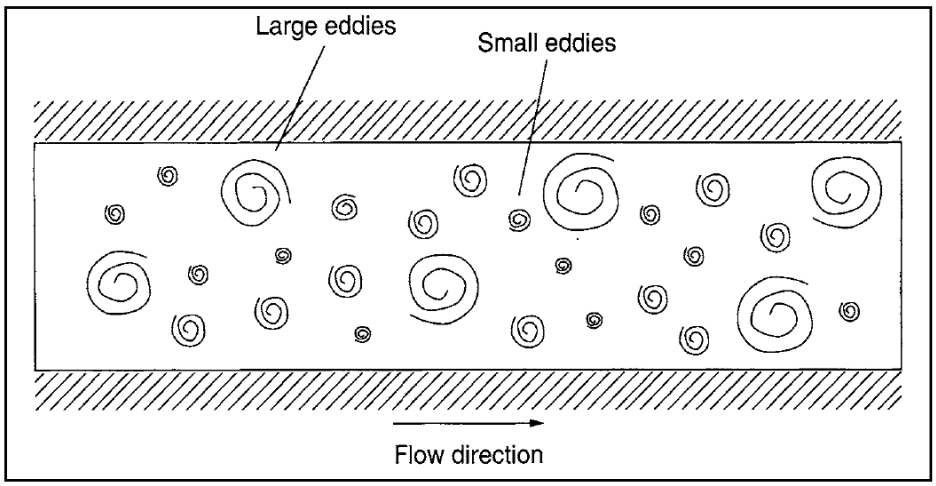

Figure 7.10: Schematic representation of a typical turbulent motion

Source: Tu et al. (2008)

DNS requires a very fine computational mesh and a small time step to predict the flow field down to the smallest length scale. In indoor flow fields, typical length scale is in the range of 0.1 mm (Murakami & Kato, 1989). Hence, this approach is extremely computationally expensive and due to the limitations in computational power of presently available computers, application of DNS to solve indoor air flow problems has not been considered as a feasible option.

In Large Eddy Simulation (Deardorff, 1970), main focus is on the large-scale eddies. The large scale eddies are generally more energetic and are the most effective transporters of the turbulent kinetic energy in the flow field than the small eddies (Tu et al., 2008). Hence, LES approach considers the behaviour of large eddies completely and only approximates the influence of the small eddies. Furthermore, when grid size is sufficiently small, the impact of the small-eddies on the flow is negligible (Malkawi & Augenbroe, 2003). In spite of this simplification, it is still computationally expensive, but much less than that of the DNS approach. However, in a three dimensional indoor flow problem, there is still a requirement for a relatively large computational effort and time to capture all the essential spatial and time scales on a sufficiently fine computational mesh with a moderate time step.

In general, DNS is considered as the preferred approach since it has the best accuracy. However, LES is the most preferred approach for flows with high Reynolds numbers or when the geometry is too complex to apply DNS (Tu, et al., 2008). The results generated by DNS or LES simulations contain extensive information on the flow behaviour, covering a broad range of length and time scales. The two approaches generally demand a high computational power and resources and hence often infeasible to be used as practical tools. Application of LES has been discussed among others by Zhang and Chen (2000) and Su, Chen, and Chiang (2001). Their predictions proved to have good agreement with the experimental measurements.

For most engineering flow problems including indoor air flows, influence of turbulence in terms of mean flow parameters is generally sufficient to quantify the turbulent flow characteristics (Tu et al., 2008). The Reynolds-averaged Navier-Stokes (RANS) approach solves statistically averaged Navier-Stokes equations using turbulent transport models. The standard k-ε model (Launder & Spalding, 1974) is the most widely used and validated turbulence model that can handle a variety of engineering flow problems (Tu et al., 2008). It is a two-equation model representing turbulent kinetic energy k and the rate of dissipation of turbulent energy ε as shown in equations 7.17 and 7.18 (Versteeg & Malalasekera, 1995).

$$l = \frac{k^{3/2}}{\varepsilon} \tag{7.17}$$

where l is the length scale and

$$\mu_t = \rho C_\mu \frac{k^2}{\varepsilon} \tag{7.18}$$

where C_μ is a dimensionless constant.

Flows within buildings fall under buoyant flow category, since they are often driven by natural air movement resulting from temperature gradients inside buildings. Rodi (1978) recommended an additional generation term to be included in the turbulent kinetic energy equation of the standard k-ε model in order to model turbulent buoyant flows. Hence, the turbulent kinetic energy equation takes the form:

$$\frac{\partial}{\partial t}(\rho k) + div(\rho k u) = div(\Gamma_k \, grad \, k) + G + B - \rho\varepsilon \tag{7.19}$$

where G is the usual generation term and B is the generation term related to buoyancy. B is expressed as:

$$B = \beta g_i \frac{\mu}{\sigma_T} \frac{\partial T}{\partial x_i} \tag{7.20}$$

where T is the temperature and g_i is the gravitational acceleration in the x_i direction. The volumetric expansion coefficient β is given by:

$$\beta = -\frac{1}{\rho}\frac{\partial \rho}{\partial T} \tag{7.21}$$

The transport equation for the dissipation of turbulent kinetic energy is given by:

$$\frac{\partial}{\partial t}(\rho\varepsilon) + div(\rho\varepsilon u) = div(\Gamma_\varepsilon \, grad \, \varepsilon) \; + C_{1\varepsilon}\frac{\varepsilon}{k}(G + B)\left(1 + C_3 R_f\right) - C_{2\varepsilon}\rho\frac{\varepsilon^2}{k} \tag{7.22}$$

where R_f is the flux Richardson number and C_3 is an additional model constant (Rodi, 1978). Rodi (1978) proposed a definition for R_f that allows $C_3 = 0.8$ to be used for both horizontal and vertical buoyant shear layers as expressed below:

$$R_f = -\frac{G_l}{2(B+G)} \tag{7.23}$$

where G_l is the buoyancy production in the lateral energy component. In the horizontal buoyant shear layer, entire buoyancy production is in the direction of gravity and hence:

$$G_l = 2B \tag{7.24}$$

In vertical buoyant shear layers, the lateral component is normal to the direction of gravity and has no contribution to buoyancy($G_l = 0$).

Accordingly, flux Richardson number is expressed as:

$R_f = -\frac{B}{B+G}$ for horizontal shear layers

$R_f = 0$ for vertical shear layers

The standard k-ε model assumes by default that the flow being modeled possesses a high Reynolds number. However, RNG k-ε model is equally applicable and valid for both low and high Reynolds number flows (Yakhot & Orszag, 1986). This is a vital aspect in order to be applied for simulating indoor air flows since the flow is generally wall-bounded and hence have regions with low Reynolds number (Chen, 1995). On the other hand, the wall functions that are used in the standard model are not necessary when the RNG k-ε model is applied (Yakhot & Orzag, 1986). The RNG k-ε model incorporates a modification to the transport ε-equation of the standard k-ε model, where the source term is expressed as (Tu, Yeoh, & Liu, 2008):

$$S_\varepsilon = \frac{\varepsilon}{\mathrm{k}}(\mathrm{C}_{\varepsilon 1}\mathrm{P} - \mathrm{C}_{\varepsilon 2}\mathrm{D}) - \mathrm{R} \tag{7.25}$$

where P, D and R represent turbulence production, destruction and rate of strain terms respectively.

Realizable k-ε model incorporates a new eddy-viscosity formula involving the variable C_μ in the turbulent viscosity expression. Furthermore, it has made changes to the transport ε-equation based on the dynamic equation of the mean-square vorticity fluctuation (Tu, Yeoh, & Liu, 2008).

Murakami and Kato (1989) compared the predictions of k-ε turbulence model with experimental measurements in a ventilated room with turbulent recirculating flows. Good agreement between the predictions and measurements were reported. Speziale, Sarkar, and Gatski (1991) and Loomans (1998) found that the RNG k-ε model performs slightly better than the standard k-ε model during indoor air flow modelling. Chen (1995) compared the performance of five different turbulence models for modelling simple indoor air flows and found that the standard and RNG k-ε models predicted the flow patterns best. Furthermore, addition of the term on rate of strain in the RNG dissipation rate equation had a significant effect on the turbulent viscosity thereby enabling RNG k-ε model to generate improved predictions on separated flows and anisotropic large-scale eddies (Gatski, Hussaini, & Lumley, 1996).

Posner, Buchanan, and Dunn-Rankin (2003) also confirmed that the RNG k-ε model shows the best agreement with the experimental data. Although the standard and RNG k-ε models are similar in nature, there are also certain crucial differences. Hence, the two models often generate substantially different predictions. Tian, Tu, and Yeoh (2006) made use of three popular turbulence models: Standard k-ε, RNG k-ε and RNG-based LES models for investigating an indoor airflow environment. The predicted air velocities have been compared and validated against experimental measurements obtained by Posner et al. (2003) in a model room. It was observed that predictions of all three turbulence models showed good agreement with experimental measurements, having captured all critical flow trends successfully. However, predictions of the RNG-based LES model provided the best agreement in terms of the air velocity. In spite of this observation, predicted velocities by the two k-ε models still showed reasonable agreement with measurements.

The shear stress transport (SST) k-ω turbulence model (Menter, 1994) has gained wide popularity in the field of indoor environmental modelling in recent times. It is a two-equation eddy viscosity model and can be applied for low Reynolds number scenarios those are typically found in indoor environments, without incorporating any additional damping functions. SST k-ω model is capable of modelling the

viscous sub-layer and related wall interactions successfully. The governing equations of the model are expressed by equations 7.26 and 7.27 (Menter, 1994):

$$\frac{\partial \rho k}{\partial t} + \frac{\partial}{\partial x_j}\left[\rho u_j k - \left(\mu + \frac{\mu_t}{\sigma_k}\right)\frac{\partial k}{\partial x_j}\right] = P_k - C_\mu \rho \omega k \tag{7.26}$$

$$\frac{\partial \rho \omega}{\partial t} + \frac{\partial}{\partial x_j}\left[\rho u_j \omega - \left(\mu + \frac{\mu_t}{\sigma_\omega}\right)\frac{\partial \omega}{\partial x_j}\right] = \alpha \frac{\omega}{k} P_k - \beta \rho \omega^2 + 2(1 - F_1)\frac{\rho}{\sigma_{\omega 2}\omega}\frac{\partial k}{\partial x_j}\frac{\partial \omega}{\partial x_j} \tag{7.27}$$

where ρ, k, ω and P_k represent density of fluid, turbulent kinetic energy, dissipation frequency of turbulent kinetic energy and production of k respectively. Eddy viscosity of the model is expressed by equation 7.28 (Menter, 1994):

$$\mu_t = \rho \frac{k}{\omega} \tag{7.28}$$

The shear stress transport formulation of the k-ω model switches its behaviour to that of k-ε model in the free stream conditions without being too sensitive to the same.

Although use of turbulence models in the RANS approach leads to certain errors in the numerical solution, it can substantially reduce the computational power requirements for CFD simulations. In spite of many encouraging success, uncertainties are still in existence during application of turbulence models in simulating indoor air flows. An important aspect to be considered with regard to modelling indoor air flows is the characterization of low-Reynolds-number turbulence (Tu et al., 2008). According to Tu et al. (2008), improper handling of low-Reynolds-number turbulence can contribute to inaccurate calculations, since indoor air flows are strongly influenced by both air velocity and turbulent fluctuations. Table 7.4 shows a comparison among main turbulence models applicable for indoor airflow modelling.

Table 7.4: Comparison of turbulence models

Model	Developer/s	Strengths	Limitations
Standard k–ε	Launder and Spalding (1974)	• Can predict airflow and turbulence reasonably well in enclosed environments with wall functions	• Valid for fully turbulent flows only • May fail under wall bounded flows
RNG k–ε	Yakhot and Orszag (1986)	• Has been widely used for predicting indoor airflows with substantial success • Majority of studies in the literature indicate that the RNG k–ε model is slightly better than the standard k–ε model in terms of the overall indoor flow simulation performance	• May fail under wall bounded flows
Realizable k–ε	Shih et al. (1995)	• Usually provides much improved results for swirling flows and flows involving separation when compared to the standard k-ε model	• May fail under wall bounded flows
Standard k–ω	Wilcox (1988)	• Performs well close to walls and in boundary layers • Works exceptionally well under strong adverse pressure gradients	• Very sensitive to free stream values
Shear Stress Transport (SST) k–ω	Menter (1994)	• Behaves as standard k-ω model near the wall boundaries and is equivalent to a transformed k-ε model in the free stream • Can capture complex flow features such as movement of vortices downstream	• Difficult to cope up with flow recovery following flow reattachment

Source/s: Extracted from Zhai et al. (2007) and Tu et al. (2008)

In modelling indoor environments, typical wall-bounded turbulent flows need to be handled on a regular basis. In this context, behaviour of flow near the envelope walls needs to be modelled in detail. It is observed that for such wall attached boundary layers, turbulent fluctuations are suppressed near the envelope walls and the viscous effects dominate in the viscous sub layer. This phenomenon generally makes the application of two-equation models such as standard k-ε, RNG k-ε and realizable k-ε

models infeasible at the near wall region, and hence requires a special procedure to model the same (Tu et al., 2008). Usually wall functions are readily used by most CFD tools in modelling near wall flow behaviour. However through this approach, near-wall region is not explicitly resolved within the CFD model (Launder & Spalding, 1974; Wilcox, 1998). As a solution to this issue, the low-Reynolds number modelling strategy may be implemented. In this method, a sufficiently fine computational mesh has to be created in the region close to the envelope element surface incorporating the boundary layer, enabling the complete resolution of the near-wall region (Neale et al., 2006). However, selecting a particular approach from the above two options entirely depends on the availability of computational resources at hand and the accuracy of the solution required (Tu et al., 2008).

In order to model near-wall flow behaviour, the region close to the wall can be characterized in terms of a dimensionless variable y^+. If y is the normal distance from the envelope wall, then the dimensionless wall distance (y^+) can be established as expressed in equation 7.29 (Neale et al., 2006; Tu et al., 2008).

$$y^+ = \frac{yu^*}{\upsilon} \tag{7.29}$$

where

y - Normal distance from the envelope wall

ν - Kinematic viscosity of fluid

u^* - Frictional velocity defined as:

$$u^* = \sqrt{\frac{\tau_w}{\rho}} \tag{7.30}$$

where τ_w and ρ denote wall shear stress and fluid density respectively. The local behaviour of flow close to the envelope element differs substantially as per the value taken by y^+ as follows (Tu et al., 2008):

- $y^+ < 5$: Viscous sub layer
- $5 < y^+ < 30$: Buffer region
- $30 < y^+ < 500$: Log-law layer

The viscous sub layer is applicable when $y^+ < 5$ and in low Reynolds number modelling the height of the first cell is generally taken approximately as $y^+ = 1$. For computational meshes with $y^+ > 30$, wall functions may be applied (Neale et al., 2006).

As per Tu et al. (2008), k-ω model performs very well close to solid walls in boundary layer flows, particularly under strong adverse pressure gradients. However, this model is very sensitive to free stream values (Tu et al., 2008) and hence is inferior to the standard k-ε model in this respect. To overcome this issue Menter (1994) developed SST k-ω model, combining both the standard k-ε and k-ω models. This retained the characteristics of the k-ω model close to the walls while gradually transforming into the standard k-ε model away from the walls towards the free stream. This combination made SST k-ω model to perform very well both close to the walls as well as in free stream conditions (Tu et al., 2008).

As per literature (Arun & Tulapurkara, 2005; Chen, 1995; Gebremedhin & Wu, 2003; Posner et al., 2003; Stamou & Katsiris, 2006), it is evident that RNG k–ε and SST k–ω are the best turbulence models to be applied for indoor flow modelling. Furthermore, Zhai et al. (2007) mentioned that many previous studies confirm that the SST k-ω model has a better overall performance than the standard k-ε model and RNG k-ε model especially with respect to indoor flow modelling. In this context, present work mainly applied RNG k–ε and SST k–ω turbulence models in predicting indoor environmental quality of buildings.

Some of the major studies on the application of CFD in predicting indoor air flow and contaminant levels have been extracted from literature and discussed below in chronological order of being published. Chen and Van der Kooi (1988) used a CFD programme and a building energy simulation programme to predict ventilation efficiency and temperature efficiency in a ventilated room having different ventilation systems and rates. Murakami et al. (1989) investigated air flow and contaminant diffusion in different types of rooms possessing various arrangements of supply and exhaust diffusers. During this study, influence of varying the number and arrangement of supply and exhaust ducts on air flow and contaminant distribution

together with the contribution of heat sources and sinks on the temperature distribution in a room were analyzed.

A CFD code has been applied for predicting thermal comfort and contaminant distribution in both mechanically and naturally ventilated offices by Awbi (1989), Awbi and Gan (1991, 1993) and Gan (1995). On comparing laminar and turbulent flow cases, it was revealed that turbulence has a major influence on air movement in a room, and use of reliable turbulent models and accurate boundary conditions are crucial in this regard.

Jacobsen and Nielsen (1993) simulated the thermal environment in a room with displacement ventilation system having heat sources. They used an extension of the k-ε turbulence model with a buoyancy factor to account for turbulent viscosity dependency on vertical temperature gradients. Alamdari, Bennett, and Rose (1994) applied CFD to simulate air flow field and temperature distribution in an open-plan office space with a displacement ventilation system.

Chen at al. (1995) applied CFD with conjugate heat transfer and radiation models to predict the thermal response of a room. During this study only surface to surface radiation was considered. Awbi (1996) investigated the performance of displacement and mixing ventilation systems in an office. He found that the displacement system could provide similar air quality in the breathing zone with only half the ventilation rate required by the mixing ventilation system.

Murakami, Kato, and Zeng (1998) analyzed the influence of occupants on the distribution of contaminants in a room. Topp et al. (1999) simulated emissions from building materials using CFD and reported that model predictions showed good agreement with experimental results. Lin, Chow, Fong and Liu (2000) applied CFD to predict profiles of CO_2, radon and moisture in a typical Hong Kong industrial workshop with displacement ventilation. It was concluded that prediction of pollutant distribution is more difficult than that of air temperature and air flow distribution. Papakonstantinou, Kiranoudis, and Markatos (2000) modelled velocity, pollutant concentrations and temperature distribution within the Athens archaeological museum using a three-dimensional CFD model. They predicted O_3, CO, SO_2, NO_x,

Pb and CO_2 concentrations indoors. A study of air quality within the breathing zone in a room with displacement ventilation was conducted by Xing, Hatton, and Awbi (2001). Xu and Chen (2001a, 2001b) developed a two-layer turbulence model to simulate indoor air flow with mixed convection. The results showed that their predictions agreed very well with the measurements. Several studies also focused on modelling energy performance and thermal comfort of buildings (Bartak et al., 2002; Beausoleil-Morrison, 2002; Zhai & Chen, 2003). Some of the recent work on indoor environment modelling includes studies conducted by Fan and Ito (2014), Zuo et al. (2014) and Gilani, Montazeri, and Blocken (2016).

Compared with the experimental approach for indoor environment analysis, CFD approach is less expensive and results are generated at a faster rate with shorter lead times. Furthermore, CFD can be applied to analyze flow and heat transfer conditions where experimental studies could prove difficult or impossible (Malkawi & Augenbroe, 2003). However, CFD results can be fully accepted only after conducting a comprehensive validation study.

7.6 Summary

This chapter explains fundamental concepts related to modelling of indoor environmental quality of buildings. It discusses the concepts on ventilation performance of buildings with reference to different mechanical ventilation configurations. Furthermore, it elaborates on the approaches for indoor environmental modelling: Semi-empirical, Zonal and CFD approach. Main turbulence models applicable in modelling indoor flows have also been discussed and compared. Finally, the chapter presents key studies related to indoor environmental modelling published in the literature.

8. MODELLING INDOOR ENVIRONMENTAL QUALITY

8.1 Overview

Modelling indoor environmental quality using the coupled Energy Simulation (ES) and Computational Fluid Dynamics (CFD) approach together with corresponding predictions have been discussed in detail in this chapter. EnergyPlus 8.0 and ANSYS Fluent 15.0 have been used as the ES and CFD tools respectively. MATLAB plays its role as the coupling platform, facilitating exchange of data between the said tools. For ease of demonstration and to manage computational power demands at an acceptable level, single-storey building considered in section 4.6.1 with its optimal envelope design has been reconsidered here. The indoor environmental quality of the building is modelled as per different standard mechanical ventilation configurations. Table 8.1 shows the thermal and electrical loads of the building considered.

Table 8.1: Thermal and Electrical loads

Load	Description
Occupancy	10 nos. of occupants involved in general office work with a specified occupancy schedule
HVAC system	Standard chilled water system
Lighting	200 W (4.17 W/m^2)
Electrical equipment	500 W (10.42 W/m^2)

CFD model of the building is shown in Figures 8.1 and 8.2.

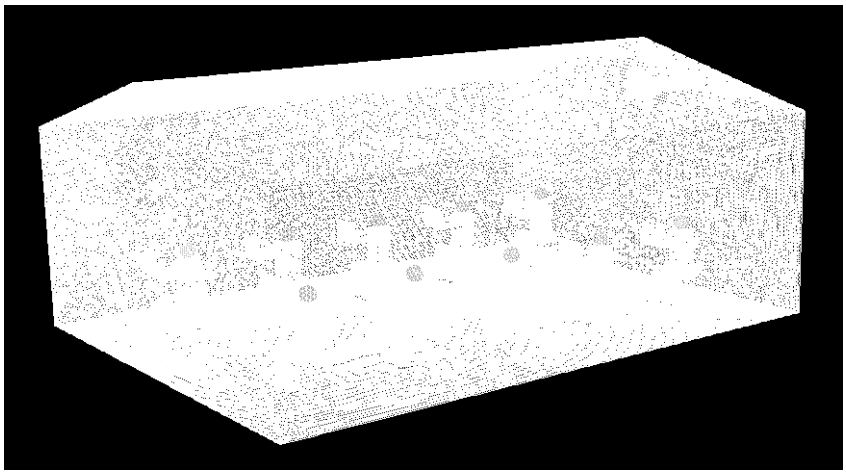

Figure 8.1: CFD model of the building

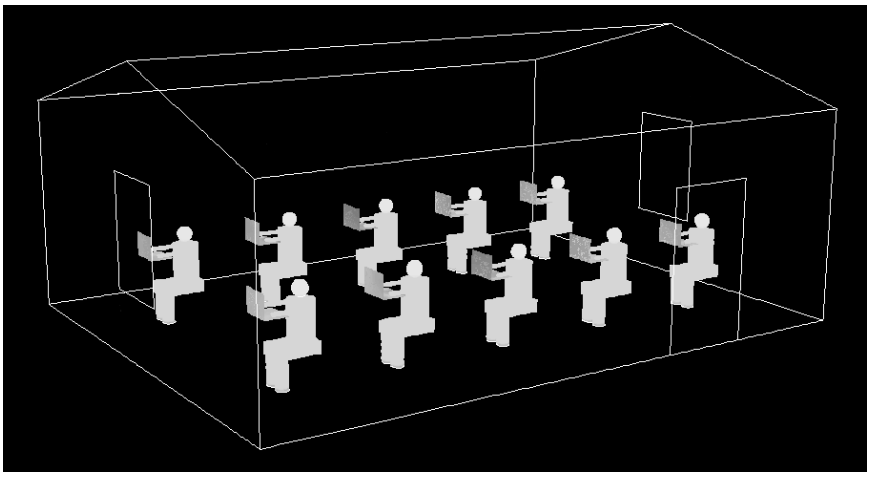

Figure 8.2: CFD model showing occupants

The CFD model consists of 1,692,867 hybrid mesh volumes in the computational domain. Computational grid has been checked against the phenomenon of "grid independence". Separate boundary meshes were generated for each surface of the building envelope to cater for convective heat transfer effects and boundary layer interactions. Average wall y-plus (y^+) has been 5.4. Table 8.2 shows boundary conditions and relevant models applied for the CFD simulations. A user defined function (UDF) was created using the C language to calculate the thermal comfort in the occupied space and it was subsequently integrated to ANSYS Fluent.

Table 8.2: Boundary conditions and models for CFD simulations

Boundary Conditions/Model	**Value/Model**
Air supply configuration	Identified mechanical ventilation configurations
Supply air temperature	16 ^{0}C
Supply air relative humidity	90%
Turbulence model	k-ε RNG
Discritization scheme	QUICK
Near-wall treatment	Finer computational mesh
Diffusion of emissions	Species transport model
Internal surface temperature	As predicted by EnergyPlus
Mass flow rate of exhaled air	2.6 x 10^{-4} kg/s per occupant
Relative humidity of exhaled air	Saturated state
Species mass fractions in exhaled air	
CO_2	0.050
H_2O	0.035
N_2	0.755
O_2	0.160

8.2 ES-CFD coupled approach

Workflow of the approach is illustrated in Figure 8.3.

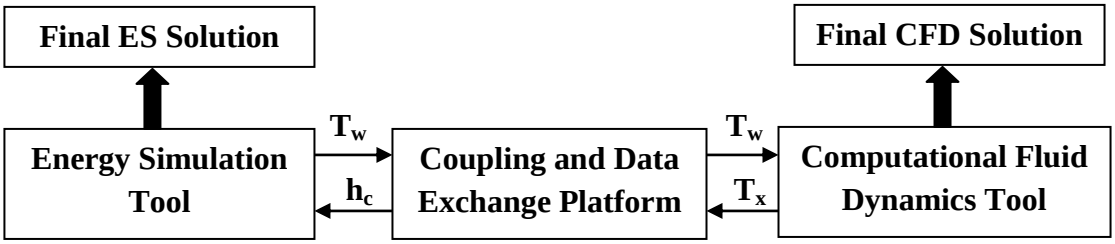

T_w - Envelope internal surface temperature

T_x - Local air temperature close to the envelope surface

h_c - Mean convective heat transfer coefficient at the envelope internal surface

Figure 8.3: Workflow of ES-CFD coupled approach

Coupled simulation was performed for the scenario that recorded the highest annual outdoor dry bulb temperature (recorded on 19th April at 12.10 pm) with reference to the weather file for Ratmalana area, which is the intended location of the building. During the simulations, Energyplus predicts internal surface temperatures of the building envelope elements and are subsequently transferred as boundary conditions for the CFD simulation run on Fluent. Then CFD simulation commences and when converged mean convective heat transfer coefficients of the internal building envelope elements are calculated and transferred back to EnergyPlus, followed by recommencement of EnergyPlus simulation. Continuation of the coupled simulation and transfer of information in between the tools through the MATLAB platform take place until consistent values are generated for the transfer variables. On completion of the coupled simulations, final ES and CFD solutions are generated.

8.3 Simulation Results

Coupled ES-CFD simulations were performed on an i5 workstation of 4 GB RAM as per different identified configurations of mechanical ventilation. Figures 8.4 to 8.10 illustrate the respective predicted indoor air flow fields for all ventilation configurations modelled.

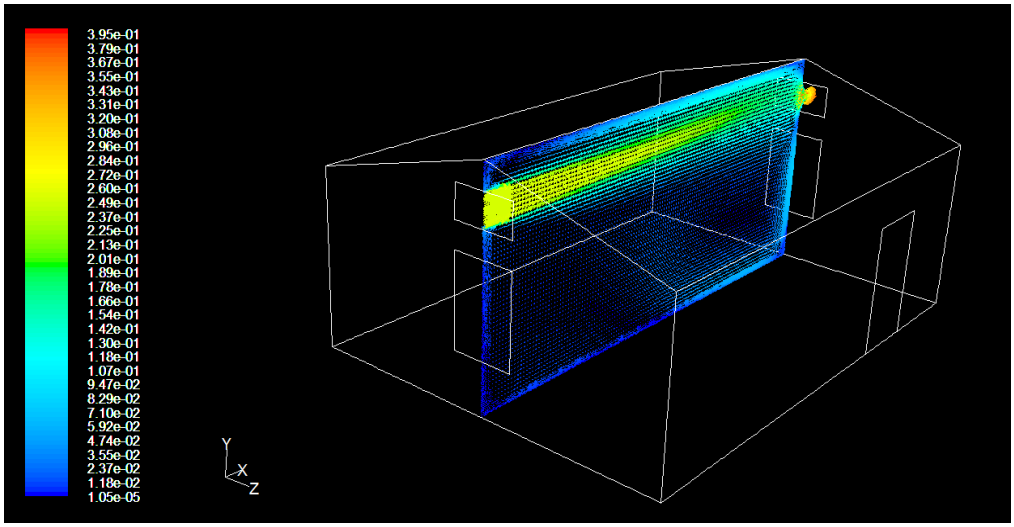

Figure 8.4: Air flow field for cavity flow ventilation

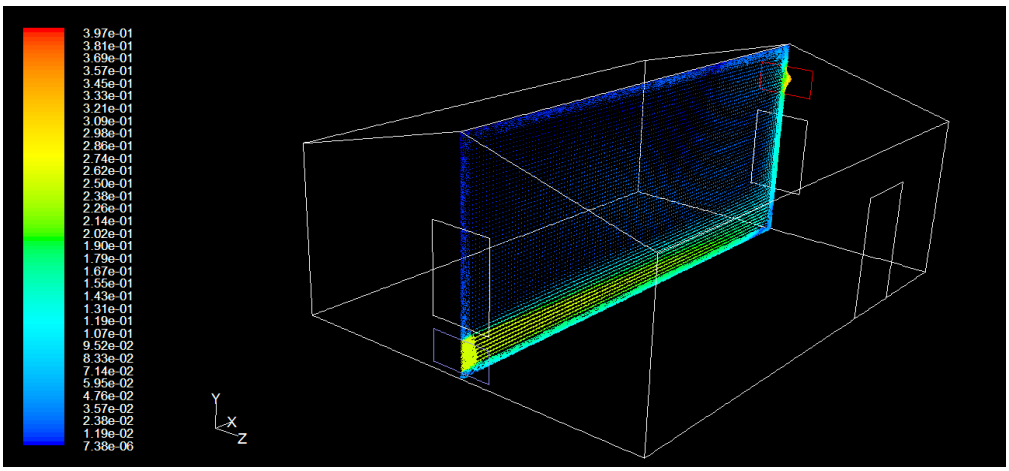

Figure 8.5: Air flow field for displacement flow ventilation

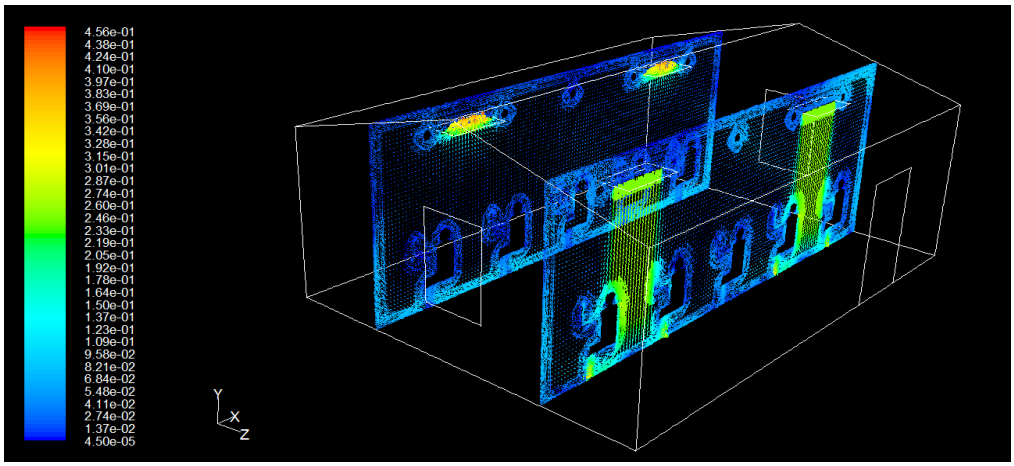

Figure 8.6: Air flow field for mixing flow ventilation – Case 1

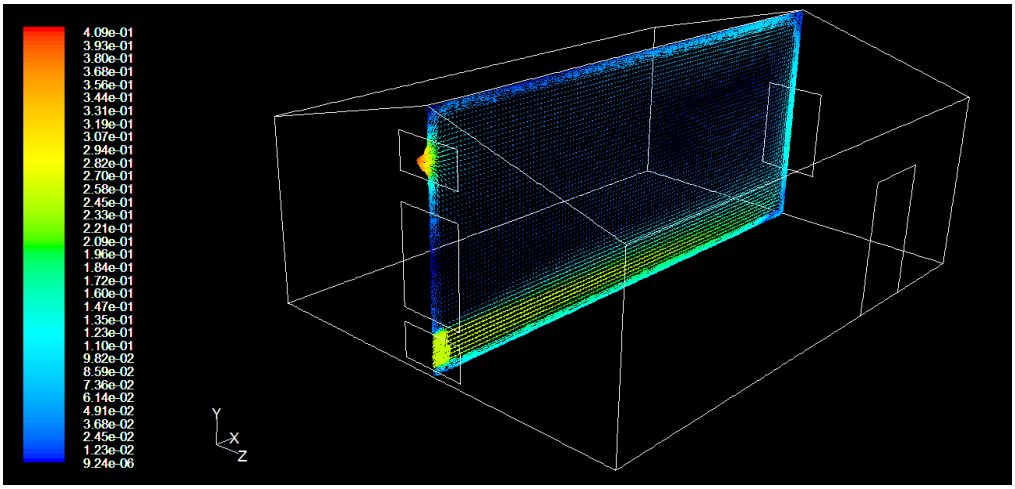

Figure 8.7: Air flow field for mixing flow ventilation – Case 2

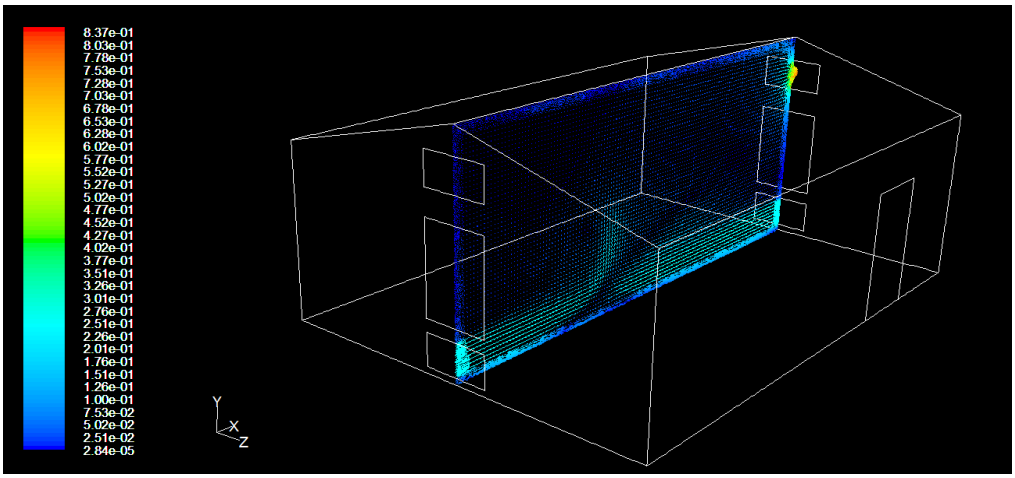

Figure 8.8: Air flow field for mixing flow ventilation – Case 3

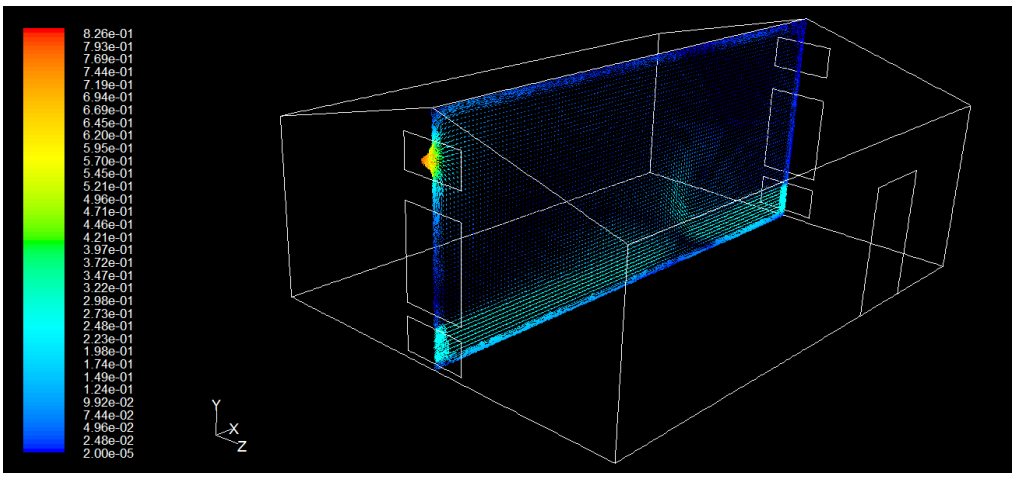

Figure 8.9: Air flow field for mixing flow ventilation – Case 4

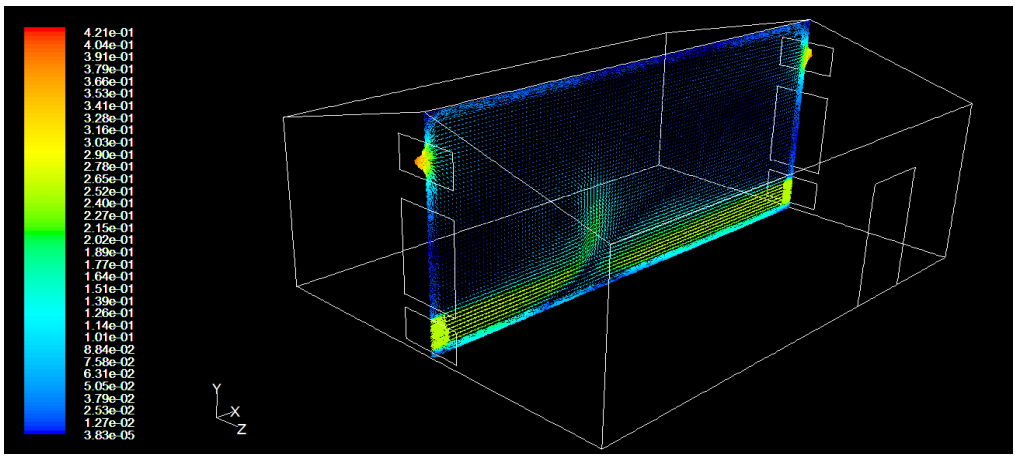

Figure 8.10: Air flow field for mixing flow ventilation – Case 5

Comparison of mean indoor environmental quality parameters on vertical occupant planes among different ventilation configurations is shown in Table 8.3.

Table 8.3: Comparison of mean values of indoor environmental quality parameters

Configuration of ventilation	**Air Temperature (^{0}C)**	**Air Velocity (ms^{-1})**	**Relative Humidity (%)**	**CO_2 Level (ppm)**	**Thermal Comfort (PMV)**
Cavity flow	28.8	0.017	55.8	1370	1.50
Displacement flow	28.6	0.021	52.8	1004	1.44
Mixing flow-Case 1	21.3	0.081	68.0	401	0.29
Mixing flow-Case 2	27.4	0.021	57.6	1133	1.29
Mixing flow-Case 3	23.1	0.030	66.9	677	0.61
Mixing flow-Case 4	23.0	0.031	68.8	770	0.61
Mixing flow-Case 5	22.7	0.031	70.9	844	0.56

The results in Table 8.3 show that the optimal indoor environmental quality on vertical occupant planes has been predicted for the mixing flow - case 1 in terms of both thermal comfort and CO_2 level among all ventilation configurations considered. Although for this case a higher relative humidity is predicted (68%), the best PMV is however expected due to lower air temperature and relatively higher air velocity compared to other configurations. This case is also expected to record the lowest CO_2 level among others.

Figures 8.11 and 8.12 show the predicted thermal comfort and CO_2 emission profiles respectively on vertical occupant planes for mixing flow ventilation – case 1.

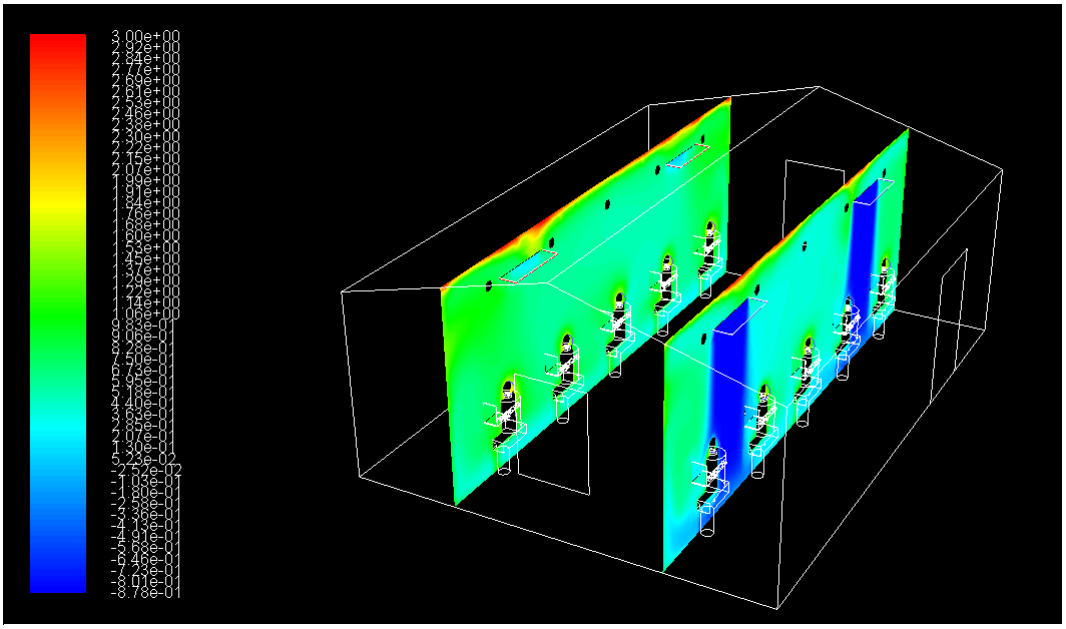

Figure 8.11: PMV thermal comfort profiles in mixing flow ventilation-Case 1

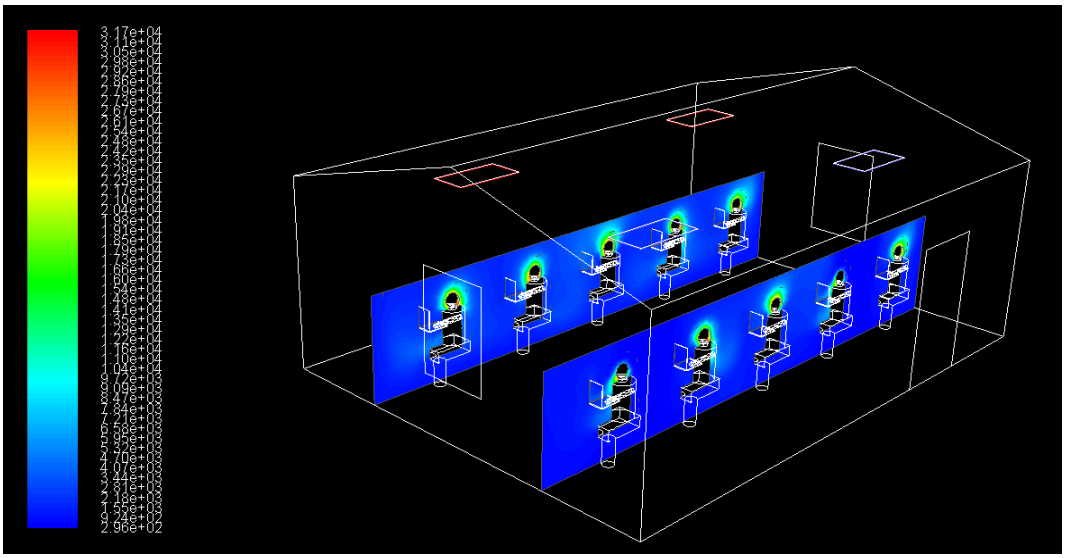

Figure 8.12: CO_2 profiles (in ppm) in mixing flow ventilation-Case 1

According to the ASHRAE standards (ASHRAE 55, 2017), thermal comfort related measurements are to be made at ankle level, waist level and neck level (0.1 m, 0.6 m and 1.1 m from floor level respectively) for seated occupants. Table 8.4 shows the predicted thermal comfort in terms of mean PMV values at the aforesaid levels for mixing flow ventilation-Case 1. Figure 8.13 illustrates predicted flow pathlines of

airborne particles released from occupants. In this configuration, it is observed that pathlines tend to spread throughout the occupied space.

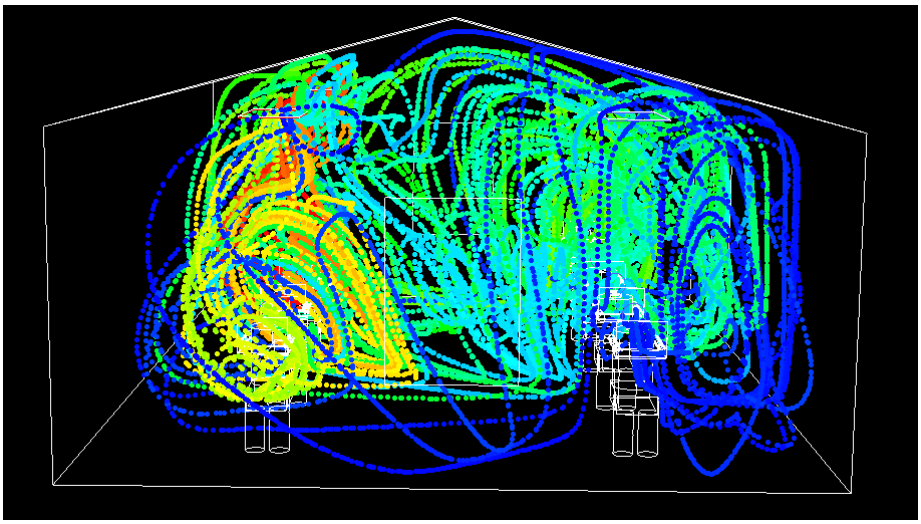

Figure 8.13: Pathlines of occupant emissions: Mixing flow ventilation-Case 1

Table 8.4: Predicted mean thermal comfort

Level	**Mean PMV on north side occupants**	**Mean PMV on south side occupants**
Ankle	0.39	-0.09
Waist	0.81	0.29
Neck	0.86	0.33

Figures 8.14, 8.15 and 8.16 show the predicted PMV at the said levels respectively.

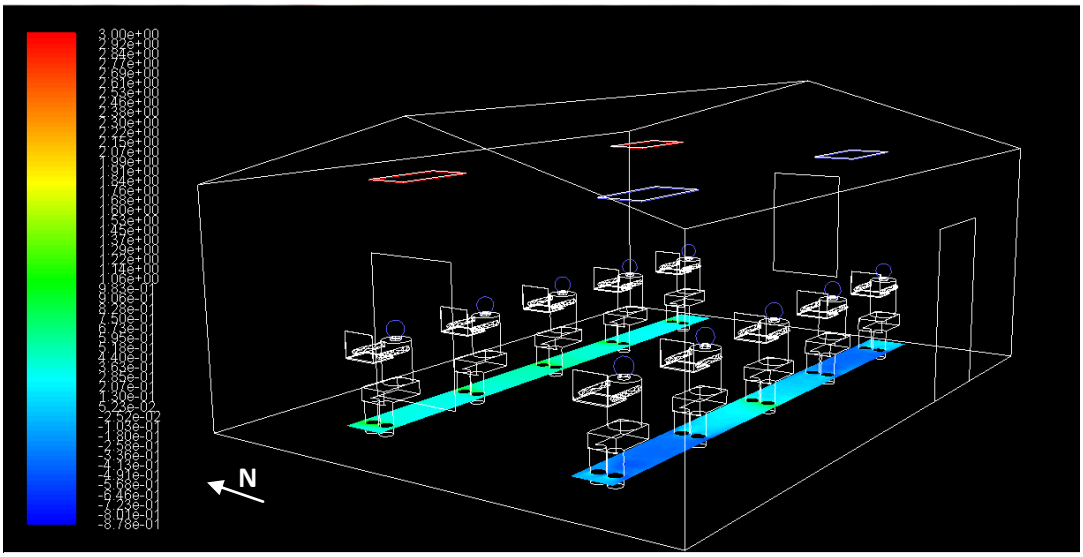

Figure 8.14: Predicted PMV at ankle level

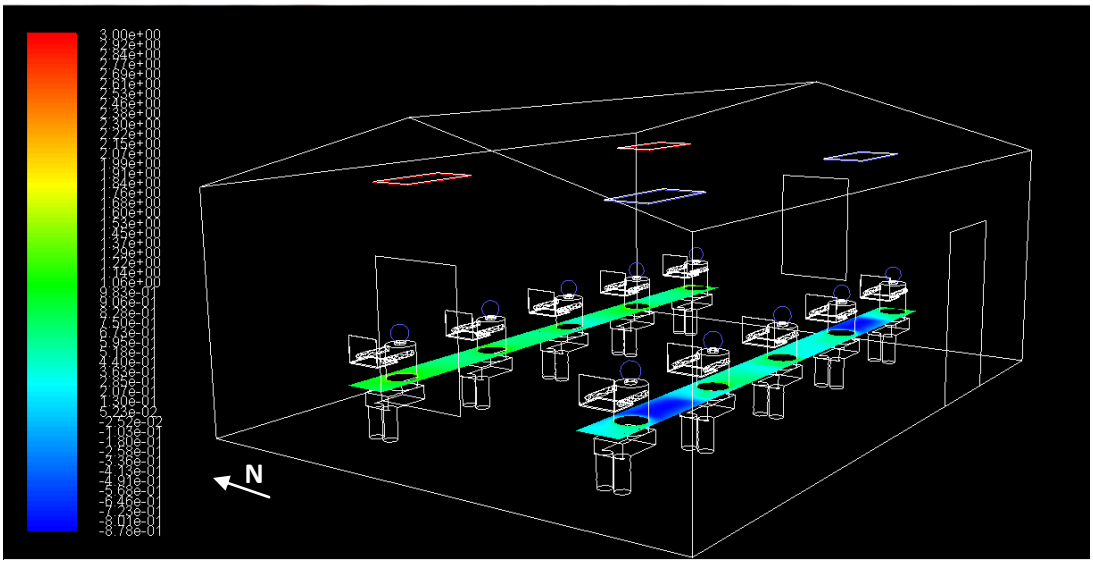

Figure 8.15: Predicted PMV at waist level

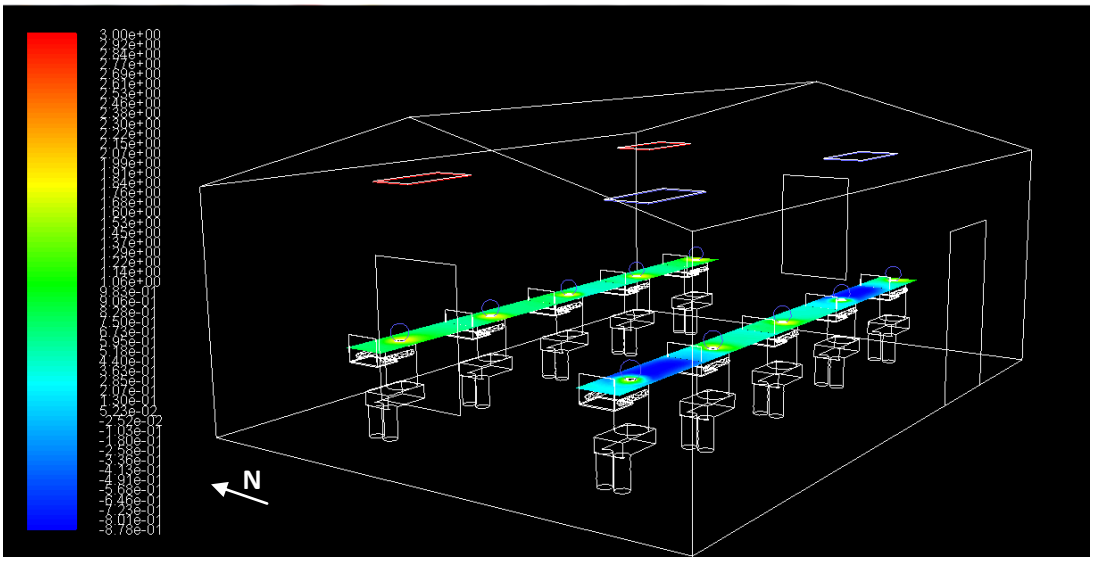

Figure 8.16: Predicted PMV at neck level

As per Table 8.4, south side occupants experience a more comfortable indoor thermal environment since all PMV values fall in between -0.5 and +0.5 which is recommended as the optimal range of PMV in the ASHRAE 55-2017 standard.

Modelling of indoor environmental quality has been performed for the scenario with maximum annual outdoor dry bulb temperature of the intended building location. The work may provide some general guidance for building designers related to the influence of the mechanical ventilation configuration on ventilation performance of a

simple building and eventually on the indoor environmental quality for human comfort and health. The computational models can be further refined by validating the CFD predictions through experimental measurements. Experimental validation of model predictions is discussed in the next chapter.

8.4 Summary

This chapter explains application of the ES-CFD coupled approach in predicting indoor environmental quality in a simple building in terms of thermal comfort and CO_2 concentrations. The predictions are made with respect to different standard mechanical ventilation configurations. Thermal comfort of occupants at standard levels has also been predicted.

9. VALIDATION OF MODEL PREDICTIONS

9.1 Overview

The validation process of model predictions on indoor environmental quality is discussed in this chapter. Postgraduate lecture room of the Department of Mechanical Engineering of the University of Moratuwa was utilized as the test facility for carrying out this task. Figures 9.1 and 9.2 show the details of the same.

Figure 9.1: Test facility

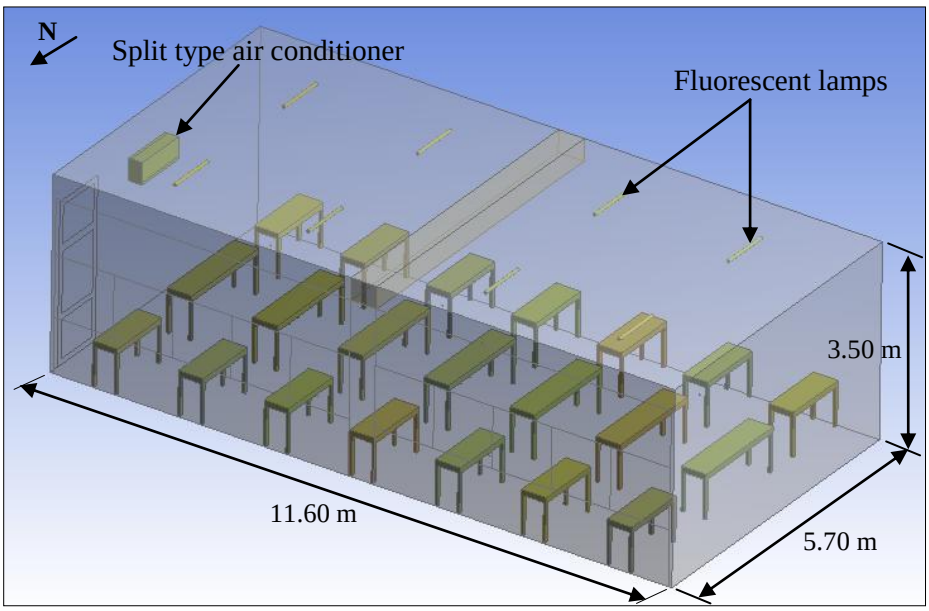

Figure 9.2: Basic features of test facility

The test facility having dimensions of 11.60 m x 5.70 m x 3.50 m as shown in Figure 9.2 is located at the fourth floor of the Mechanical Engineering building complex. It has three walls made of standard brickwork and the remaining being a partitioned wall that carries 10 nos. of glass sections each of 1.10 m x1.10 m. Figure 9.3 shows the details of the same.

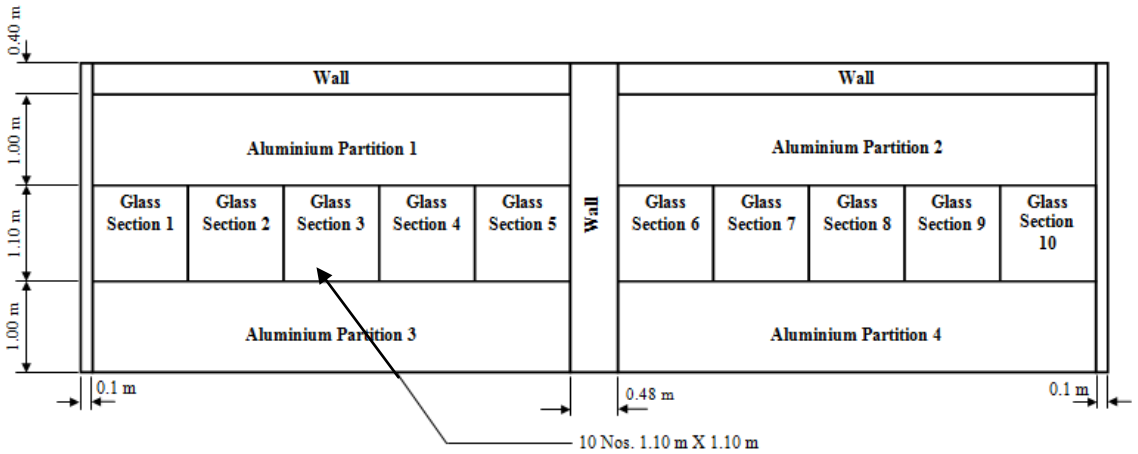

Figure 9.3: Details of north wall

The east wall has a door with dimensions of 2.92 m x 1.04 m made of glass and Aluminium partitions as shown in Figure 9.4.

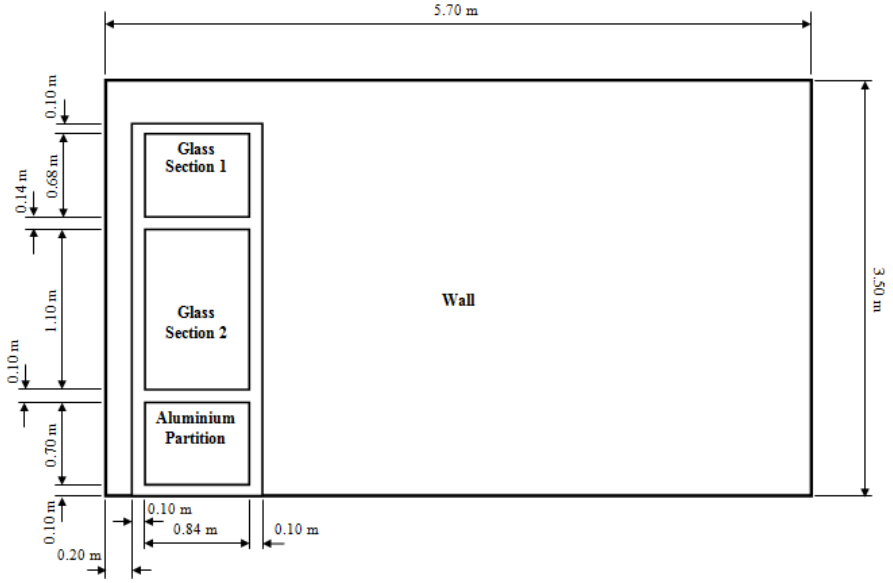

Figure 9.4: Details of east wall

Conditioned air is supplied to the occupied space by a split type air conditioner of 18000 BTU/h. The room is illuminated by 8 nos. of fluorescent lamps each of 20 W.

It consists of 14 nos. of tables each of 1.22 m x 0.46 m and 7 nos. of tables, each with dimensions of 1.84 m x 0.46 m.

9.2 Experimental Design

Experimental design was performed as follows according to the guidelines specified in the relevant standards (ASHRAE 55, 2017; ISO 16000-1, 2004):

- Measurements were made at specified occupants' workstations in the building space.
- Measurement locations included centre of the room and at 1.0 m inwards from the centre of each of the walls.
- Measurements were taken at locations where the most extreme values of thermal parameters are observed to occur (Such as diffuser inlet and outlet, near envelope walls etc.)
- Measurements were made sufficiently away from the boundaries of the occupied zone and any surfaces to allow for air circulation around sensors.
- Humidity of indoor air was measured at the centre of the occupied space.
- Indoor thermal and flow measurements were taken at 1.1 m from floor level for seated occupants.
- The minimum measuring period for determining the mean air velocity at any location to be three minutes.
- The measurements were taken for duration of two hours to establish the nature of the temperature cycle. An automatic recorder was used in taking measurements.
- Mean values of clothing and activity levels of the occupants were determined immediately one hour prior to measuring thermal parameters.
- Locations of measurement for CO_2 were at the centre of the space and at two other key locations at a height of 1.1 m above floor level (neck level of occupants).

Figure 9.5 shows the relevant experimental design layout.

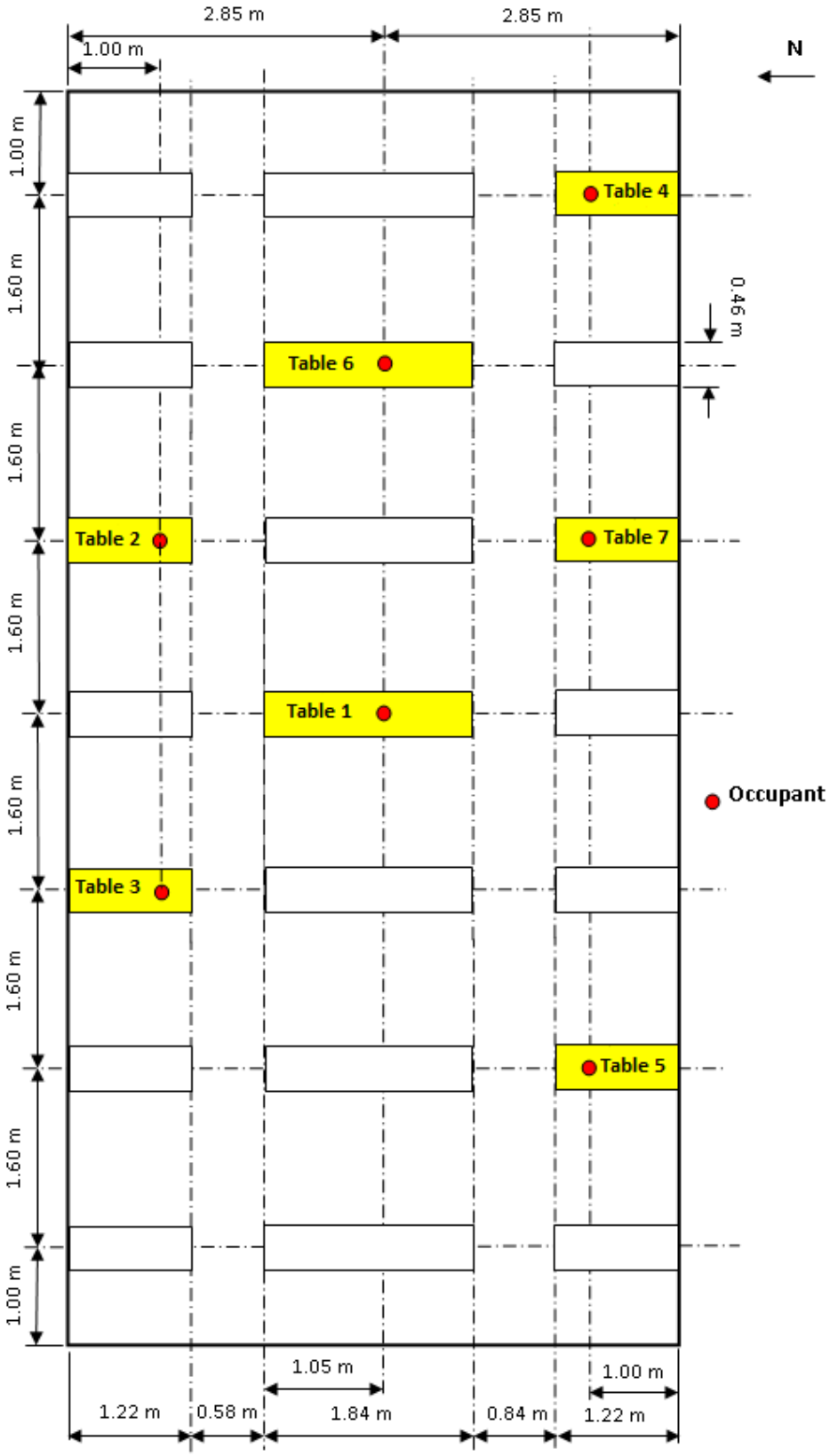

Figure 9.5: Plan view of the experimental design layout

9.3 Measuring equipment

Several equipment and tools of high precision have been used in taking measurements. They are compatible with the following standards for taking measurements in moderate thermal environments:

- ISO7726: Thermal environments (Instruments and methods for measuring physical quantities)
- ISO7730: Ergonomics of the thermal environment (Analytical determination and interpretation of satisfaction of thermal environment using calculation of PMV and PPD indices and local thermal comfort criteria)

A brief description on each of the equipment and tools is given below.

9.3.1 Omni-directional Anemometer (Swema 03)

This equipment shown in Figure 9.6 is capable of measuring air velocity and air temperature at a particular point in the occupied space. It is designed with a fast microcontroller and a small sensing element to achieve good dynamic qualities for response time and turbulence.

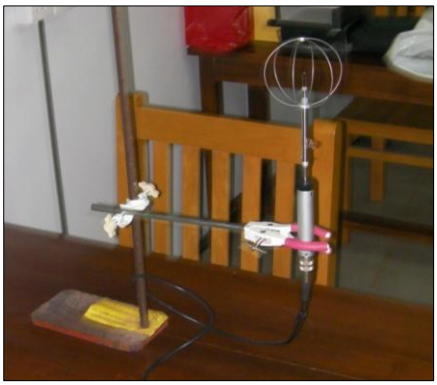

Figure 9.6: Omni-directional Anemometer (Swema-03)

The sensors are directional independent and sensitive for low air velocities that are typical for indoor flows. The equipment has exceptionally low self convection. The anemometer has a sampling frequency of 10 Hz with a time constant of 0.1 s. It can measure air velocities from 0.05 ms^{-1} to 3.00 ms^{-1} at an accuracy of ±0.04 ms^{-1} and also air temperatures within the range from 10 ^{0}C to 40 ^{0}C at an accuracy of ±0.5 °C.

Omni-directional anemometer can be set up with multiple probes and linked with the software programme SwemaMultipoint. Data transfer from the device can be performed through USB or RS485.

9.3.2 Black globe Temperature Sensor (Swema 05)

Black globe temperature sensor, shown in Figure 9.7 has a globe diameter of 150 mm with a 200 mm long rod of 10 mm diameter. The equipment is capable of measuring air temperatures from 0 ^{0}C to 50 ^{0}C at an accuracy of ±0.1 °C. The recommended sampling frequency is 10 Hz. The communication of measured data from the device to the data logger is made through USB and RS485. Data from the Omni-directional anemometer and Black globe temperature sensor can be used to calculate mean radiant temperature and operative temperature at a particular location in the occupied space.

Figure 9.7: Black globe temperature sensor (Swema-05)

9.3.3 Air humidity sensor (HygroClip2-S)

This equipment shown in Figure 9.8 is of 15 mm diameter and 83 mm long. It measures relative humidity and temperature of air using the Rotronic sensing element and digital calibration. The recommended sampling frequency is 10 Hz. It is capable of measuring relative humidity from 0 to 100% at an accuracy of ±0.8 % and also air temperature from -40 ^{0}C to 60 ^{0}C with an accuracy of ±0.3 °C. Communication of data takes place through USB.

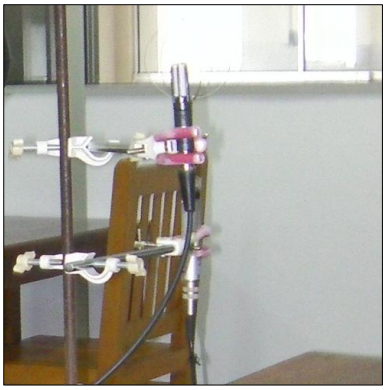

Figure 9.8: Air humidity sensor (HygroClip2-S)

9.3.4 Data logging software (SwemaMultipoint 3.5.1)

SwemaMultipoint 3.5.1 software is capable of logging measured data from different locations of an occupied space. It has three separate windows: for setup and storing data, presenting data on online graphs and the ISO 7730 window. The programme collects and saves data received from up to six Swema measurement devices and two HygroClip2 sensors. Data from each sensor is saved in an individual file that can be opened with MS Excel. Connections are through USB or RS485. Parameters calculated in SwemaMultipoint 3.5.1 include: PMV, PPD, Draught, Mixing ratio, Dew point, Wet bulb temperature and Operative temperature. The GUI of the SwemaMultipoint 3.5.1 is shown in Figure 9.9.

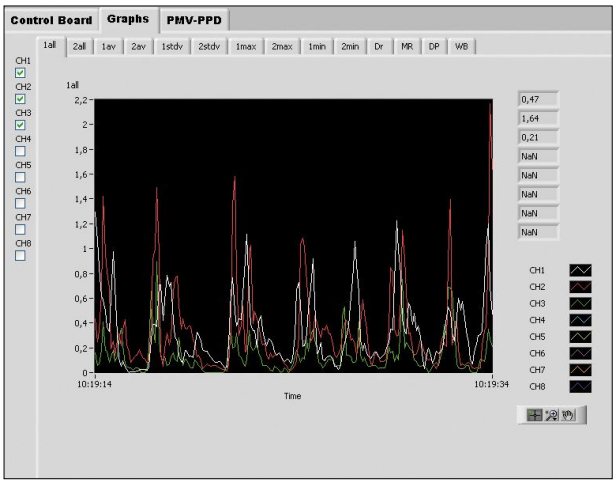

Figure 9.9: GUI of SwemaMultipoint 3.5.1 software

9.3.5 Thermal imaging camera (Fluke Ti400)

Figure 9.10: Thermal imaging camera (Fluke Ti400)

Thermal imaging camera shown in Figure 9.10 was utilized to measure surface temperature of building envelope elements to be applied as boundary conditions in the CFD simulations. This is capable of taking temperature measurements from -20 °C to 1200 °C with an accuracy of ±2%. Fluke Ti400 was also used for generating thermal images of occupants during the experiments.

9.3.6 Indoor air quality monitor (IQM 60)

Figure 9.11: Indoor air quality monitor (IQM 60)

IQM 60 equipment shown in Figure 9.11 was used to measure CO_2 concentration at selected locations in the occupied space. It has a range of measurement from 0 to 5000 ppm with an accuracy of ±3%. Data is logged to a removable secure digital (SD) card for post processing.

9.3.7 Other equipment

Other equipment used in conducting measurements is shown in Figure 9.12.

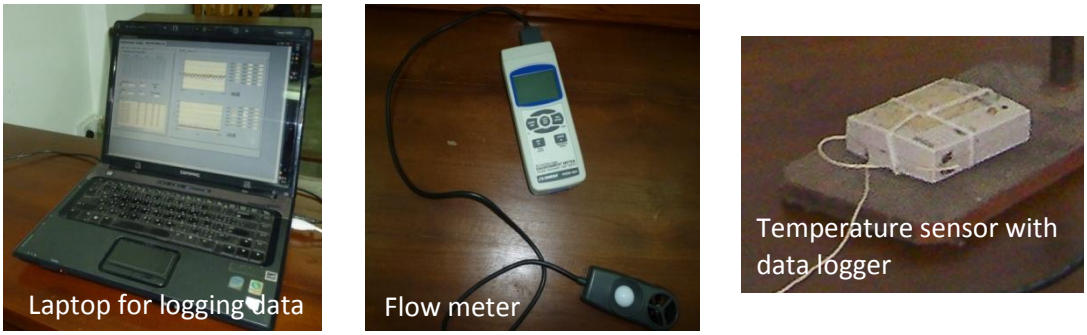

Figure 9.12: Other measuring equipment

9.4 Measurement process

Measuring tools and equipment were placed at the following locations of the test facility as per Table 9.1.

Table 9.1: Placement of measuring equipment

Location	Equipment
Table 1	Swema 03, Swema 05, HygroClip2-S and IQM 60
Table 2	Swema 03
Table 3	Swema 03 and IQM 60
Table 4	Swema 03
Table 5	Swema 03
Table 6	Swema 03
Table 7	Swema 03 and IQM 60
Air supply port	Flow meter and temperature sensor with data logger
Air discharge port	Temperature sensor with data logger

Measuring devices and tools were connected to the laptop computer in order to facilitate data logging through the USB port as shown in Figure 9.13. Prior to taking measurements, test room with the occupants was allowed to attain steady state conditions. Data acquisition was performed as shown in Figures 9.14 and 9.15. Data from the measuring devices were allowed to transfer to the data logger at 0.1 s time intervals. The measurements were taken continuously for a period of two hours. Thermal images of occupants were taken with the thermal imaging camera. The

occupants were also asked to complete a structured questionnaire related to their thermal sensation at 20 minute intervals during this period.

Figure 9.13: Measuring equipment setup

Figure 9.14: Acquisition of thermal data

Figure 9.15: Acquisition of CO_2 data

9.5 Modelling test facility

9.5.1 Creation of geometrical model

The geometrical model shown in Figure 9.16 was created using the DesignModeler software in the ANSYS Workbench. Seated thermal manikins were developed as per measured data of an average person and each of them has a body surface area of 1.52 m^2.

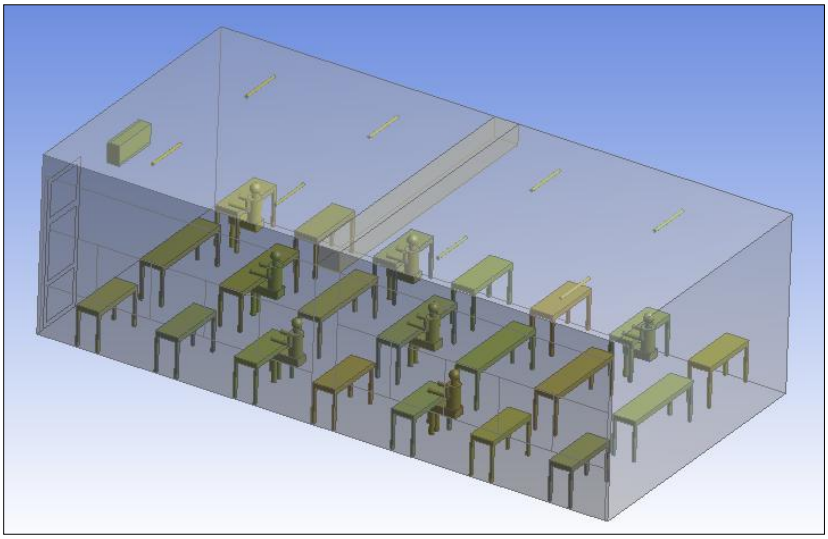

Figure 9.16: Geometrical model of test facility

9.5.2 Creation of computational model

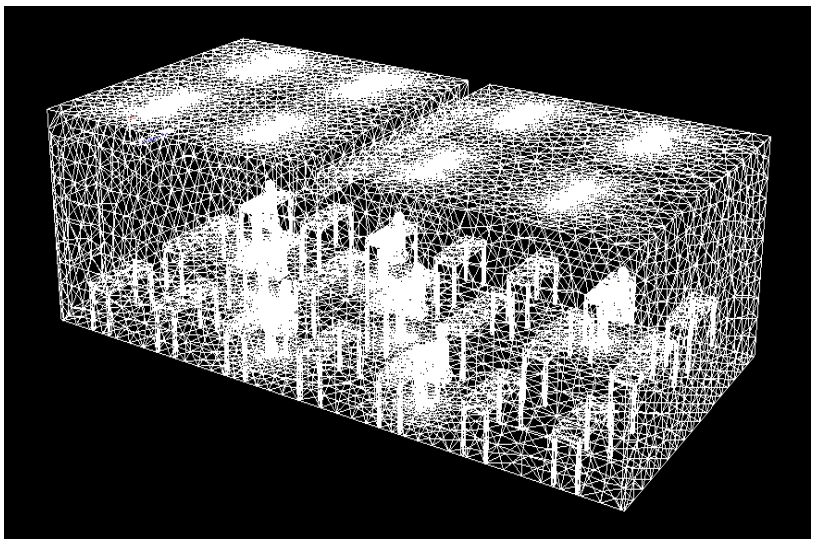

Figure 9.17: Computational model of test facility

Figure 9.17 shows the computational model of test facility created on ANSYS Workbench. It consists of 2,401,000 hybrid mesh volumes in the computational domain. Number of mesh volumes was finalized after checking against the phenomena of "grid independence". Average wall y-plus (y^+) has been 3.2. Tables 9.2 and 9.3 show relevant models and boundary conditions applied for the CFD simulations respectively.

Table 9.2: Models for CFD simulations

Parameter	**Model or Approach**
Turbulence model	Standard k-ε model/ RNG k-ε model/ Realizable k-ε model/ k-ω SST model
Radiation model	Discrete transfer model (DTRM) and Discrete ordinates model (DO)
Discritization scheme	Quadratic upstream interpolation for convective kinematics (QUICK) scheme
Near-wall treatment	Finer surface mesh
Pressure-velocity coupling	Coupled scheme
Diffusion of emissions	Species transport model in ANSYS Fluent
Buoyancy effects	Boussinesq model

Table 9.3: Boundary conditions

Parameter	**Value/Status**
Supply air temperature	17 ^{0}C (Measured value)
Supply air relative humidity	82% (Measured value)
Internal surface temperatures (^{0}C) (As per measurements taken)	
North Wall	30.8
South Wall	30.8
East Wall	31.0
West Wall	31.4
Floor	30.2
East-side Slab	35.2
West-side Slab	31.4
Wall Partition 1	30.6
Wall Partition 2	31.4
Wall Partition 3	30.4
Wall Partition 4	30.8
Mass flow rate of exhaled air	1.6 x 10^{-4} kg/s per occupant
Boundary Conditions	
Supply port	Velocity inflow
Discharge port	Constant pressure outlet
Building envelope elements	Isothermal walls
Occupants	Wall with a constant heat flux
Nose of an occupant	Mass inflow boundary of CO_2 and moisture

Separate boundary meshes were created for each envelope surface of the test room in order to capture boundary layer interactions and wall convective heat transfer effects. All building envelope elements were modelled as isothermal walls assigned with relevant measured temperatures. Boundary condition of an occupant was taken as a wall with a constant heat flux of 55 W/m^2. Furthermore, nose of a particular occupant was assigned with a mass inflow boundary of CO_2 and moisture.

Buoyancy effects are significant in indoor flows. Hence, this aspect was addressed in the computational model in two ways. Firstly, influence of gravity was incorporated in the model. Moreover, Boussinesq model that modifies the source term due to gravity in the momentum equations was applied. Boussinesq eddy-viscosity hypothesis assumes that turbulent stresses in the governing equations can be related to the mean strain rate algebraically.

Simulations were conducted using k-ε and k-ω SST turbulence models. A UDF using C language was created to determine PMV and PPD values at each node point in the computational domain. For PMV calculations, mean radiant temperature, metabolic rate of occupants and clothing insulation have been assigned with 29 ^{0}C (measured value), 1.0 Met and 0.7 clo respectively. The CFD simulations were run on an Intel Core i5 3.2 GHz workstation of 4.0 GB RAM. Steady state CFD solutions were generated in par with the ASHRAE standards.

9.6 Comparison of model predictions against measurements

9.6.1 Overview

Standard k-ε model (Launder & Spalding, 1972), RNG k-ε model (Yakot & Orszag, 1986), Realizable k-ε model (Shih, Liou, Shabbir, Yang, & Zhu, 1995) and k-ω SST model (Menter, 1994) were applied in the CFD simulations. However, all k-ε models failed to generate an acceptable solution in this regard possibly due to poor performance at the boundary layer. Only k-ω SST model was able to produce a reliable CFD solution among those considered. This was in agreement that k-ω SST model has always shown good near-wall performance and has been able to produce better heat transfer predictions in modelling indoor flows as mentioned in the

literature (Vieser, Esch, & Menter, 2002; Zhai et al., 2007). In free stream conditions away from the solid surfaces, k-ω SST model and all k-ε models behaved in a similar manner. However, close to the solid surfaces such as building envelope elements, furniture and occupants, all k-ε models performed poorly, especially in the region of viscous sub-layer. This became worse since there were many such solid surfaces in the computational domain of the building. Furthermore, standard k-ε model failed possibly due to buoyant flows existing in the indoor environment. Because of this reason, a low-Reynolds number turbulence model such as k-ε RNG model was used. However, it also failed within the boundary layer, since this model still largely depends on the eddy-viscosity hypothesis. In order to facilitate turbulence modelling with k-ω SST model, a fine computational model comprised of 2,401,000 mesh volumes was generated having a lower y+ value of 3.2.

9.6.2 Indoor air velocity

Figure 9.18 compares indoor air velocity model predictions against measurements.

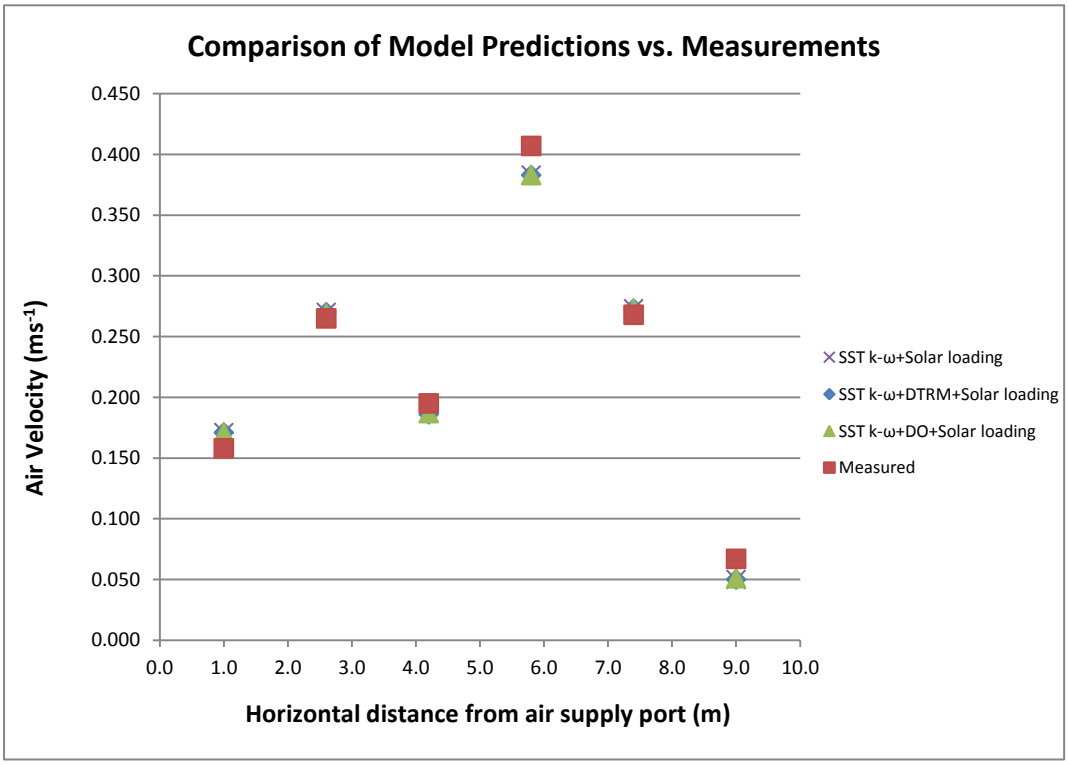

Figure 9.18: Model predictions against measurements: Air velocity

From the Figure 9.18 it is evident that there exists a good agreement between the model predictions and measurements of air velocity in the building space. The best agreement is shown by the k-ω SST model incorporated with Discrete Ordinates (DO) radiation model together with solar loading. Other models also show fairly good agreement with the measured data. It is also observed that inclusion of radiation models have not influenced much on the air velocity in the occupied space.

9.6.3 Indoor air temperature

Figure 9.19 illustrates a comparison between indoor air temperature model predictions and measurements.

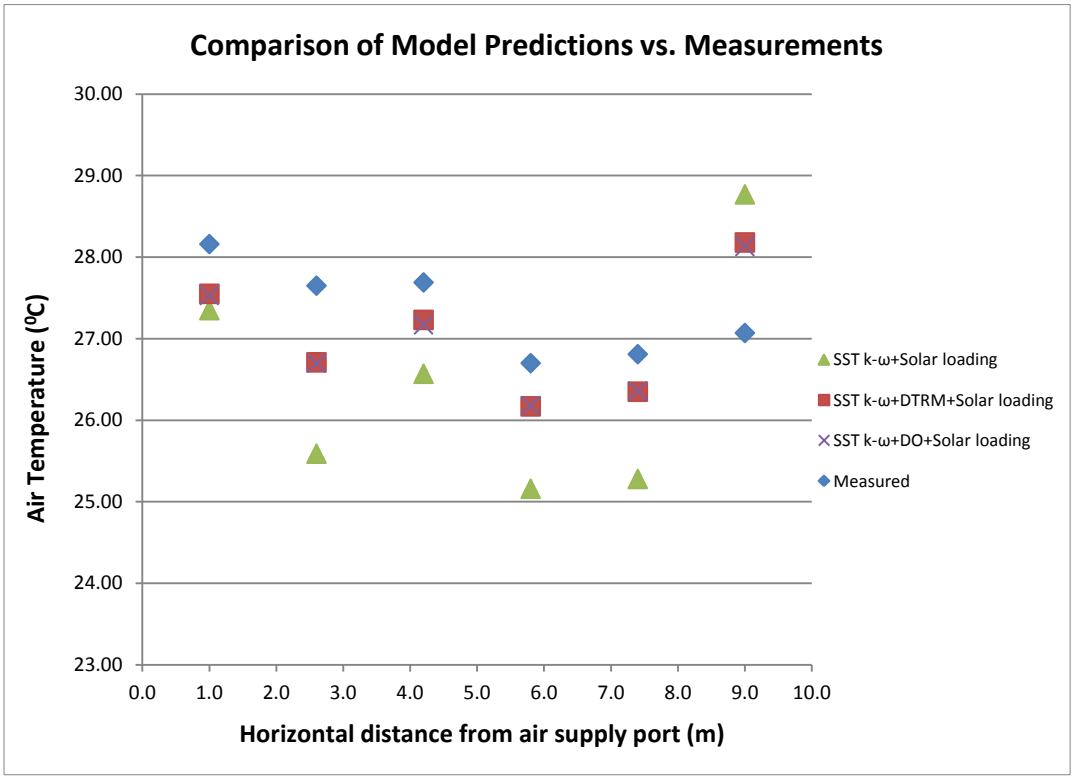

Figure 9.19: Model predictions against measurements: Air temperature

Predicted air temperature within the test facility also showed a fairly reasonable agreement against the measurements. The best agreement has been recorded by the k-ω SST model incorporated with Discrete Ordinates radiation model and solar loading. The maximum discrepancy observed in this regard is only 4%. It is evident

that application of radiation models has created a substantial influence on the air temperature predictions.

9.6.4 Thermal comfort

Figures 9.20 and 9.21 show a comparison of model predictions and measurements of thermal comfort in terms of PMV and PPD values.

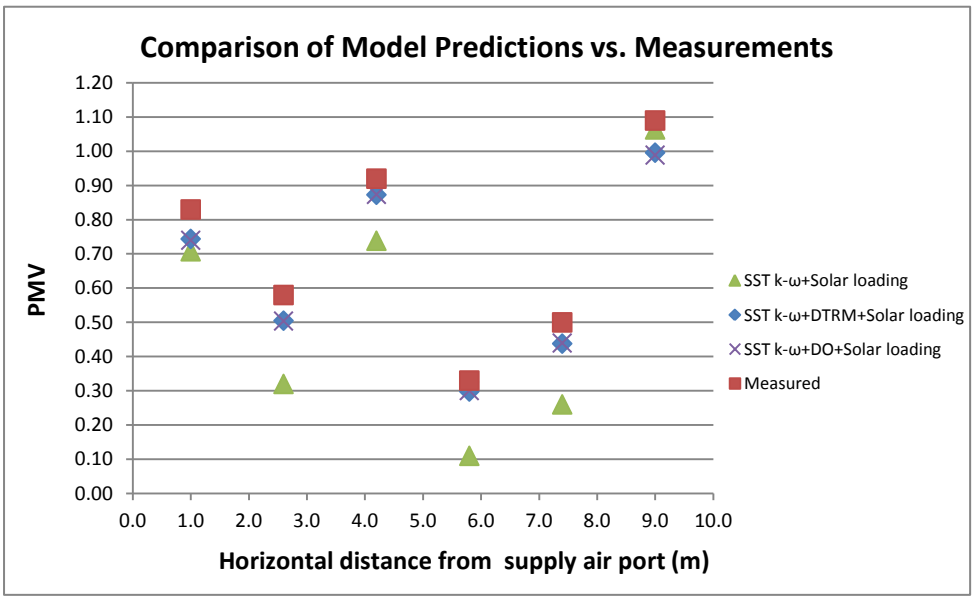

Figure 9.20: Model predictions against measurements: PMV

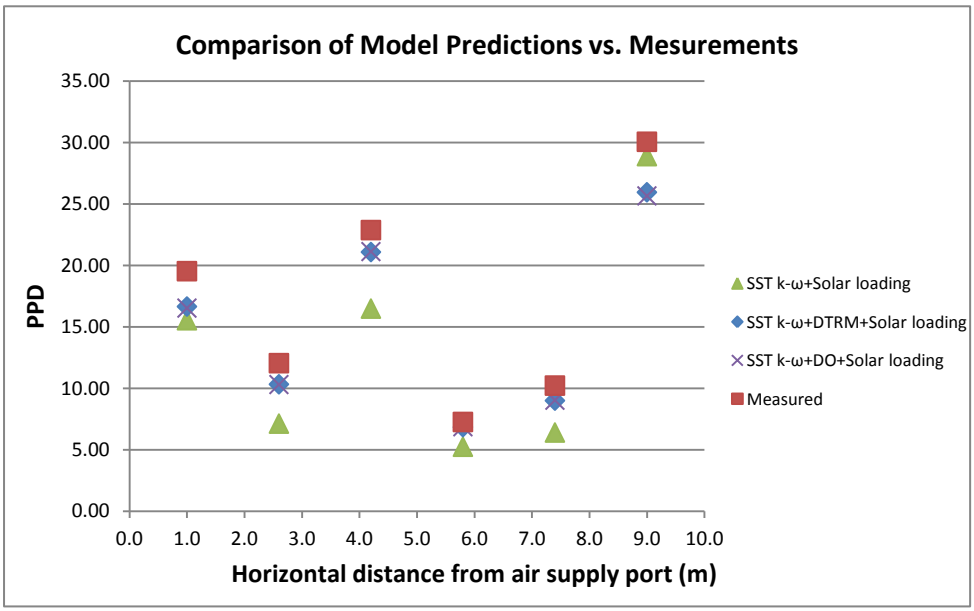

Figure 9.21: Model predictions against measurements: PPD

A fairly good agreement is recorded by k-ω SST model when incorporated with both DTRM and DO radiation models against measurements. The maximum discrepancy recorded in this regard is 13.1%. Figure 9.22 shows the predicted thermal comfort profile of k-ω SST with DO radiation model and solar loading at the centre plane.

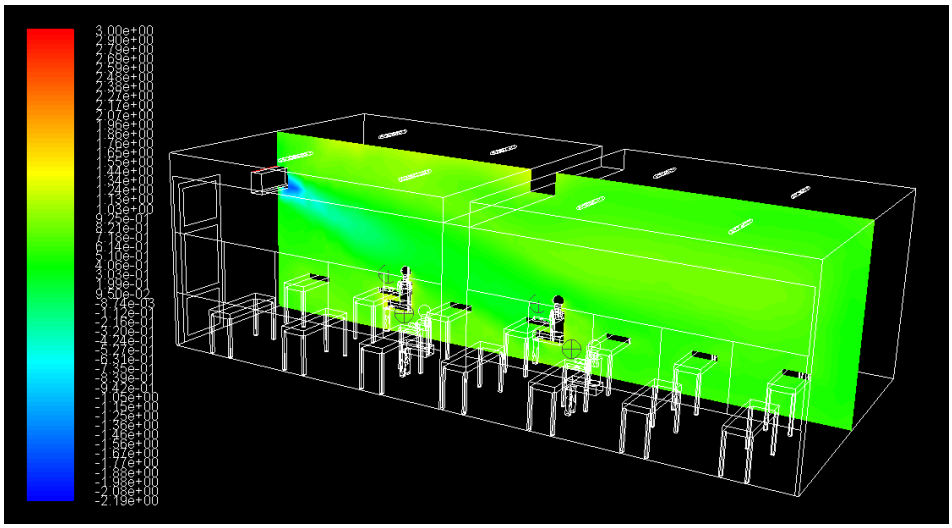

Figure 9.22: Predicted PMV profile in the centre plane: k-ω SST and DO model

9.6.5 CO_2 concentration

Comparison of model predictions against measurements of CO_2 concentration in the occupied space is shown in Figure 9.23.

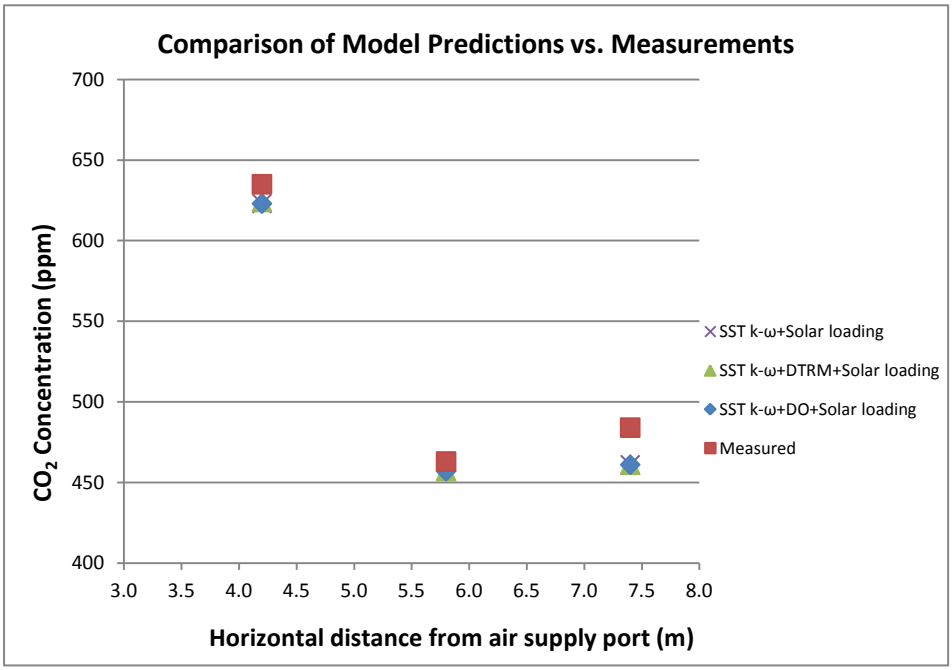

Figure 9.23: Model predictions against measurements: CO_2 concentration

The measurements were taken at three recommended locations including the centre of the building space as per standards (ISO 16000-1, 2004). The model predictions are in good agreement with measurements. The best agreement is recorded by the k-ω SST model incorporated with Discrete Transfer radiation model and solar loading. The maximum discrepancy recorded in this case is approximately 5%. However, it is observed that influence of radiation models on the predicted CO_2 level at a particular location in the occupied space is not significant. Moreover, maximum concentration of CO_2 measured at key positions within the test facility is 635 ppm, which stays well below the allowable level of 1000 ppm recommended by ASRAE standards.

9.7 Summary

This chapter explains the validation process of model predictions through measurements conducted in an actual indoor environment. It elaborates on the experimental design, measurement procedure and tools and equipment used. The computational model of the test facility has been simulated using different turbulence and radiation models. It is observed that model predictions show a fairly close agreement with measurements.

10. CONCLUSION

10.1 Performance-based modelling and optimization

Building performance modelling and simulation has become one of the most important tools available to the building designers and policy makers at present. However, the true potential of building performance modelling is not yet fully made use of in the modern building construction industry. Instead, mostly prescriptive building standards imposed either by the local or national authorities are followed or implemented by the building designers. Prescriptive standards stipulate mandatory and prescriptive criteria for generic building elements related to building services, equipment and energy supply conditions to be complied by the user. This includes building envelope, HVAC equipment, lighting system, service hot water system, power supply and auxiliary equipment. Hence, prescriptive standards establish only the minimum performance levels for the buildings but do not indicate the optimal level of achievement. On this basis, most building envelope designs end up being sub optimal designs. However, performance based standards proceed one step further and attempt to optimize performance of buildings through which substantial savings on energy cost can be achieved while meeting the design intent. Hence, by adopting building performance modelling coupled with generic optimization, it is possible to come up with optimal or near optimal building envelope designs subjected to predefined constraints. Present work firstly, concentrated on how this approach could be implemented in optimizing the performance of buildings in terms of building envelope elements with respect to annual energy consumption and life cycle cost. On this context, an objective function is established depending on the specified performance criteria.

During present work two independent objective functions; namely; annual energy consumption and life cycle cost were established. The said objective functions were considered separately. A penalty function was incorporated as needed in order to ensure that optimal solutions do not aggravate the thermal comfort of the occupied space. A particular objective function was minimized with respect to a set of independent variables operating under predefined constraints. The list consists of

both continuous and discrete variables. The study considered variables related to the building envelope geometry (e.g., Building orientation), envelope configuration related variables (e.g., Window-to-Wall Ratio, Location of fenestrations, Wall material, Roof material etc.) and shading related variables (e.g., Overhang depth). All variables are of continuous type except wall and roof materials which can be classified as discrete variables. Continuous variables are controlled by box constraints having upper and lower bounds. Discrete variables are managed by selective constraints. The constraints for the envelope variables were setup based on practical limitations of construction. Any whole building energy simulation tool, including EnergyPlus is not in a position to compute the value of the objective function alone. The process was supported by the user developed codes included in the initiation file of GenOpt, using inputs received from EnergyPlus simulations at each time step of the optimization process.

Objective function for annual energy consumption is the sum of the individual energy usage quantities related to heating, cooling, lighting and process and non-process equipment. In the Sri Lankan context, building cooling is the dominant component whereas contribution due to heating is minimal. Optimal window-to-wall ratio (WWR) was determined upon the compromise established among cooling load, demand for artificial lighting and availability and usage of daylight. When WWR is increased, demand for artificial lighting can be reduced substantially by exploiting natural daylight. On the other hand, a higher WWR will lead to an increased cooling load. Hence a compromise is reached so that the annual energy consumption becomes a minimum. The case studies show that notable saving on annual energy consumption and life cycle cost could be achieved by optimizing building envelope through energy modelling coupled with generic optimization approach. Notable changes in the building orientation and window-to-wall ratio could be observed in the optimal envelope designs compared to the base designs. Furthermore, it is observed that reduction in window-to-wall ratio in the optimal envelope design leads to a considerable increase in energy consumption for lighting. However, it is compensated through a substantial energy saving on building cooling, which is the dominating factor, which contributes to the annual energy consumption of the

building. Locations of fenestrations on the optimal building envelope also have undergone notable changes compared to that of the base design. Among typical building wall and roof material used in Sri Lanka, brickwork and Calicut tiles combination produced the maximum percentage of saving in annual energy consumption in all case studies. Furthermore, the optimal envelope design led to a better level of thermal comfort for the occupants. Thermal comfort for the building was determined by the weighted average of the Predicted Mean Vote ($PMV_{weighted}$) calculated as per cooling load of each thermal zone of the building.

Objective function for the life cycle cost is the sum of the investment cost and the present values of operating costs incurred at different points during the lifetime of the building. Investment costs include the costs incurred on the construction of walls and windows and capital cost of the HVAC system. Escalation of electrical energy and fuel prices and rate of inflation were also considered in the analysis. Operating energy costs become the dominant component in the objective function. The case studies clearly show that substantial saving on life cycle cost could be achieved by implementing the present approach irrespective of the combinations of material being used on the envelope. Notable changes in the building orientation and window-to-wall ratio were observed in the optimal envelope designs compared to the base designs. Furthermore, it was observed that reduction in window-to-wall ratio in the optimal envelope design lead to a notable increase in the construction cost of walls. However, it is compensated through a substantial saving on building energy costs, which is the dominating aspect which contributes to the life cycle cost of the building. Among the common wall and roof material combinations, brickwork and Calicut tiles combination produced the maximum percentage of saving in life cycle cost for all case studies, as in the case of annual energy consumption. Also the optimal envelope design led to a better level of thermal comfort for the occupants as in the case of annual energy consumption.

Different optimization algorithms were tested by conducting many numerical experiments during present work. This included direct search algorithms (Coordinate search algorithm, Hooke-Jeeves algorithm and Nelder and Mead algorithm), gradient based algorithms (Discrete Armijo Gradient algorithm and Levenberg-Marquardt

algorithm) and a hybrid algorithm (GPSPSOCCHJ algorithm). It was observed that the two gradient based algorithms and the Nelder and Mead direct search algorithm failed during numerical experiments in terms of stability and not being able to produce an acceptable solution. Hooke-Jeeves algorithm performed better in terms of stability but had the tendency of getting trapped in local minima. According to literature (Wetter & Wright, 2004; Nguyen et al., 2014) hybrid algorithms show an impressive capability to deal with discontinuous, highly constrained multimodal problems as frequently found in building simulation outputs. During numerical experiments, hybrid algorithm GPSPSOCCHJ generated the best results confirming the recommendations found in the literature as given above.

Performance of any optimization algorithm depends on its control parameters. Hence several numerical experiments had to be conducted to come up with an acceptable set of values for the parameters that would successfully carryout the optimization process. However, complete refining of the said parameters was not performed since it was a highly time consuming and a tedious task. Instead, an acceptable set of values that produced reliable results during the numerical experiments were assigned to the parameters of the algorithm.

Optimization process was attempted with different initial conditions and each ended with the same unique optimal solution with respect to all case studies considered using the GPSPSOCCHJ algorithm. To ensure that optimization algorithm actually converged to a global minimum, considerable number of parametric runs based on practical values of possible envelope element combinations was performed for all case studies. However, none of the parametric runs produced a lower value for the objective functions than that generated by GenOpt with respect to optimal solutions. Hence, it can be concluded that solutions obtained through present approach are very likely to be the global minima of the solution space for the two objective functions within the scope of this study. According to the literature (Hasan et al., 2008), a brute-force search is the best method to check the aforementioned condition. This is an exhaustive search that systematically enumerates all possible candidate solutions (Hasan et al., 2008). However, since it is a highly time consuming and a tiring exercise, it was not implemented during the present study. Furthermore, a sensitivity

analysis has been performed with respect to plant efficiencies for all building case studies and this showed negligible sensitivity on the respective optimal solutions due to variations in plant efficiencies.

One should clearly understand that, actual building conditions and performance could only be matched through a well calibrated building simulation, something considered to be a difficult task in practice. Hence, performance based methods demand additional efforts in order to make use of their full potential. In this context, building designers are expected to possess competencies related to building performance modelling tools together with the usage of optimization techniques. Therefore, the lessons learnt through application of performance based modelling coupled with generic optimization during present work can contribute to the Sri Lankan building sector substantially, which still remains mostly as an unexplored area.

10.2 Challenges in making reliable predictions

Although combined performance modelling and generic optimization has proved to be an efficient tool in optimizing performance of buildings, there are certain drawbacks that need to be addressed for making enhanced level of predictions. Main source of drawbacks is the inherent limitations possessed by whole building simulation tools. EnergyPlus adopts a “nodal” approach in modelling thermal processes taking place in a building by applying deliberate simplifications. The underlying simplifying assumptions lead to limitations explained in Chapter 6. Application of Computational Fluid Dynamics (CFD) can be considered as the best possible option to address the said issues. CFD tools can predict airflow paths and velocities within a thermal zone of a building accurately. Hence, CFD is capable of determining the temperature field within building space and convective heat transfer coefficients at building envelope elements. This information is vital for Energy Simulation (ES) tools to predict building energy consumption accurately. Furthermore, CFD also requires information related to envelope surface temperatures and heat fluxes through the building envelope from ES tools, to be used as boundary conditions in order to generate indoor air flow and temperature fields. Hence,

information generated by both ES and CFD tools are complementary and integration of the said tools results in more accurate predictions on building performance.

ES and CFD tools can be coupled based on different strategies. In internal coupling, both hard and loose approaches are highly computationally expensive. Hence during present work, external coupling (loose coupling) approach was adopted and ES and CFD tools were coupled on a common platform through one-step static data exchange mechanism. However, even with this approach, coupled simulations were limited only for two key scenarios, since computational time and effort were still considerably high. Scenarios related to maximum and minimum outdoor dry bulb temperature of the building location were modelled for two types of buildings. A substantial discrepancy related to mean envelope wall convective heat transfer coefficients predicted by ES only and ES-CFD coupled approach was observed. Hence on this basis, discrepancy of prediction with respect to building energy consumption between ES only and ES-CFD coupled approach was more than 20% in certain scenarios. Although this finding agrees very well with the available literature, a comprehensive experimental validation is needed for confirming the same.

Application of ES-CFD coupled approach for the process of generic optimization of building performance was considered. Three different approaches were proposed in this regard. In the first approach, ES and CFD tools were supposed to carry out complementary data exchange at every iterative step of the generic optimization process. However, this approach was not feasible due to extreme computational demands. Second approach was to exchange data between the two tools at certain specific iterative steps of the generic optimization process. This strategy was not as computationally expensive as the previous approach. However, intermittent data transfer between the two systems lead to stability and convergence issues during the optimization process. In the third approach, generic optimization process was first completed and subsequently ES-CFD coupled simulation was implemented for the optimal envelope design in order to generate a more refined solution for building performance. Although this approach had the least accuracy, it was the only feasible approach due to manageable computational demands. This approach was demonstrated using two case studies.

10.3 Indoor environmental quality

Application of CFD in predicting indoor environment quality was extensively discussed. ES-CFD approach was adopted in predicting air temperature, velocity, relative humidity, thermal comfort and CO_2 concentration in a simple building with respect to seven identified mechanical ventilation configurations. This was a quite challenging task since indoor flows are associated with low Reynolds number buoyancy flows. CFD tool did not have the provision of directly predicting the thermal comfort of the occupied space. Hence, a user-defined function was developed using C language and subsequently integrated with the CFD tool. The results provide with PMV data at each node point of the computational domain. With this analysis, thermal comfort data at microscopic level of the occupied space are available to the designers, compared to a single PMV value that represents the entire occupied space as given in relevant ASHRAE standards. Furthermore, thermal comfort on occupants at ankle level, waist level and neck level was predicted.

The analysis included a comparison of ventilation performance among the different air supply configurations considered. It was observed that, mixing flow ventilation through diffusers located at ceiling level produced the best indoor environmental quality among the configurations considered. This was observed with respect to both thermal parameters and CO_2 levels within the building space.

Modelling of indoor environment has only been conducted using the RANS approach in CFD due to limited computational resources possessed by the researcher. However, the building performance predictions could have been more accurate had the computationally expensive LES approach been utilized. Furthermore, indoor environmental quality has been assessed only in terms of thermal comfort and CO_2 concentration. Prediction of other indoor pollutant levels, acoustical quality and visual quality of the building would have added substantial value to this study.

10.4 Validation of predictions

Several tools were utilized in developing the computational model of the test facility. Simulations were conducted using several turbulence models in order to predict the indoor flow field. However, only k-ω SST model could generate an acceptable solution and all k-ε turbulence models failed in this regard as explained in chapter 9. Checking the CFD solution against "grid independence" was really cumbersome due to numerous options available in the mesh generation tool and limitations in computational power at hand.

Measurements were taken with respect to air temperature, air velocity, relative humidity and CO_2 concentration in an actual indoor environment in order to validate computational model predictions. Experimental design was conducted as specified in the ASHRAE 55-2017 and ISO 16000-1: 2004 standards. Several precision measuring instruments such as Omni-directional anemometers, Black globe temperature sensor, Air humidity sensors, data logging tools etc. have been used in taking thermal and flow measurements. Calibrating measuring equipment took a fairly long period of time. Several pilot test runs were conducted prior to taking the final set of measurements. Obtaining measurements under steady state conditions was a big challenge and every effort was made to maintain the same during the period of measurement. Measurement of thermal and flow parameters was restricted to a height of 1.1 m from floor level due to technical limitations of the equipment used. CO_2 measurements were recorded at the same height as recommended in the ISO 16000-1 standards. Since building envelope elements were modelled as isothermal walls, surface temperature measurements at multiple locations of a particular element were recorded to minimize the error. The model predictions with respect to all indoor environmental parameters showed a fairly good agreement with the actual measurements. Inclusion of a radiation model was crucial in predicting air temperature and thermal comfort in the building space. However, influence of the radiation model was not significant in the case of predicting air velocity and CO_2 levels. Discrete ordinates radiation model incorporated with solar loading recorded the best agreement with measurements in the overall analysis. Computational model

can be further refined for making better predictions, if more advanced computational resources and tools are utilized.

10.5 Concluding remarks

As far as the four research objectives are concerned, first three objectives have been fully achieved during the study using relevant methodologies and tools as described in the thesis. The fourth objective on validating model predictions against actual measurements has been achieved only to a moderate extent. This is mainly due to the practical constraints and issues associated with the task concerned. It is not feasible to practically measure the energy performance of buildings with the optimal envelope design recommended by the study, since they are still in the conceptual early design stage. Hence, taking actual measurements on energy performance related to the optimal envelope designs of the said building case studies considered in the study are not feasible at this stage. However, energy performance of an existing building in Sri Lanka predicted by EnergyPlus using the same approach can be successfully validated by conducting actual measurements, especially with reference to green building certification programmes. Experiments on IEQ were conducted only for the scenario of maximum annual outdoor dry bulb temperature in order to validate computational model predictions related to the test facility. It would have been ideal if several experimental sessions had been conducted during different time periods of the year in this regard. However, this was not possible due to time constraints. Hence it can be concluded that only partial validation of model predictions has been accomplished during the study.

The methodology suggested as the outcome of the research can be conceptually applied to any complex building configuration. However, two major challenges need to be addressed in this regard. Technically it is a huge challenge to model a full-scale multi-storey building operating under dynamic conditions with complex interactions of energy and indoor air quality. Developing the computational model, assigning appropriate boundary conditions for the same and subsequently conducting time consuming simulations on high-end computers will be an exhaustive and costly endeavour. Hence, the approach can be initially applied for simple buildings and selected parts of a complex building, allowing reasonable time for the approach to

become a standard feasible practice in the building sector. On the other hand, professionals involved need to be trained extensively on modelling tools and methodologies. In most developing economies building designers, engineers, architects and contractors adopt prescriptive standards imposed by the respective local authorities at present. This approach only specifies the minimum standards to be met in terms of different systems of the building. The proposed performance-based approach will enable design and construction of buildings with enhanced or optimal performance while meeting both the design intent and minimum standards to be complied with. However, this goal can only be accomplished through dedication and commitment of all stakeholders in the building construction sector.

10.6 Directions for future work

One area that has great potential for future work is the analysis and optimization of personal thermal comfort systems, which can be considered as a new challenge for the building energy simulation community. This includes systems such as personal ventilation, cooling/heating chair etc. In such systems, ambient temperature will be different from that of the occupant's task zone. Hence, modelling and optimizing the same will be more challenging compared to conditioned occupied spaces of conventional nature.

10.7 Summary

This chapter gives a summary of work conducted and main contributions of the study. It also explains challenges, issues and limitations encountered during this endeavour together with directions for future work.

LIST OF REFERENCES

Adams, B., Bohnhoff, W., Dalbey, K., Eddy, J., Eldred, M., & Gay, D. (2010). *DAKOTA: A multi-level parallel object-oriented framework for design optimization, parameter estimation, uncertainty quantification and sensitivity analysis: v.5.0 user's manual.* Livermore, CA: Sandia National Laboratory.

Alamdari, F., Bennett, K., & Rose, P. (1994). Air flow and temperature distribution within an open-plan building space using displacement ventilation system. *Proceeedings of 4th International conference on air distribution in rooms.* Krakow, Poland: Roomvent '94.

Alfano, F., Bellia, L., Boerstra, A., Dijken, F., Ianniello, E., & Lopardo, G. (2010). *Indoor environment and energy efficiency in schools - part 1 principles.* Brussels: REHVA (Federation of European Heating and Air-conditioning Associations).

Al-Homoud, M., & Degelman, L. (1994). The framework of an optimization model for the thermal design of building envelopes. *Proceedings of the 9th Symposium on Improving Building Systems in Hot and Humid Climates,* (pp. 100-109). Arlington, TX.

Al-Homoud. (1997). Optimum thermal design of office buildings. *International Journal of Energy Research 21,* 941-957.

Ambiente Interior e Eficiência Energética nas Escolas (2010). Ingenium Edições, Lda., Manual REHVA. Lisboa: REHVA.

ANSI/ASHRAE standard 55-2017: Thermal environmental conditions for human occupancy. Atlanta, USA: ASHRAE.

Arens, A. (2000). *Evaluation of Dispalcement Ventilation for use in High-Ceiling Facilities.(MSc Thesis).* Cambridge: Massachusetts Institute of Technology.

Arun, M., & Tulapurkara, E. (2005). Computation of turbulent flow inside an enclosure with central partition. *Progress in Computational Fluid Dynamics 5*, 455-465.

ASHRAE Handbook of Fundamentals (2013). Atlanta, USA: ASHRAE.

Attia, S. (2012). *Computational optimization zero energy building design: Interviews with 28 international experts.* Louvain la Neuve: Université Catholique de Louvain.

Awbi, H. (1989). Application of computational fluid dynamics in room ventilation. *Building and Environment 24*, 73-84.

Awbi, H., & Gan, G. (1991). Computational fluid dynamics in ventilation. *Proceedings of CFD for Environmental and Building Services Engineer* (pp. 67-79). London: Institution of Mechanical Engineers.

Awbi, H., & Gan, G. (1993). Evaluation of the overall performance of room air distribution. *Proceedings of the Indoor Air Quality and Climate* (pp. 283-288). Helsinki: Indoor Air '93.

Awbi, H. (1996). A CFD study of the air quality at the breathing zone. *Proceedings of Indoor Air '96* (pp. 1009-1014). Nagoya, Japan: Indoor Air '96.

Baker, A., Williams, P., & Kelso, R. (1994). Development of a robust finite element CFD procedure for predicting indoor room air motion. *Building and Environment*, 261-273.

Bambrook, S., Sproul, A., & Jacob, D. (2011). Design optimization for a low energy home in Sydney. *Energy and Buildings 43*(7), 1702-1711.

Baños, R., Manzano-Agugliaro, F., Montoya, F., Gil, C., Alcayde, A., & Gómez, J. (2011). Optimization methods applied to renewable and sustainable energy: A review. *Renewable and Sustainable Energy Reviews 15*(4), 1753-1766.

Bartak, M., Beausoleil-Morrison, I., Clarke, J., Denev, J., Drkal, F., Lain, M., . . . Stankov, P. (2002). Integrating CFD and building simulation. *Building and Environment 37(8)*, 865-872.

Beausoleil-Morrison, I., & Clarke, J. (1998). The Implications of Using the Standard k - e Turbulence Model to Simulate Room Air Flows which are not Fully Turbulent. *Proceedings of ROOMVENT 98* (pp. 99-106). Stockholm: ROOMVENT.

Beausoleil-Morrison, I. (2000). *The adaptive coupling of heat and air flow modeling within dynamic whole-building simulation (PhD Thesis).* Glasgow: University of Strathclyde.

Beausoleil-Morrison, I. (2001). The adaptive coupling of Computational Fluid Dynamics with whole building thermal simulation. *Proceedings of the 7th International IBPSA Conference* (pp. 1259-1266). Rio de Janeiro: IBPSA.

Beausoleil-Morrison, I. (2002). The adaptive conflation of computational fluid dynamics with whole building thermal simulation. *Energy and Buildings 34(9)*, 857-871.

Belegundu, D., & Chandrupatla, T. (2011). *Optimization Concepts and Applications in Engineering* (2nd ed.). London: Cambridge University Press.

Bernal, W., Behl, M., Ngheim, T., & Mangharam, R. (2012). MLE+: a tool for integrated design and deployment of energy efficient building controls. *Proceedings of the 4th ACM Workshop on Embedded Sensing Systems for*

Energy-Efficiency in Buildings (pp. 123-130). Toronto, Ontario, Canada: BuildSys '12.

Bluyssen, P. (1996). *Methods and sensors to detect indoor air pollutants perceived by the nose.* TNO report 96 - BB I- R0873.

Bluyssen, P. (2009). *The Indoor Environment Handbook: How to make buildings healthy and comfortable* (1st ed.). London: Earthscan.

Bouchlaghem, N. (2000). Optimizing the desgn of building envelopes for thermal performance. *Automation in Construction 10(1),* 101-112.

Building Energy Software Tools. (2016). Retrieved from TRNSYS: https://www.buildingenergysoftwaretools.com/software/trnsys

Butler, D. (2002). *Air conditioning using displacement ventilation to maximize free cooling.* BRE's Environmental Engineering Centre.

Caldas, L.; Norford, L. (2002). A design optimization tool based on a genetic algrithm. *Automation in Construction 11(2),* 173-184.

Carson, Y., & Maria, A. (1997). Simulation Optimization: Methods and Applications. *Proceedings of the 29th Winter Simulation Conference* (pp. 118-126). Atlanta: IEEE Computer Society Washington, DC, USA.

Castro-Lacouture, D., Sefair, J., Flórez, L., & Medaglia, A. (2009). Optimization model for the selection of materials using a LEED-based green building rating system in Colombia. *Building and Environment 44(6),* 1162-1170.

Ceylan, H., & Myers, G. (1980). Long-time solutions to heat conduction transients with time-dependent inputs. *ASME Journal of Heat Transfer 102(1),* 115-120.

Chen, Q., & Van der Kooi, J. (1988). Accuracy: A Computer Program for Combined Problems of Energy Analysis, Indoor Airflow, and Air Quality. *ASHRAE Transactions, 94 (2),* 196-214.

Chen, Q., Peng, X., & Van Passen, A. (1995). Prediction of room thermal response by CFD technique with conjugate heat transfer and radiation models. *ASHRAE Transaction 101*, 50-60.

Childs, K., Argeles, C., Henderson, H., Horst, S., & Malin, N. (2006). *Indoor Air Quality: Interior Design and Global Impacts.* Washington DC: American Society of Interior Designers.

Clarke, J. (2001). *Energy Simulation in Building Design* (2nd ed.). Oxford: Butterworth-Heinemann.

Cofaigh, E., Fitzgerald, E., Alcock, R., McNicholl, A., Peltonen, V., & Marucco, A. (1999). *A Green Vitruvius: Principles and Practice of Sustainable Architecture Design* (1st ed.). London: James & James (Science Publishers).

Commercial Buildings Energy Consumption Survey (2003). Washington, DC: Energy Information Administration, U.S. Department of Energy.

Crawley, D., Lawrie, L., Frederick, C., Winkelmann, C., Buhl, W., Huang, Y., . . . Glazer, J. (2001). EnergyPlus: creating a new-generation building energy simulation program. *Energy and Buildings 33(4),* 319-331.

Crawley, D., Hand, J., Kummert, M., & Griffith, B. (2005). *Contrasting the capabilities of building energy performance simulation programs.* Washington DC: U.S. Department of Energy.

D'Angelo, J., & West, D. (2000). *Mathematical thinking: Problem solving and proofs.* London: Prentice-Hall.

Dar, J. (2017). *Core concepts in MATLAB Programming.* lulu.

D'Cruze, N., & Radford, A. (1987). A multi-criteria model for building performance and design. *Building and Environment 22(3),* 167-179.

Deardorff, J. (1970). A numerical study of three-dimensional turbulent channel flow at large Reynolds numbers. *Journal of Fluid Mechanics. 41 (2),* 453–480.

Djunaedy, E., Hensen, J., & Loomans, M. (2003). Towards external coupling of building energy and airflow modeling programs. *ASHRAE Transactions 109(2),* 771-787.

Djunaedy, E., Hensen, J., & Loomans, M. (2004). Selecting an appropriate tool for airflow simulation in buildings. *Building Services Engineering Research and Technology 25(3),* 269–278.

Djundaedy, E. (2005). *External coupling between building energy simulation and computational fluid dynamics (PhD Thesis).* Eindhoven: Technische University Eindhoven.

Ellis, P., Griffith, N., Torcellini, P., & Crawley, D. (2006). Automated multivariate optimization tool for energy analysis. *Proceedings of the 2nd National IBPSA-USA Conference* (pp. 42-48). Cambridge: SimBuild2006.

Energy Technology Perspectives (2016). Paris: International Energy Agency/The Organisation for Economic Co-operation and Development.

EnergyPlus Engineering Reference (2013). Washington, DC: US Department of Energy.

ESP-r Whole Building Simulation Tool Overview. (2011). Retrieved from http://www.esru.strath.ac.uk/Programs/ESP-r_overview.htm

Fan, Y., & Ito, K. (2014). Optimization of indoor environmental quality and ventilation load in office space by multilevel coupling of building energy simulation and computational fluid dynamics. *Building Simulation 7(6),* 649–659.

Fesanghary, M., Asadi, S., & Geem, Z. (2012). Design of low-emission and energy efficient residential buildings using a multi-objective optimization algorithm. *Building and Environment 49,* 245-250.

Feustel, H., & Sherman, M. (1989). A Simplified Model for Predicting Air Flow in Multizone Structures. *Energy and Buildings 13(3),* 217-230.

Feustel, H., & Dieris, J. (1992). A survey on air flow models for multizone structures. *Energy and Buildings 18(2),* 79-100.

Feustel, H. (1998). *COMIS — An International Multizone Air-Flow and Contaminant Transport Model.* Berkeley: Lawrence Berkeley National Laboratory.

Fonseca, C., & Flemming, P. (1998). Multi-objective optimization and multiple constraints handling with evolutionary algorithms - part 1: A unified formulation. *IEEE Transactions on Systems, Man and Cybernetics, Part A 28(1),* 26-37.

Gan, G. (1995). Evaluation of room air distribution systems using computational fluid dynamics. *Energy & Buildings 23(2),* 83-93.

Gatski, T., Hussaini, M., & Lumley, J. (1996). *Simulations and Modeling of Turbulent Flows.* New York: Oxford University Press.

Gebremedhin, K., & Wu, B. (2003). Characterization of flow field in a ventilated space and simulation of heat exchange between cows and their environment. *Journal of Thermal Biology 28(4),* 301–319.

Gilani, S., Montazeri, H., & Blocken, B. (2016). CFD simulation of stratified indoor environ ment in displacement ventilation: Validation and sensitivity analysis. *Building & Environment 95,* 299-313.

Global Status Report (2016). Paris: Global Alliance for Buildings and Construction.

Goldberg, D. (1989). *Genetic Algorithms in Search, Optimization and Machine Learning* (1st ed.). London: Addison-Wesley.

Gupta, C. (1970). A systematic approach to optimum thermal design. *Building Science 5(3-4),* 165-173.

Gupta, C., & Spencer, J. (1970). Building design for optimum thermal performance. *Australia Refrigeration, Air-conditioning and Heating,* 18-25.

Han, Y., Liu, X., & Chang, L. (2014). Comparison of software for building energy simulation. *Journal of Chemical and Pharmaceutical Research 6(3),* 467-471.

Hasan, A., Vuolle, M., & Siren, K. (2008). Minimisation of life cycle cost of a detached house using combined simulation and optimisation. *Building and Environment,* 2022-2034.

Healthy Housing Reference Manual (2006). Washington DC: United States Department of Health and Human Services.

Hooke, R., & Jeeves, T. (1961). Direct search solution of numerical and statistical problems. *Journal of the Association for Computing Machinary 8(2),* 212-229.

Hoskins, J. (2003). Health Effects due to Indoor Air Pollution. *Indoor and Built Environment 12(6),* 427-433.

International Energy Outlook (2016). Washington, DC: Energy Information Administration, U.S. Department of Energy.

ISO 16000-1:2004: Indoor air - Part 1: General aspects of sampling strategy. ISO.

Jacobsen, T., & Nielsen, P. (1993). Numerical modeling of thermal environment in a displacement-ventilated room. *Proceedings of the 6th International Conference on Indoor Air Quality and Climate* (pp. 301-306). Helsinki: Indoor Air '93.

Jagemar, L. (1996). *Design of energy efficient buildings.* Goteborg: PhD thesis.

Jedrzejuk, H., & Marks, W. (2002). Optimization of shape and functional structure of buildings as well as heat source utilization. *Building and Environment 37(11),* 1037-1043.

Kämpf, J., & Robinson, D. (2009). A hybrid CMA-ES and HDE optimisation algorithm with application to solar energy potential. *Applied Soft Computing 9(2),* 738-745.

Kämpf, J., Wetter, M., & Robinson, D. (2010). A comparison of global optimisation algorithms with standard benchmark functions and real-world applications using EnergyPlus. *Journal of Building Performance Simulation 3(2),* 103-120.

Kennedy, J., & Eberhart, R. (1995). Particle swarm optimization. *Proceedings of the IEEE international conference on neural networks IV* (pp. 1942–1948). Piscataway: IEEE.

Khalil, E. (2014). *Air Distribution in Buildings* (1st ed.). New York: Talor & Francis Group.

Knebel, D. (1983). *Simplified Energy Analysis Using the Modified Bin Method.* Atlanta, GA: American Society of Heating, Refrigerating and Air-Conditioning Engineers.

Knipe, E., & Day, T. (1986). Building energy simulation:Looking before you leap. *J. Property Mnt.,* 19-22.

Kumar, A., Ashutosh, S., & Sodha, M. (1989). Optimum distribution of insulation over various components of an air-conditioned building. *Building and Environment 24(2)*, 169-178.

Kusuda, T. (2001). Early history and future prospects of building system simulation. *Proceedings of the Building Simulation '99* (pp. 3-15). Kyoto: IBPSA.

Launder, B., & Spalding, D. (1974). The numerical computation of turbulent flows. *Computer Methods in Applied Mechanics and Engineering 3(2)*, 269-289.

Li, K., Pan, L., Xue, W., Jiang, H., & Mao, H. (2017). Multi-Objective Optimization for Energy Performance Improvement of Residential Buildings: A Comparative Study. *Energies 10(2)*, 245.

Lin, Z., Chow, T. T., Fong, K., & Liu, J. (2000). CFD Simulation of concentration of gaseous impurities in a typical Hong Kong industrial workshop. *Proceedings of ROOMVENT 2000* (pp. 167-172). Reading, UK: ROOMVENT 2000.

Lomas, K. (1996). The UK Applicability Study: An evaluation of thermal simulation programs for passive solar house design. *Building and Environment 31*, 197-206.

Lombard, L., Ortiz, J., & Pout, C. (2008). A review on buildings energy consumption information. *Energy and Buildings 40(3)*, 394-398.

Loomans, M. (1998). *The measurement and simulation of indoor air flow (PhD Thesis).* Eindhoven: Eindhoven University of Technology.

Loutzenhiser, P., Manz, H., Moosberger, S., & Maxwell, G. (2009). An empirical validation of window solar gain models and the associated interactions. *International Journal of Thermal Sciences 48(1)*, 85-95.

Lucon, O., Ürge-Vorsatz, D., Zain Ahmed, A., Akbari, H., Bertoldi, P., Cabeza, L., . . . Gadgil, L. (2014). Buildings. In O. Edenhofer, R. Pichs-Madruga, Y. Sokona, ,. E. Farahani, S. Kadner, & K. Seyboth, *Climate Change 2014: Mitigation of Climate Change* (pp. 671-738). New York: Cambridge University Press.

Maile, T., Fischer, M., & Bazjanac, V. (2007). *Building Energy Performance Simulation Tools - A Life-Cycle and Interoperable Perspective.* USA: Stanford University.

Malkawi, A., & Augenbroe, G. (2003). *Advanced Building Simulation.* New York: Spon Press.

Menter, F. (1994). Two-equation eddy-viscosity turbulence models for engineering applications. *AIAA Journal 32(8)*, 1598-1605.

Mitchell, R., & Kaplan, J. (1968). Non-linear constrained optimization by a non-random complex method. *Journal of Research of the National Bureau of Standards 72C (4)*, 249-258.

Mumovic, D., & Santamouris, M. (2009). *A Handbook of Sustainable Building Design and Engineering: An Integrated Approach to Energy, Health and Operational Performance* (1st ed.). London: Earthscan.

Murakami, S., & Kato, S. (1989). Numerical and experimental study on room airflow - 3-D predictions using the k-ε turbulence model. *Building and Environment, 24(1)*, 85-97.

Murakami, S., Kato, S., & Zeng, J. (1998). Combined simulation of airflow, radiation and moisture transport for heat release from human body. *Proceedings of the 6th International conference on air distribution in rooms* (pp. 141-150). Stockhom: ROOMVENT'98.

Neale, A., Derome, D., Blocken, B., & Carmeliet, J. (2006). CFD calculation of convective heat transfer coefficients and validation – Part 2: Turbulent flow, Annex 41. Kyoto, April 2006.

Negendahl, K., & Nielsen, T. (2015). Building energy optimization in the early design stages: A simplified method. *Energy and Buildings 105*, 88-99.

Negrão, C. (1995). *Conflation of computational fluid dynamics and building thermal simulation (PhD thesis).* Glasgow: University of Strathclyde.

Negrão, C. (1998). Integration of computational fluid dynamics with building thermal and mass flow simulation. *Energy and Buildings 27*, 155-165.

Nelder, J., & Mead, R. (1965). A simplex method for function minimization. *The Computer Journal 7(4)*, 308-313.

Nguyen, A. (2013). *Sustainable housing in Vietnam: Climate responsive design strategies to optimize thermal comfort (PhD Thesis).* Belgique: University of Liege.

Nguyen, A., Reiter, S., & Rigo, P. (2014). A review on simulation-based optimizationmethods applied to building performance analysis. *Applied Energy 113*, 1043-1058.

Nielson, P. (1974). *Flow in air conditioned rooms. (Ph.D. Thesis).* Copenhagen: Technical University of Denmark.

Nielsen, T. (2002). *Optimization of buildings with respect to energy and indoor environment (PhD Thesis).* Lyngby: Technical University of Denmark.

Nielsen, T., & Svendsen, S. (2002). Life cycle cost optimization of buildings with regard to energy use, thermal indoor environment and daylight. *International Journal of Low Energy and Sustainable Buildings 2*, 1-16.

Palonen, M., Hasan, A., & Siren, K. (2009). A Genetic algorithm of optimization of building envelope and HVAC system parameters. *Proceedings of the 11th International IBPSA Conference* (pp. 159-166). Glasgow: IBPSA.

Palonen, M., Hamdy, M., & Hasan, A. (2013). MOBO A new software for multi-objective building performance optimization. *Proceedings of the 13th Conference of International Building Performance Simulation Association* (pp. 2567-2574). Chambery, France: IBPSA.

Papakonstantinou, K., Kiranoudis, C., & Markatos, N. (2000). Mathematical modelling of environmental conditions inside historical buildings: The case of the Archaeological Museum of Athens. *Energy and Buildings 31*, 211-220.

Patankar, S. (1980). *Numerical Heat Transfer and Fluid Flow*. Minnesota: Taylor & Francis.

Peippo, K., Lund, P., & Vartiainen, E. (1999). Multivariate optimization of design trade-offs for solar low energy buildings. *Energy and Buildings 29(2),* 189-205.

Posner, J., Buchanan, C., & Dunn-Rankin, D. (2003). Measurement and prediction of indoor air flow in a model room. *Energy and Buildings 35*, 515-526.

Powell, M. (1964). An efficient method for finding the minimum of a function of several variables without calculating derivatives. *The Computer Journal 7(2),* 155-162.

Rodi, W. (1978). *Turbulence models and their application in hydraulics: A state-of-the art review - SFB 80/T/127.* Baden-Württemberg, Germany: University of Karlsruhe.

Rosenbrock, H. (1960). An automatic method for finding the greatest or least value of a function. *The Computer Journal 3(3),* 175-184.

Roy, R., Hinduja, S., & Teti, R. (2008). Recent advances in engineering design optimization: challenges and future trends. *CIRP Annals- Manufacturing Technology 57(2),* 697-715.

Sahab, M., Toropov, V., & Gandomi, A. (2013). *A review on traditional and modern structural optimization: problems and techniques* (1st ed.). Oxford: Elsevier.

Santamouris, M., Synnefa, A., Assimakopoulos, M., Livada, I., Pavlou, K., & Papaglastra, M. (2008). Experimental investigation of the air flow and indoor carbon dioxide concentration in classrooms with intermittent natural ventilation. *Energy and Buildings 40(10),* 1833-1843.

Seem, J. (1987). *Modeling of heat transfer in buildings (PhD Thesis).* Madison: Thesis, University of Wisconsin-Madison.

Shih, T., Liou, W., Shabbir, A., Yang, Z., & Zhu, J. (1995). A New k-ε Eddy Viscosity Model for High Reynolds Number Turbulent Flows—Model Development and Validation. *Computers Fluids 24(3),* 227-238.

Skistad, H., Mundt, E., Nielsen, P., Hagström, K., & Railio, J. (2004). *Displacement Ventilation in Non-Industrial Premises.* REHVA Guidebook 1: Brussels.

Speziale, C., Sarkar, S., & Gatski, T. (1991). Modelling the pressure-strain correlation of turbulence : an invariant dynamical systems approach. *Journal of Fluid Mechanics 227*, 245-272.

Spitler, J., Pedersen, C., Fisher, D., Menne, P., & Cantillo, J. (1991). An experimental facility for investigation of interior convective heat transfer. *ASHRAE Transactions 97(1)*, 497-504.

Stamou, A., & Katsiris, I. (2006). Verification of a CFD model for indoor airflow and heat transfer. *Building and Environment 41(9)*, 1171-1181.

Su, M., Chen, Q., & Chiang, C. (2001). Comparison of different subgrid-scale models of Large Eddy simulation for indoor airflow modeling. *ASME Transactions 123*, 628-639.

Suh, W., Park, C., & Kim, D. (2011). Heuristic and meta-heuristic optimization for energy performance of a post office building. *Proceedings of the 12th Conference of International Building Performance Simulation Association* (pp. 704-711). Sydney: IBPSA.

The European Portal for Energy Efficiency in Buildings. (2010). Retrieved from http://www.buildup.eu/en/learn/tools/esp-r

The Inside Story: A guide to indoor air quality (1995). Washington DC: United States Environmental Protection Agency.

Tian, Z., Tu, J., & Yeoh, G. (2006). On the numerical study of contaminant particle concentration in indoor air flow. *Building and Environment 41*, 1504-1514.

Topp, C., Nielsen, P., & Heiselberg, P. (1999). Modelling Emission from Building Materials with Computational Fluid Dynamics. *Proceedings of the 8th International Conference on Indoor Air Quality and Climate* (pp. 737-742). Edinburgh: Aalborg University.

Transient System Simulation Tool (TRNSYS) 17. (2012). Retrieved from https://sel.me.wisc.edu/trnsys/features/t17updates.pdf

Tu, J., Yeoh, G., & Liu, C. (2008). *Computational Fluid Dynamics: A Practical Approach.* Oxford: Butterworth-Heinemann.

Underwood, C., & Yik, F. (2004). *Modelling methods for energy in buildings* (1st ed.). London: Blackwell Publishing Ltd.

Versteeg, H., & Malalasekera, W. (1995). *Computational Fluid Dynamics: The finite volume method.* London: Addison Wesley Longman Ltd.

Vieser, W., Esch, T., & Menter, F. (2002). *CFX Technical Report: Heat transfer predictions using advanced two-equation turbulence models.* CFX-VAL10/0602.

Wang, B., Xia, X., & Zhang, J. (2014). A multi-objective optimization model for the life-cycle cost analysis and retrofitting planning of buildings. *Energy and Buildings 77*, 227-235.

Wang, L., & Chen, Q. (2005). On Solution Characteristics of Coupling of Multizone and CFD Programs in Building Air Distribution Simulation. *Proceedings of the 9th International IBPSA Conference* (pp. 1315-1322). Montreal: IBPSA.

Wang, L. (2007). *Coupling of multizone and CFD programs for building airflow distribution and contaminant transport simulations. (PhD Thesis).* Lafayette: Purdue University.

Wang, L., & Wong, N. (2008). Coupled simulations for naturally ventilated residential buildings. *Automation in Construction 17*, 386-398.

Wang, W., Zmeureanu, R., & Rivard, H. (2005). Applying multi-objective genetic algorithms in green building design optimization. *Building and Environment 40(11)*, 1512-1525.

Wargocki, P. (2009). Ventilation, thermal comfort, health and productivity. In D. Mumovic, & M. Santamouris, *A handbook of sustainable building design and engineering: An integrated approach to energy, health and operational performance.* London: Earthscan.

Wetter, M., & Wright, J. (2004). Comparison of deterministic and probabilistic optimization algorithms for non-smooth simulation-based optimization. *Building and Environment 39(8),* 989-999.

Wetter, M. (2009). *GenOpt Generic Optimization Program User Manual v. 3.0.0, Technical Report LBNL-5419.* Berkeley: Lawrence Berkeley National Laboratory.

Wetter, M. (2011). *GenOpt 3.1.0: Generic Optimization Program User Manual.* Berkeley: Lawrence Berkeley National Laboratory.

Wigginton, M., & Harris, J. (2002). *Intelligent Skins* (1st ed.). Oxford: Butterworth-Heinemann.

Wilcox, D. (1988). Reassessment of the Scale-Determining Equation for Advanced Turbulence Models. *AIAA Journal 26*, 1299-1310.

Wilcox, D. (1998). *Turbulence modeling for CFD.* La Cañada, California: DCW Industries.

Wilson, J., & Templeman, A. (1976). An approach to the optimum thermal design of office buildings. *Building and Environment 11(1)*, 39-50.

World Health Organization. (2018). Retrieved from Global Health Observatory (GHO) data: Mortality from household air pollution http://www.who.int/gho/phe/indoor_air_pollution/burden/en/

Wu, F., Jacobs, D., Mitchell, C., Miller, D., & Karol, M. (2007). Improving Indoor Environmental Quality for Public Health: Impediments and Policy Recommendations. *Environmental Health Perspectives 115(6)*, 953-957.

Xing, H., Hatton, A., & Awbi, H. (2001). A study of the air quality in the breathing zone in a room with displacement ventilation. *Building and Environment 36*, 809-820.

Xu, W., & Chen, Q. (2001a). A two-layer turbulence model for simulation indoor airflow Part I. Model development. *Energy and Buildings 33*, 613-625.

Xu, W., & Chen, Q. (2001b). A two-layer turbulence model for simulation indoor airflow Part II. Applications. *Energy and Buildings 33*, 627-639.

Yakot, V., & Orszag, S. (1986). Renormalization-group analysis of turbulence. *Physical Review Letters 57(14)*, 1722–1724.

Yan, D., & Jiang, Y. (2005). An overview of an integrated building simulation tool-Designer's simulation toolkit (DeST). *Proceedings of the Building Simulation 2005* (pp. 1393-1400). Montreal, Canada: IBPSA.

Zhai, Z., Chen, Q., Klems, J., & Haves, P. (2001). Strategies for coupling energy simulation and computational fluid dynamics programs. *Proceedings of the 7th International IBPSA Conference* (pp. 59-66). Rio de Janeiro, Brazil: IBPSA.

Zhai, Z., Chen, Q., Haves, P., & Klems, J. (2002). On approaches to couple energy simulation and CFD programs. *Building and Environment 37(8)*, 857-864.

Zhai, Z., & Chen, Q. (2003). Solution characters of iterative coupling between energy simulation and CFD programs. *Energy and Buildings 35*, 493-505.

Zhai, Z., Gao, Y., & Chen, Q. (2004). Pressure boundary conditions in multi-zone and CFD program coupling. *Proceedings of the 1st National IBPSA-USA Conference*. Boulder: SimBuild 2004.

Zhai, Z., Zhang, Z., Zhang, W., & Chen, Q. (2007). Evaluation of various turbulence models in predicting airflow and turbulence in enclosed environments by CFD: Part-1: summary of prevent turbulence models. *HVAC&R Research 13(6)*, 853–870.

Zhang, R., Lam, K., Yao, S., & Zhang, Y. (2012). Coupled EnergyPlus and CFD for Annual Natural Ventilation Simulation. *Proceedings of the 5th National Conference of IBPSA-USA* (pp. 329-336). Madison: Simbuild 2012.

Zhang, W., & Chen, Q. (2000). Large Eddy simulation of indoor airflow with a filtered dynamic subgrid scale model. *International Journal of Heat and Mass Transfer 43*, 3219-3231.

Zuo, W., Wetter, M., Li, D., Jin, M., Tian, W., & Chen, Q. (2014). Coupled simulation of indoor environment, HVAC and control system by using fast fluid dynamics and the Modelica buildings library. *Proceedings of the Building Simulation Conference 2014* (pp. 56-63). Atlanta, GA: Building Simulation Conference 2014.

APPENDIX A

User code to calculate PMV in buildings

```
#DEFINE USE_FLUENT_IO_API 0
#INCLUDE "UDF.H"
#INCLUDE "STDLIB.H"
#INCLUDE "SPECIES.H"
DEFINE_ON_DEMAND(TCDTRM)
{
DOMAIN *D;
THREAD *T;
CELL_T C;
FILE *FP;
INT I;                  // NUMBER OF ITERATIONS
INT X;                  // CELL INDEX
INT Y;                  // CELL INDEX
FLOAT RLH[2401000];     // RELATIVE HUMIDITY (%)
REAL CLO;               // CLOTHING (CLO)
REAL MET;               // METABOLIC RATE (MET)
REAL WME;               // EXTERNAL WORK (MET)
REAL TA;                // AIR TEMPERATURE (0C)
REAL TR;                // MEAN RADIANT TEMPERATURE (0C)
REAL VEL;               // AIR VELOCITY (M/S)
REAL PA;                // PARTIAL WATER VAPOUR PRESSURE (PA)
REAL FNPS;              // SATURATED VAPOUR PRESSURE (KPA)
REAL ICL;               // THERMAL INSULATION OF CLOTHING (M2K/W)
REAL TCL;               // SURFACE TEMPERATURE OF CLOTHING (0C)
REAL M;                 // METABOLIC RATE (W/M2)
REAL W;                 // EXTERNAL WORK (W/M2)
REAL MW;                // INTERNAL HEAT PRODUCTION IN THE HUMAN BODY (W/M2)
REAL FCL;               // CLOTHING AREA FACTOR
```

```
REAL HCF;          //HEAT TRANSFER COEFFICIENT BY FORCED CONVECTION (W/M2K)
REAL HCN;          //HEAT TRANSFER COEFFICIENT BY NATURAL CONVECTION (W/M2K)
REAL HC;           // CONVECTIVE HEAT TRANSFER COEFFICIENT (W/M2K)
REAL TAA;          // AIR TEMPERATURE (K)
REAL TRA;          // MEAN RADIANT TEMPERATURE (K)
REAL HL1;          // HEAT LOSS DIFFERENCE THROUGH SKIN
REAL HL2;          // HEAT LOSS BY SWEATING (COMFORT)
REAL HL3;          // LATENT RESPIRATION HEAT LOSS
REAL HL4;          // DRY RESPIRATION HEAT LOSS
REAL HL5;          // HEAT LOSS BY RADIATION
REAL HL6;          // HEAT LOSS BY CONVECTION
REAL TS;           // THERMAL SENSATION TRANSFER COEFFICIENT
REAL EPS;          // STOPPING CRITERIA DURING ITERATION
REAL TCLA;         //FIRST GUESS FOR SURFACE TEMPERATURE OF CLOTHING
REAL P1,P2,P3,P4,P5; // CALCULATION TERMS
REAL XN,XF;        // ITERATIVE SOLUTIONS
REAL PMV;          // PREDICTED MEAN VOTE
REAL PPD;          // PREDICTED PERCENTAGE DISSATISFIED
D=GET_DOMAIN(1);
FP = FOPEN("R_H_DTRM.TXT","R");
X=1;
WHILE (X<2401001)
{
FSCANF(FP,"%F", &RLH[X]);
X++;
}
EPS=0.00015;
CLO=0.7;
MET=1.1;
```

```
WME=0.0;
TA=0.0;
ICL=0;
TCL=0;
M=0;
W=0;
MW=0;
FCL=0;
VEL=0;
FNPS=0;
PA=0;
HCF=0;
TAA=0;
TRA=0;
TS=0;
TCLA=0;
I=0;
P1=P2=P3=P4=P5=0;
HL1=HL2=HL3=HL4=HL5=HL6=0;
XN=XF=0;
HCN=0;
HC=0;
PMV=0;
PPD=0;
Y=1;
ICL=0.155*CLO;
M=MET*58.15;
W=WME*58.15;
MW=M-W;
WHILE (Y<2401001)
{
```

```
IF(ICL<=0.078) FCL=1.0+1.29*ICL;ELSE FCL=1.05+0.645*ICL;
THREAD_LOOP_C(T,D)
{
BEGIN_C_LOOP(C,T)
{
TA=C_T(C,T)-273.00;
TR=29;
VEL=SQRT(POW(C_U(C,T),2)+POW(C_V(C,T),2)+POW(C_W(C,T),2));
FNPS=EXP(16.6536-4030.183/(TA+235));
PA=RLH[Y]*10.0*FNPS;
//FPRINTF(FP1,"%F\N", RLH[Y]); Y++;
HCF=12.1*SQRT(VEL);
TAA=TA+273.00;
TRA=TR+273.00;
TCLA=TAA+(35.5-TA)/(3.5*((6.45*ICL)+0.1));
P1=ICL*FCL;
P2=P1*3.96;
P3=P1*100;
P4=P1*TAA;
P5=308.7-(0.028*MW)+P2*POW((TRA/100),4);
XN=TCLA/100.0;
XF=XN;
FOR(I=0;I<150;I++)
{
XF=(XF+XN)/2;
HCN=2.38*POW(FABS(100.0*XF-TAA),0.25);
IF(HCF>HCN) HC=HCF;ELSE HC=HCN;
XN=(P5+P4*HC-P2*POW(XF,4))/(100+P3*HC);
IF(FABS(XN-XF)<EPS)BREAK;
}
TCL=100.0*XN-273.00;
```

```
HL1=3.05*0.001*(5733.0-6.99*MW-PA);
IF(MW>58.15) HL2=0.42*(MW-58.15);ELSE HL2=0;
HL3=1.7*0.00001*M*(5867.0-PA);
HL4=0.0014*M*(34.0-TA);
HL5=3.96*FCL*(POW(XN,4)-POW((TRA/100.0),4));
HL6=FCL*HC*(TCL-TA);
TS=0.303*EXP(-0.036*M)+0.028;
PMV=TS*(MW-HL1-HL2-HL3-HL4-HL5-HL6);
PPD=100.0-95.0*EXP(-0.03353*POW(PMV,4)-0.2179*POW(PMV,2));
IF (PMV>3.0) PMV=3.0;
IF (PMV<-3.0) PMV=-3.0;
IF (PPD>100) PPD=100;
IF (PPD<5) PPD=5;
C_UDMI(C,T,0)=PMV;
C_UDMI(C,T,1)=PPD;
}
END_C_LOOP(C,T)
}
}
FCLOSE(FP);
}
```